DYNAMIC CRACK PROPAGATION IN ELASTIC-PLASTIC SOLIDS

Thesis by

Xiaomin Deng

In Partial Fulfillment of the Requirements

for the Degree of

Doctor of Philosophy

California Institute of Technology

Pasadena, California

1990

(Submitted May 3, 1990)

To my parents, my wife, my family
and my motherland, China

ACKNOWLEDGEMENTS

I would like to thank my thesis advisor, Prof. Ares J. Rosakis, for his steady support and great guidance during the entire course of this study. I am very grateful to Prof. John F. Hall for his excellent lectures and stimulating thoughts on the finite element method. I am deeply indebted to Profs. Wolfgang G. Knauss and James K. Knowles, and to the late Profs. Charles D. Babcock, Jr., and Eli Sternberg for many helpful discussions on the general subject of Solid Mechanics. I must also thank Prof. Thad Vreeland for his encouragement and interest throughout my stay at Caltech, and Prof. G. Ravichandran for his many valuable suggestions regarding this work. Further, I wish to express my sincere appreciation to the members of my thesis examining committee, Profs. J.F. Hall, W.G. Knauss, J.K. Knowles, A.J. Rosakis and T. Vreeland, Jr., for patiently reading my thesis and for their constructive comments on the thesis.

Thanks are also to the entire Solid Mechanics Group of the Graduate Aeronautical Laboratories. In particular, I greatly appreciate the many seemingly endless, useful discussions with Drs. Sridhar Krishnaswamy, R. Narasimhan, Hareesh V. Tippur and Alan T. Zehnder. The help of Mr. Carl Schultheisz is gratefully acknowledged.

I am thankful to our secretary Theresa Thalken for her cheerfulness and miscellaneous help, to Jean Anderson and Pat Gladson of the Aeronautics Library for their excellent work and help, and to our Lab technician Ken Wang for his various assistance.

I am very grateful to many wonderful American people I have met on and off campus during my stay at Caltech. Their friendship and understanding have made me, a student from China, felt like at home during those past years. I am especially grateful to Mrs. Ruth Hadley and Dr. Carmer Hadley for their parental love and encouragement.

I would further like to express my gratitude to all my Chinese friends in the states, at home and in other countries, and to all my fellow Chinese students at Caltech, in particular, to Dr. Zhikun Hou. They have been very supportive, helpful, and entertaining.

The Josephine de Kármán Fellowship, the Li Ming Fellowship, and the Chinese Government Scholarship are gratefully acknowledged. I am also thankful to the National Science Foundation for financial support for attending a summer institute at the San Diego Supercomputer Center.

The present work was carried out with the funding of the Office of Naval Research, Contract Nos. N00014-85-K-0596 and N00014-90-J-1340, and the National Science Foundation, Grant No. MSM-84-51204. The finite element computation was performed on the SCS-40, Cray X/MP and Cray Y/MP computers of the San Diego Supercomputer Center. Link to the computer network was provided by the Caltech Campus Computing Organization.

Finally and most importantly, I wish to thank my parents and other members of my family for their constant love and care for me. I am especially indebted to my wife, Jingyan, for her love, patience and support.

ABSTRACT

The present finite element study addresses several issues of interest pertaining to the phenomenon of dynamic crack propagation in elastic-plastic solids. Three classes of materials, namely elastic-perfectly plastic materials, linear hardening materials and power-law hardening materials, are considered. The materials are assumed to obey the von Mises yield criterion and the associated flow rule.

Under conditions of Mode I, plane stress, steady state and small scale yielding, we investigated the structures of the near-tip stress and deformation fields. A preliminary asymptotic analysis for crack-tip stress and velocity fields in elastic-perfectly plastic solids was provided to reveal and explain some special features of the crack tip fields observable only in the case of rapid crack propagation. We studied the theoretical basis of a fracture criterion based on the dynamic stress intensity factor for crack growth in materials which fail in a locally ductile manner. We explored the behavior of crack tip fields under non-K-dominance conditions and its effects on the dynamic fracture toughness vs. crack propagation speed relationship.

An Eulerian finite element scheme is employed. Finite element meshes with extremely small elements near the crack tip are carefully designed. The ratio of the crack tip plastic zone size to that of the element nearest to the crack tip is of the order of 1.6×10^4. In order to overcome numerical difficulties associated with crack-tip strain singularities and the use of small near-tip elements, an efficient stress integration algorithm is devised. The existing stress state determination procedure is modified to prevent the occurrence of negative plastic flow and to avoid mistakenly treating elastic unloading as plastic flow. The above measures are proven to be essential for the convergence of the numerical solution.

TABLE OF CONTENTS

CHAPTER 1

INTRODUCTION

All engineering structures contain or will develop cracks, either as natural defects or as a result of fabrication and assembly processes. A short crack may grow through mechanisms such as fatigue, corrosion cracking, etc., and might, under certain circumstances, become unstable. An unstable crack propagates dynamically in a structure, with a speed usually in the range of $20 \sim 60\%$ of the material elastic shear wave speed. For a structure made of 4340 steel, for example, the crack speed would be on the order of one thousand to two thousand meters per second. This rapid separation of material would seriously damage the integrity and function of the structure, and even lead to complete structural failure.

Interest in dynamic crack propagation has been increasing. For the most part, this is because structural designs which preclude crack instability under all conditions can be far too costly, and there are, in addition, applications where the larger-scale unstable extension of a crack would have catastrophic consequences. It is recognized that fracture failures of structures, such as transmission pipelines, offshore oil production platforms, welded ships, railroad tracks, aircraft and spacecraft, bridge girders, pressurized containers, and nuclear reactor pressure vessels, etc., can be prevented by stopping propagating cracks before the structural integrity of the unit is completely lost. It is therefore important for the engineers, when designs preventing crack instability are impossible or inadequate, to configure structural systems in favor of the timely arrest of unstable cracks. Careful scientific study of crack arrest phenomena is thus indispensible. Crack arrest is intimately related to the behavior of the running crack immediately preceeding the arrest. Precise

treatments of crack arrest phenomena must then start from analyses of propagation events and propagation criteria.

It is under this impetus towards understanding crack growth and arrest phenomena that we undertook the present investigation. We present in this thesis the result of a detailed finite element study on dynamic crack propagation in elastic-plastic solids, under Mode I plane stress and steady state conditions. Finite element computations were conducted under small-scale yielding conditions with and without far-field K-dominance to be defined later.

In this study, we intend to address several important issues relevant to dynamic crack propagation pheonomena. First of all, we will try to reveal features of the asymptotic structures of crack tip stress and deformation fields, both for quasi-statically growing cracks and for dynamically propagating cracks. We do this for three classes of elastic-plastic solids, namely, elastic-perfectly plastic materials, power hardening materials and linear hardening materials.

In carrying out the computation, we adopted an Eulerian type finite element formulation (Dean and Hutchinson, 1980), which is based on a weak form of the integral representation of the virtual work principle. The so-called Tangent Predictor-Radial Return method (see Schreyer, Kulak and Kramer, 1979) is modified to calculate stresses in the plastic range by numerically integrating the elastic-plastic, incremental constitutive law, such that the computed stress state automatically satisfies, for elastic-perfectly plastic and linear hardening materials, the yield condition at the end of a strain increment. Furthermore, the existing procedures implementing the stress integration algorithms are improved to eliminate the occurrence of negative plastic flow, and to avoid mistakenly treating elastic unloading as plastic flow. Numerical errors due to the appearance of negative plastic flow may cause deterioration of the numerical solution with oscillations and even divergence, which, for example, can be encountered in elastic-plastic computations for crack growth

problems.

Secondly, we will investigate the issue of fracture criteria for dynamic crack growth. Instead of directly assuming the dependence of the fracture toughness or the critical stress intensity factor on the crack tip velocity, we employ a crack tip local criterion and then abstract from numerical data such a dependence, which is compared with good agreement to experimental measurements performed on metallic materials.

Finally we will explore what happens to the findings of the above studies when small-scale yielding conditions with K-dominance do not hold. A parametric study will be conducted concerning the influence of the nonsingular terms in the elastic far-field on quantities such as the size and shape of the crack tip active plastic zone, the near-tip stress and deformation field variations, and the dynamic fracture toughness vs. the crack propagation speed relationship.

In section 1.1 of this chapter, a brief review will be given regarding elastodynamic analyses of crack propagation phenomena, which forms the basis of our later discussions. Section 1.2 is concerned with a commonly used concept in linear elastic fracture mechanics, namely the concept of small-scale yielding, and with issues regarding its extension to the case of dynamic crack propagation. Observations about discrepancies among experimental results related to fracture criteria are then discussed in section 1.3. Finally in section 1.4 the overview of this thesis is given.

1.1 ELASTODYNAMIC ANALYSES

Most of the work done in the area of dynamic crack propagation has assumed that materials are homogeneous and that they are linearly elastical (although isotropy is not generally assumed in the literature, it is assumed during the course of our discussion). Early investigations concentrated on theoretical analyses of problems of special geometries, loading conditions and/or crack propagation patterns.

The pioneering work of Yoffe (1951) was concerned with the problem of a Mode I crack of fixed length translating steadily through a body subjected to uniform remote tension. The steady motion of a semi-infinite Mode I crack was then analyzed by Craggs (1960). Some years later, Nilsson (1972) studied the case of steady propagation of a Mode I crack, along the centerline of an infinitely-long, finite-width strip subjected to uniform edge displacement conditions.

While the above considered only steady state situations, analyses were also performed for transient problems under the constraint of constant crack velocity (Broberg, 1960; and Baker, 1962). Studies by Kostrov (1966) and by Eshelby (1969) on Mode III nonuniform crack extension problems lifted the restriction of constant crack speed. The plane strain problem of crack growth at nonuniform rates under general loading conditions was treated by Freund (1972a, b, 1973, and 1974).

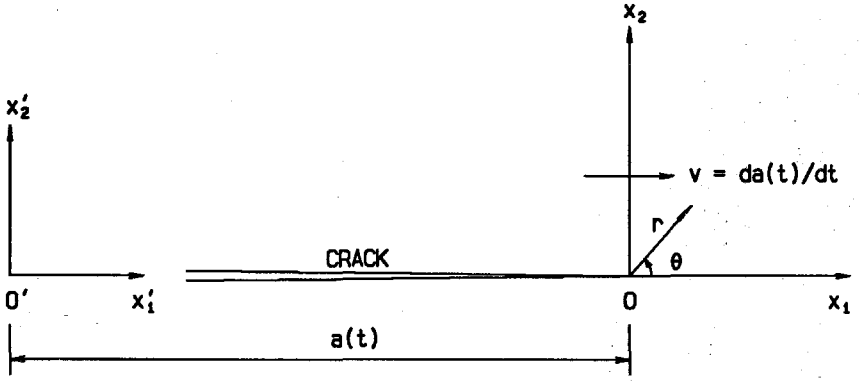

FIGURE 1.1.1 A diagram of crack propagation, where (x_1',x_2') is a fixed reference coordinate system, (x_1,x_2) is a moving system with origin at the crack tip, and (r,θ) is the associated polar coordinate system.

As more particular problems were solved (see reviews by Freund, 1976; Rose, 1976; Sih and Chen, 1977; and Chen and Sih, 1977), it was discovered that while the problems studied may involve either steady state or transient state, and may vary in geometry, loading and crack speed conditions, their solutions share a common

asymptotic feature near the crack tip. That this is true for all growing cracks with smooth trajectories is demonstrated by general elastodynamic near-tip asymptotic analyses of the stress and deformation fields (see Rice, 1968a; Sih, 1970; Freund and Clifton, 1974; Nilsson, 1974; Achenbach and Bazant, 1974; Burgers, 1980; Freund, 1980; and Nishioka and Atluri, 1983). The stress state, in a local polar (r,θ) coordinate system fixed at the crack tip (see Fig.1.1.1), can be expressed as (for definitions of order symbols see Erdélyi, 1956)

$$\sigma_{ij} = \frac{K_N^d(t)}{\sqrt{2\pi r}}\Sigma_{ij}^N(\theta, v) + O(1), \quad (N = I, II, III) \quad \text{as } r \to 0, \tag{1.1.1}$$

for pure Mode I, Mode II and Mode III fracture cases, respectively. Here Σ_{ij}^N $(i,j = 1,2,3)$ are known universal functions of θ and crack velocity v, and K_I^d, K_{II}^d and K_{III}^d are the dynamic stress intensity factors in Mode I, Mode II and Mode III respectively, representing the strength of the singular stress field. The stress intensity factors uniquely characterize the singular stress field which is then usually called the K-field. Moreover, they are also a measure of the energy release rate (the energy power supplied to the crack tip region per unit fracture area). Indeed, as shown by several investigators (Broberg, 1967; Atkinson and Eshelby, 1968; Eshelby, 1969; Kostrov and Nikitin, 1970; Sih, 1970; Achenbach and Brock, 1971; and Freund, 1972c) the energy release rate at the crack tip is proportional to the squares of the stress intensity factors, with universal coefficients dependent only on the instantaneous crack speed v. Attempts are then made to introduce fracture criteria based on the stress intensity factors. In the Mode I case, for example, it is often postulated that during crack propagation the instantaneous value of the stress intensity factor is equal to a function of crack tip speed, which is a material property. The criterion takes the form

$$K_I^d(t) = K_{ID}(v). \tag{1.1.2}$$

Here the stress intensity factor $K_I^d(t)$ represents the driving force of the crack motion, and is determined by the history of the geometric and loading conditions of a

specific problem up to the present time t. On the other hand, the quantity K_{ID}, a material property, represents the resistance of the material to the crack motion, and its functional dependence on v can only be determined through experiments. K_{ID}, together with its velocity dependence, is termed the dynamic (propagation) fracture toughness. Care must be taken not to confuse K_{ID} with the dynamic (initiation) fracture toughness K_{Id}.

Note that K_{ID} is usually used to denote the plane strain toughness, but will be used in this study, unless otherwise stated, as a generic symbol for dynamic fracture toughness. Occasionally, under plane stress conditions, K_{ID} will be replaced with K_{Ic}^{d}, the plane stress dynamic fracture toughness. Similarly, K will be used as a generic notation for the stress intensity factor.

1.2 THE SMALL-SCALE YIELDING CONCEPT

The autonomous, universal structure of the asymptotic singular K-field at a propagating crack tip, and the hypothesis of the critical stress intensity factor criterion (1.1.2) form the basis of the current dynamic fracture mechanics. This is evidenced by the large number of publications devoted to the theoretical and numerical evaluation of stress intensity factors, and to the experimental determination of the dynamic fracture toughness of materials. However, it is the very underlying assumptions, which lead to the near-tip singular stress field, that are violated at the crack tip. As we know, linear elastodynamic analyses predict infinite stresses and strains at the crack tip which real materials cannot sustain. Plasticity and large strains must come into effect. Also as the crack tip traverses rapidly through a body, material points near the path of the crack tip experience large strain rates. Thus for rate sensitive solids, rate effects have to be considered. Plasticity and rate sensitivity produce large energy dissipation which in turn generates a large amount of heat, raising the crack tip temperature up to as high as several hundreds to several thousands of degree centigrade (see Fuller, Fox and Field, 1975; Weichert and

Schoenert, 1978; and Zehnder and Rosakis, 1990b). As a result, material properties at the crack tip may change during fast crack propagation. It then seems clear that, if the concept of the K-field and the critical stress intensity factor criterion (1.1.2) are to provide any applications at all in engineering practice, the influence zone of the crack tip nonlinearity and/or inelasticity effects must be confined to a tolerable region.

It is fortunate that for quasi-static fracture initiation and slow stable (short range) crack growth, such crack tip confining regions do often exist in practical applications. The rationale for admitting the singular stress distribution at the crack tip is thus explanable in terms of the so-called small-scale yielding (SSY) concept (Rice, 1967, 1968a, b). In this concept, it is assumed that, in the vicinity of the crack tip, the potentially large stresses are relieved by plastic flow in a region whose size is much smaller than the crack length or any other characteristic geometric scale. It is further assumed that the plastic zone is engulfed all around by an elastic region which is dominated by the singular K-field. The success of the linear elastic analysis of quasi-static fracture problems, or as is usually called, the linear elastic fracture mechanics (LEFM), is virtually based on the SSY assumption. This is because when the SSY assumption is met, as it is in many engineering applications involving quasi-static fracture, the stress intensity factor K totally characterizes the stress and strain fields for the localized fracture process, and the energy release rate calculated from the K-field represents the actual energy release rate. The critical stress intensity factor criterion for (quasi-static) crack initiation is thus based on a strong physical ground.

However, the situation is physically different for propagating cracks. When a crack propagates, the crack tip plastic flow leaves a wake of residual plasticity behind. While the plastic effect may be confined to a small region almost everywhere around the crack tip, it will always extend far behind the tip along the two crack surfaces. As a result, SSY is not strictly applicable, and the stress intensity

factor loses its physical meaning, i.e., it is no longer strictly a measure of the energy release rate. Nonetheless, there are many engineering situations where the SSY concept may still apply, if it is extended to allow for the existence of plastic wakes along crack faces. Thus it is of great importance that we investigate the following questions: First, under the extended SSY conditions (i.e., when the K-field does dominate the crack tip surrounding area except near the crack surfaces), will the stress intensity factor still be the characterizing parameter for the localized fracture process? Second, if the answer to the first question is negative, will the stress intensity factor approximately characterize the fracture process? What are the major influences on the accuracy of the approximation? Finally, if the stress intensity factor is not related to the fracture process at all, what will be the replacing parameters? Obviously, in the search for answers to the above questions, analyses incorporating crack tip nonlinear and inelastic behaviors are necessary.

1.3 EXPERIMENTAL OBSERVATIONS

Concerns for the elastodynamic treatment of crack propagation phenonmena also arise because of experimental observations. Many discrepancies have been noticed, not only between experimental results and theoretical predictions or assumptions, but also among experimental results themselves. Pioneered by Post et al.(Post, 1954; and Wells and Post, 1958) on the measurement of stress field around a propagating crack, early experiments were able to show that observed crack terminal speeds are of the order of 0.5$\sim$0.8 of the Rayleigh wave speed, instead of the theoretically predicted Rayleigh wave speed itself (see Schardin, 1959; and Bowden, Brunton, Field and Heys, 1967). The validity of this is demonstrated by many later experiments. The emphasis here however, is on the measurement of the dynamic fracture toughness $K_{ID}(v)$. Due to the advent of better optical techniques, many experiments on fast crack propagation were conducted during the past few years. Unfortunately, the discoveries are not always encouraging. While experimen-

tal results by Kobayashi and Dally, 1977, 1980; Bilek, 1980; Kanazawa, Machida, Teramoto and Yoshinari, 1981; Brickstad, 1983; Rosakis, Duffy and Freund, 1984; and Zehnder and Rosakis, 1990a support the idea of a unique material dependent K_{ID} vs. v relationship, those by Kobayashi and Mall, 1978; Brickstad and Nilsson, 1980; Ravi-Chandar, 1982; Kalthoff, 1983; Ravi-Chandar and Knauss, 1987; and Takahashi and Arakawa, 1987 do not find such a uniqueness.

This uniqueness versus nonuniqueness question has become one of the current key issues of dynamic fracture mechanics. An point to note here is that, before we jump to any definite conclusions, we must be assured that all experimental results are intepreted adequately. Since almost all the experiments are conducted on thin plates of relatively small dimensions, and conditions of plane stress and K-dominance are assumed, care must be taken that the underlying assumptions for the experiments are not violated. This subject has recently been studied extensively by Krishnaswamy and Rosakis (1990a) and Krishnaswamy, Rosakis and Ravichandran (1990). Naturally the question of the existence of a plane stress K-dominant region will account for some of the observed discrepancies. However, the difference in the micromechanics of material decohesion should be responsible for many of the observed phenomena. As pointed out by Broberg (1968, 1971), a fracture process zone exists at the front of a crack tip, where material inhomogeneities such as microcracks and microvoids may nucleate, grow and coalesce. For different materials, the operative microfracture mechanism within the process zone will be different. Namely, for materials which behave ductilely at the crack tip, void growth and coalescence are predominant, whereas for materials which behave in a brittle manner, the growth and coalescence of microcracks will be dominant (see Broek, 1968; Ashby, 1979; Curry and Knott, 1980; and Ravi-Chandar and Knauss, 1984). A closer examination of the experiments tells us that most of the experiments in favor of the uniqueness idea are conducted on materials such as metals which fail in a locally ductile manner, while those against it are usually conducted on more

brittle materials such as polymers.

Advances in the understanding of crack propagation in materials which fail in a locally ductile manner have been obtained through some recent numerical studies. In a combined theoretical and numerical study of Mode III elastic-plastic crack propagation problems, Freund and Douglas (1982) used a critical plastic strain criterion (McClintock, 1956, 1958; and McClintock and Irwin, 1964) and obtained theoretical K vs. v curves which resemble those from experiments showing unique $K_{ID}(v)$ relations. In a separate investigation on the problem of Mode I elastic-plastic crack propagation under plane strain, Lam and Freund (1985) used a different fracture criterion, i.e., the critical crack opening angle criterion (Rice and Sorensen, 1978; and Rice, Drugan and Sham, 1980), and again obtained theoretical K vs. v curves with the same qualitative tendency. It should be noted here that these criteria are mostly suited for metals that fail in a locally ductile manner.

Although above comparisons are made between theoretically generated K *vs.* v curves for Mode III (anti-plane strain) and Mode I plane strain, and experimental results which are more closely related to Mode I plane stress, they do strongly indicate that it is indeed possible to explain experimental observations in terms of material local behaviors at the crack tip.

1.4 OVERVIEW OF CURRENT STUDY

The need for the study of nonlinear and inelastic behaviors at the crack tip now becomes apparent. It comes from the fact that so much effort has been spent on the elastodynamic treatment of crack propagation problems that more fundamental analyses are necessary to back it up. In addition, it is motivated from the expectation that a better understanding of the crack propagation phenomena can only be gained through the use of more realistic analyses.

Thus far substantial work on elastic-plastic analyses of crack propagation prob-

lems have concentrated on anti-plane strain and plane strain cases (see reviews in later chapters), from which we see steady effort has been made by the scientific community in order to understand the onset of ductile crack growth, the slow stable crack extension and the dynamic crack propagation from the point of view of material elastic-plastic behaviors at the crack tip. It is fair to say that quite a good understanding has been obtained through this effort, although many issues do remain open.

On the other hand, however, plane stress elastic-plastic analyses for growing cracks are still in a much less developed state, despite the fact that many experiments of this kind are performed on relatively thin plates and results are interpreted under plane stress conditions. This may be partly because the field equations for elastic-plastic studies in plane stress are somewhat more involved, hence analyses become more complicated, and perhaps partly because of the doubt on the practical importance of plane stress analyses near the crack edge where three-dimensional effects are present.

Nonetheless, we believe, our undertstanding of elastic-plastic crack tip fields would not be complete if the equivalent plane stress or generalized plane stress cases were not investigated, again, due to the fact that many engineering structures are made of thin sheets, and that almost all experiments are performed on thin plate specimens, of which many assume plane stress conditions. Furthermore, because of the complicated three-dimensional character of the stress and deformation fields near the crack edge, plane stress solutions cannot be ruled out in favor of plane strain counterparts, until a complete three-dimensional picture is clearly obtained. On the other hand, although some advances have been made in three-dimensional analyses(see, for example, Rosakis, Ravi-Chandar and Rajapakse, 1988), which are usually impossible to cope with analytically and are very costly to perform numerically, conclusive results await the emergence of accurate two-dimensional analyses and/or accurate three-dimensional experimental measurements, at least in

the sense of numerical calibrations of computer codes.

As we mentioned above, analytical and numerical investigations of dynamic crack propagation phenomena in elastic-plastic solids under plane stress conditions are rare. For example, analytical solutions are usually valid only at the crack tip, called the asymptotic solutions, or valid along the prospectively crack line, called the crack-line solutions. Yet due to the fact that analytical solutions often involve complicated mathematics and sometimes many simplifying assumptions, numerical solutions are indispensible for checking the correctness of analytical solutions. Besides, in situations where analytical solutions are not available or when certain key parameters characterizing crack tip fields are not obtainable through local analyses, full field numerical computations are extremely appealing.

In this thesis we present the results of a detailed finite element investigation of the problem of dynamic crack propagation in elastic-plastic solids under Mode I plane stress and steady state conditions. Investigations were conducted under small-scale yielding conditions with and without elastic far-field K-dominance (see chapter 7). The materials are assumed to obey the J_2 flow theory of plasticity and its associated flow rule. The ratio of the crack tip plastic zone size to the size of the element nearest to the crack tip is of the order of 1.6×10^4. This high spatial resolution of the near-tip mesh was chosen to allow for the investigation of the asymptotic structure of fields very near the propagating crack tip. Results are reported for a wide range of Mach numbers (the ratio of crack speed to material elastic shear wave speed), and are compared with available analytical and numerical solutions, and with experimental measurements.

In Chapter 2 we describe the Eulerian-type finite element formulation of the problem and give details of our finite element mesh design and specifications. A stress integration algorithm is proposed, which improves the popular Tangent Predictor-Radial Return algorithm in that the calculated stress state satisfies au-

tomatically, for elastic-perfectly plastic and linear hardening materials, the yield condition at the end of a strain increment. Moreover, the existing solution procedures implementing the stress integration algorithms are modified to eliminate the occurrence of negative plastic flow, and to avoid incorrectly treating elastic unloading as plastic flow. At the end of this chapter, we discuss how the finite element results are to be post-processed and presented in the current study.

An important aspect of fracture mechanics research is the investigation of the asymptotic structure of crack tip local fields, and the identification of controlling parameters which hopefully reflect the gross behavior of the crack tip fracture process zone and are to be used in fracture criteria. Hence Chapters 3, 4 and 5 are concentrated on near-tip stress and deformation fields for elastic-perfectly plastic materials, for isotropic linear hardening materials and for isotropic power-law hardening materials, respectively. Detailed discussions will be performed concerning comparisons with available crack tip asymptotic solutions.

In Chapter 6, we study fracture criteria for elastic-plastic solids. Theoretical K_{Ic}^{d} (the dynamic *plane stress* fracture toughness) versus v (the crack propagation speed) curves are generated based on a local fracture criterion near the crack tip and are compared, with good agreement, to experimental measurements corresponding to dynamic crack growth in thin 4340 steel plates, whose material characteristics match those of the calculations.

In Chapter 7 we investigate the effects of non-K-dominance on the near-tip elastic-plastic fields and on K_{Ic}^{d} versus v relations. This study would substantiate the findings of previous chapters and is revelant to the subject of proper interpretation of experimental results since under laboratory conditions K-dominance may not always exist.

Finally Chapter 8 summarizes the main findings of the current study and concludes with comments and suggestions.

CHAPTER 2

NUMERICAL PROCEDURE

2.1 INTRODUCTION

Two types of finite element formulations are usually used in the investigations of crack growth phenomena, especially in circumstances where crack tip stress and deformation fields and fracture criteria are of main concern.

In the first formulation, the crack tip advances along the prospective crack line in a stationary finite element mesh. In order to govern the procedure, it is necessary to assume a fracture criterion *a priori*. If the crack tip is made to advance by untying the crack tip finite element node, the procedure is called a nodal release procedure (see Andersson, 1973; de Koning, 1977; and Sorensen, 1978, 1979). If, on the other hand, it is done by deforming the crack tip elements such that the crack tip shifts ahead, it is called a moving element procedure (see, for example, Atluri and Nishioka, 1985).

Nodal release procedures are commonly used for problems involving stable crack growths in elastic-plastic solids. For example, Andersson (1973) and de Koning (1977) devised such procedures for quasi-static crack growth in Mode I plane stress by assuming a constant crack tip opening angle criterion, whereas Sorensen (1978, 1979) applied such procedures for stable crack growth in Mode III using a critical plastic strain criterion, and in Mode I plane strain using a critical stress intensity factor criterion.

In the second formulation, which is of an Eulerian type, the whole finite element mesh translates with the crack tip, or relatively speaking, materials convect through the mesh downstreamwise. However, in order to compensate for the loss of information about previous crack growth, a steady state condition must be assumed and the boundary conditions must be hypothesized. This formulation was originated by Dean and Hutchinson (1980) for steady state quasi-static crack growth in Mode III and in Mode I plane strain, and was adopted later by Freund and Douglas (1982) for steady state dynamic crack propagation in Mode III and by Lam and Freund (1985) for steady state dynamic crack propagation in Mode I plane strain.

One of the shortcomings of the Eulerian-type formulation is that it can only be used in problems involving steady state crack growth and where conditions such as small-scale yielding can be assumed. Yet compared with the advancing tip formulation, it has many advantages. First of all, the Eulerian formulation does not need a fracture criterion assumed *a priori*, which makes the formulation more flexible in this sense. Secondly, due to mathematical difficulties, analytical crack tip stress and deformation fields are usually obtained asymptotically under steady state conditions. Hence, direct comparisons between those two types of solutions are possible. Thirdly, in the advancing tip formulation, the crack tip shifts ahead in a discrete manner, according to an experimental input or a process devised artificially. This may cause fictitious oscillations in numerical results, and more importantly, inconsistencies may arise in the sense that different tip-shifting procedures may yield different results. This possibility is especially true for dynamic crack propagation where wave motions are inevitable. Finally, due to a steady state-peculiar solution procedure used in the Eulerian formulation, which will be discussed later, solutions can be obtained for a group of elastic-plastic materials once and for all, including elastic and elastic-perfectly plastic materials as special cases.

The Eulerian-type finite element formulation is employed in the current study, which will enable us to investigate the steady state crack tip stress and deformation

fields as well as fracture criteria at the same time. The numerical formulation of this study and some related issues are presented in detail in the following sections.

2.2 GOVERNING EQUATIONS

In this section, the governing equations are presented for dynamic crack propagation in elastic-plastic solids under Mode I plane stress, steady state, and small-scale yielding conditions. All field quantities will be referred to a Cartesian rectangular coordinate system and its associated polar coordinate system as shown in Fig. 1.1.1. The origin of the coordinate system is fixed at, and translates with the crack tip (hence the name Eulerian-type for the finite element formulation to be discussed in section 2.3).

For convenience, it is assumed hereafter, unless otherwise stated, that all physical quantities are denoted by hatted symbols. The usual indicial notation and its associated conventions will be used. The following nondimensional quantities are then introduced:

$$\left.\begin{aligned} \underline{x} &= \underline{\hat{x}}/(K/\sigma_0)^2, \\ \underline{u} &= \underline{\hat{u}}/(K^2/E\sigma_0), \\ \underline{\sigma} &= \underline{\hat{\sigma}}/\sigma_0, \\ \underline{\varepsilon} &= \underline{\hat{\varepsilon}}/\varepsilon_0, \\ m &= v/c_s, \end{aligned}\right\} \tag{2.2.1}$$

where $\underline{\hat{x}}$, $\underline{\hat{u}}$, $\underline{\hat{\sigma}}$, $\underline{\hat{\varepsilon}}$ and v are respectively the position vector, the displacement vector, the stress tensor, the strain tensor, and the crack propagation velocity, K is the far-field dynamic stress intensity factor specified by the small-scale yielding conditions, σ_0 is the initial yield stress in tension, m is called the Mach number, E is the Young's modulus, $\varepsilon_0 = \sigma_0/E$ is the initial yield strain in tension, $c_s = \sqrt{\mu/\rho}$ is the elastic shear wave speed, $\mu = E/2(1+\nu)$ is the elastic shear modulus, ν is the Poisson ratio, and ρ is the mass density of the material.

Under steady state conditions, it is required that the crack propagates at a constant speed, and that the material time derivative or the time rate of any field quantity, say q, is replaced by the spatial gradient $-v\partial q/\partial \hat{x}_1$. In light of this, the field governing equations for crack growth in homogeneous isotropic elastic-plastic solids can be presented in normalized form as follows.

The equation of motion can be written as

$$\nabla \cdot \underline{\sigma} = \frac{m^2}{2(1+\nu)} \frac{\partial^2 \underline{u}}{\partial x_1^2}, \tag{2.2.2a}$$

$$\underline{\sigma}^{\top} = \underline{\sigma}, \tag{2.2.2b}$$

where $\nabla = \underline{e}_i \frac{\partial}{\partial x_i}$, with $\underline{e}_i$ being the unit base vector of the Cartesian coordinate system, and the superscript "$\top$" denotes the transpose of a vector or a tensor. The infinitesimal strain-displacement relation can be expressed as

$$\underline{\varepsilon} = \frac{1}{2}[\nabla \underline{u} + (\nabla \underline{u})^{\top}]. \tag{2.2.2c}$$

For an isotropic homogeneous material obeying the J_2 flow theory of plasticity and the associated flow rule, the Huber-von Mises yield criterion

$$F(\underline{\sigma}, \varepsilon_e^p) \equiv J_2(\underline{S}) - \frac{1}{3}\sigma^2(\varepsilon_e^p) = 0, \tag{2.2.3a}$$

is assumed, where $\underline{S}$ and J_2 are respectively the deviatoric stress tensor and its second invariant, defined respectively by

$$S_{ij} = \sigma_{ij} - \frac{\sigma_{kk}}{3}\delta_{ij}, \tag{2.2.3b}$$

$$J_2 = \frac{1}{2}\underline{S} \cdot \underline{S}, \tag{2.2.3c}$$

σ is the current yield stress in tension and is usually called the flow stress, and ε_e^p is the effective plastic strain given by

$$\varepsilon_e^p = \int \sqrt{\frac{2}{3}\dot{\underline{\varepsilon}}^p \cdot \dot{\underline{\varepsilon}}^p}\ dt, \tag{2.2.3d}$$

where $\dot{\underline{\varepsilon}}^p$ is the plastic strain rate tensor. The dependence of the flow stress σ on ε_e^p is called the hardening rule, which describes the hardening behavior of the material. If σ is a constant, then it models an elastic-perfectly plastic solid.

From the above relations, the associated flow rule can be written as

$$\dot{\underline{\varepsilon}}^p = \dot{\lambda}\underline{S}, \tag{2.2.4}$$

where $\dot{\lambda}$ is called the plastic strain rate proportionality coefficient, or simply the plastic multiplier or the flow factor, and it takes zero value for elastic stress states and is nonnegative for currently yielded stress states.

Now the Prandtl-Reuss strain rate decomposition assumption states that

$$\dot{\underline{\varepsilon}} = \dot{\underline{\varepsilon}}^e + \dot{\underline{\varepsilon}}^p, \tag{2.2.5a}$$

with the elastic strain rate tensor $\dot{\underline{\varepsilon}}^e$ related to the stress rate tensor $\dot{\underline{\sigma}}$ through

$$\dot{\underline{\sigma}} = \underline{C}\ \dot{\underline{\varepsilon}}^e, \tag{2.2.5b}$$

where $\underline{C}$, normalized by the Young's modulus E, is the fourth-order elasticity modulus tensor of the solid, with the usual primary and secondary symmetries.

Generally, the set of nonlinear elastic-plastic equations (2.2.3-5) can be linearized to yield the classic small strain incremental stress-strain relationship (see, for example, Deng and Rosakis, 1990)

$$\dot{\underline{\sigma}} = \underline{C}^{ep}\dot{\underline{\varepsilon}}, \tag{2.2.6a}$$

where $\underline{C}^{ep}$ is the fourth-order elastic-plastic tangent stiffness tensor defined by

$$\underline{C}^{ep} = \underline{C} - \frac{(\underline{C}\ \underline{S}) \otimes (\underline{C}\ \underline{S})}{A + \underline{S} \cdot (\underline{C}\ \underline{S})}, \tag{2.2.6b}$$

where "$\otimes$" is the tensor outer product operator, and A is a material parameter given by

$$A = \frac{2}{3}\sigma\frac{d\sigma}{d\varepsilon_e^p}\sqrt{\frac{2}{3}\underline{S} \cdot \underline{S}}. \tag{2.2.6c}$$

If (2.2.3a) is used, it is seen that

$$A = \frac{4}{9}\sigma^2 \frac{d\sigma}{d\varepsilon_e^p}. \tag{2.2.6d}$$

Note that the derivative $\frac{d\sigma}{d\varepsilon_e^p}$ depends on the specific material model employed.

In this study, we consider three groups of material models, namely elastic-perfectly plastic materials, linear hardening materials, and power-law hardening materials. The materials are characterized by their uniaxial stress-strain relations, which are extended to multiaxial stress states through the use of the flow stress, the effective plastic strain, and the effective stress σ_e which is defined as

$$\sigma_e = \sqrt{\frac{3}{2}\underline{S}\cdot\underline{S}} = \sqrt{3J_2}. \tag{2.2.7}$$

The elastic-perfectly plastic model works for very low and nonhardening materials. Its uniaxial stress-strain relation is expressed in normalized form by

$$\sigma = \begin{cases} \varepsilon, & \text{if } \sigma_e \leq 1; \\ 1, & \text{if } \sigma_e \geq 1. \end{cases} \tag{2.2.8a}$$

The uniaxial stress-strain relation for strain hardening (or equivalently work hardening for J_2 flow theory (see Bland, 1956) solids are more complicated, but can generally be very well-approximated by means of polygonal lines (see Phillips, 1951), the simplest of which is described by the linear hardening model. Portrayed by two straight lines, the σ-ε curve is expressed as

$$\sigma = \begin{cases} \varepsilon, & \text{if } \sigma_e \leq 1; \\ 1 + \frac{\alpha}{(1-\alpha)}\varepsilon_e^p, & \text{if } \sigma_e \geq 1, \end{cases} \tag{2.2.8b}$$

where ε_e^p is, in the uniaxial case, the same as the plastic strain defined by

$$\varepsilon_e^p = \varepsilon - \sigma,$$

α is the hardening parameter of this bilinear material such that $0 \leq \alpha \leq 1$ and it is defined by

$$\alpha = \frac{E_t}{E},$$

E_t being the slope of the hardening line. It is noted that $\alpha = 1$ and 0 correspond to the elastic and elastic-perfectly plastic cases respectively.

A more realistic model for hardening materials was first proposed by Ludwig (1909) and later modified by Ramberg and Osgood (1943), which is widely known as the power-law hardening material model and is supported by many experiments on metals. In this model, the uniaxial stress-strain relation is described as

$$\begin{cases} \sigma = \varepsilon, & \text{if } \sigma_e \leq 1; \\ \varepsilon_e^p = \sigma^n - \sigma, & \text{if } \sigma_e \geq 1, \end{cases} \tag{2.2.8c}$$

where the exponent n is the hardening parameter such that $0 \leq n < +\infty$. When n is set to zero it models elastic materials, and at the limit $n \to \infty$, the elastic-perfectly plastic case is recovered.

Under small-scale yielding conditions, the crack tip far-field for dynamic crack propagation is characterized uniquely by the dominant singular elastic K-field. The explicit two-dimensional field variations are given, for example, by Freund (1976) for Mode I plane strain. As first noted by Bishop (1952), dynamic elastic solutions for plane strain always have counterparts in plane stress. Hence without any difficulty, we list below the normalized singular stress and displacement distributions:

$$\sigma_{11} = B[(1 + 2\alpha_l^2 - \alpha_s^2)\frac{cos(\theta_l/2)}{\sqrt{r_l}} - \frac{4\alpha_l\alpha_s}{1+\alpha_s^2}\frac{cos(\theta_s/2)}{\sqrt{r_s}}], \tag{2.2.9a}$$

$$\sigma_{22} = B[-(1 + \alpha_s^2)\frac{cos(\theta_l/2)}{\sqrt{r_l}} + \frac{4\alpha_l\alpha_s}{1+\alpha_s^2}\frac{cos(\theta_s/2)}{\sqrt{r_s}}], \tag{2.2.9b}$$

$$\sigma_{12} = 2\alpha_l B[\frac{sin(\theta_l/2)}{\sqrt{r_l}} - \frac{sin(\theta_s/2)}{\sqrt{r_s}}], \tag{2.2.9c}$$

$$u_1 = 4(1+\nu)B[\sqrt{r_l}cos(\theta_l/2) - \frac{2\alpha_l\alpha_s}{1+\alpha_s^2}\sqrt{r_s}cos(\theta_s/2)], \tag{2.2.9d}$$

$$u_2 = 4(1+\nu)\alpha_l B[-\sqrt{r_l}sin(\theta_l/2) + \frac{2}{1+\alpha_s^2}\sqrt{r_s}sin(\theta_s/2)], \tag{2.2.9e}$$

where

$$B = (1 + \alpha_s^2)/D\sqrt{2\pi},$$

$$D = 4\alpha_l\alpha_s - (1+\alpha_s^2)^2,$$

$$\alpha_l = \sqrt{1-(v/c_l)^2} = \sqrt{1-(c_s/c_l)^2 m^2},$$

$$\alpha_s = \sqrt{1-(v/c_s)^2} = \sqrt{1-m^2},$$

$$r_l e^{i\theta_l} = x_1 + i\alpha_l x_2,$$

$$r_s e^{i\theta_s} = x_1 + i\alpha_s x_2,$$

and c_l being the elastic longitudinal wave speed. Note here that the only difference between the elastic solutions for plane strain and for plane stress lies in the value of the ratio $(c_s/c_l)^2$, which is expressed in terms of the Poisson ratio as

$$(\frac{c_s}{c_l})^2 = \frac{1-\hat{\nu}}{2}, \tag{2.2.10a}$$

where

$$\hat{\nu} = \begin{cases} \nu, & \text{for plane stress;} \\ \nu/(1-\nu), & \text{for plane strain.} \end{cases} \tag{2.2.10b}$$

For the purpose of later computations, we give the displacement spatial deritives with respect to x_1 as follows:

$$\frac{\partial u_1}{\partial x_1} = 2(1+\nu)B[\frac{cos(\theta_l/2)}{\sqrt{r_l}} - \frac{2\alpha_l\alpha_s}{1+\alpha_s^2}\frac{cos(\theta_s/2)}{\sqrt{r_s}}], \tag{2.2.11a}$$

$$\frac{\partial u_2}{\partial x_1} = 2(1+\nu)B[\alpha_l\frac{sin(\theta_l/2)}{\sqrt{r_l}} - \frac{2\alpha_l}{1+\alpha_s^2}\frac{sin(\theta_s/2)}{\sqrt{r_s}}]. \tag{2.2.11b}$$

Finally, it is reminded that the actual equations for plane stress problems must be simplified in conjuction with the following conditions

$$\sigma_{3i} = 0 \qquad (i = 1,2,3), \tag{2.2.12}$$

from which the out-of-plane strain ε_{33} can be computed. For clarity of discussion, those derivations are omitted here.

2.3 FINITE ELEMENT FORMULATION

The mechanics problem of a crack advancing in a plate under small-scale yielding conditions can be formulated with the help of the boundary layer concept (Rice, 1967, 1968a, b). It is argued that mathematically the solution for the above problem can be obtained by treating a new problem, namely that of a semi-infinite crack propagating in an infinite plate, for which the stress state described by Eq.(2.2.9) is achieved as $r \to \infty$. Since numerically it is difficult to model an infinite region, usually a region of finite size is instead considered. As pointed out by Dean (1983), a size larger than ten times that of the crack tip active plastic zone will suffice to produce reasonable results. In fact, one can study directly a region which just encompasses the crack tip and its active plastic zone by utilizing a modified variational principle (Hilton and Hutchinson, 1971; and Sham, 1983), which, while it saves some degrees-of-freedom for a finite element computation, makes the formulation of the problem much more complicated.

Eulerian Formulation

Now suppose the region under consideration occupies a domain V with boundary B, which is composed of two sets of sub-boundaries: B_t where traction is specified and B_u where displacement is prescribed. Assume further that $\delta\underline{u}$ is the virtual displacement vector, and that $\delta\underline{\varepsilon}$ is the associated infinitesimal virtual strain tensor given by

$$\delta\underline{\varepsilon} = \frac{1}{2}[\nabla\delta\underline{u} + (\nabla\delta\underline{u})^{\top}].$$

From the principle of virtual work, we have

$$\int_V \delta\underline{\varepsilon} \cdot \underline{\sigma}\ dV = \int_V \delta\underline{u}^{\top} \cdot [-\frac{m^2}{2(1+\nu)}\frac{\partial^2\underline{u}}{\partial x_1^2}]\ dV + \int_{B_t} \delta\underline{u}^{\top} \cdot \underline{t}\ dB_t, \qquad (2.3.1a)$$

where $\underline{t}$ is the boundary traction vector and is related to the singular stress fields Eq.(2.2.9) through

$$\underline{t} = \underline{\sigma}\ \underline{n},$$

$\underline{n}$ being the outward unit normal vector of the boundary surface.

When the divergence theorem is applied to the first term on the right-hand side of Eq.(2.3.1a), the weak form of Eq.(2.3.1a) is obtained as

$$\int_V [\delta\underline{\varepsilon} \cdot \underline{\sigma} - \frac{m^2}{2(1+\nu)} \frac{\partial \delta \underline{u}^\top}{\partial x_1} \cdot \frac{\partial \underline{u}}{\partial x_1}] \; dV = \int_{B_t} \delta \underline{u}^\top \cdot [\underline{t} - \frac{n_1 m^2}{2(1+\nu)} \frac{\partial \underline{u}}{\partial x_1}] \; dB_t, \quad (2.3.1b)$$

where n_1 is the first component of $\underline{n}$. Note here that the admissibility condition for the virtual displacement, i.e., $\delta \underline{u} = 0$ on B_u, has been used in deriving (2.3.1b). This weak form is the basis of our finite element formulation.

From the decomposition assumption in Eq.(2.2.5a) and the Hooke's law expressed in Eq.(2.2.5b), it is true that

$$\underline{\varepsilon} = \underline{\varepsilon}^e + \underline{\varepsilon}^p, \text{ and } \underline{\sigma} = \underline{C} \; \underline{\varepsilon}^e, \quad (2.3.2a)$$

Hence we obtain

$$\underline{\sigma} = \underline{C} \; (\underline{\varepsilon} - \underline{\varepsilon}^p). \quad (2.3.2b)$$

Substitution of Eq.(2.3.2b) into Eq.(2.3.1b) readily produces

$$\int_V [\delta\underline{\varepsilon} \cdot \underline{C} \; \underline{\varepsilon} - \frac{m^2}{2(1+\nu)} \frac{\partial \delta \underline{u}^\top}{\partial x_1} \cdot \frac{\partial \underline{u}}{\partial x_1}] \; dV =$$

$$\int_V \delta\underline{\varepsilon} \cdot \underline{C} \; \underline{\varepsilon}^p \; dV + \int_{B_t} \delta \underline{u}^\top \cdot [\underline{t} - \frac{n_1 m^2}{2(1+\nu)} \frac{\partial \underline{u}}{\partial x_1}] \; dB_t, \quad (2.3.3)$$

After performing the usual finite element discretization procedure, a system of nonlinear algebraic equations can be derived as

$$(\underline{K}_s + \underline{K}_d) \; \underline{U} = \underline{F}_t + \underline{F}_u + \underline{F}_d + \underline{F}_p, \quad (2.3.4)$$

where $\underline{K}_s$ and $\underline{K}_d$ are respectively the global stationary, elastic stiffness matrix of the finite element system, and the contribution due to dynamic or inertia effects, $\underline{U}$ is the unknown global nodal point displacement vector, $\underline{F}_t$ and $\underline{F}_u$ are respectively the global force vector due to specified boundary tractions and boundary displacements, which collectively form the stationary, elastic force vector, and $\underline{F}_d$ and $\underline{F}_p$ are respectively the contributions to the global force vector due to dynamic and plastic effects. Note that the nonlinearity of the system of equations comes only from the last force vector which is due to the accumulated plastic strains. All those global vectors and matrices are assembled from their counterparts for all the elements according to the standard assembly procedure. If we assume for a generic element that it occupies a domain V^e whose boundary B^e is consisted of the traction boundary B_t^e and the displacement boundary B_u^e, where superscript "e" denotes a quantity for the element, then the aforementioned counterparts for this element will be

$$\underline{K}_s^e = \int_{V^e} \underline{B}^\top \underline{C}\ \underline{B}\ dV^e, \tag{2.3.5a}$$

$$\underline{K}_d^e = \int_{V^e} -\frac{m^2}{2(1+\nu)} \frac{\partial \underline{N}^\top}{\partial x_1} \frac{\partial \underline{N}}{\partial x_1}\ dV^e, \tag{2.3.5b}$$

$$\underline{F}_t^e = \int_{B_t^e} \underline{N}^\top \underline{t}\ dB_t^e, \tag{2.3.5c}$$

$$\underline{F}_u^e = -(\underline{K}_s^e + \underline{K}_d^e)\ \underline{U}_0^e, \tag{2.3.5d}$$

$$\underline{F}_d^e = \int_{B_t^e} -\frac{n_1 m^2}{2(1+\nu)} \underline{N}^\top \frac{\partial \underline{u}}{\partial x_1}\ dB_t^e, \tag{2.3.5e}$$

$$\underline{F}_p^e = \int_{V^e} \underline{B}^\top \underline{C}\ \underline{\varepsilon}^p\ dV^e, \tag{2.3.5f}$$

where $\underline{N}$ is the usual finite element shape function matrix, $\underline{B}$ is the associated geometric matrix, $\underline{U}_0^e$ is a vector composed of zeros for degrees-of-freedom with unknown nodal displacement values, and specified values for degrees-of-freedom with prescribed nodal displacements. All the integrals are calculated numerically by means of the Gauss Quadrature, i.e., they are approximated by summations over

Gauss integration points of their values at each Gauss point multiplied by a Gauss weighting value.

The system of equations (2.3.4) is solved for the unknown nodal displacement vector $\underline{U}$ using the solution procedure first proposed by Dean and Hutchinson (1980), which is peculiar to the steady state Eulerian formulation. Since the force vector of the system in Eq.(2.3.4) is unknown *a priori* due to the presence of the unknown plastic strains, it is solved essentially by initializing and updating $\underline{\varepsilon}^p$ and hence $\underline{F}_p$, and by iterating through Eq.(2.3.4). For completeness, the solution procedure is described as follows.

We choose a material hardening model, say the linear hardening (or pow-law hardening) model, start with a value for the hardening parameter α (or n) which corresponds to the elastic case, i.e., $\alpha = 1$ (or $n = 1$). This renders $\underline{\varepsilon}^p$ and hence $\underline{F}_p$ zero, which makes (2.3.4) solvable immediately and a solution for $\underline{U}$ can be obtained.

We then gradually change the value of the hardening parameter such that a material with less strain hardening is under consideration, i.e., we gradually decrease α (or increase n). For each such new material, the solution for the previous material is used as the initial guess, and iteration is performed until a certain convergence criterion is met.

At each iteration step, the displacement solution for the previous step is used to obtain the strain distribution for the current iteration. Under steady state conditions, since the material time derivative for any field quantity is transferred into the negative spatial derivative of this quantity with respect to x_1 and multiplied by the crack velocity v, then the history of this field quantity for any particular material particle is stored instantaneously along a horizontal line from the crack front boundary to the back boundary. To this end, strain history, or more precisely the strain rate distribution, can be calculated from the strain distribution computed

previously. Hence stresses and plastic strains can be obtained by integrating the incremental constitutive law in Eqs.(2.2.3) through (2.2.5) from the leading edge of the finite element mesh along horizatal lines downstreamwise.

Mesh Specifications

It is appropriate at this moment to describe briefly our finite element mesh design and its specifications, before further discussions about stress state determination and iteration procedures are mentioned. Shown in Fig. 2.3.1 in our normalized coordinates is a schematic of the finite element meshes used in the present computation. The domain of interest is modelled by a rectangle, where the middle point of its bottom boundary coincides with the current crack tip position. The crack surface lies along the bottom from the lower left corner to the crack tip, and accordingly the line from the crack tip to the lower right corner represents the symmetry plane. The length of the domain is twice its height which, with the normalization for the coordinates, is 4.5, which is about 15 times larger than the active plastic zone size.

The rectangular domain is discretized by a network of horizontal and vertical lines, whose intervals decrease rapidly towards the bottom line and the center vertical line, resulting in increasingly small elements near the crack tip. The divided areas are simply represented by four-noded isoparametric rectangular elements with 2×2 Gauss integration points, although it is noted in plane strain that it is best to subdivide the quadrilateral element into four triangular ones and then to condense out the degrees-of-freedom corresponding to the inner element node (Nagtegaal, Parks, and Rice, 1974), in order to avoid element stiffening or locking (see Malkus and Hughes, 1978) due to material incompressibility caused by large plastic strains. This type of finite element meshes gives rise to horizontal lines composed of Gauss quadrature points, along which stress integrations are to be performed.

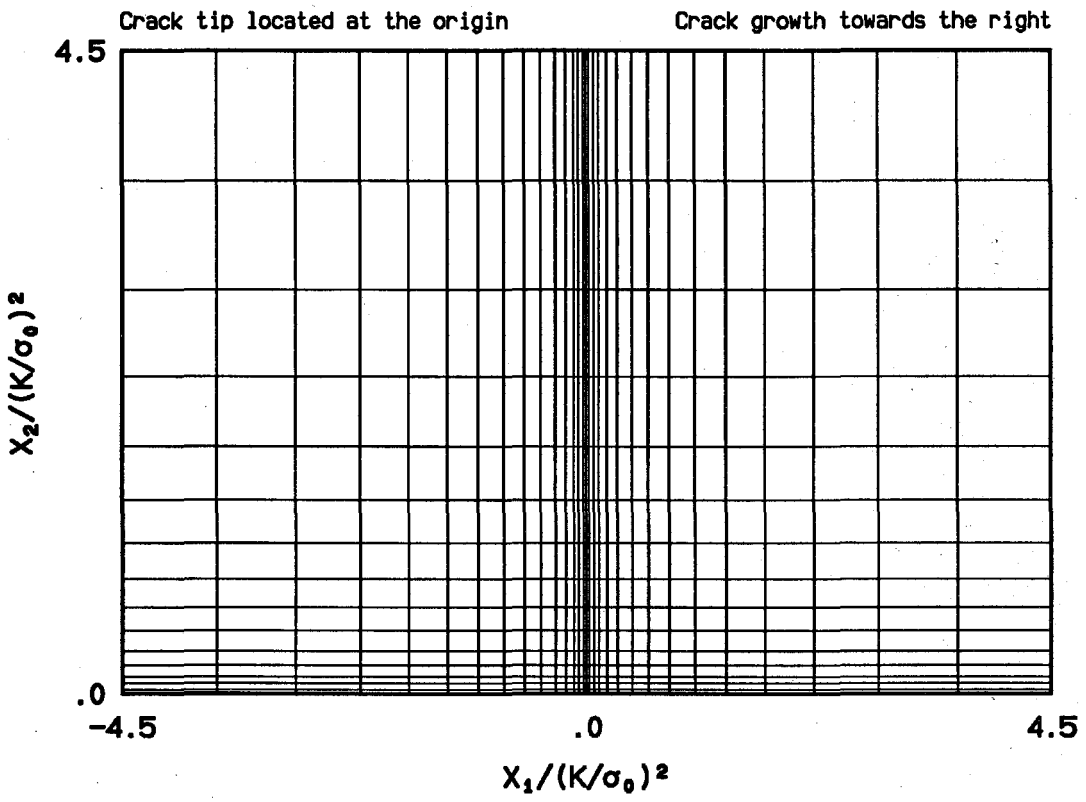

FIGURE 2.3.1 A coarse representation of the finite element mesh used in the present computation.

Two meshes of high resolutions are used in our computation. They are different in that the numbers of the horizontal and vertical lines of the mesh networks and the variations of the intervals between those lines are different. In the finer mesh, the network of lines results in 4050 elements with 4186 nodes, and the ratio of the plastic zone size to that of the smallest near-tip element is on the order of 1.6×10^4. In the slightly coarser mesh, there are 1800 elements, and the plastic zone size is about 0.8×10^4 times the size of the smallest near-tip element. Comparisons between numerical results obtained from those two meshes demontrate very good agreement, which will be discussed in later chapters.

The boundary conditions are prescribed in accordance with the small-scale yielding assumption. At the front and the top boundaries, the far-field displacement

distribution in Eq.(2.2.9d, e) are specified, whereas at the back, where displacements are altered to a large extent due to the existence of residual plasticity in the wake, traction conditions corresponding to the stress field in Eq.(2.2.9a, b, c) are applied, with necessary updating near the plastic wake. And as usual, the traction-free condition and the symmetry condition are used respectively at the bottom before and behind the crack tip.

Stress State Determination

For displacement-based finite element formulations, which is the case in the current study, stresses are calculated by integrating Eq.(2.2.6a) numerically, along a path in the strain space. It should be realized that, due to the discretization process involved in a finite element computation, strain rates can not be obtained exactly. Rather, they are approximated by finite strain increments.

In order to choose an appropriate algorithm for the integration of stresses, or as is usually said for the determination of stress state, the following factors should be considered. From the viewpoint of accuracy and convergence of numerical solutions, we tend to use small time steps and fine element meshes, in the hope of better following the true strain history. The fine mesh requirement is particularly important in our case where, due to the use of the Eulerian formulation, the time history of any field quantity is converted into a spatial variation, which is stored along horizontal lines parallel to the direction of crack propagation. On the other hand, cost considerations force us to do just the opposite. In order to compromise in both ways, we have to find an efficient as well as accurate stress state determination algorithm.

There are several algorithms at our disposal, such as the Radial Return method (Wilkins, 1964),the Tangent Stiffness method (Marcal, 1965), which is commonly combined with a radial return at the end of an increment, and is accordingly called

the Tangent Predictor-Radial Return method (see Schreyer, Kulak, Kramer, 1979), and the Secant Stiffness method (Rice and Tracey, 1973; and Tracey, 1976).

The Secant Stiffness method is attractive, in that the calculated stress state at the end of a strain increment satisfies automatically the yield condition. However, when it is applied to hardening materials (see Tracey, 1976), an assumption regarding the slope of the uniaxial stress-plastic strain curve, $\frac{d\sigma}{d\varepsilon_e^p}$, must be made, irrespective of the actual material behavior. For example, for linear hardening materials, the slope is a constant, while the assumed or calculated value varies.

The Tangent Stiffness method, or its modified version, the Tangent Predictor-Radial Return method, are the easiest to implement in plane stress. The disadvantage is that, at the end of an increment, the calculated stress usually does not lie on the yield surface when it is currently yielded. Rather, a radial return to the yield surface must be performed to avoid greater error accumulations in the future.

In order to achieve the fine points of the above two methods, the Tangent Predictor-Radial Return method is adopted in this study, but with proper modifications. Note that the method is based on the linearized stress-strain rate relationship in Eq.(2.2.6a), which is obtained through the differential form of the yield condition in Eq.(2.2.3a), or the consistency condition as it is usually called (see, for example, Deng and Rosakis, 1990). Modifications are obtained by improving the consistency condition when the strain increments, and hence the stress increments, are not infinitesimal. The detail is presented in the following, with rates replaced by finite increments. For convenience, the derivations are obtained in terms of deviatoric stress and strain tensors, and under general three-dimensional conditions.

Without loss of generality, consider a currently yielded stress state $\underline{\sigma}$, and a strain increment $\Delta\underline{\varepsilon}$ which is in a plastic path. Then by definition, we have

$$\frac{1}{2}\underline{S}\cdot\underline{S} = \frac{1}{3}\sigma^2(\varepsilon_e^p), \qquad (2.3.6a)$$

where the deviatoric stress tensor $\underline{S}$ is defined in Eq.(2.2.3b). The exact consistency condition for continued yielding for a finite stress increment, which is the yield condition at the end of the increment, can be written as

$$\frac{1}{2}(\underline{S}+\Delta\underline{S})\cdot(\underline{S}+\Delta\underline{S})=\frac{1}{3}\sigma^2(\varepsilon_e^p+\Delta\varepsilon_e^p). \tag{2.3.6b}$$

The deviatoric stress increment tensor $\Delta\underline{S}$ is calculated through the elastic response of the material

$$\Delta\underline{S}=2\mu(\Delta\underline{e}-\Delta\underline{e}^p), \tag{2.3.7a}$$

where μ is the elastic shear modulus normalized by the Young's modulus E, and $\underline{e}$ is the deviatoric strain tensor defined by

$$e_{ij}=\varepsilon_{ij}-\frac{\varepsilon_{kk}}{3}\delta_{ij}. \tag{2.3.7b}$$

The effective plastic strain increment $\Delta\varepsilon_e^p$ is given by

$$\Delta\varepsilon_e^p=\sqrt{\frac{2}{3}\Delta\underline{\varepsilon}^p\cdot\Delta\underline{\varepsilon}^p}, \tag{2.3.8a}$$

where the plastic strain increment tensor $\Delta\underline{\varepsilon}^p$ is described by the associated flow rule as

$$\Delta\underline{\varepsilon}^p=\Delta\lambda\underline{S}, \tag{2.3.8b}$$

with $\Delta\lambda$ being the nonnegative, finite flow factor.

Substitution of Eq.(2.3.8b) into Eq.(2.3.8a) and Eq.(2.3.7a) yields

$$\Delta\varepsilon_e^p=\frac{2}{3}\sigma^2(\varepsilon_e^p)\Delta\lambda, \tag{2.3.9}$$

$$\Delta\underline{S}=2\mu(\Delta\underline{e}-\Delta\lambda\underline{S}), \tag{2.3.10}$$

where use is made of Eq.(2.3.6a) and the fact that $\Delta\underline{e}^p=\Delta\underline{\varepsilon}^p$ due to the plastic incompressibility, which is implied by Eqs.(2.3.8b) and (2.2.3b).

It is noted here that the conventional Tangent Stiffness method, or the Tangent Predictor-Radial Return method, are obtained if the consistency condition in Eq.(2.3.6b) is linearized both in $\Delta\underline{S}$ and in $\Delta\varepsilon_e^p$. To improve the approximation of this condition, its left-hand side is kept complete, while its right-hand side is expanded in Taylor series form, which is then used with first few terms. In the present study, the first three terms are retained, giving us a second-order approximation. In doing so, with the help of Eq.(2.3.9), we are left with

$$\frac{1}{2}(\underline{S}+\Delta\underline{S})\cdot(\underline{S}+\Delta\underline{S}) = \frac{1}{3}\sigma^2+\frac{4}{9}\sigma^2\frac{d\sigma}{d\varepsilon_e^p}\Delta\lambda+\frac{4}{27}\sigma^2[(\frac{d\sigma}{d\varepsilon_e^p})^2+\sigma\frac{d^2\sigma}{d(\varepsilon_e^p)^2}](\Delta\lambda)^2, \quad (2.3.11)$$

where σ is the current flow stress, which is evaluated at the current effective plastic strain ε_e^p.

Then, Eqs.(2.3.6a), (2.3.10) and (2.3.11) can be solved for $\Delta\lambda$ to arrive at the expression

$$\Delta\lambda = \frac{2\mu(\underline{S}+\mu\Delta\underline{e})\cdot\Delta\underline{e}}{b(1+\sqrt{1-\frac{ac}{b^2}})}, \quad (2.3.12a)$$

where

$$a = \frac{4}{3}\sigma^2\left(\mu^2-\frac{1}{9}[(\frac{d\sigma}{d\varepsilon_e^p})^2+\sigma\frac{d^2\sigma}{d(\varepsilon_e^p)^2}]\right), \quad (2.3.12b)$$

$$b = \frac{2}{3}(\mu\sigma^2+3\mu^2\underline{S}\cdot\Delta\underline{e}+\frac{1}{3}\sigma^2\frac{d\sigma}{d\varepsilon_e^p}), \quad (2.3.12c)$$

$$c = 2\mu(\underline{S}+\mu\Delta\underline{e})\cdot\Delta\underline{e}. \quad (2.3.12d)$$

Note that the strain increment should be small enough, such that

$$1-\frac{ac}{b^2}\geq 0. \quad (2.3.12e)$$

Now the substitution of Eq.(2.3.12a) into Eq.(2.3.10) will yield the modified incremental deviatoric stress-strain relation

$$\Delta\underline{S} = 2\mu\left[\underline{I}-\frac{2\mu\underline{S}\otimes(\underline{S}+\mu\Delta\underline{e})}{b(1+\sqrt{1-\frac{ac}{b^2}})}\right]\Delta\underline{e}, \quad (2.3.13)$$

where $\underline{I}$ is the fourth-order identity tensor. Eqs.(2.3.12a) and (2.3.13), which will be used in this study with radial return, form the stress integration algorithm, called here the Modified Tangent Predictor-Radial Return method. It can be seen that, when applied to elastic-perfectly plastic, or linear hardening materials, this method gives a stress estimate which satisfies automatically the yield condition at the end of an increment. Hence no radial return is needed. When it is adopted for power-law hardening solids, it still gives a better approximation to the consistency condition than the original tangent stiffness-based methods. In such a case, radial return is still necessary. Note that in actual numerical computations, $\Delta\underline{S}$ can be calculated more efficiently by using Eq.(2.3.10) directly if $\Delta\lambda$ is calculated first.

Remember that for a general initial stress state $\underline{\sigma}$ and strain increment $\Delta\underline{\varepsilon}$, a contact stress state $\underline{\sigma}^C$ must be determined, and used in place of $\underline{\sigma}$ in equations (2.3.6-13). It is done as follows. Suppose that the stress state $\underline{\sigma}$ is inside the yield surface, and that the stress state denoted by

$$\underline{\sigma}^T = \underline{\sigma} + \underline{C}\Delta\underline{\varepsilon},$$

called the *trial stress state*, is outside the yield surface. Then there exists a transitional stress state, called the *contact stress state*, which is determined through the transition parameter R, such that

$$\underline{\sigma}^C = \underline{\sigma} + R\underline{C}\Delta\underline{\varepsilon}$$

lies exactly on the yield surface. Care must be taken in order to obtain the correct value for R, which will be discussed explicitly later in the iteration procedure.

A final point to note is that large strain increments will be encountered near the crack tip, where large strain gradients exist due to strain singularity at the tip. In fact, due to this singular behavior, it is generally true that the finer the mesh is, the larger the increments will be, unless the rate of the decreasing grid size, when the crack tip is approached, is no less than that of the strain gradient. One way to

improve on this is to use subdivision of the strain increment, and to integrate the subincrements one by one to obtain the final stress state for the total strain increment. Actually, the necessity of subdividing the strain increment $\Delta\underline{\varepsilon}$ is observed by many investigators, as discussed by Marques (1984). With subincrementation the stress integration is performed for each subincrement $\Delta\underline{\varepsilon}/M$, where M is the subincrementation number determined according to a certain rule. Taking into consideration the fact that plastic strain updating is essential in the present finite element formulation, M is chosen in this case to be proportional to the normalized effective plastic strain increment which is estimated with original strain increment, such that for each subincrement, the estimated effective plastic strain increment is small compared to the initial yield strain ε_0.

Iteration Procedure

We present in this subsection the detailed procedure for the iteration of the system of equations (2.3.4), which can be rewritten as

$$\underline{K}\ \underline{U} = \underline{F} + \underline{F}^p, \tag{2.3.14}$$

where $\underline{K} = \underline{K}_s + \underline{K}_d$, $\underline{F} = \underline{F}_t + \underline{F}_u + \underline{F}_d$, and $\underline{F}^p = \underline{F}_p$. Note that the only term that needs to be updated in Eq.(2.3.14) is $\underline{F}^p$, which accounts for the plasticity effects. Theoretically speaking, since the small-scale yielding condition is not exactly satisfied along the crack flank due to the existence of the residual plasticity wake, tractions and displacements at the trailing edge of the finite element mesh must be updated accordingly. In such a case, the part of $\underline{F}$ which is contributed from the back boundaries must be updated too. For convenience of discussion, we shall include this part in $\underline{F}^p$. It is discovered from our computations that while the updating of $\underline{F}_t$ at the back hardly affects the fields at the crack tip area, the updating of $\underline{F}_d$ (or $\underline{F}_u$ if one chooses to use the displacement boundary conditions there) does make substantial difference, especially for higher crack speeds.

Now let $T \in [0,1]$ be a generic hardening parameter, which equals $(1-\alpha)$ for bilinear materials and $(1-\frac{1}{n})$ for power-law hardening materials. At the limit $T=1$, the elastic-perfectly plastic material model is assumed. Solutions are first obtained for $T=0$ and then for increasing discrete T values, until $T=1$ if it is desired, according to the solution procedure described at the begining of this section.

At each iteration step, the spatial distribution of the stress field is calculated through

$$\underline{\sigma}(x_1,x_2) = \underline{\sigma}(x_1-\triangle x_1, x_2) + \triangle\underline{\sigma}(x_1,x_2). \tag{2.3.15a}$$

The stress increment $\triangle\underline{\sigma}$ is computed by the Modified Tangent Predictor-Radial Return method we proposed, in connection with the subincrementation technique discussed above, from the strain increment $\triangle\underline{\varepsilon}$ defined by

$$\triangle\underline{\varepsilon}(x_1,x_2) = \underline{\varepsilon}(x_1,x_2) - \underline{\varepsilon}(x_1-\triangle x_1, x_2). \tag{2.3.15b}$$

Convergence at each T-step, i.e., at each T value, is said to have been reached at the $(k+1)$-th iteration, if the following criterion is met simutaneously for every choice of i, j, and α:

$$\frac{\|\sigma_{ij}^{k+1} - \sigma_{ij}^{k}\|_2}{\|\sigma_{ij}^{k+1}\|_2} \leq \epsilon, \tag{2.3.16a}$$

$$\frac{\|\varepsilon_{ij}^{k+1} - \varepsilon_{ij}^{k}\|_2}{\|\varepsilon_{ij}^{k+1}\|_2} \leq \epsilon, \tag{2.3.16b}$$

$$\frac{\|u_{\alpha}^{k+1} - u_{\alpha}^{k}\|_2}{\|u_{\alpha}^{k+1}\|_2} \leq \epsilon, \tag{2.3.16c}$$

where i,j have the values of 1, 2 and 3, α has the values of 1 and 2, $\|\bullet\|_2$ is the standard 2-norm, and ϵ is the error tolerance which is a small positive number. The stress and strain norms are summed over all Gauss integration points, and the displacement norm is summed over all nodal points. ϵ is taken to be around 1.0×10^{-4} in the current computation.

Now suppose that $\underline{K}$ and $\underline{F}$ have been calculated and that a displacement solution $\underline{U}_k$ at the k-th iteration is just obtained for Eq.(2.3.14), the $(k+1)$-th solution can then be determined according to the following procedure:

1. Set $\underline{F}^p_{k+1}$ to zero.
2. Start loop over elements.
3. Form nodal displacement vector $\underline{U}^e$ for the current element.
4. Start loop over Gauss integration points.
5. Compute strain $\underline{\varepsilon} = \underline{B}\ \underline{U}^e$ and strain increment $\Delta\underline{\varepsilon}$ for the current Gauss point.
6. Assuming elastic behavior, compute the trial stress increment $\Delta\underline{\sigma}^T$ and the trial stress state

$$\underline{\sigma}^T = \underline{\sigma}_{prev} + \Delta\underline{\sigma}^T$$

for the current Gauss point at the location (x_1, x_2), where the subscript "prev" denotes the stress state at the previous Gauss point, which is at the location $(x_1 - \Delta x_1, x_2)$. Compute their corresponding deviatoric tensors $\Delta\underline{S}^T$ and $\underline{S}^T$.

7. Check the value of the yield function $F(\underline{\sigma}^T, \varepsilon^p_e)$ according to Eq.(2.2.3a). Note that at this moment, the current yield surface is represented by σ, through the hardening rule $\sigma(\varepsilon^p_e)$, where σ and ε^p_e are respectively the flow stress and the effective plastic strain at the previous Gauss point. If $F \leq 0$ then jump to step 16, otherwise continue.
8. If the stress state at the previous Gauss point $\underline{\sigma}_{prev}$ is on the yield surface denoted by σ, then check the sign of the inner product

$$2\mu\underline{S}_{prev} \cdot \Delta\underline{e} = \underline{S}_{prev} \cdot \Delta\underline{S}^T.$$

If the product is nonnegative, set the elastic portion parameter R to zero and go to next step, otherwise determine R from

$$R = \frac{-2\underline{S}_{prev} \cdot \Delta\underline{S}^T}{\Delta\underline{S}^T \cdot \Delta\underline{S}^T}.$$

However, if the previous stress state is inside the yield surface, R should be calculated from

$$R = \frac{-b + \sqrt{b^2 + ac}}{a},$$

where

$$a = \Delta \underline{S}^T \cdot \Delta \underline{S}^T,$$

$$b = \underline{S}_{prev} \cdot \Delta \underline{S}^T,$$

$$c = \frac{2}{3}\sigma^2 - \underline{S}_{prev} \cdot \underline{S}_{prev}.$$

9. Compute the contact stress $\underline{\sigma}^C = \underline{\sigma}_{prev} + R \cdot \Delta \underline{\sigma}^T$, the excess stress $\Delta \underline{\sigma}^{Exc} = \underline{\sigma}^T - \underline{\sigma}^C = (1-R)\Delta \underline{\sigma}^T$, and the portion of strain increment where plasticity occurs $\Delta \underline{\varepsilon}^{Exc} = (1-R)\Delta \underline{\varepsilon}$.

10. Estimate subincrementation number M, and compute the trial stress subincrement $d\underline{\sigma} \equiv \Delta \underline{\sigma}^{Exc}/M$ and the strain subincrement $d\underline{\varepsilon} \equiv \Delta \underline{\varepsilon}^{Exc}/M$.

11. Start loop over subincrements.

12. Compute for the current subincrement $\Delta\lambda_m$ using the stress state $\underline{\sigma}_{m-1}$ of the previous subincrement and the strain subincrement $d\underline{\varepsilon}$, or the trial stress subincrement $d\underline{\sigma}$.

13. Compute for the current subincrement the stress state $\underline{\sigma}_m$ according to our Modified Tangent Predictor-Radial Return method.

14. Compute for the current subincrement the effective plastic strain subincrement $(d\varepsilon_e^p)_m$, the effective plastic strain $(\varepsilon_e^p)_m = (\varepsilon_e^p)_{m-1} + (d\varepsilon_e^p)_m$, and the flow stress σ_m through the hardening rule.

15. End loop over subincrements.

16. Compute plastic strain $\underline{\varepsilon}^p$ for the current Gauss point, and add its contribution to $\underline{F}_p^e = \int_{V^e} \underline{B}^\top \underline{C}\ \underline{\varepsilon}^p\ dV^e$.

17. End loop over Gauss integration points.

18. Assemble $\underline{F}_{k+1}^p$.

19. End loop over elements.

20. Solve $\underline{K}\ \underline{U}_{k+1} = \underline{F} + \underline{F}^p_{k+1}$ for $\underline{U}_{k+1}$.
21. Check convergence according to the criterion in Eq.(2.3.16).

It is worth pointing out that step 8 in the above procedure is an improved version of those in wide use today. With the check on the sign of the inner product, negative $\Delta\lambda$ values, which is physically wrong, can be avoided, and elastic unloading will not be mistakenly treated as plastic flow (Deng and Rosakis, 1990). This measure is particularly important in circumstances where complex loading and/or large increments are involved. As mentioned earlier, for example, in the current investigation large strain increments are inevitable due to large strain gradients near the crack tip. Moreover, as the crack propagates, or equivalently, as the stress integration sweeps the crack tip from its front to its back, severe nonproportional loading will be experienced by the material particles passing by the crack tip.

2.4 POST-PROCESSING

It is known for displacement-based finite element formulations that best accuracy for stress calculation is achieved at Gauss integration points, rather than at nodal points. Hence, stress and strain values are usually computed at Gauss points, although displacements are obtained at nodal points. For practial applications, however, values at locations other than Gauss points are often desirable. In such circumstances, the finite element results are manipulated in a certain manner in order to obtain desirable approximations.

In the present study, for example, the value of a field quantity at the centroid of an element is taken to be the average of the values at all the Gauss points of the element. Hence, due to the special arrangement of our finite element network, field variations can be observed directly along horizontal and vertical lines composed of element centroids, if the above averaging procedure is employed. Yet, field variations along circular and radial lines, which are centered at the crack tip, are not readily

available. For that, we need a general but consistent post-processing algorithm, which converts Gauss point values of field quantities into nodal values. We then can use standard procedures to interpolate those nodal values for every element to yield approximations at desired locations.

Global Least Square Smoothing

There are generally two types of post-processing algorithms, namely local smoothing and global smoothing, among which are those using least square fitting techniques (Hinton, Campbell, 1974; and Majorana, Odorizzi, and Vitaliani, 1985). A local smoothing is performed on each single element, which usually produces nonunique values at a common node, such that the nodal value is obtained by averaging those values from all the elements sharing the node. On the other hand, global smoothing is performed on all elements at once, which, although usually more expensive, generates unique nodal values.

In the current study, a global smoothing algorithm proposed by Hinton and Campbell (1974) is adopted. This approach uses a global least square fitting, resulting in a system of linear algebraic equations, with the nodal values as unknows and the Gauss point values as sources. The coefficient matrix for this algebraic system depends only on the interpolation functions to be used with the nodal values, and it can be factorized, stored and used over and over again for the smoothings of all the field quantities of many problems with the same finite element mesh. The savings are even greater if one uses the same interpolation functions for the smoothing procedure as those for the original finite element computations, provided that the Gauss point values of those functions are stored. In fact, this is exactly the situation with which we are dealing, since we use the same finite element discretization and the same interpolation functions for all materials and all crack propagation speeds.

The global smoothing approach with least square fitting is described as follows.

Suppose that $g(\underline{x})$ is a field quantity which is a function of position $\underline{x}$, $\underline{G}$ is a vector composed of all the unknown nodal values of $g(\underline{x})$, and $\underline{G}^e$ is the unknown nodal value vector of $g(\underline{x})$ for a generic element with domain V^e. Then $g(\underline{x})$ can be approximated by

$$\hat{g}(\underline{x}) = \underline{N}(\underline{x}) \cdot \underline{G}^e, \tag{2.4.1}$$

where $\underline{N}(\underline{x})$ is a vector composed of the shape functions used in the original finite element computation. The principle of least square fitting states that $\underline{G}$ is such that the functional

$$\Phi = \sum^{e} \int_{V^e} [\hat{g}(\underline{x}) - q(\underline{x})]^2 \ dV^e \tag{2.4.2}$$

is minimum, where the sum is over all elements, and $q(\underline{x})$ is an approximation for $g(\underline{x})$ appropriately interpolated or extropolated from the Gauss point values of $g(\underline{x})$. The minimum is achieved when

$$\frac{\partial \Phi}{\partial \underline{G}} = 0. \tag{2.4.3}$$

From Eqs.(2.4.1) through (2.4.3), the following system of linear algebraic equations can be obtained for $\underline{G}$ after performing the standard finite element discretization process:

$$\underline{K} \ \underline{G} = \underline{F}, \tag{2.4.4}$$

where $\underline{K}$ and $\underline{F}$ are assembled from their counterparts for all elements, namely those

$$\underline{K}^e = \int_{V^e} \underline{N} \ \underline{N}^\top \ dV^e, \tag{2.4.5a}$$

$$\underline{F}^e = \int_{V^e} \underline{N} \ q(\underline{x}) \ dV^e. \tag{2.4.5b}$$

Note that when the Gauss points for the original finite element computation are used for the evalution of Eq.(2.4.5b), $q(\underline{x})$ can be replaced by the the original finite element results at these Gauss points.

Numerical Data Presentation

After the nodal values for field quantities are obtained using the global least square smoothing approach described above, we can begin to interpolate those quantities within an element with the shape functions for the original finite element computation. In this subsection, we will illustrate how the numerical data is to be presented in this study.

When referred to a polar coordinate system (r, θ) centered at the crack tip, the stress and deformation fields for a propagating crack in an elastic-plastic solid are generally dependent on both r and θ. Even in the case of an elastic-perfectly plastic material for which the stresses are asymptotically independent of r, numerical discretization errors will inevitably introduce fictitious r-dependence, especially at locations away from the crack tip. Hence it is desirable to present angular field variations along circular lines around the crack tip, other than along rectangular paths as is usually done in the literature.

In the current study, all data for angular field variations are extracted from finite element locations along a semicircle of radius $0.2033 \times 10^{-3}(K/\sigma_0)^2$ for the finer mesh, which is about one thirteen-hundredth of the active plastic zone size, and of radius $0.6411 \times 10^{-3}(K/\sigma_0)^2$ for the coarser mesh, which is about one four-hundredth of the active plastic zone size. This circular path lies at least five elements away from the crack tip.

CHAPTER 3

ELASTIC-PERFECTLY PLASTIC SOLIDS

3.1 INTRODUCTION

The subject of crack growth in elastic-perfectly plastic solids has attracted very much attention during the last 30 years or so. Particularly, studies for crack tip stress and deformation fields, which form the basis of further fracture analyses, are among the favorites of many investigators. Those studies have greatly promoted our understanding of many ductile fracture phenomena, such as the increased material resistance to continued crack extension, and the effect of inertia on dynamic crack propagation. Yet this subject is far from closed. As of today, for example, many of the available analyses only offer partially complete solutions. In some instances, the solutions are inconclusive. In the worst case, solutions are just not available, the Mode I quasi-static crack growth under plane stress being one example.

In the following, a comprehensive literature survey is given first, covering all anti-plane strain, plane strain and plane stress or generalized plane stress cases. It highlights certain common patterns or characteristics of available solutions. Critical reviews are given for some key issues which are of most concern here.

Numerical results are then presented for the current full field finite element investigation of Mode I crack growth in elastic-perfectly plastic solids in plane stress under steady state and small-scale yielding conditions. quasi-static crack growth is discussed first, followed by treatment on dynamic crack propagation. In the quasi-static case, we concentrate on comparisons with the results of similar studies, namely with finite element solutions by Dean (1983), Luo, Zhang and Hwang (1984),

and Narasimhan, Rosakis and Hall (1987a). In the dynamic case, details are given regarding the evolutive variations of the crack tip active plastic zones, the stress and the deformation fields, with respect to crack propagation velocities. The so-called crack-line solution by Achenbach and Li (1984a, b, c), and the recent asymptotic solution by Gao (1987) will be discussed. All computations are performed with the Poisson ratio $\nu = 0.3$. All logarithmic values used in figures are based on the natural number e.

Anti-Plane Strain

Hult and McClintock (1956) were the first to study crack tip fields in elastic plastic solids. They considered the problem of a quasi-statically loaded Mode III stationary crack in an elastic-perfectly plastic material. They found that the crack tip plastic zone is located at the front of the crack tip and that strains in the plastic zone are as singular as $\frac{1}{r}$ as $r \to 0$, where r is the radial distance from the crack tip. This strong singularity results in a nonzero crack opening displacement at the crack tip (Rice, 1968a). Under small-scale yielding conditions, the plastic zone shape is a circle in contact with the crack tip and with a diameter of $R_0 = \frac{K_{III}^2}{\pi \tau_0^2}$ (Rice, 1966, 1968a), where K_{III} is the stress intensity factor in Mode III and τ_0 is the yield stress in shear, and the effect of yielding is to shift the elastic singularity ahead as if the crack tip were at the center of the plastic zone (Irwin and Koskinen (1963)). Hult (1957) and McClintock (1958, 1963, 1965) also studied the strain distribution at the front of a quasi-statically growing crack tip, again in an elastic-perfectly plastic solid, whereas Rice (1968a) was the first to give a complete expression for the strains along the crack line under steady state conditions. His result was confirmed, under SSY conditions, by the crack line solution of Achenbach and Dunayevsky (1984). A full field solution under steady state and SSY conditions, including the plastic zone shape, was given by Chitaley and McClintock (1971) with some errors noted by Rice (1973), Broberg (1975) and Gao (1980). Chitaley and McClintock showed that the

plastic zone ahead of the crack, the primary plastic zone, can be approximated by a centered fan composed of radial stress characteristic lines, with an angular span (measured from the crack line) of $\theta_p \doteq 19.69^o$ and a radial linear span of $R_p \doteq R_0$, and that at the crack flank there is a reverse loading zone, the secondary plastic zone, with an angular span of $\theta_s \doteq 0.37^o$. While the $[ln(\frac{R_p}{r})]^2$ strain singularity just ahead of the crack tip obtained by the above investigators was verified by the asymptotic analysis of Rice (1982) from the point of view of a general formulation, and by the finite element (FEM) full field analyses to be discussed below, the shape and size of the plastic zone given by Chitaley and McClintock were not confirmed by any of them. Sorensen (1978) performed a FEM computation utilizing a nodal release procedure to simulate the crack growth process, and found that the results rapidly converge to a steady state solution after a few node releases, but that R_p is 4% smaller than R_0, and that θ_p is about 45^o. No secondary plastic zone was detected. Dean and Hutchinson (1980) used an Eulerian-type FEM formulation peculiar to steady state problems, obtained a R_p which is 10% larger than R_0, and $\theta_p \doteq 60^o$. They reported that the primary plastic zone could be characterized by a centered fan with all the stress characteristic lines emanating from the crack tip only for $|\theta| < 20^o$. No secondary plastic zone was noticed either. Steady state FEM studies of this problem with finer meshes were conducted by Douglas (1981) and Lam (1982), whose results essentially agree with each other, showing that R_p is about 13% smaller than R_0 and $\theta_p \doteq 55^o$. Besides, Douglas's calculation shows a small region of reversed plastic flow in the wake along the crack faces. His result also suggests that the characteristic line direction at any point within 20^o of the x_1-axis is nearly radial, thus confirming Dean and Hutchinson's earlier finding. It is interesting to note that no complete numerical angular stress and strain variations were ever reported. Nevertheless it can be concluded that the strain distribution along the crack line is clearly understood, but the exact shape and size of the plastic zone remain elusive. A FEM calculation with higher spatial resolution may be necessary.

The investigation of Mode III dynamic crack propagation in elastic-plastic solids was pioneered by Slepyan (1976), for a steadily growing crack in an elastic-perfectly plastic solid. His asymptotic results, which show continuous angular stress and strain distributions, as verified by other investigators utilizing different solution schemes (Achenbach, Burgers and Dunayevsky, 1979; Achenbach, Dunayevsky, 1981a, b; Gao and Nemat-Nasser, 1983a; and Lin, 1985), show features distinct from quasi-static analysis. It is seen that the crack tip is preceded by a centered fan plastic sector and trailed by another plastic sector of uniform stress, with no elastic unloading sector in between, and the angle separating the two sectors is given by

$$\theta^* = -tan^{-1}(\frac{1}{m}), \tag{3.1.1}$$

where m is the ratio of crack speed to the elastic shear wave speed. The centered fan is composed of radial characteristic lines which do not coincide with the principal shear lines when crack speed is nonzero (Achenbach, Burgers and Dunayevsky, 1979; Achenbach, Dunayevsky, 1981a, b; and Douglas, Freund and Parks, 1981). While the strain component ε_{13} is bounded everywhere for fixed crack speed, and the component ε_{23} is as singular as lnr at the crack tip, they both become infinite at fixed distance when m goes to zero. In particular, in the centered fan sector,

$$\varepsilon_{23} = \frac{\tau_0}{\mu}\frac{(1-m)}{2m} ln(\frac{R}{r}), \quad \text{as} \quad r \to 0, \tag{3.1.2}$$

where μ is the shear modulus, and R is an undetermined constant by the asymptotic analysis, on the same order as the plastic zone size R_p measured along the crack line. The crack tip opening displacement, expressed by

$$\delta = 2u_3 \mid_{\theta=\pi} = \frac{\pi\tau_0}{\mu m} r, \tag{3.1.3}$$

increases rapidly as m decreases. It is important to note that, as m approaches zero, the dynamic asymptotic solution does not tend to the quasi-static limit. First, to name a few examples, no elastic sectors appear in the limit; second, the strains

and crack tip opening displacement are not defined (for fixed r), instead, they become unbounded. An explanation for this inconsistency is as follows: The dynamic asymptotic solution has only a limited range of dominance around the crack tip, and the dynamic zone shrinks onto the crack tip as $m \to 0$. This is clearly demonstrated by the crack line solutions discussed below. Dunayevsky and Achenbach (1982a), Freund and Douglas (1982), Achenbach and Li (1984b), and Achenbach, Li and Nishimura (1985) using different methods, managed to obtain exact solutions along the crack line in the active plastic zone, valid up to the plastic boundary. The crack line solution is shown to reduce to the correct dynamic asymptotic form, for any m in the range $0 < m < 1$, if the distance x ahead of the crack tip is such that

$$(\frac{x}{R_p})^{\frac{2m}{(1+m)}} \ll 1, \tag{3.1.4}$$

and tend to the correct limit as m approaches zero for any fixed point on the crack line (Freund and Douglas (1982)). From the last expression, it is indeed observed that the size of the dominamce zone of the dynamic asymptotic solution becomes vanishingly small as m becomes smaller and smaller. This means that the current dynamic asymptotic solution cannot capture the full feature of the crack tip fields for low and intermediate crack speeds and hence is of limited use as far as a fracture criterion is concerned. Rather, in order to characterize crack propagation transitional behavior from low speeds to higher ones, the full field solution, or at least an asymptotic solution including higher order terms, which recovers the quasi-static one as crack speed goes to zero, should be used in a fracture criterion. However, higher order asymptotic analyses are extremely difficult, if not impossible, to perform, and full field solutions can usually only be obtained numerically. In this sense, crack line solutions have their advantages.

Numerical investigations of this problem are rare, in spite of their importance as a check for asymptotic solutions and as a means to relate local quantities to global ones. A full field finite element analysis, under SSY and steady state conditions, was provided by Douglas (1981). The strain distribution at crack front is shown to

agree quite well with the exact crack line solution. The active plastic zone, scaled by $\frac{K_{II}^2}{\tau_0^2}$, is found to shrink in the crack line direction and to grow in height, as the crack speed increases. However the theoretically anticipated all around plastic zone feature is not revealed, instead, the plastic zone is sited ahead of the crack. Further, in contrast to the behavior described by Eq.(3.1.3), the crack tip profile seems to be invariant to crack speeds (Douglas, Freund and Parks, 1981). This situation may exist because the range of the dynamic asymptotic solution is too small and the mesh used is not fine enough to capture the dynamic behavior. It is also quite possible that this may be attributed to the nature of the numerical procedure used. In this procedure, field quantities are integrated along stream lines parallel to the crack faces, from positive x_1 to negative x_1 locations, a scheme peculiar to the FEM formulation used for steady state problems. Large errors are carried over to the crack flank when integration sweeps the crack tip region where large errors are inevitable due to the discretization process. The effect of these carry-over errors are most pronounced just behind the crack tip. Thus information extracted from elements or nodal points just behind the crack tip, e.g., the crack tip opening angle, must be interpreted with caution. This is an important point which has not been given enough attention. As we mentioned at the beginning of this paragraph, no other numerical studies, especially of the angular stress and strain distributions were available, either as checks for the asymptotic analyses, or as checks for the accuracy and reliability of the numerical schemes themselves.

Plane Strain

Elastic-plastic fields around a sharp crack tip, for the case of in-plane fracture modes, were first investigated independently by Rice (1967, 1968a) and by Cherepanov (1967). Under Mode I plane strain and contained-yielding conditions, they noticed that the well-known Prandtl slip line solution (see Hill, 1950) can be used to represent the near-tip field for a stationary crack in a nonhardening

solid. According to this solution, plastic yielding sectors fully surround the crack tip, among which are two constant stress sectors, one at the front and the other at the back, and one centered fan sector in between. The stresses are found to be bounded and continuous, and are completely determined by the equilibrium and yield conditions. Rice further pointed out that strains can have singularities only in the centered fan sector where, in particular, ε_{rr} and $\varepsilon_{\theta\theta}$ are bounded, and $\varepsilon_{r\theta}$ varies as $\frac{1}{r}$. Moreover, analogous to the Mode III case, there is a finite, discrete crack opening displacement at the tip. Similar slip line solutions were also obtained by Hutchinson (1968b) for Mode II plane strain, and by Shih (1973) and Dong and Pan (1988) for mixed Mode I and Mode II plane strain. For all the cases, the angular strain variations are nonunique and cannot be determined by a local analysis. That is, they depend on the solution to an entire boundary value problem. It should be noted here that by using the slip line solutions elastic incompressibility is implied. Consequently, slip line solutions are in general valid only in the immediate vicinity of a crack tip, where plastic strains are presumably dominant and the incompressibility condition is expected to be very well-approximated.

The first study on the asymptotic elastic-plastic fields around an in-plane extending crack was made by Rice (1968a). He considered the case of a Mode I plane strain crack growing quasi-statically and steadily in an incompressible elastic-perfectly plastic solid. In this preliminary investigation, he discovered that, if the Prandtl slip line field is assumed, then in the centered fan sector strains and velocity components all vary as $ln(\frac{R}{r})$ as the tip is approached, where R is an undetermined constant by the local analysis. His results were then extended to nonsteady conditions by Rice (1973) and Cherepanov (1974), and to elastically compressible materials by Rice and Sorensen (1978), but with the same Prandtl slip line field. It was later found, independently by Slepyan (1974) (for Tresca solids), Gao (1980) and also Gao and Hwang (1981a), and Rice, Drugan and Sham (1980), that the centered fan sector cannot be joined by a constant stress plastic sector at its rear boundary,

rather, an elastic unloading sector must be placed in between, if the nonnegative plastic work principle is to be satisfied. The origin of this negativeness of plastic work comes from the discontinuity in the velocity component v_r along the common radial boundary where the two concerned plastic sectors connect each other. While $v_r \to +\infty$ as $r \to 0$ along the centered fan side, v_r is necessarily bounded along the constant stress side. Hence when the boundary is crossed from the centered fan to the other side, the positive shear stress component $\sigma_{r\theta}$ does infinite amount of negative work. The correct assembly of crack tip sectors for the case of Poisson ratio $\nu = 0.5$ is as follows: A constant stress sector at the crack front, followed by a centered fan sector, then joined by an elastic sector and finally trailed by another constant stress sector. Slepyan's solution covered the cases of both Mode I and Mode II and general ν, for materials obeying the Tresca yield condition and its associated flow rule, which coincides with the von Mises yield condition and the Prandtl-Reuss flow rule when $\nu = 0.5$. Also found in Rice, Drugan and Sham's work, for von Mises solids, is an approximate solution for the case of $\nu \neq 0.5$ under general non-steady-state conditions, with the same type of assembly of sectors, and with the assumption that the deviatoric stress component $s_{33} \to 0$ as $r \to 0$ in all plastic sectors. In a later study, Rice (1982), for the $\nu \neq 0.5$ case, made some corrections to the previous one and noticed the need for plastic sectors with $s_{33} \neq 0$, which are neither constant stress sectors nor can be represented in terms of slip lines. He also gave a general formulation for the investigation of asymptotic structures of near-tip stress and deformation fields around quasi-statically advancing cracks, for materials of arbitrary yield condition and of the associated flow rule type, including anisotropic response. As pointed out by Gao (see Gao (1983)), the assembly of crack tip sectors for $\nu = 0.5$ cannot be used for general ν cases, due to the fact that there will be a small zone in the elastic sector right behind the centered fan, where the von Mises yield condition is violated. He then proposed that the elastic sector be placed between two plastic sectors of $s_{33} \neq 0$ type, one joining the centered fan, the other connecting the crack flank. Following Gao's observa-

tion, Drugan, Rice and Sham (1982) were able to obtain a complete solution for non-steady-state crack growth, which has the feature that all stress components are continuous and bounded, resulting in a discontinuity in the velocity component v_r at $\theta = \frac{\pi}{4}$ where the constant stress sector at the crack front meets the centered fan. Due to the mathematical complexities involved, the angles separating the different sectors were determined via a numerical procedure. An incorrect value in the calculated angles was noticed by Hwang and Luo (1988), resulting from an algebraic error in the computation (Rice, 1989, private communication). Nonetheless the main features of the crack tip fields are now understood to be as follows. Stresses are continuous and resemble very much the Prandtl slip solution, an indication that the growing crack is characterized by strain fields more than by stress fields. The dominating singularity of the accumulated crack tip strains are due to contributions from the centered fan plastic sector only, which starts at $\theta = \frac{\pi}{4}$. Hence the strains are as singular as $ln(\frac{R}{r})$, in and behind the centered fan, and are less singular than that at the crack front, where R is a constant length scale undetermined by the asymptotic analyses. Thus it is observed again that maximum strain concentration does not occur ahead of the crack tip.

Finite element studies of Mode I plane strain quasi-static crack growth in elastic-perfectly plastic solids were usually performed under small-scale yielding conditions and for $\nu = 0.3$. Two types of formulations were frequently used. The first one, introduced originally by Andersson (1973), involves progressively unloading nodes ahead of the crack tip in conjunction with a certain pre-assumed crack growth criterion, thus simulating a crack advancing from its stationary state, which is customarily referred to as the nodal release approach. The advantage of this approach is that the transient process of crack extension can be revealed, and usually a steady state can be reached at the end after some node releases. The second procedure, the so-called steady state or Eulerian formulation mentioned before, was first used by Dean and Hutchinson (1980). In this formulation, it is assumed that a

steady state has been reached such that the crack speed and the loading parameters, etc., are all invariant to the crack growth, hence a mesh moving with the crack tip can be used, and all field quantities can be computed according to some convection rules required by the steady state condition. In this case, no criterion is assumed *a priori*.

Sorensen (1979) performed a FEM computation by utilizing a nodal release procedure according to the achievement of the static similarity solution of Tracey (1976), with hypothetical load histories which might be found in service, reflecting the different K levels required to obtain appropriate similarity solutions. A mesh size of about 20 times the maximum extent of the active plastic zone is used to approximate the small-scale yielding condition. The smallest element size is about one-eleventh of the maximum active plastic zone size. His results show that the crack tip stress distribution is similar to that of the Prandtl slip line solution, and the crack tip profiles in the steady state reveal a vertical tangent at the tip. However, no near-tip elastic unloading sector is discovered in this study, which may be attributed to the coarse mesh used. In much the same way, Sham (1983) conducted a FEM study, but with a much finer mesh, particularly around the crack path. He adopted a modified variational principle developed by Hilton and Hutchinson (1971) to model the small-scale yielding condition, hence allowing the plastic zone to spread very close to the mesh boundary, concentrating degrees-of-freedom in the plastic zone region, thus making full use of the computer capability. The smallest element size is about one one-hundredth of the maximum extent of the active plastic zone. As expected, his results agrees very well with the theoretically predicted stress distributions and crack opening profile. Particularly, a well-defined elastic unloading sector, which moves with the advancing crack tip, was clearly shown at a loaction anticipated by the asymptotic analysis.

The steady state formulation was employed by Dean and Hutchinson (1980), and by Lam (1982) (see also Parks, Lam and McMeeking, 1981, and Lam and

Freund, 1985) in their finite element studies. They used meshes whose spatial resolutions are about the same as that of Sham, i.e., the smallest element size is about one one-hundredth of the maximum extent of the plastic zone. Their results are essentially in agreement with available asymptotic analyses, as far as stress distribution is concerned. However, there is no clear wedge-shaped elastic unloading region shown in their results, although some indications for the existence of a trailing elastic sector was present in the solutions of Lam et al. (Parks, Lam and McMeeking, 1981; and Lam, 1982). An apparent reason for this disagreement with the prediction of asymptotic analyses is that the mesh refinements used by these investigators are not sufficient to reveal the details around the tip region. However, considering the fact that unloading was detected by Sham's results which employs a mesh of similar finess at the tip but with a different formulation, it seems that this can, to some extent, be attributed to the steady state formulation itself. As we have pointed out in the discussion for Mode III crack growth, in the steady state formulation, errors are carried over from the crack tip to regions along the crack flank, which are most pronounced immediately behind the tip. It can be seen from the results of Dean and Hutchinson that, the traction-free condition along the crack faces is not very well satisfied, in comparison with Sham's results. It appears that in order to reduce this error, a mesh of high spatial resolution near the crack tip has to be used.

quasi-static solutions are valid when inertia effects are negligible. The inclusion of dynamic terms in the equations of motion, which accounts for the inertia effects, may produce crack tip fields distinct from the quasi-static counterparts, as has been clearly seen for the Mode III case. Many investigators have offered solutions for steady state dynamic crack growth of Mode I plane strain cracks in elastic-perfectly plastic solids. Slepyan (1976) and Achenbach and Dunayevsky (1981a, b) obtained solutions for Tresca materials obeying associated flow rules for the case of small m, the Mach number for crack propagation defined as the ratio of crack tip speed to

the elastic shear wave speed of the material. Their solutions agree with each other when $m \rightarrow 0$ as far as in-plane stress distribution is concerned, and are otherwise different. Lin (1985) found a solution for general m values, which recovers those by Slepyan and by Achenbach and Dunayevsky in the limit $m = 0$. The main features of the above solutions are that plastic sectors are all around the crack tip and that stresses and strains are continuous and bounded. In contrast, Gao and Nemat-Nasser (1983a) provided a solution which predicts totally different behaviors, for an incompressible material obeying the von Mises yield condition and the Prandtl-Reuss flow rule, which coincide with the Tresca yield condition and its associated flow in this special case, i.e. Poisson ration $\nu = 0.5$. Later Gao (1985) repeated the above asymptotic analysis for general ν. Their results show that certain stress and strain components possess discontinuities along a radial line whose position depends on the value of m, and that strains have logarithmatic singularities everywhere around the tip. No elastic unloading sectors were found either. As pointed out by Lam and Freund (1985), however, if discontinuities in the stress components are ruled out, then the analysis of Gao and Nemat-Nasser will yield a generalization of the Achenbach and Dunayevsky result which is valid for arbitrary values of m. Further effort has been made by Leighton, Champion and Freund (1987) in order to "identify a discriminating feature among the proposed asymptotic solutions." They reconsidered the problem for the special case of $\nu = 0.5$. In their analysis, a proof is given as to the boundedness of the hydrostatic stress (i.e., the mean stress), and hence of all the other stresses. They argued that, if the principle of maximum plastic work is to be satisfied, then the stresses have to be continuous around the propagating crack tip, which necessarily results in the boundedness of velocity and strain components. But as to the general ν cases, such a discriminating feature has not yet been firmly established. Under small-scale yielding conditions, a full field finite element computation of the Eulerian-type was performed by Lam and Freund (1985) for the case of $\nu = 0.3$ with the von Mises yield condition and the Prandtl-Reuss flow rule, for a wide range of Mach numbers. They reported that for an

extremely small crack speed, namely $m = 10^{-6}$, the finite element results show close agreement for stresses, except for σ_{33}, with those of Achenbach and Dunayevsky, which alone, we think, does not necessarily mean that the solution of the later authors is more reasonable than others (see remarks in the next paragraph). The numerical results of Lam and Freund also clearly indicate the possibility of elastic unloading behind the primary active plastic zone, particularly for the higher crack speeds considered, which is a puzzling phenomenon contradictory to the asymptotic predictions. It seems, however, that this cannot be attributed to the possibility that the range of validity of the asymptotic solutions is small, since, for example, as m increases, the range of validity grows and the deviation of the numerical calculation away from the analytic solution should decrease rather than increase.

A few observations, along with some remarks, can be made regarding the above investigations. Firstly, in the limit $m = 0$, the dynamic crack tip fields do not tend to the quasi-static ones, which shows again the restricted applicability of asymptotic analyses for rapidly propagating cracks, as has demonstrated for the Mode III case. Secondly, the asymptotic solutions by Achenbach and Dunayevsky and by Lin used the Tresca yield condition and its associated flow rule, and assumed that the stress component σ_{33} was the intermediate principal stress, which was not known *a priori*. If this is true, then the relation $\sigma_{33} = \nu(\sigma_{11} + \sigma_{22})$ will hold. However, a close examination reveals that this assumption, hence the resulting solutions, are valid only for a certain range of ν values. As shown by above solutions, the plastic sectors, both at the crack front and at the crack faces, are constant stress sectors where $\sigma_{12} = 0$ from the symmetry conditions along the crack line and from the traction-free conditions along the crack flank. Consequently both σ_{11} and σ_{22} are principal stresses there. Hence the Poisson ratio ν must be such that σ_{33} is between σ_{11} and σ_{22}, otherwise the solution is not valid. For small m values, for example, the asymptotic solutions hold only if $\nu > \frac{\pi}{2(1+\pi)} + O(m^2) \doteq 0.3793 + O(m^2)$. This observation can be used to explain the comparisons between the asymptotic

solutions and the finite element results of Lam and Freund (1985), who reported, for the case of $\nu = 0.3$ and m very small (essentially the quasi-static value), that while their in-plane stresses agree quite well with the asymptotic solutions of Achenbach and Dunayevsky, the σ_{33} component differs very much from each other, with their numerical value being closer to the Prandtl solution. This is not surprising since as $m \rightarrow 0$, all the available dynamic asymptotic in-plane stresses tend to the values of the Prandtl field, and the numerical solution tends to the quasi-static one, which closely resembles the Prandtl solution, as discussed before. Besides, the asymptotic value for σ_{33} is obviously much smaller than σ_{11} and σ_{22}, for an angular region from the crack line to about $\theta = 100°$, as seen from Fig. 2 of the paper by Lam and Freund. On the other hand, it seems that Slepyan in his solution noticed the need to modify the solution when the aforementioned assumptions were violated, but he didn't resolve this issue. Thirdly, in order to identify the right asymptotic solution, full field, high resolution numerical computations must be conducted and strain and velocity variations should be compared with available asymptotic solutions.

Although not of great practical importance, solutions for the Mode II crack growth would be theoretically very appealing as they might provide insights for the equivalent Mode I case. However, the situation for Mode II case here is even more puzzling than the Mode I case just discussed. As far as the current authors are aware, there are only two asymptotic solutions, proposed for elastically incompressible media. Following the work of Slepyan (1976) for Mode I, Lo (1982) obtained a Mode II solution, which predicts all around plastic sectors at the crack tip, with bounded and continuous stress variations. While the strain components $\varepsilon_{11} = -\varepsilon_{22}$ are finite at the tip, the component ε_{12} is as singular as lnr. As the Mach number $m \rightarrow 0$, the stresses approach those of the slip line solution of Hutchinson (1968b) for a stationary crack. But just as for the Mode I case, the solution by Gao and Nemat-Nasser (1984) shows very different features. In the first place, there is an elastic unloading zone behind the crack. Secondly, stresses and strains again pos-

sess angular discontinuities. Thirdly, all strains are as singular as lnr. Finally, in the limit $m = 0$, stresses approach a solution for a stationary crack tip, which is different from that of Hutchinson in that the elastic sector at the crack flank still exists. No full field solutions are available for comparison.

Plane Stress

An analysis for elastic-plastic fields around a stationary crack tip in an elastic-perfectly plastic solid under plane stress conditions was performed by Hutchinson (1968b). He constructed a stress characteristic line field, with a centered fan sector in front of the crack tip and two constant stress sectors behind it. As in the plane strain case, strains can have singularities only in the centered fan, with $\varepsilon_{\theta\theta}$ and $\varepsilon_{r\theta}$ varying as $\frac{1}{r}$, and ε_{rr} bounded. Note here that, as in the case of Mode III and Mode I plane strain, the $\frac{1}{r}$ strain singularity would produce a nonzero crack opening displacement at the crack tip (see, for example, the finite element results of Narasimhan and Rosakis, 1988). In contrast to the plane strain case, however, the stress component σ_{rr} is discontinuous across the radial line which separates the two constant stress sectors. Similar stress characteristic line solutions were also obtained by Shih (1973) for Mode II plane stress, by Shih (1973), and Dong and Pan (1989) for mixed Mode I and Mode II plane stress. Just as for the plane strain case, the angular strain variations are nonunique and cannot be determined from a local analysis. That is, they depend on the solution to an entire boundary value broblem. It should be noted here that, by using the stress characteristic solutions, elastic incompressibility is implied. Consequently, stress characteristic line solutions are in general valid only in the immediate vicinity of a crack tip, where plastic strains are presumably dominant and the incompressibility condition is expected to be very well-approximated.

For quasi-static plane stress crack growth in elastic-perfectly plastic solids, a preliminary analysis was given by Rice (1982) regarding the structure of possible

elastic and plastic sectors around the crack tip. He demonstrated that only two types of plastic sectors are possible: a constant stress sector where the Cartesian components of the stress tensor are constant, and a centered fan sector in which the polar components of the stress tensor can be expressed as

$$\left.\begin{aligned} \sigma_{\theta\theta} &= \pm 2\tau_0 cos(\theta - \theta_1), \\ \sigma_{rr} &= \pm \tau_0 cos(\theta - \theta_1), \\ \sigma_{r\theta} &= \pm \tau_0 sin(\theta - \theta_1), \end{aligned}\right\} \tag{3.1.5}$$

where τ_0 is the yield stress in shear and θ_1 is an arbitrary constant. He also showed that the velocity components are necessarily logarithmically singular in the centered fan with amplitudes determined by the stress distribution in Eq.(3.1.5). However, it seems that there is no successful assembly of complete crack tip fields for Mode I crack growth, although Ponte Castañeda (1986) succeeded in assembling a crack tip field for a Mode II crack. Achenbach and Dunayevsky (1984), Achenbach and Li (1984c) and Guo and Li (1987) proposed crack line solutions based on the assumptions that the stress component σ_{22}, and hence σ_{11}, are uniform along the crack line up to the elastic plastic boundary, and that the plastic solutions can be matched to an appropriate elastic solution, which may not be unique, at the boundary. Their solutions suffer from the fact that the constancy assumption of σ_{22} and σ_{11} along the crack line is not valid, as is shown by the finite element studies to be discussed below, by the perturbation analysis of Krishnaswamy and Rosakis (1990b) and our numerical results to be presented in this chapter.

Much understanding of the subject has been gained through some recent finite element investigations performed by Dean (1983), Luo, Zhang and Hwang (1984), and Narasimhan, Rosakis and Hall (1987a), under small-scale yielding conditions. All the investigators studied the elastic-perfectly plastic case. While Dean and Luo et al. used the Eulerian-type formulation for steady state crack growth, Narasimhan et al. adopted the nodal release procedure to simulate a crack advancing from its stationary state. They presented results regarding the plastic zone shape, stress dis-

tributions and crack opening profiles. Narasimhan et al. also gave the tensile plastic strain variation along the crack line, and investigated the regions of hyperbolicity and ellipticity for elastic-perfectly plastic solids, with some evidence showing that inside the active plastic zone ahead of the crack, an elliptic region may extend all the way up to the crack tip as a wedge of increasingly small angular extent as the tip is approached along the crack line. This finding can probably explain the intriguing situation encountered by asymptotic analyses. These studies did not discuss the angular dependence of strain components.

No asymptotic solutions for dynamic crack propagation in elastic-perfectly plastic solids were available until recently. Applying the method used for the quasi-static case, Achenbach and Li (1984a, b) proposed a crack line solution for steady state Mode I crack growth under similar assumptions, namely that σ_{22} and σ_{11} are uniform along the crack line up to the elastic plastic boundary, etc. Again, this solution suffers from the fact that the underlying assumptions are not valid, as shown by our finite element results to be presented in this study. Gao (1987) gave a solution with full angular stress and strain continuity. It is shown that the crack tip is surrounded by two plastic sectors, one ahead of the crack and the other behind it, and one elastic sector in between, and that strains possess $ln(\frac{R}{r})$ singularity at the tip, where R is a constant undetermined by the asymptotic analysis. No confirmations have been made as to the appropriateness of this solution.

3.2 QUASI-STATIC CRACK GROWTH

The subject of crack tip asymptotic fields for quasi-static crack growth under conditions of Mode I plane stress and small-scale yielding was previously investigated, using the finite element method, by Dean (1983), by Luo, Zhang and Hwang (1984), and Narasimhan, Rosakis and Hall (1987a). In order to capture the main features of their results and to interpret them correctly, it is noted here that those investigations are both similar and different in many ways.

First of all, the numerical formulations are different. Dean, Luo et al. studied steady state crack growth, and accordingly they employed the Eulerian finite element formulation originated by Dean and Hutchinson (1980). Narasimhan et al., on the other hand, looked into the transient fracture process of a crack beginning from its stationary state. Hence, they adopted a nodal release procedure first introduced by Sorensen (1979), which simulates stable crack growth by progressively releasing crack tip element nodes according to the achievement of critical stress intensity factor values.

Yet the above fact does not prohibit comparisons between results from the two different numerical formulations, although care must be exercised. As indicated by the results of Narasimhan et al., the transient solution near the crack tip rapidly converges to a steady one, after the nodal release procedure is carried out several times. The same is reported by Sorensen (1979) for Mode I plane strain. In fact it can be shown analytically that the stress and deformation fields at the crack tip are asymptotically in a steady state, provided that crack growth is quasi-static, or that the partial time derivatives in the crack tip moving Cartesian coordinate system are bounded. This would mean that solutions from different numerical formulations are comparable near the crack tip, and that whether they are comparable away from the tip-region depends on the extent the transient computation is carried out.

Secondly, it is noted that the finite element meshes used by those investigators are not of the same fineness. It is helpful to bear in mind that the ratio of the active plastic zone size to that of the smallest crack tip element is about 35 in Dean's computation and about 140 in the other two computations. It is expected that a finer mesh will usually yield a higher accuracy.

Finally, the validity of comparisons between results of those different studies mentioned above will depend very much on the way the results are post-processed and presented. For example, an angular variation of a field quantity around the

crack tip should be extracted from the numerical data along a circular path centered at the tip and the magnitude of the variations will generally depend on the radius of the path, whether it is due to the true radial dependence of this quantity, or due to the existence of the finite element discretization error. It is worth recalling that rectangular paths are used for stress distributions in the above presentations.

In our study, we followed Dean's method and employed a near-tip mesh of high spatial resolution, with the ratio of plastic zone size to the smallest element size on the order of 1.6×10^4, which is much finer than the previous ones. We also use circular paths for angular field variations. Thus we tend to believe that our solution represents a better approximation for steady state crack tip fields. For this reason and because of the fact that not all field quantities of interest were published in the earlier studies, we feel it is beneficial to document our results here.

The Active Plastic Zone

The active plastic zone is located at the front of the crack tip and it spreads out along the prospective crack line, as shown in Fig. 3.2.1. Its size R_p, measured along $\theta = 0^0$, is about $0.265(K/\sigma_0)^2$, where σ_0 is the initial yield stress in tension, and K is the stress intensity factor indicating the current load level. Its height $H_p \doteq 0.084(K/\sigma_0)^2$ is measured from the crack line. The angular span θ_p of the active plastic zone, measured from the crack line again, is approximately 45^0.

Also shown in Fig. 3.2.1 is the active plastic zone obtained by Dean (1983), utilizing the same finite element solution scheme. It is seen, however, that his result gives a larger plastic zone shape. In particular his R_p is as large as $0.31(K/\sigma_0)^2$, even greater than that for a stationary crack, which is about $0.29(K/\sigma_0)^2$ according to a recent detailed finite element study by Narasimhan and Rosakis (1988). Both Luo et al. and Narasimhan et al. reported R_p to be around $0.28(K/\sigma_0)^2$. Note that the results of Narasimhan et al. were obtained at the end of the twentieth node

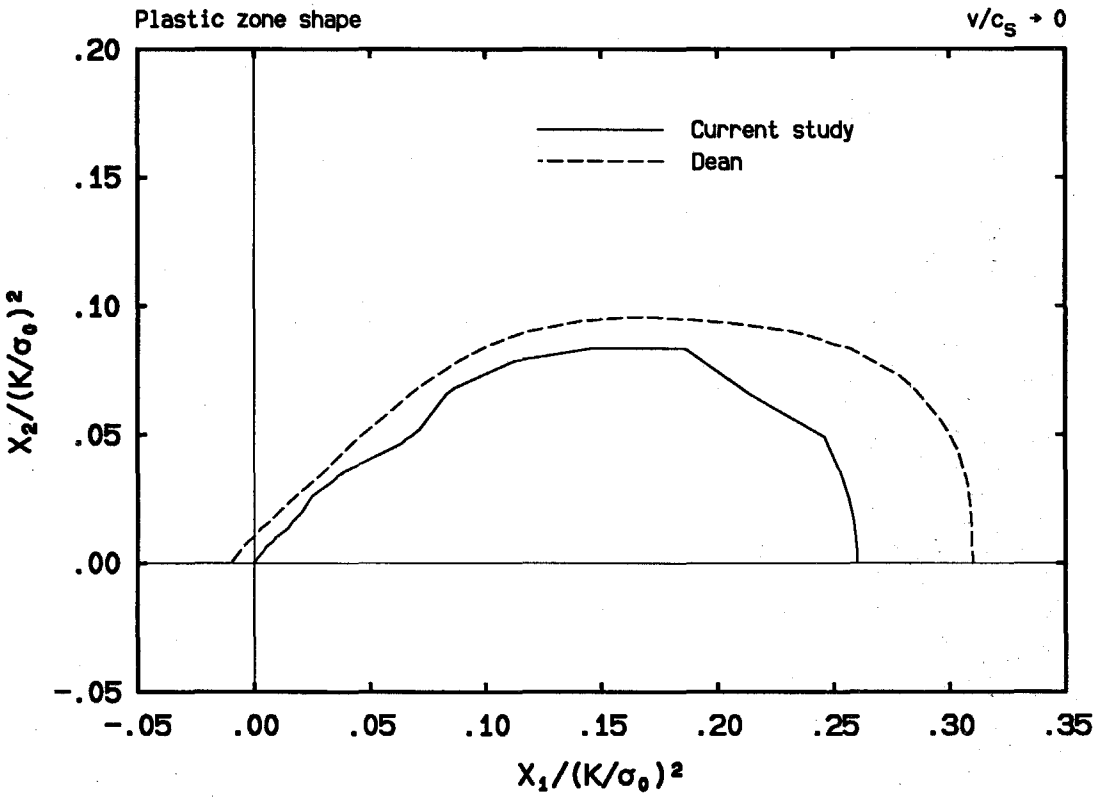

FIGURE 3.2.1 The shape of the crack tip active plastic zone compared with that by Dean (1983) in normalized coordinates, with the origin located at the crack tip.

release where the crack has advanced quasi-statically a distance of $0.04(K/\sigma_0)^2$. In other words, as the crack extends, the active plastic zone shrinks along the prospective crack line. The same is observed in the Mode III case where Sorensen (1978) noted that R_p is about 4% smaller than the stationary value at the end a of few node releases. If we recall that the results by Sorensen and by Narasimhan et al. were for a transient crack, and that the active plastic zone size is not a local issue, we may then assume that R_p for the steady state case should be even smaller. This is indeed manifested by the Mode III calculations of Douglas (1981) and Lam (1982), whose solutions show that R_p should be about 13% smaller than the stationary counterpart. Considering the similarities between Mode III and Mode I plane stress fracture, as pointed by McClintock and Irwin (1964), it is plausible

to expect a similar result in plane stress. It is also interesting to notice that R_p obtained by Dean and Hutchinson (1980) for steady state quasi-static Mode III crack growth is also much higher (10%) than its stationary value, contrary to the findings of more detailed studies by Douglas and Lam as mentioned above.

The 45^0 angular extent of the active plastic zone at the crack tip is confirmed by the results of Dean, Narasimhan et al. This seems to be expected since very near the crack tip, the elastic-plastic boundary angle appears to be a local quantity, thus it should be close to the steady state value. Strangely, however, the angle shown by Luo et al. is almost 90^0, which we think is due to numerical errors.

Angular Field Variations

In order to examine the angular variations of field quantities and to minimize the effects of any real or numerically created radial dependence, data regarding the angular variations of field quantities are extracted from near-tip finite elements along a circular path of radius approximately $2.0 \times 10^{-4}(K/\sigma_0)^2$, which is about 5 elements away from the crack tip.

The angular variations of the crack tip stress field are shown in Fig. 3.2.2a for the effective stress and the polar stress components, and in Fig. 3.2.2b for Cartesian rectangular stress components. Comparisons with finite element solutions by Dean, by Narasimhan et al., and Luo et al. are included.

It is seen from Fig. 3.2.2a that while the angular variations of stress components $\sigma_{\theta\theta}$ and $\sigma_{r\theta}$ are quite similar to those of the stress characteristic line solution by Hutchinson (1968b), the σ_{rr} component behaves very differently. In Hutchinson's solution, which is for a stationary crack, there is a discontinuity in σ_{rr} at an angle of about 150^0. Moreover, his solution reveals that σ_{rr} reaches $-\sigma_0$ at the traction-free crack surface, and thus the stress state there is actively yielded. However, in the present quasi-static crack extension case, no discontinuity and no reverse loading

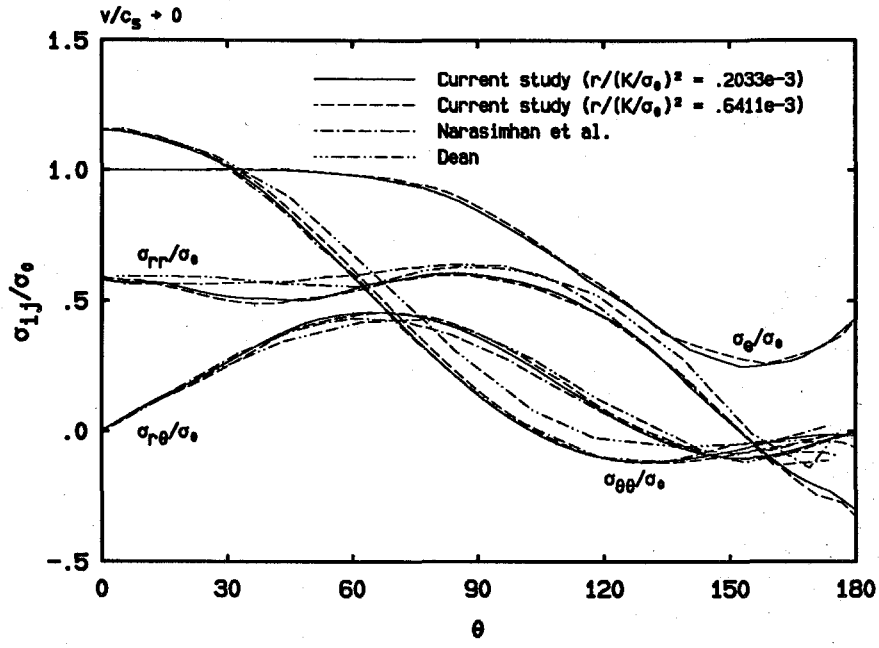

FIGURE 3.2.2a Angular variations of the effective stress and the polar stress components, compared with the results by Dean (1983) and Narasimhan, Rosakis and Hall (1987a).

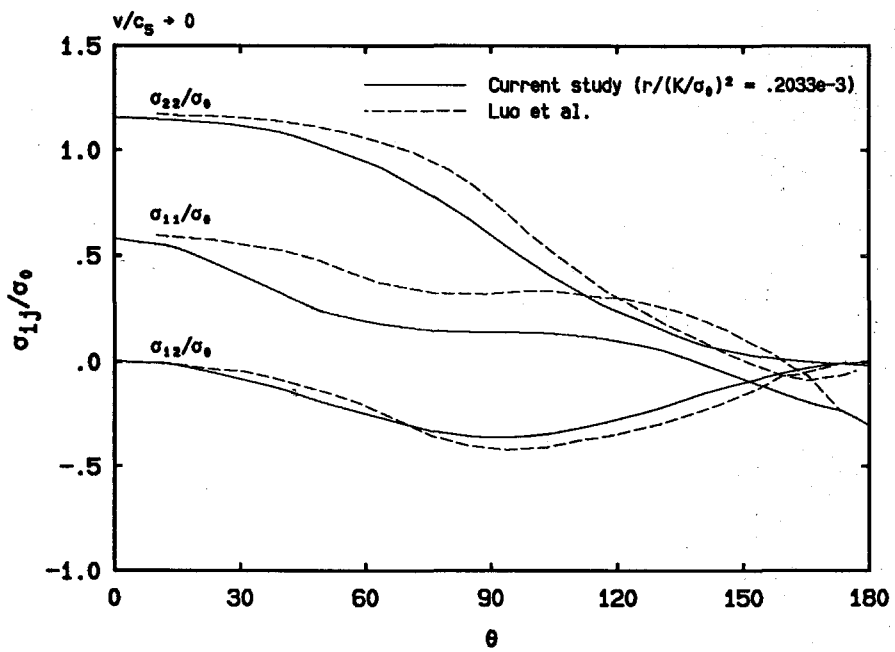

FIGURE 3.2.2b Angular variations of the Cartesian stress components, compared with the results by Luo, Zhang and Hwang (1984).

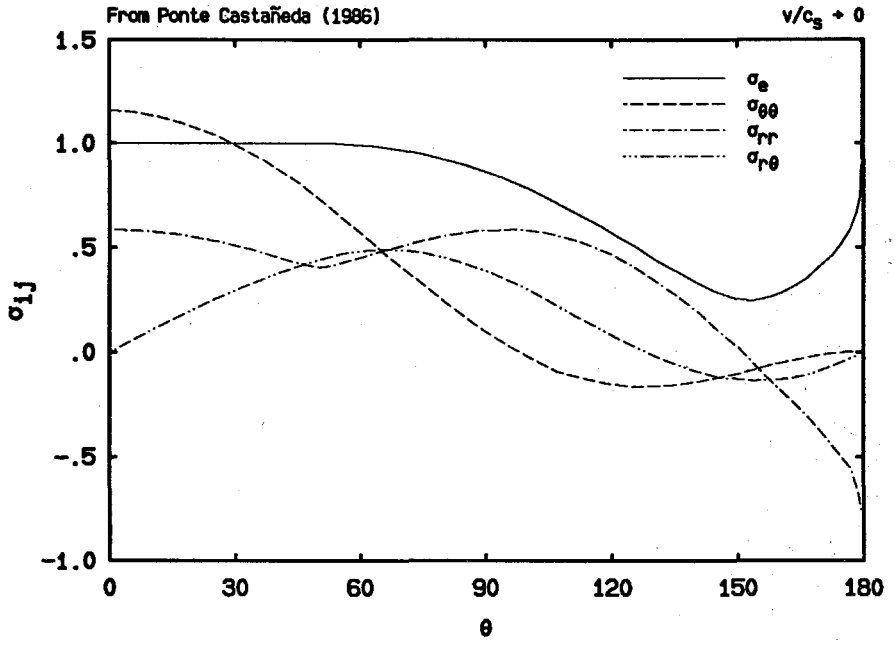

FIGURE 3.2.2c Angular variations of the effective stress and the polar stress components in their original normalized forms for low-hardening bilinear solids (Ponte Castañeda, 1987a).

at the back of the crack tip are observed, although the present numerical solution does clearly indicate a compressive zone for σ_{rr} along the crack flank.

Further, in accord with observations from the active plastic zone shape, it is found that the effective stress σ_e deviates from 1.0 or the value of the yield stress at approximately $\theta = 45^0$ where elastic unloading takes place. It is also obvious that there is a tendency of reverse plastic loading at the back of the crack tip, but it seems that this tendency is not strong enough to reach yielding.

Overall comparisons as shown in the figures tell that agreement is best with those of Narasimhan et al., good with Dean's, and bad with the ones by Luo et al. Actually the comparison is almost perfect with Narasimhan et al. for $\sigma_{\theta\theta}$, $\sigma_{r\theta}$ and for σ_{rr}, except that σ_{rr} of the latter authors' solution prematurely flattens out near the crack surface. As to Dean's solution, it is seen that $\sigma_{r\theta}$ obviously deviates at the crack surface from the traction-free condition and that at the same time σ_{rr}

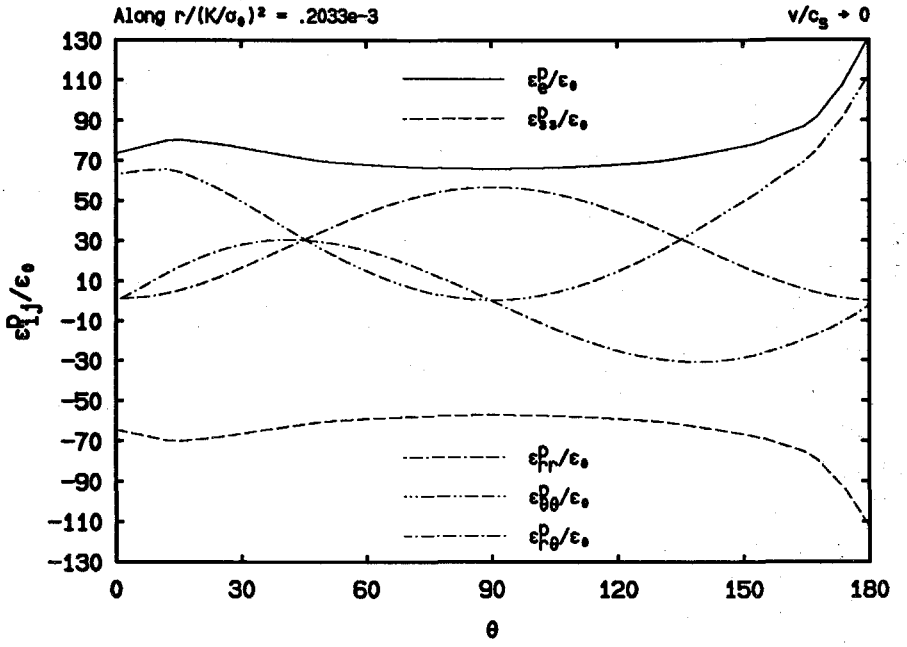

FIGURE 3.2.3a Angular variations of the effective plastic strain, the out-of-plane plastic strain, and the polar plastic strain components.

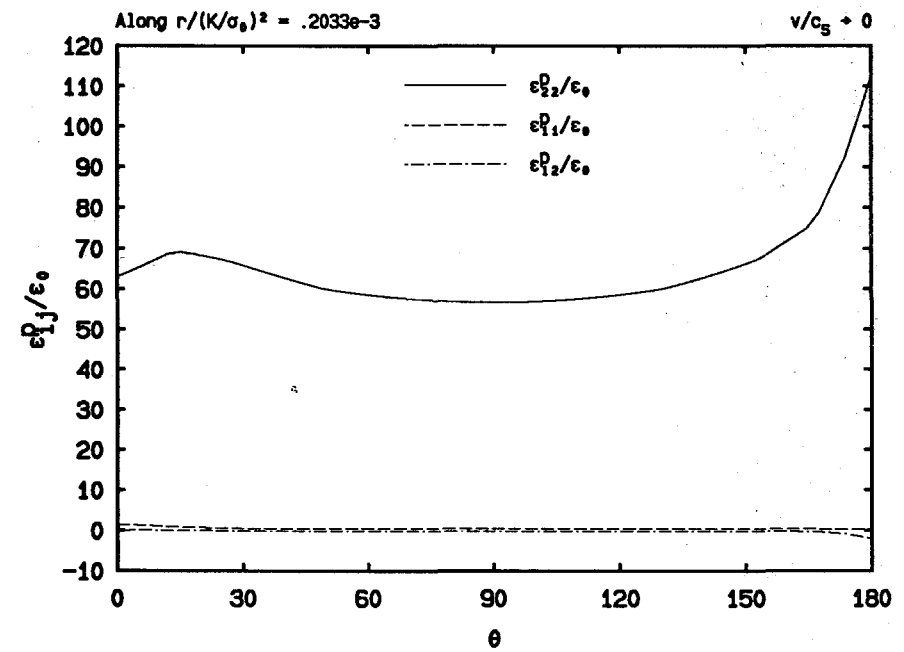

FIGURE 3.2.3b Angular variations of the Cartesian plastic strain components.

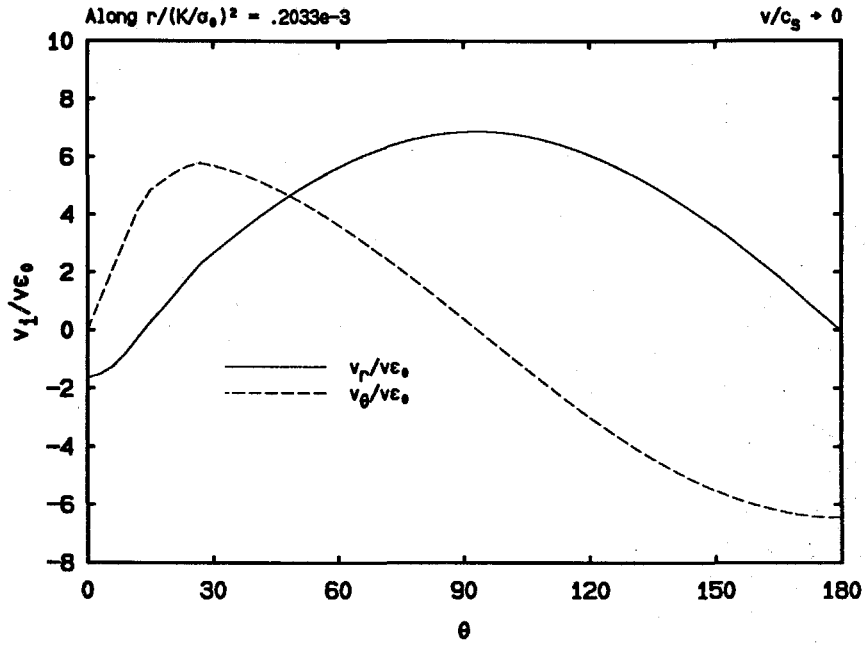

FIGURE 3.2.4a Angular variations of the polar velocity components.

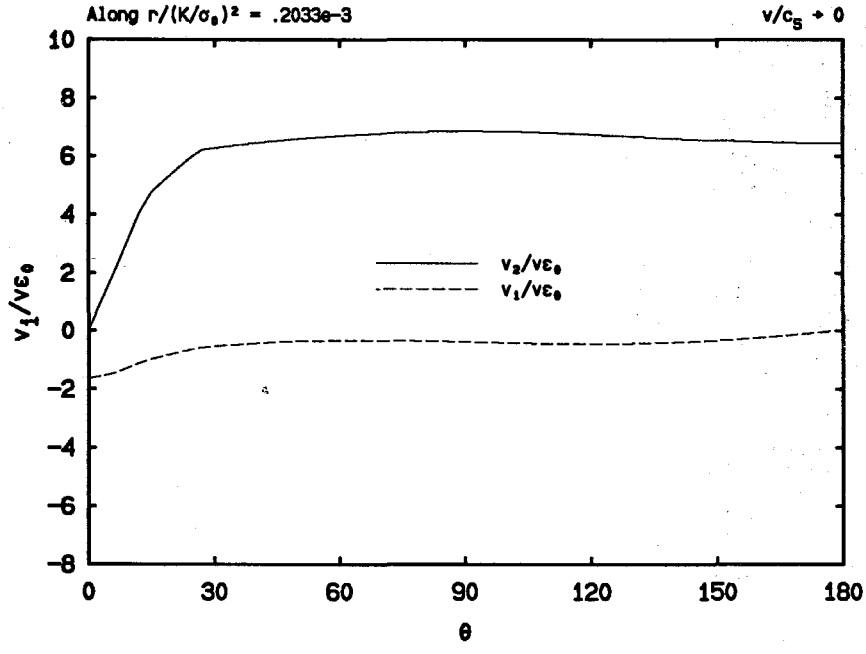

FIGURE 3.2.4b Angular variations of the Cartesian velocity components.

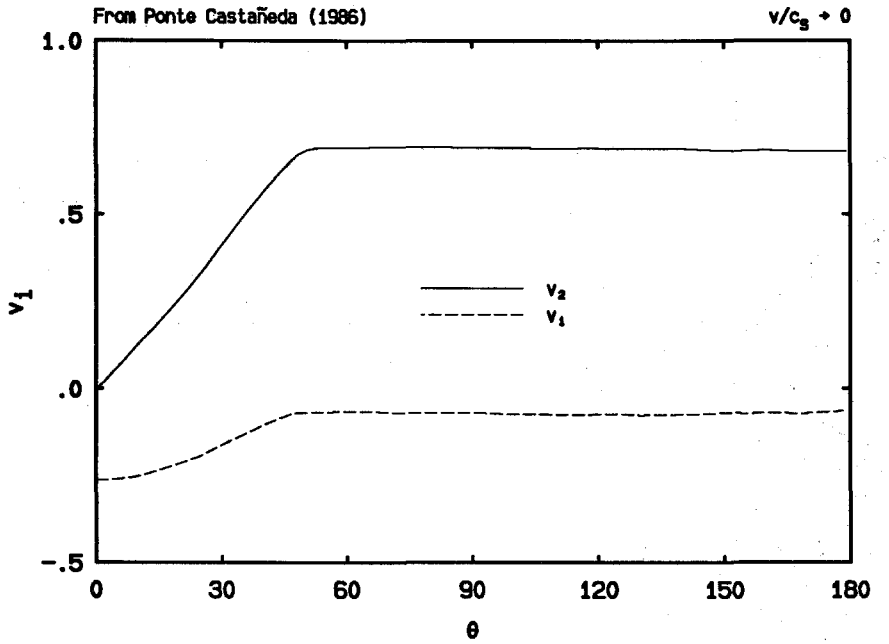

FIGURE 3.2.4c Angular variations of the Cartesian velocity components in their original normalized forms for low-hardening bilinear solids (Ponte Castañeda, 1987a).

tends to zero. It is of our opinion that this is due to the possibly large discretization error accumulated at the crack tip and carried over to the area behind the crack tip. At this stage, we would like to call your attention to the fact that we utilized a much finer mesh than the previous investigators, and that our data are drawn from a circular path much nearer to the crack tip. Besides, the results by Luo et al. and Narasimhan et al. are for a rectangular path about $1.0\times10^{-2}(K/\sigma_0)^2$ away from the crack tip, which inherently adds some radial dependence to the stress variations. It is also helpful to point out that the low-hardening limit solution by Ponte Castañeda (1987a) for bilinear elastic-plastic materials (see Fig. 3.2.2c) strongly resembles our solution, particularly for σ_{rr} near the crack flank and in the range $\theta \in (20^0, 80^0)$ where it heads down and then rises. Note that for comparison purposes, the finite element results from a slightly coarser mesh (see section 3.3 for more detail) and along a farther circular path whose normalized radius is $r/(K/\sigma_0)^2 = .6411 \times 10^{-3}$ is also included in Fig. 3.2.2a. Excellent agreement between the two finite element

solutions is observed, as is expected.

Angular plastic strain variations are shown in Figs. 3.2.3a and 3.2.3b,with strains being normalized by ε_0, the initial yield strain in tension. From the distributions of polar components we observe for most of the angular range that the in-plane components behave in a sinusoidal-like fashion and that the effective plastic strain ε_e^p and the out-of-plane component ε_{33}^p are fairly flat. This behavior becomes apparent if the variations of the rectangular components are first examined. From Fig. 3.2.3b it can be seen that while the 1-1 and 1-2 components are almost identically zero, the 2-2 component is predominantly large and it undergoes only small percentage changes for most of the angular ranges. A simple tensorial transformation will then give rise to the observed phenomena in Fig. 3.2.3a. Note that the plastic strains outside the active plastic zone are the residual plastic strains determined at the elastic-plastic boundary. The rapid rising part of ε_{22}^p, and hence ε_e^p and ε_{33}^p, near the crack flank are due to the accumulated plastic strains at the crack tip, which theoretically may be unbounded if the strains are singular at the crack tip in the active plastic zone.

We present in Figs. 3.2.4a and 3.2.4b the results of the velocity field normalized by $v\varepsilon_0$, where v is the crack speed. From Fig. 3.2.4a we see that the tangential component v_θ starts at $\theta = 0$ with zero value, apparent due to the symmetry condition, and ends negatively at $\theta = \pi$, whereas the radial component v_r starts negatively and ends with zero. But the rectangular velocity component distribution tells a more interesting story. It is seen that v_1 is always negative and v_2 is always positive, and that both v_1 and v_2 increase initially and then level off at about $\theta = 30^0$, with v_2 having a much larger absolute value after $\theta \doteq 15^0$. Actually in the elastic zone, which is about 45^0 to 180^0, the Cartesian components should have asymptotically logarithmic singularities with constant coefficints (see, for example, Rice, 1982 or Ponte Castañeda, 1987a). In fact, it can be shown that the coefficient for v_1 must be zero if there is no reverse yielding along the crack flank. Therefore the

slight velocity variations in the elastic zone are due to their bounded or less singular terms. Note also that the Cartesian velocity component variations are qualitatively very similar to those of the asymptotic low-hardening solutions for bilinear solids (Ponte Castañeda, 1987a) as shown in Fig. 3.2.4c.

Radial Field Variations

Radial stress variations along the prospective crack line are shown in Fig. 3.2.5a, covering the elastic-plastic transitional region, and in Fig. 3.2.5b with a detailed view of the crack tip zone. Note that the radial distance is normalized by $(K/\sigma_0)^2$. At the crack tip it is seen that σ_{11} and σ_{22} take values very close to τ_0 and $2\tau_0$ respectively, where τ_0 is the initial yielding stress in simple shear. This finding is somehow in agreement with the asymptotic results in Eq.(3.1.5) if θ_1 is taken to be zero as suggested by Rice (1982). Away from the tip σ_{11} is found to increase monotonically all the way up to the elastic-plastic boundary, whereas σ_{22} slightly decreases. This result contradicts the assumption employed by many crack line solutions (Achanbach and Dunayevsky, 1984; Achenbach and Li, 1984c; and Guo and Li, 1987) that σ_{22}, and hence σ_{11}, are identically constant in the plastic zone along the crack line. It is also observed that further away from the elastic-plastic boundary, but in the elastic region, σ_{11} and σ_{22} tend to coincide with each other, which means they are, as expected, approaching the far-field singular elastic solution. A comparison to the results of Narasimhan et al. is made in Fig. 3.2.5b with very good agreement.

Figs. 3.2.6a and 3.2.6b are for the crack line plastic strain distributions. It is found in Fig. 3.2.6a that ε_{22}^p and hence ε_e^p greatly exceed ε_{11}^p in magnitude and possess logarithmic-like singularities as the crack tip is approached. This singular behavior is more clearly demonstrated by the log-scale plot in Fig. 3.2.6b where a linear relation exists in the crack tip region, which strongly suggests that both ε_e^p and ε_{22}^p vary as lnr as the crack tip is approached. Luo et al. (1984) also

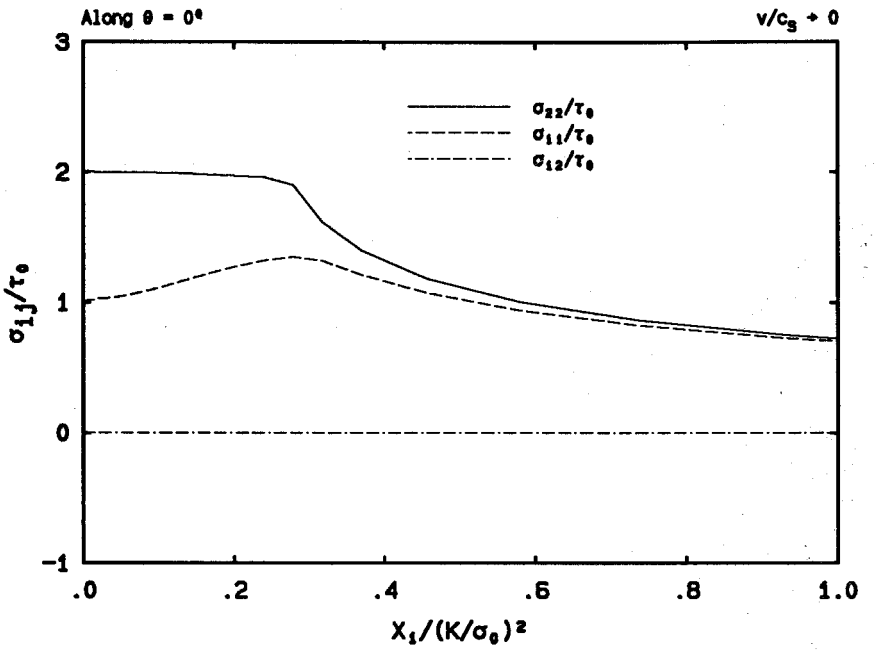

FIGURE 3.2.5a Radial distributions of the stress components at crack front.

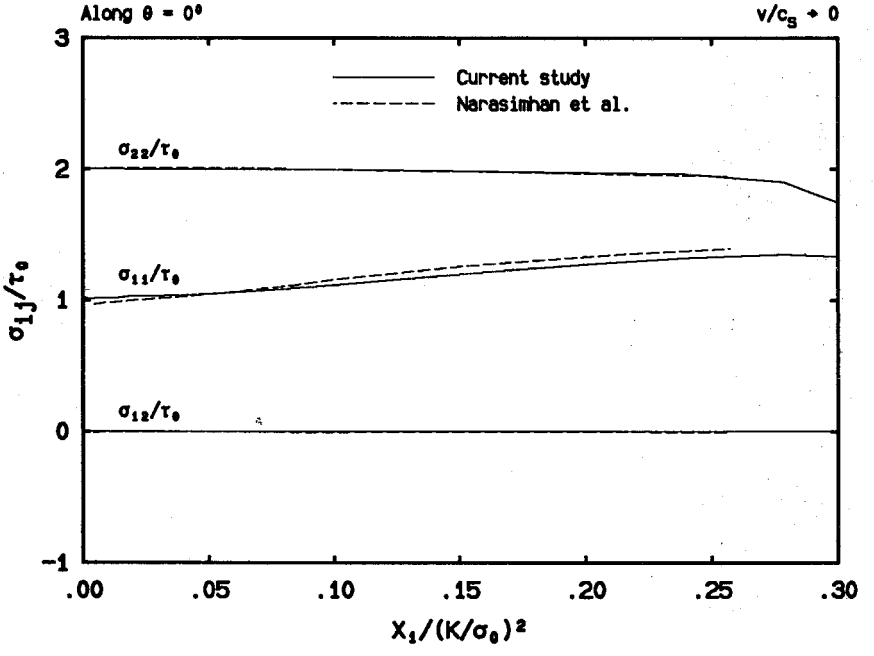

FIGURE 3.2.5b Detailed view of the radial dependence of the stress components at crack front.

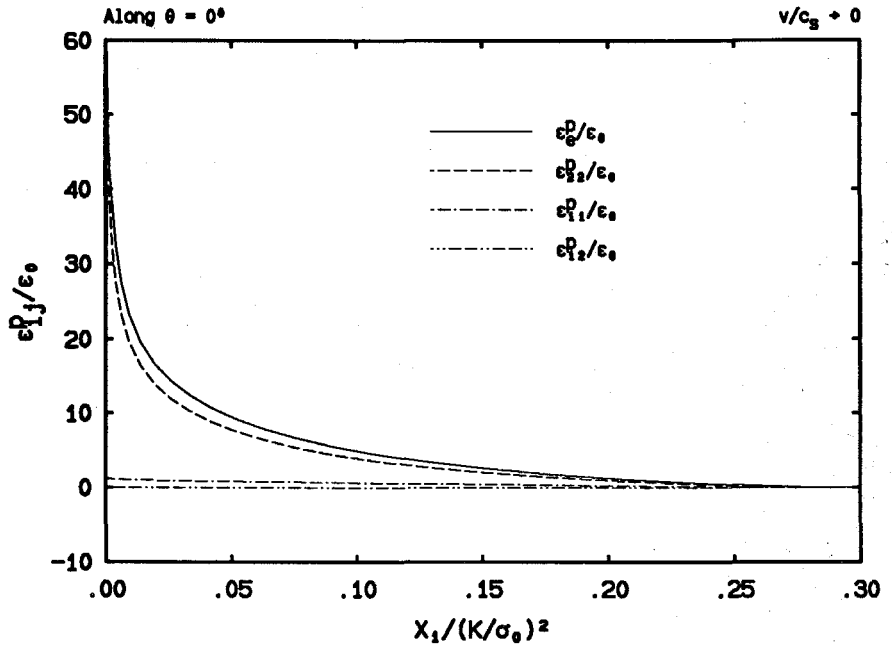

FIGURE 3.2.6a Radial distributions of the plastic strain components at crack front.

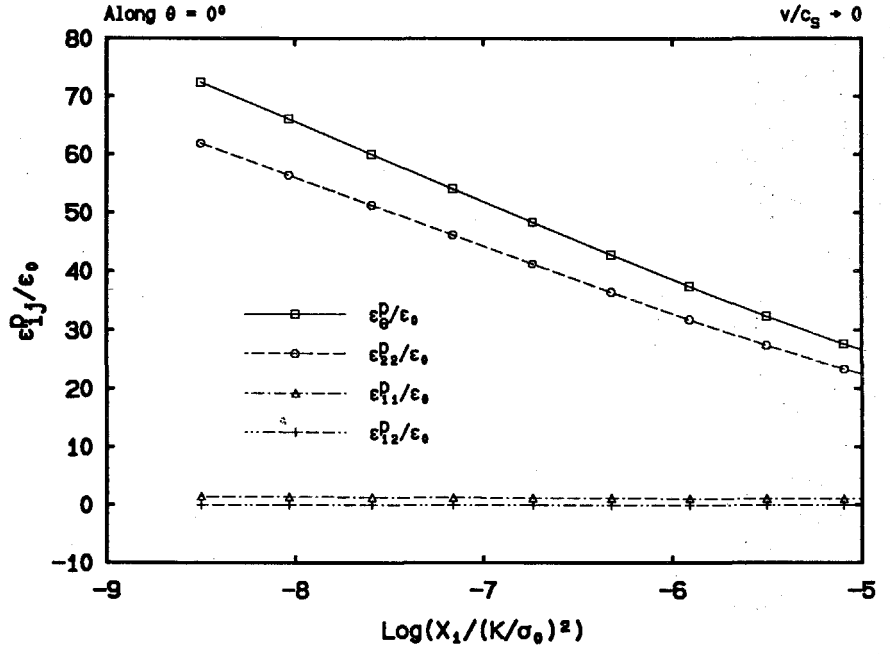

FIGURE 3.2.6b Radial distributions of the plastic strain components at crack front, plotted against the logarithmic values of the normalized distance.

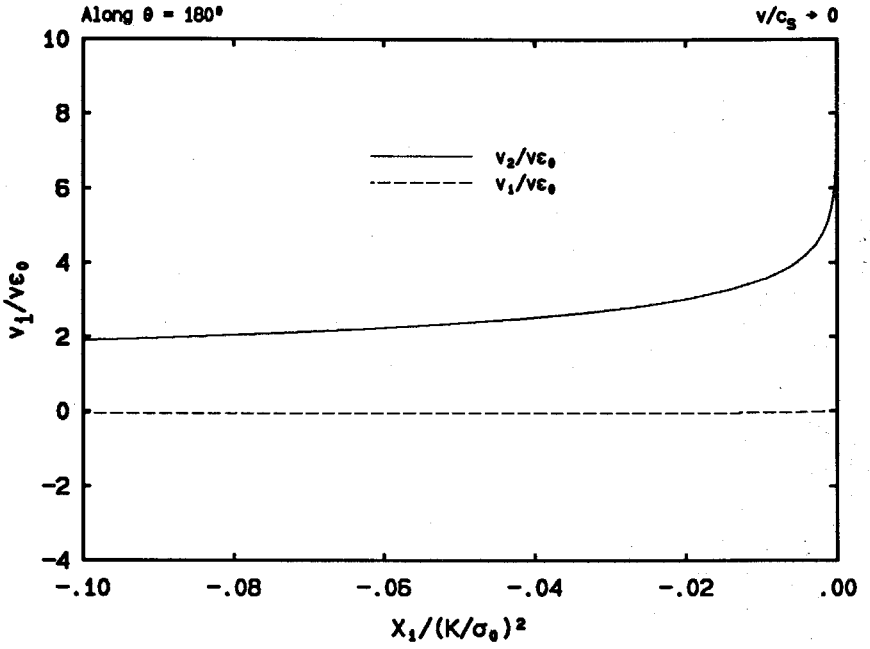

FIGURE 3.2.7a Radial distributions of the velocity components at crack front.

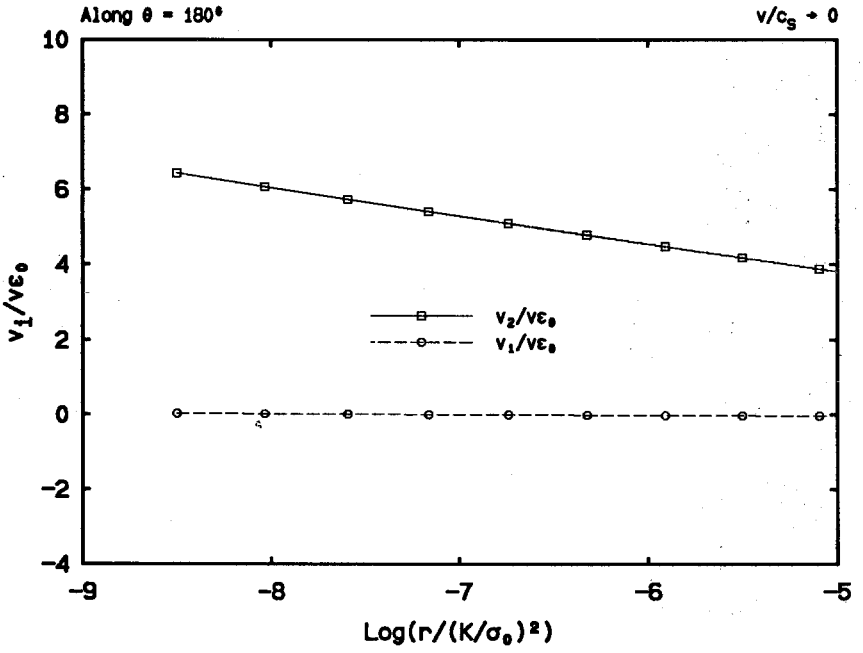

FIGURE 3.2.7b Radial distributions of the velocity components at crack front, plotted against the logarithmic values of the normalized distance.

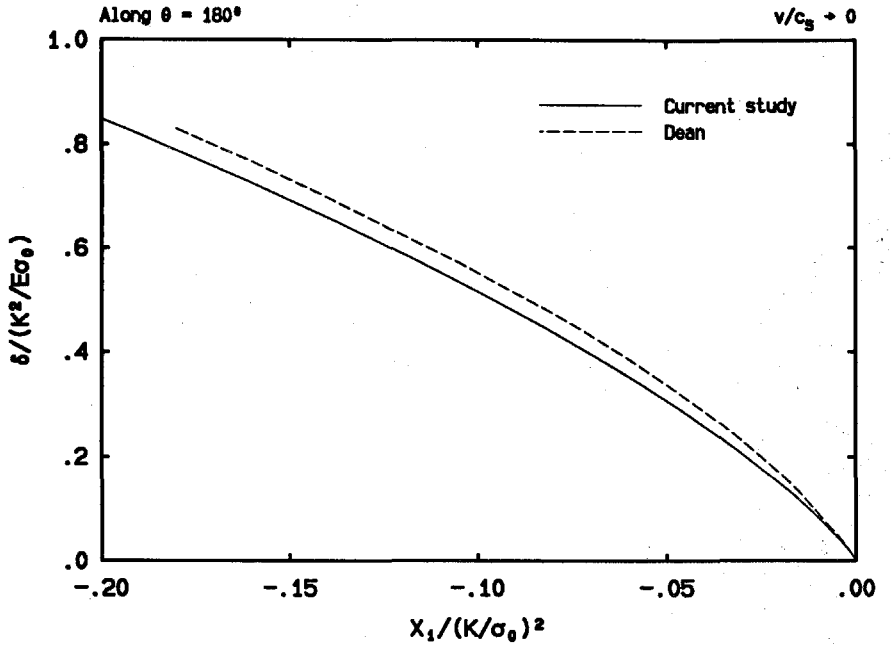

FIGURE 3.2.8 Radial dependence of the crack opening displacement.

discovered such a singular tendency. As to the 1-1 component, a horizontal line is observed in Fig. 3.2.6b, which indicates that ε_{11}^p almost has no lnr dependence. The 1-2 component is found to be identically zero as is expected from the symmetry condition.

Presented in Figs. 3.2.7a and 3.2.7b are the velocity component variations along the crack flank. It is seen from Fig. 3.2.7a that while v_1 is almost invariably zero, v_2 behaves singularly near the crack tip. The log-scale plot in Fig. 3.2.7b tells that this is a logarithmic singularity as can be predicted by a simple asymptotic analysis.

Finally we proceed to examine the crack opening displacement profile as shown in Fig. 3.2.8, where the opening displacement δ (twice of the vertical displacement component u_2) is normalized by $K^2/E\sigma_0$ with E being the Young's modulus. Note that while in the stationary case there is a blunt opening at the crack tip, here in the quasi-static case we observe a sharp crack opening. This conclusion is also confirmed by Dean (1983) except that he predicted a somewhat larger crack opening profile as

shown in Fig. 3.2.8. Analytically, since velocities possess *lnr* singularity, the crack profile should then behave like *rlnr* as the crack tip is approached, and hence it intersects the crack surface with a right angle. Our numerical results, however, do not show such an infinite slope at the crack tip, which is probably due to the finite element discretization error.

Asymptotic Analysis

There is as yet no successful assembly of crack tip asymptotic fields for quasi-static Mode I plane stress crack growth in elastic-perfectly plastic solids. We summarize here some observations and try to shed light on this somewhat illusive problem.

First of all, when a constant stress sector is adjacent to a centered fan sector, its velocity components must be less singular than those in the centered fan, i.e., less singular than *lnr*, if the maximum plastic work principle is to be satisfied. This can be derived from the constitutive law, and from the fact that along the interface boundary, the deviatoric polar stress component S_{rr} equals zero at the centered fan side and hence also at the constant stress sector side. This is because the maximum plastic work principle requires that the stresses be continuous across the boundary (see, for example, Narasimhan and Rosakis, 1987). Hence, it can be shown that plastic strains in such a constant stress sector cannot have logarithmic singularities.

Secondly, a constant stress sector cannot immediately follow a centered fan sector if the maximum plastic work principle is employed. Just as in the plane strain case, if a centered fan sector is followed by a constant stress sector, then when the boundary between the two sectors is crossed as the crack extends, the positive shear stress $\sigma_{r\theta}$ does infinitely negative work as r goes to zero, which is in violation of the maximum plastic work principle. This is because the radial velocity component v_r tends to be infinitely positive on the centered fan side as the crack

tip is approached. Whereas due to the reduced singularity of v_r on the side of the constant stress sector, the magnitude of v_r tends to be much less there. Hence the difference in v_r from the centered fan to the constant stress sector is infinitely negative as the crack tip is approached.

Thirdly, a constant stress sector is not likely to exist at the crack front and be followed by a centered fan sector, since otherwise the plastic strains would not, as we discussed above, possess a logarithmic-like singularity when the crack tip is approached. It is, however, demonstrated by our detailed numerical results that they should behave logarithmically.

Finally, if a centered fan sector is to exist at the crack front, it appears that it is valid along the crack line only at the limit $r = 0$. In other words, the centered-fan field variations, and the strain rate distribution in particular, do not hold on any length scale away from the crack tip. As shown by our finite element solution, the asymptotic values for σ_{rr} and $\sigma_{\theta\theta}$ at $r = 0$ along the crack line are τ_0 and $2\tau_0$ respectively, and $\sigma_{r\theta} = 0$ due to the symmetry condition, whereas away from the crack tip, it is clearly seen that σ_{rr} rises above τ_0 and $\sigma_{\theta\theta}$ steadily decreases from $2\tau_0$, which means that the stresses are in an elliptic plastic state (see Kachonov, 1974). Since a parabolic characteristic line is a line along which the two principal stress values are equal to $\pm\tau_0$ and $\pm 2\tau_0$ respectively, it is then expected that the parabolic line (see results by Narasimhan, Rosakis and Hall, 1987a), which divides the centered fan in the hyperbolic state from the parabolic state, terminates at the crack tip and is only tangent to the crack line there. A higher order asymptotic analysis by Krishnaswamy and Rosakis (1990b), in connection with the finite element analysis of Narasimhan, Rosakis and Hall (1987a), also demonstrates this point. One of the immediate consequences of this is that it may prohibit an integration of strain rates to obtain plastic strains along the crack line. In other words, instead of obtaining a $ln^2(r)$ plastic strain singularity along $\theta = 0$ as suggested by Rice (1982) and Narasimhan, Rosakis and Hall (1987a), we would only get a lnr

singularity, which seems to agree with our numerical observations.

3.3 DYNAMIC CRACK PROPAGATION

Published studies on the stress and deformation fields around a rapidly propagating crack tip in an elastic-perfectly plastic solid under plane stress or generalized plane stress conditions are rare. Achenbach and Li (1984a, b) proposed a crack line solution for Mode I steady state which assumes that σ_{22} and hence σ_{11} are constant along $\theta = 0$ from the crack tip up to the elastic-plastic boundary, which is then used to extract a theoretical K_{Ic}^d vs. v curve, where K_{Ic}^d is the plane stress fracture toughness, and v the crack tip speed. However, to interpret their findings correctly, it is necessary to verify the assumptions which form the very basis of their analysis. There are no such verifications available as of today.

Gao (1987) on the other hand obtained an analytic Mode I solution valid asymptotically in the crack tip area. Due to the mathematical complexities involved in the analysis and due to the limited data presented in his paper, it is difficult to judge with confidence whether this solution is unique or appropriate. Besides, from the experience of Mode III fracture, it is suspected that any first-order asymptotic dynamic solution would only have a restricted near-tip domain of validity which decreases rapidly as the crack tip velocity goes to zero. This poses a problem when one is interested in getting a crack-velocity dependence for a certain physical quantity, say for the dynamic fracture toughness.

It is apparent then that detailed full field numerical studies will greatly help to resolve the issues mentioned above. To our best knowledge, the results presented in the following document the first published effort to investigate numerically the stress and deformation fields under plane stress conditions.

Two mesh designs with slightly different near-tip mesh refinements were used in our study. The finer mesh, which has a ratio of plastic zone size to the smallest

near-tip element size on the order of 1.6×10^4, is employed to study a typical dynamic case, namely the case for $m = 0.3$, where m is the ratio of the crack tip speed to the material elastic shear wave speed. The slightly coarser mesh is used, for cost considerations, to carry out computations for the whole range of m values from 0.0 to 0.4, where $m = 0$ describes the quasi-static crack growth. The evolutionary variations of field quantities with respect to m are thus obtained.

The Active Plastic Zones

The variation of the active plastic zone shapes with respect to the Mach number m is shown in Fig. 3.3.1a, where the coordinates are nondimensionalized through the usual normalization $(K/\sigma_0)^2$, with K being the dynamic stress intensity factor, and σ_0 the initial yield stress in tension. It is observed that as m or the normalized crack speed increases, the active plastic zone shrinks along the crack line from size $0.265(K/\sigma_0)^2$ at $m = 0.0$ to $0.255(K/\sigma_0)^2$ at $m = 0.4$, and it spreads out from size $0.084(K/\sigma_0)^2$ to about $0.15(K/\sigma_0)^2$ in the direction perpendicular to the crack line, which almost doubles the quasi-static value. The near-tip angular extent of the active plastic zone also grows as m becomes larger, actually from 45^0 at $m = 0.0$ to about 90^0 at $m = 0.4$, as shown by an expanded view of the crack tip zone in Fig. 3.3.1b. From this figure, a secondary active plastic zone, or a reversed yielding zone, is clearly revealed for $m = 0.35$ and 0.4 near the crack flank. The variations of the angular extent of the primary near-tip active plastic zones with respect to m is shown in Fig. 3.3.1c. This type of plastic zone arrangement is very similar to the findings of Douglas (1981) for Mode III dynamic crack propagation, utilizing the same finite element technique as used in this study. While the asymptotic solution by Slepyan (1976) for Mode III predicts an allaround plastic zone, which is not confirmed by Douglas's investigation, Gao's Mode I plane stress asymptotic solution anticipates an elastic unloading sector behind the primary active plastic zone, which is somewhat consistent with our numerical results.

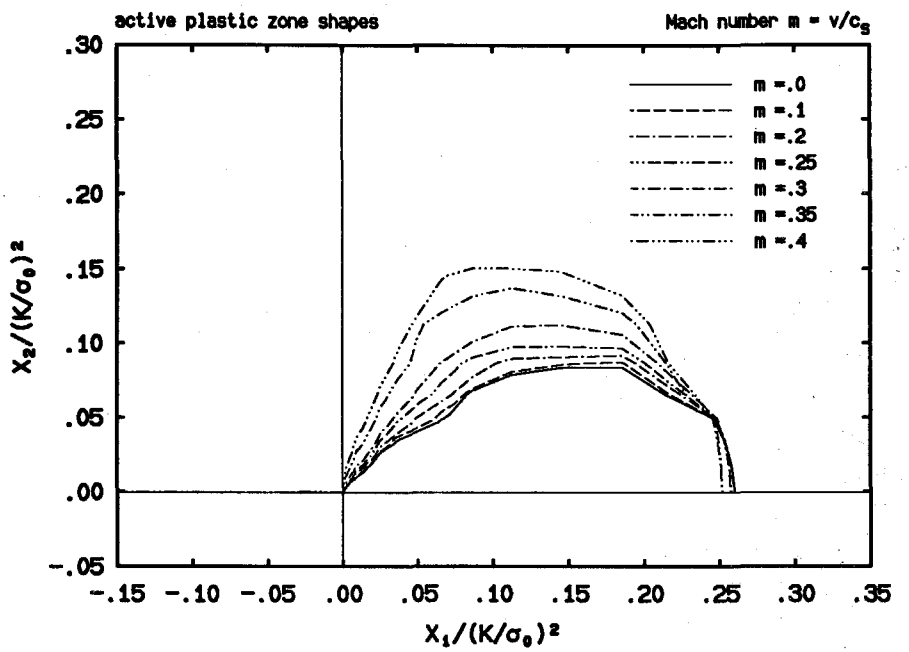

FIGURE 3.3.1a Active plastic zone shapes for various normalized crack propagation velocities, with the origin located at the crack tip.

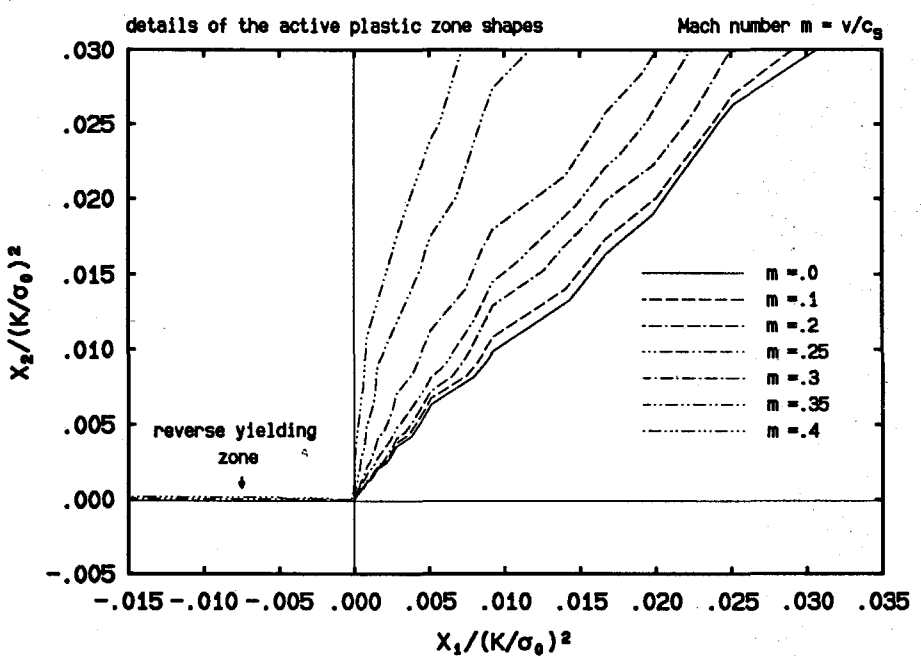

FIGURE 3.3.1b Detailed view of the active plastic zone shapes at the crack tip for various normalized crack propagation velocities, with the origin located at the crack tip.

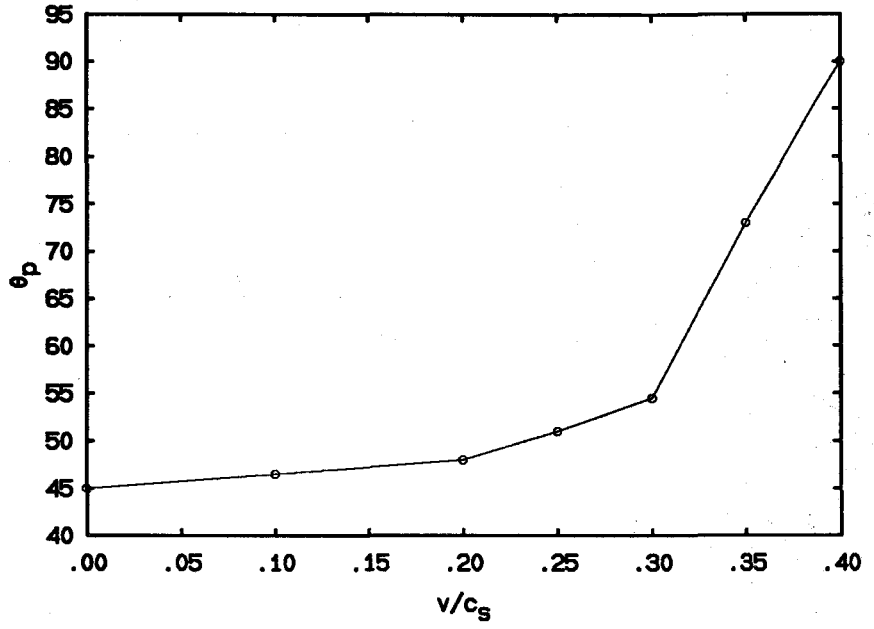

FIGURE 3.3.1c The variations of the angular extent of the near-tip active plastic zones with respect to the normalized crack speed.

Angular Field Variations

As in the quasi-static case, our angular field variations are obtained from finite element data extracted from locations about 5 elements away from the crack tip along a circular path with a distance to the tip of $0.2033 \times 10^{-3}(K/\sigma_0)^2$ for the finer mesh, which is about one thirteen-hundredth of the plastic zone size, and of $0.6411 \times 10^{-3}(K/\sigma_0)^2$ for the coarser mesh, which is about one four-hundredth of the plastic zone size.

In conjunction with the above observed reverse yielding phenomenon, the angular effective stress distribution presented in Fig. 3.3.2a gives details regarding the evolutionary tendency toward a secondary active plastic zone at the back of the crack tip, where σ_e, the effective stress, regains its yielding value σ_0 for $m = 0.35$ and 0.40. The asymptotic solution by Gao (1987) shows, however, that the secondary active plastic zone exists for all values of m from 0.0 to 0.3. Especially, he

found that the angular extent of this reverse yielding zone increases as m decreases, which is strongly contrary to our findings.

Fig. 3.3.2a also tells that the effective stress deviates from σ_0 at about $\theta = 45^0$ for $m = 0.0$, and 90^0 for $m = 0.4$, thus confirming our earlier discoveries pertaining to the angular extent of the primary active plastic zones at the crack front. Again Gao's results predict different active plastic zone angles, which, in his calculations, are always larger than 90^0.

Next we discuss the θ-dependence of other stress components as shown in Fig. 3.3.2b. First we want to point out that the symmetry condition at the crack front and the traction-free condition at the back are well satisfied. We emphasize this because with the Eulerian-type finite formulation we employed, stresses are obtained through integration of the incremental constitutive law, along lines parallel to the crack line, from crack front downstream to the area behind the crack tip. When the integration sweeps the crack tip, the inevitable large discretization error at the crack tip is carried over to regions behind. It is then expected that most discretization errors are accumulated along the crack flank and the momentum-balance iterations are mostly carried out to minimize the error there. Hence the satisfaction of the boundary conditions at the crack surface is a major indication of a converged numerical solution.

It is then seen from Fig. 3.3.2b that the changes of $\sigma_{\theta\theta}$ with respect to θ are smooth for all values of m, and that while the changes in σ_{rr} and $\sigma_{r\theta}$ are smooth for lower m values, a kink develops for higher m values, notably for the case of $m = 0.4$ at $\theta \doteq 90^0$, where the boundary between the active plastic zone and the elastic unloading zone is located approximately. This seems to agree qualitatively with the analytic predictions by Gao (1987), although quantitatively large differences exist.

The angular variations of the Cartesian rectangular stress components are shown in Fig. 3.3.2c, for the typical case of $m = 0.3$. It is found that σ_{22} and

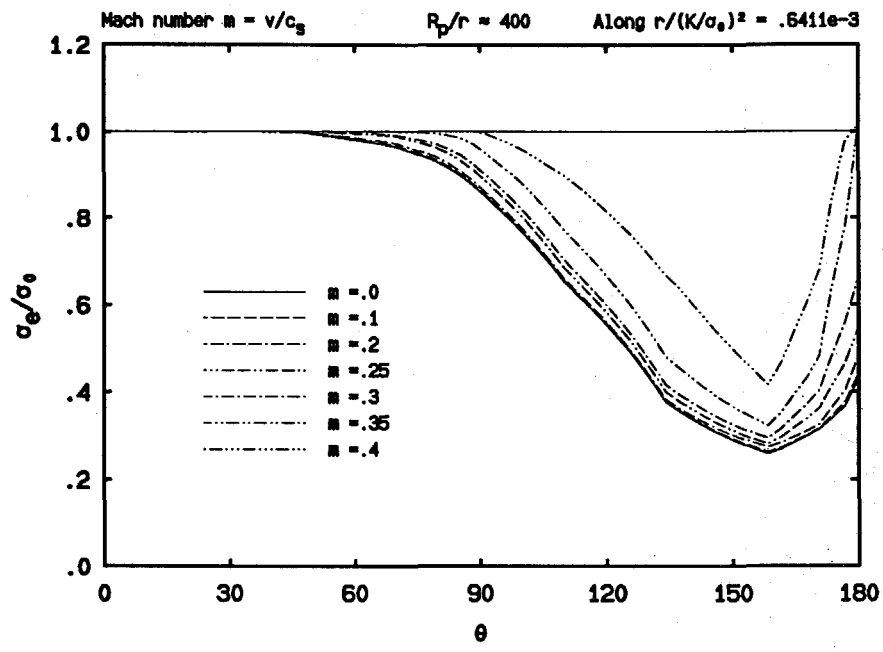

FIGURE 3.3.2a The angular dependence of the effective stress for various normalized crack speeds.

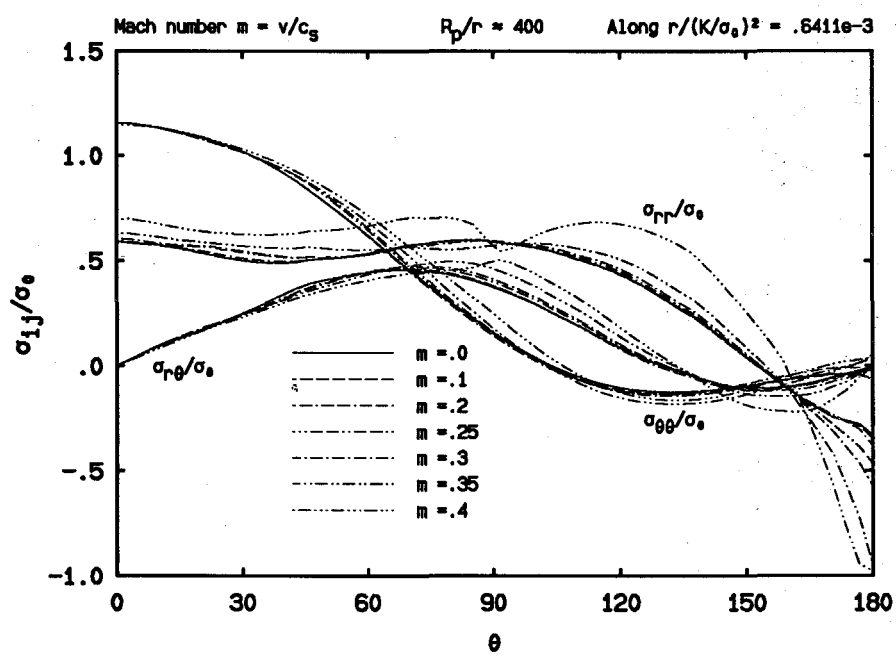

FIGURE 3.3.2b The angular dependence of the polar stress components for various normalized crack speeds.

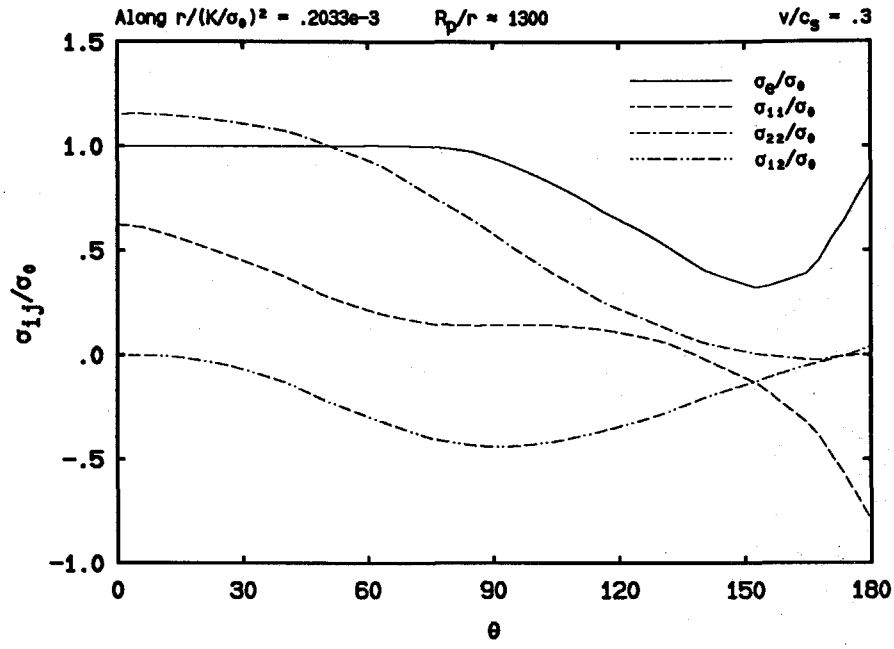

FIGURE 3.3.2c The angular dependence of the Cartesian stress components for $v/c_s = 0.3$.

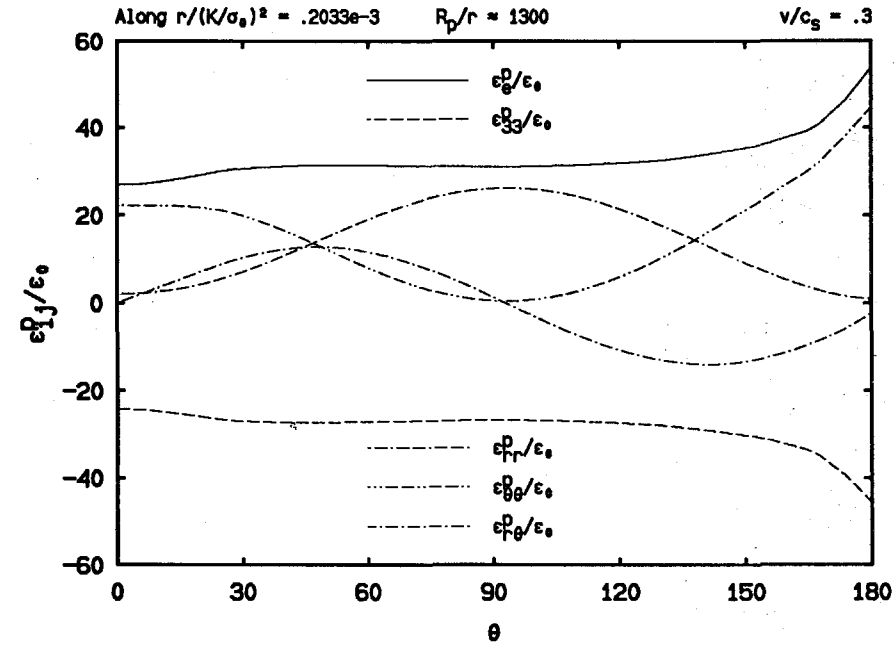

FIGURE 3.3.3a The angular dependence of the effective plastic strain, the out-of-plane plastic strain and the polar plastic strain components for $v/c_s = .3$.

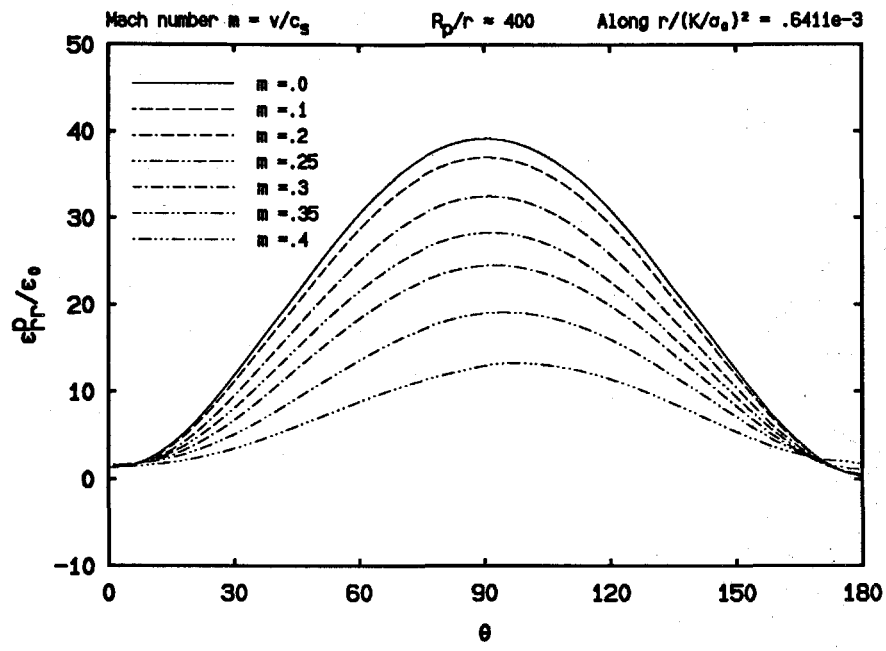

FIGURE 3.3.3b The angular dependence of the r-r polar plastic strain component for various normalized crack speeds.

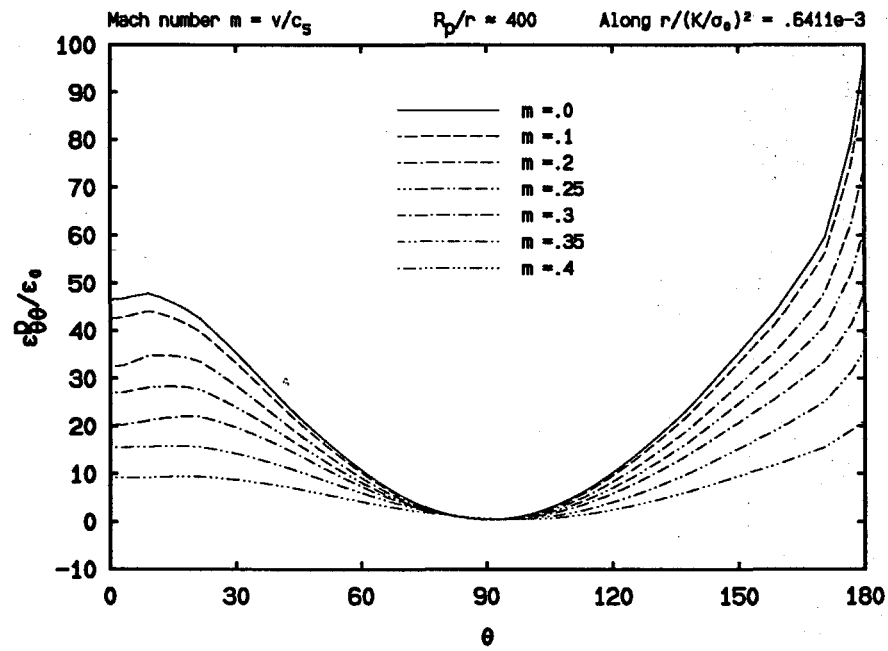

FIGURE 3.3.3c The angular dependence of the θ-θ polar plastic strain component for various normalized crack speeds.

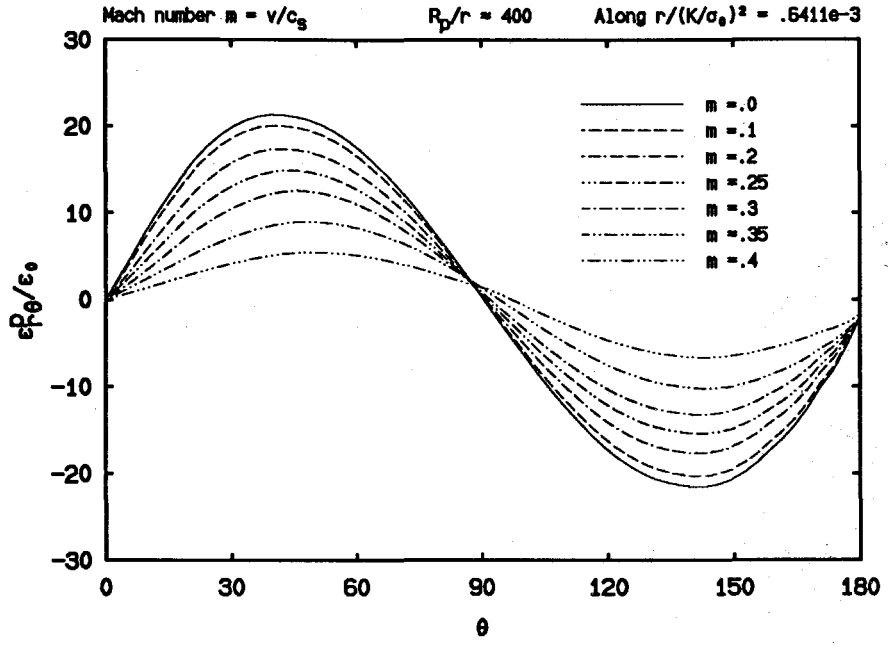

FIGURE 3.3.3d The angular dependence of the r-θ polar plastic strain component for various normalized crack speeds.

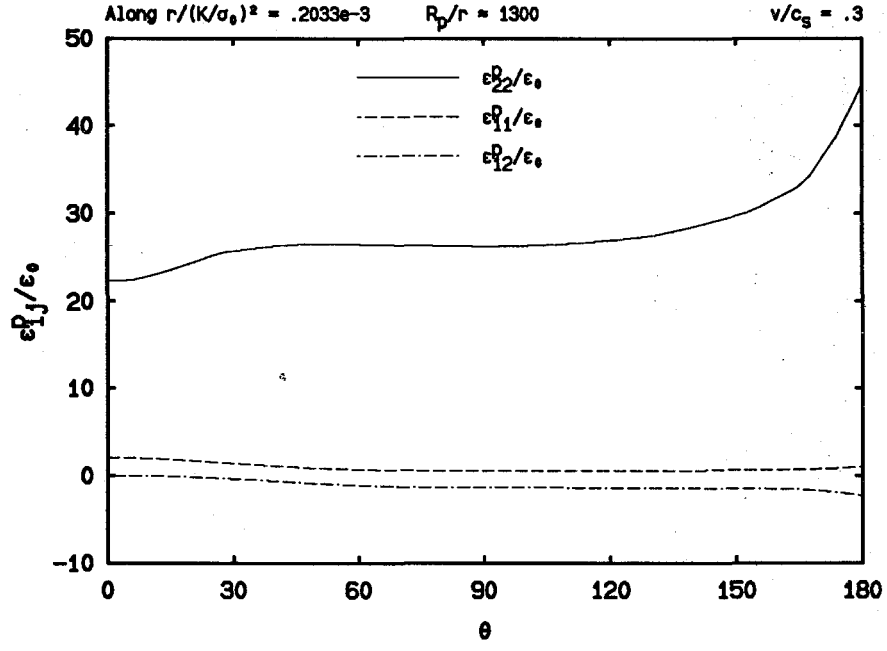

FIGURE 3.3.3e The angular dependence of the Cartesian plastic strain components for $v/c_s = .3$.

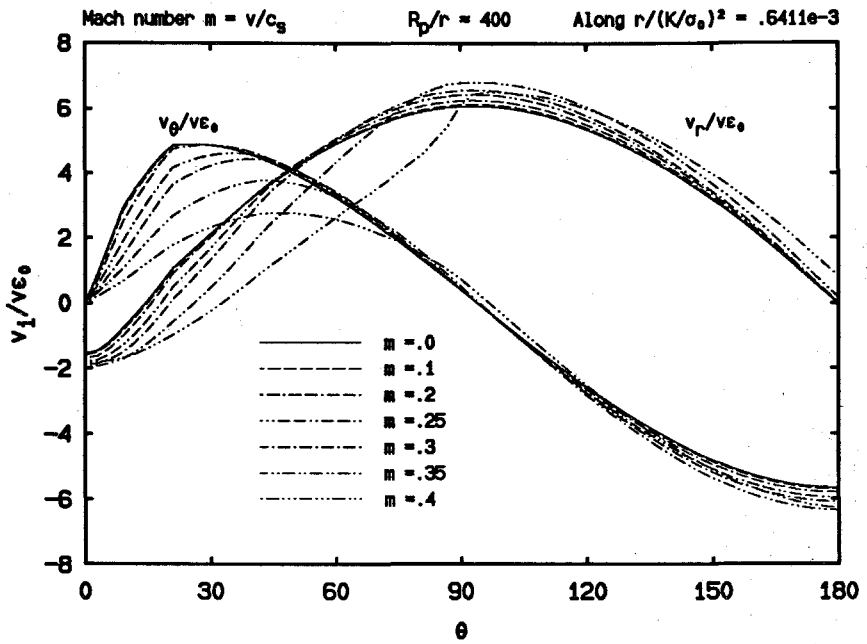

FIGURE 3.3.4a The angular dependence of the polar velocity components for various normalized crack speeds.

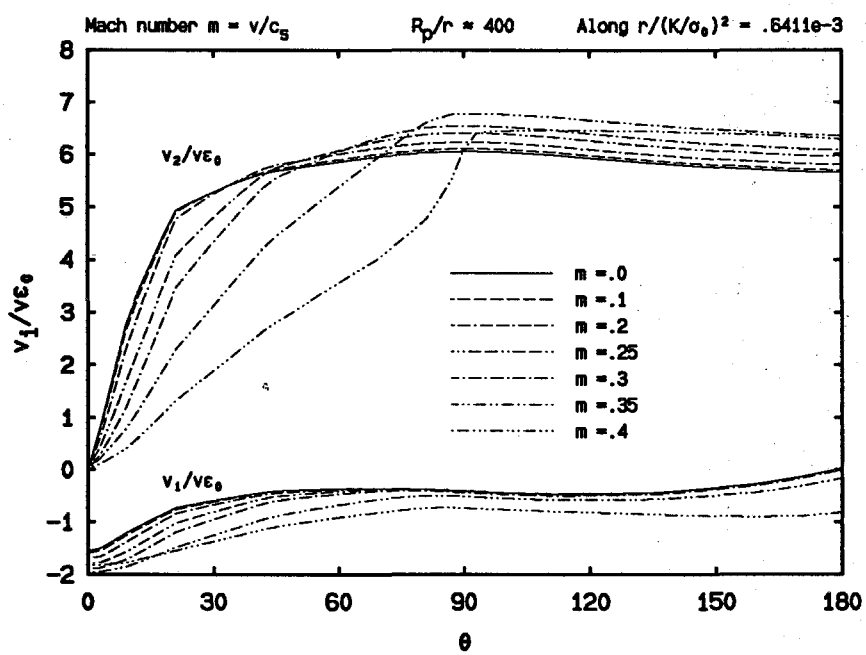

FIGURE 3.3.4b The angular dependence of the Cartesian velocity components for various normalized crack speeds.

σ_{12} are respectively always positive and negative except near the crack surface, whereas σ_{11} changes sign when θ reaches approximately 135^0.

Next the plastic strain variations are illustrated. Remember that the plastic strains outside the active plastic zones are the residual plastic strains. Fig. 3.3.3a shows the θ-dependence of the polar components of the plastic strain, the effective plastic strain and the out-of-plane plastic strain for $m = 0.3$. It is seen that the polar components exhibit, just as in the quasi-static case, sinusoidal-like behaviors, while ε_e^p and ε_{33}^p remain fairly flat for most of the θ ranges and rise up near the crack flank, which are apparently due to the residual plastic strains accumulated at the crack tip (theoretically they should tend to infinity if the plastic strains in the active plastic zone are singular). The sinusoidal-like behaviors are in fact present in all our calculated cases, whose progressive changes are shown in Figs. 3.3.3b, 3.3.3c and 3.3.3d, respectively, for ε_{rr}^p, $\varepsilon_{\theta\theta}^p$ and $\varepsilon_{r\theta}^p$.

This phenomenon is easily explained if the angular variations of the Cartesian rectangular plastic strain components are examined. It is discovered from Fig. 3.3.3e, for the case of $m = 0.3$, that throughout the angular range, the 2-2 component is dominantly larger than the 1-1 and 1-2 components, which means that the effective plastic strain, through its definition, and the out-of-plane plastic strain, through the plastic incompressibility, are dominated by ε_{22}^p. Hence, they behave like ε_{22}^p as seen from the figures. The predominance of the 2-2 Cartesian component certainly also accounts for the sinusoidal behaviors of the polar components, which becomes clear if a tensorial transformation is performed. It is also worth mentioning that as the crack speed goes up, the magnitude of ε_{22}^p decreases and that of ε_{11}^p increases.

The angular variations of the velocity field around the crack tip are shown in Fig. 3.3.4a for the polar components and in Fig. 3.3.4b for the Cartesian components. It is observed that v_r starts negatively at $\theta = 0^0$ and ends at values close to

zero, whereas v_θ starts at zero, as expected due to symmetry conditions, and ends at negative values. For all m values we considered, both v_r and v_θ curves go up steadily (i.e., with positive slopes) initially and then fall down consistently all the way to the crack surface. The Cartesian components also share the initial positive slope characteristic and remain that way approximately up to the elastic-plastic boundary where they level off until they meet the crack surface.

We would like to emphasize the observation that at $\theta = 180^0$, v_1 is very close to zero for $m < 0.3$, and it apparently becomes nonzero as m becomes larger, especially for $m = 0.4$, which, in our opinion, has to do with the fact that as m becomes larger, a secondary active plastic zone develops along the crack flank. We will show in the subsection of asymptotic analysis that if there is no reverse plastic reloading zone at the back of the crack tip, then v_1 is less singular than lnr, whereas v_2 is as singular as lnr in the elastic unloading zone including $\theta = 180^0$, which implies that the magnitude of v_1 there is extremely small when compared with that of v_2. However, if there is a plastic reloading zone at the back of the crack tip, then both v_1 and v_2 should possess the same lnr singularity as r approaches zero, but the coefficient for the v_1 singularity is not necessarily zero.

Radial Field Variations

Many interesting characteristics can be observed from the radial distributions of stress and deformation fields, which are also very important for the studies of fracture criteria and for the search for appropriate asymptotic solutions.

Fig. 3.3.5a describes for $m = 0.3$ the crack front stress variations with respect to the normalized radial distance and covering regions both inside and outside the plastic zone. It is obvious from the figure that outside the plastic zone (note that the plastic zone size is about $0.26(K/\sigma_0)^2$), both σ_{11} and σ_{22} become smaller as the distance from the crack tip becomes larger, and eventually they intersect each other

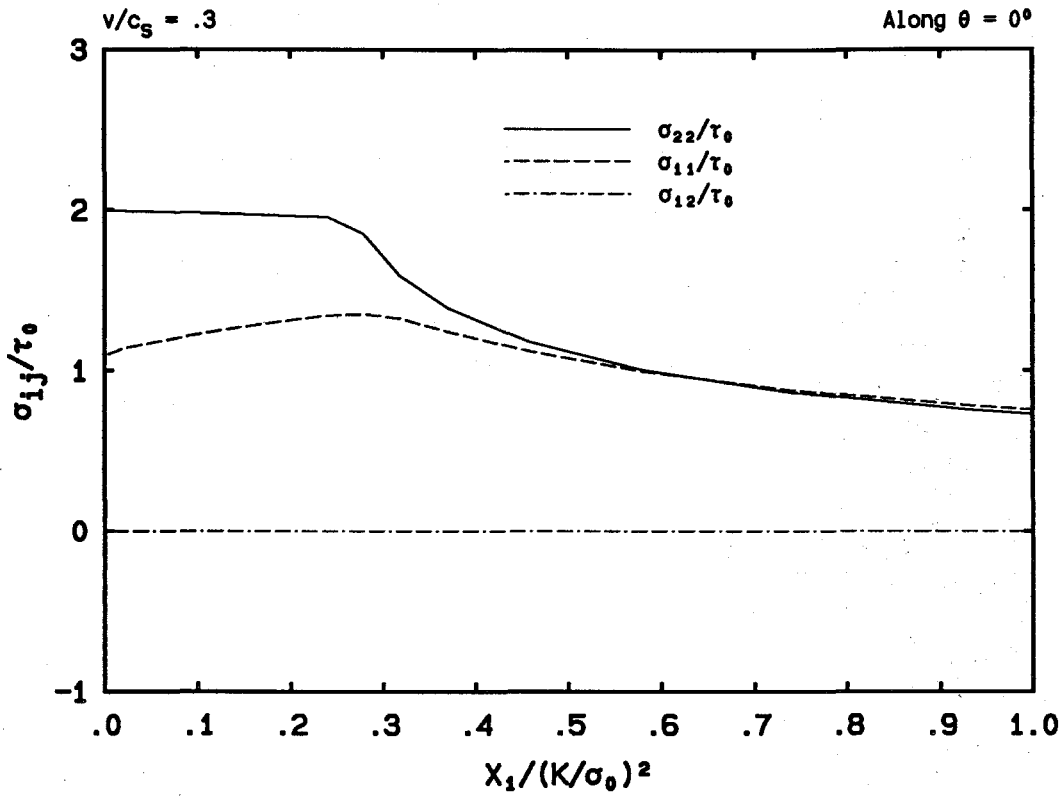

FIGURE 3.3.5a The radial dependence of the stress components at crack front along the prospective crack line for $v/c_s = .3$.

and then change their relative magnitudes as required by the dynamic asymptotic K-field specified on the crack front boundary. While inside the plastic zone, it is seen that as the distance increases, σ_{11} increases sharply whereas σ_{22} only decreases slightly, and that σ_{11} has a crack tip asymptotic value clearly greater than τ_0, i.e., greater than its quasi-static counterpart, whereas σ_{22} has an asymptotic value about $2\tau_0$ which is almost the same as the quasi-static value.

A more detailed asymptotic view of the radial stress distributions along the crack line is presented in Figs. 3.3.5b and 3.3.5c for all cases of crack propagation speeds we considered. It is discovered that while σ_{11} increases as m goes up (see Fig. 3.3.5b), σ_{22} actually decreases, although slightly, as m goes up.

At this point we would like to point out a strong inconsistency of the solution

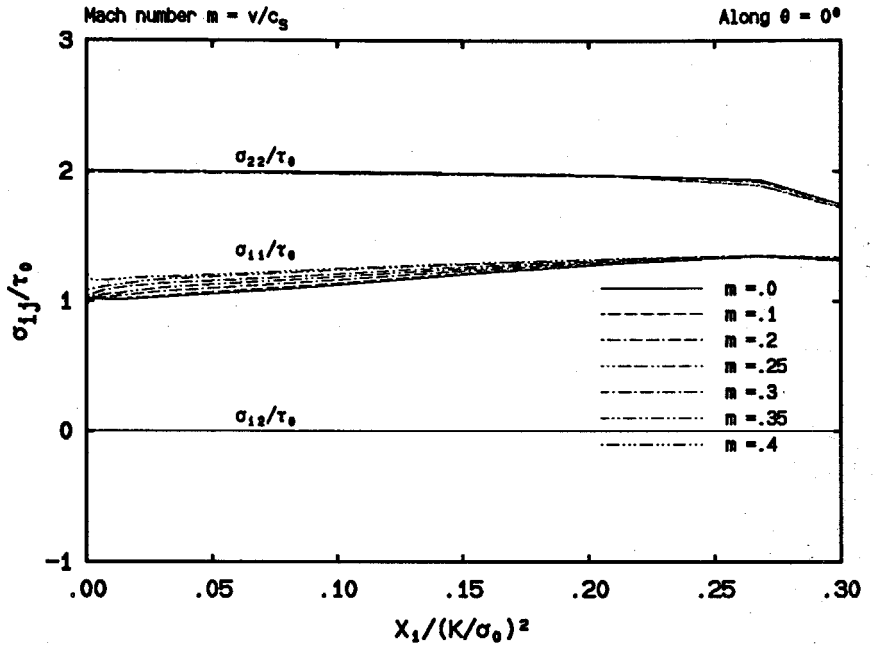

FIGURE 3.3.5b The radial dependence of the stress components at crack front for various normalized crack speeds.

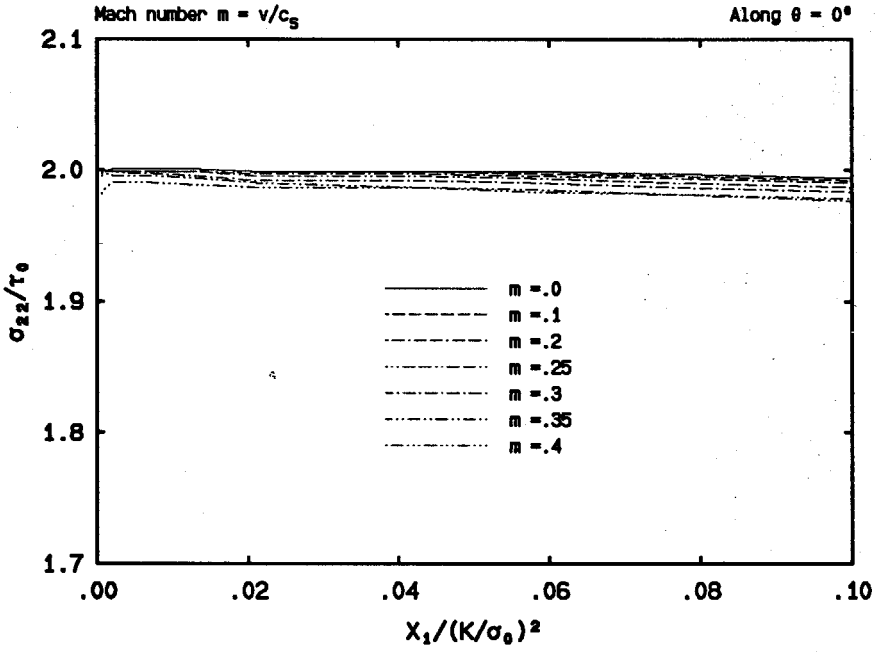

FIGURE 3.3.5c The radial dependence of the 2-2 stress component at crack front for various normalized crack speeds.

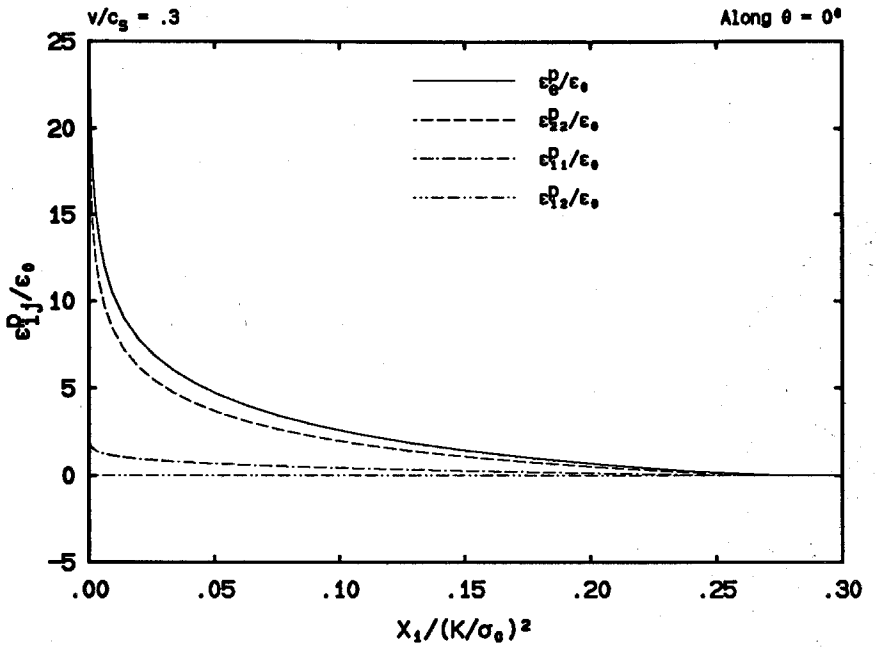

FIGURE 3.3.6a The radial dependence of the plastic strain components at crack front for $v/c_s = .3$.

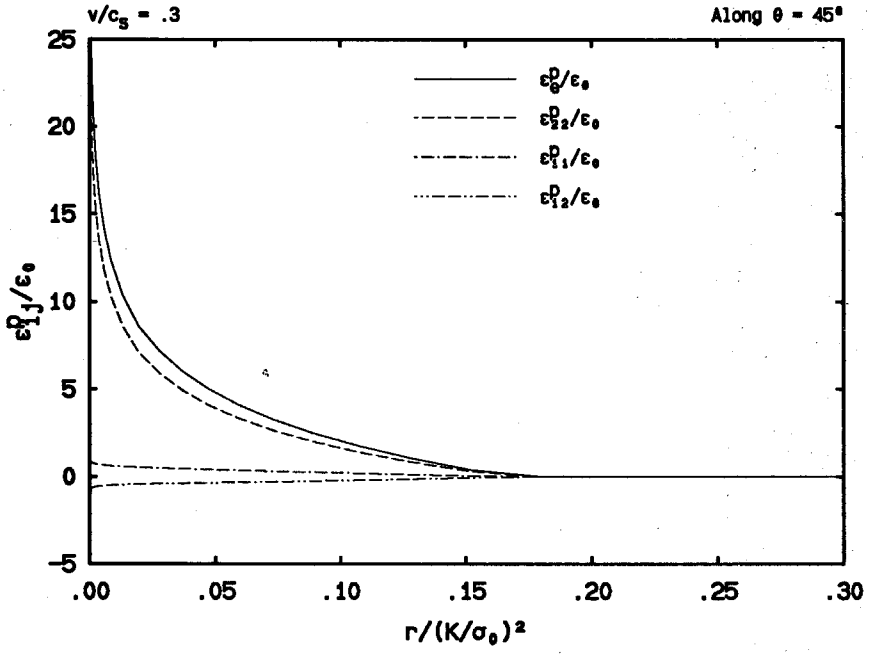

FIGURE 3.3.6b The radial dependence of the Cartesian plastic strain components along the radial line $\theta = 45^0$ for $v/c_s = .3$.

by Gao (1987) with our numerical findings. It can be seen from Fig. 3 and Fig. 4 of Gao's paper that the value of σ_{11} at $\theta = 0^0$ for $m = 0.3$ is smaller than τ_0, or smaller than that for $m = 0$ (also refer to Fig. 5 of his paper).

Our numerical solutions also showed approximate linear radial variations of both σ_{11} and σ_{22}. Note also that the 1-2 component of the stress field is always zero, satisfying the symmetry condition at $\theta = 0^0$.

The strong r-dependence of the 1-1 stress component noted in Figs. 3.3.5a and 3.3.5b are apparently in disagreement with the assumption made in the crack line solutions by Achenbach and Li (1984a, b), namely the assumption that $\sigma_{22}(r)$ and hence $\sigma_{11}(r)$ are constants in the plastic zone. The assumption is introduced in their series expansion solution in order to increase the number of equations to equal the number of unknowns.

The radial dependence of crack tip plastic strains is shown in Fig. 3.3.6 through Fig. 3.3.9. First of all, the typical variations along the radial lines $\theta = 0^0$ and 45^0 are depicted in Figs. 3.3.6a and 3.3.6b respectively for $m = 0.3$, where we see that very near the crack tip, the 2-2 plastic strain component, and hence the effective plastic strain, demonstrate much stronger radial dependence than the 1-1 and 1-2 components, which confirms our earlier observations from their angular variations (see Fig. 3.3.3e). However we cannot rule out the possibility that ε^p_{11} and ε^p_{12} are singular as $r \to 0$, although their magnitudes will be very small compared to the magnitude of ε^p_{22}.

The radial variations of the 1-1 plastic strain component for various m values are illustrated in Figs. 3.3.7a and 3.3.7b. It is clear from Fig. 3.3.7a that ε^p_{11} does show large slopes near the crack tip, especially for larger m values, which indicates a somewhat singular behavior. In fact in the log-scale plot illustrated in Fig. 3.3.7b, where data are from the fifth to the eighth elements away from the crack tip, approximate linear relations are observed, which strongly suggests

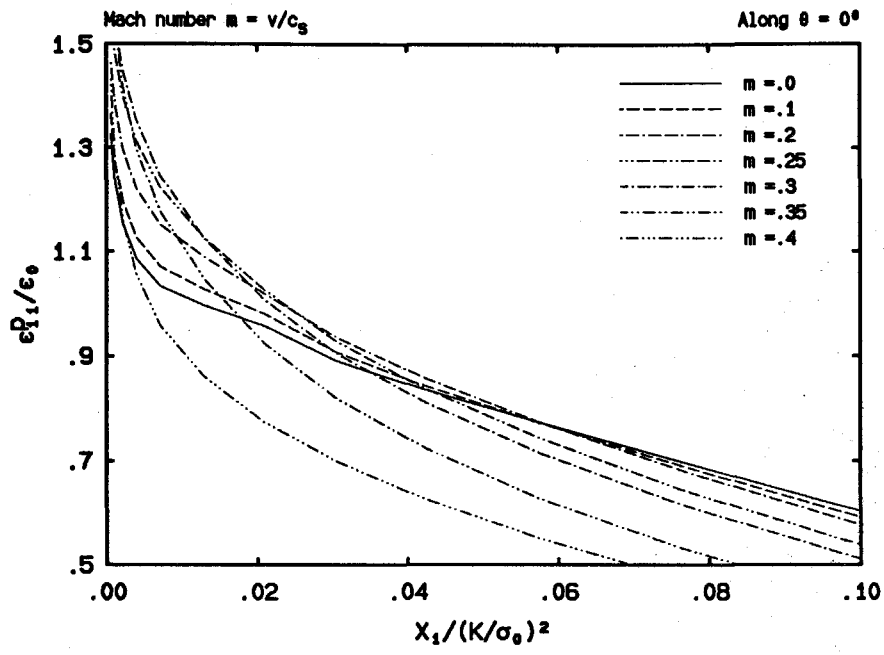

FIGURE 3.3.7a The radial dependence of the 1-1 plastic strain components at crack front for various normalized crack speeds.

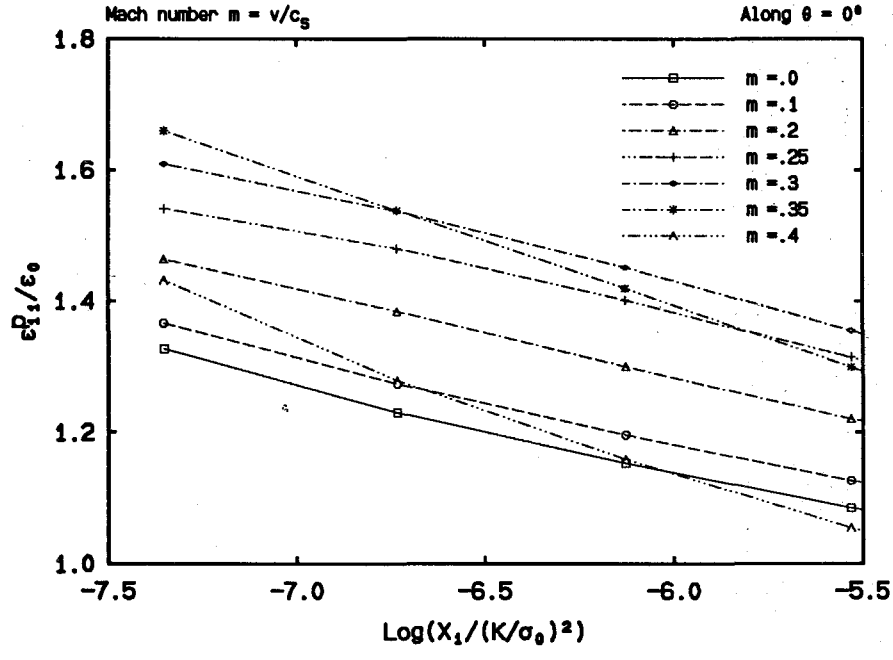

FIGURE 3.3.7b The radial dependence of the 1-1 plastic strain components at crack front for various normalized crack speeds, plotted against the logarithmic value of the normalized distance.

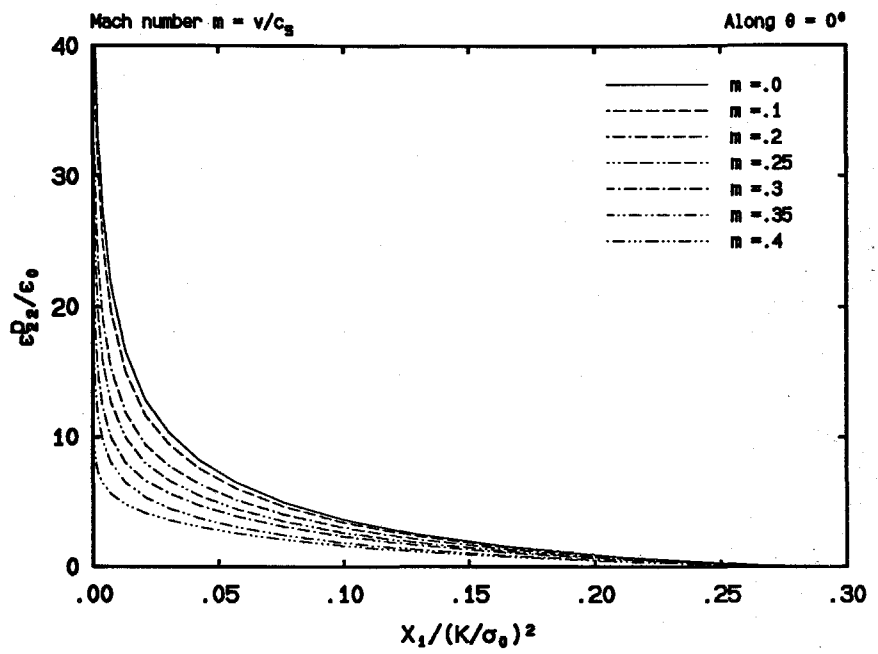

FIGURE 3.3.8a The radial dependence of the 2-2 plastic strain components at crack front for various normalized crack speeds.

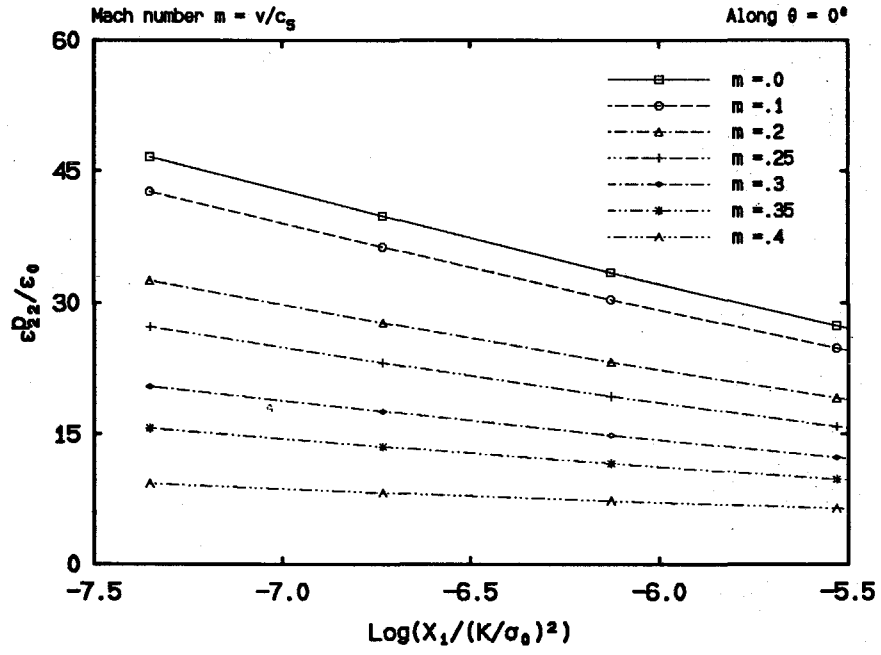

FIGURE 3.3.8b The radial dependence of the 2-2 plastic strain components at crack front for various normalized crack speeds, plotted against the logarithmic values of the normalized distance.

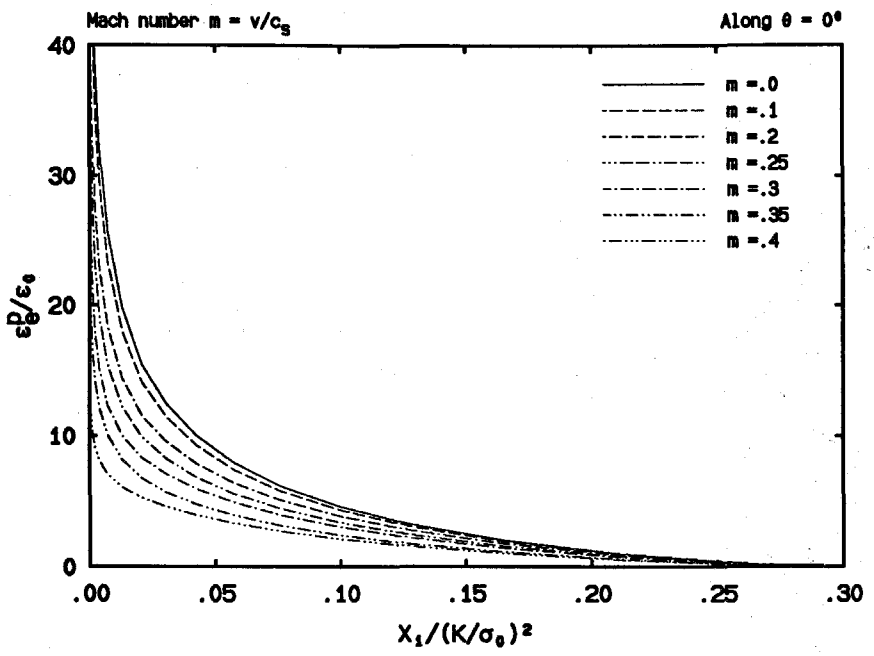

FIGURE 3.3.9a The radial dependence of the effective plastic strain at crack front along for various normalized crack speeds.

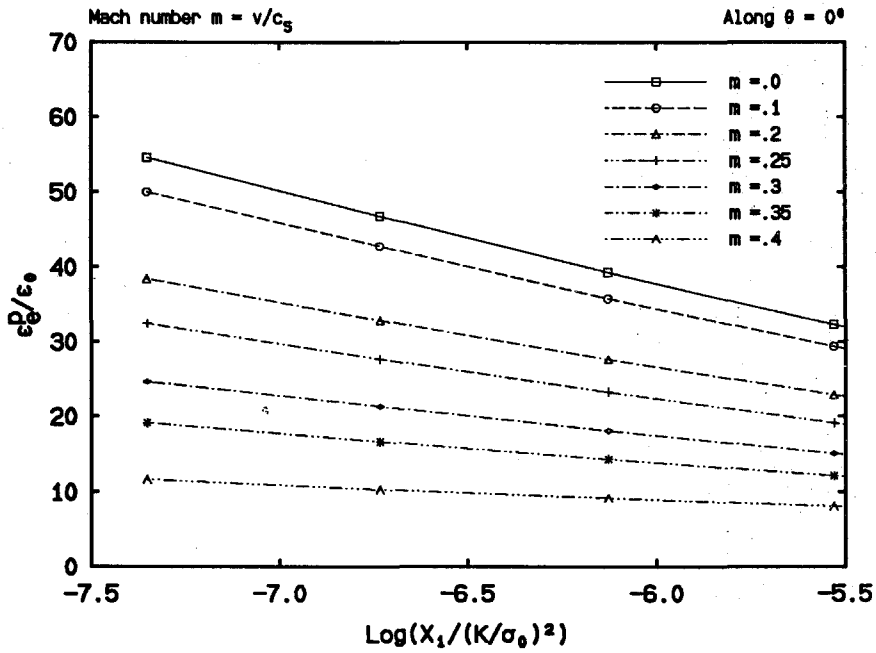

FIGURE 3.3.9b The radial dependence of the effective plastic strain at crack front for various normalized crack speeds, plotted against the logarithmic values of the normalized distance.

a logarithmic singularity. Another characteristic of the 1-1 component variation is that its magnitude tends to flip over to lower values as the normalized distance increases, which is shown in both figures.

The evolutionary radial variation of the plastic strain component ε_{22}^p along the crack line is shown in Fig. 3.3.8a. One of the characteristics of this variation is that as m increases, the magnitude of this dominant plastic strain component decreases. It is observed that strong singularity exists at the crack tip. Actually, the straight lines observed in Fig. 3.3.8b strongly indicate that ε_{22}^p behaves as lnr as the crack tip is approached.

This logarithmic strain singularity for dynamic crack propagation in elastic-perfectly plastic solids were also reported for Mode III (see, for example, Slepyan, 1976) and Mode I plane strain (Gao and Nemat-Nasser, 1983a; and Gao, 1985). It is noted here that in the incompressible plane strain case, a proof is offered by Leighton, Champion and Freund (1987) stating that stress discontinuities are not permissible if the maximum plastic work principle is to be satisfied. Hence they showed that velocity or strain singularities of the lnr type are not permitted for this special case. Gao (1987), in his Mode I plane stress asymptotic solution, assumed directly that strains and consequently velocities behave as lnr as $r \to 0$.

Since the plastic strains are dominated by ε_{22}^p near the crack tip, it is expected that the effective plastic strain behaves as ε_{22}^p near the tip. Figs. 3.3.9a and 3.3.9b verify this. Here it is worth pointing out that since ε_e^p is a measure of plastic straining, then from Fig. 3.3.9a, it can be said that as crack speed increases, plastic straining at the crack front becomes less severe. This reduced plastic straining phenomenon in fact has been found, as reviewed in the introduction section, in all three fracture modes, and from stationary cracks to extending cracks. Thus if a certain loading is to be maintained for a certain plastic straining, it is then obvious that for a higher level of plastic straining, the loading level must also be raised. Thus

to achieve the same plastic straining level at the crack front, a higher loading must be applied for a crack to run with a higher speed. We will disscuss this observation in more detail in Chapter 6, where fracture criteria are investigated.

The radial distributions of the Cartesian velocity components are presented in Fig. 3.3.10 for v_2 and in Fig. 3.3.11 for v_1, which are of more interest in the sense that asymptotic solutions are usually obtained in terms of velocities instead of strains. Note that the normalized velocities are plotted against the logarithmic values of the normalized distance, along two radial lines, namely along $\theta = 45^0$ and 135^0. It is discovered that while v_2 behaves, especially for lower m values, as lnr at the crack tip, its strength becomes much smaller for higher m values. Yet, interestingly enough, the opposite is observed for v_1. For small m values, approximately horizontal lines are observed, which indicates no or little lnr dependence, whereas as m increases, the linear curves are found to increase their slope significantly, which indicates strong lnr dependence.

Also of some interest are the radial variations of the velocity field along the crack flank, which is shown in Fig. 3.3.12. It is seen that the magnitude of v_2 decreases rapidly as the distance from the crack tip increases, but it is not clear from our results if v_2 will tend to zero as the distance continues to increase. The v_1 component is found to equal approximately zero at all distances from the tip.

The lnr-velocity singularities indicated by the above finite element results and the changes of their magnitudes with respect to the crack propagation speed will be further discussed in the subsection on asymptotic analysis. At the same time, it is worth pointing out that the asymptotic analysis given by Gao (1987) assumed, to start with, that strain field has lnr singularity. Hence he essentially assumed a velocity field with lnr singularity. Morover, from the form of the velocity field he used, it can be derived that only the velocity component $v_1(r, \theta)$ will have the assumed lnr singularity, whereas the velocity component $v_2(r, \theta)$ is bounded in his

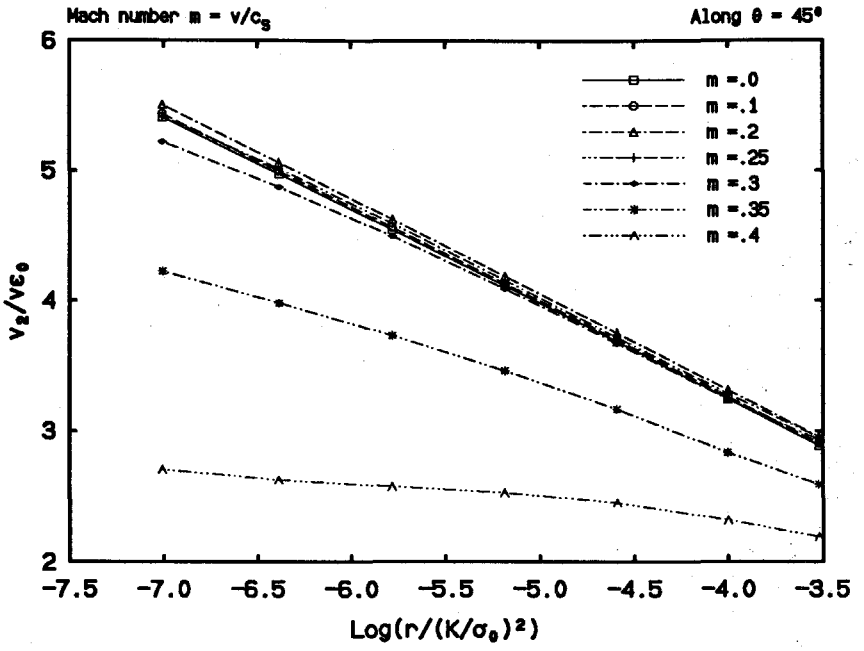

FIGURE 3.3.10a The radial dependence of v_2 in its normalized form plotted against $Log(r/(\frac{K}{\sigma_0})^2)$ along $\theta = 45^0$ for various normalized crack speeds.

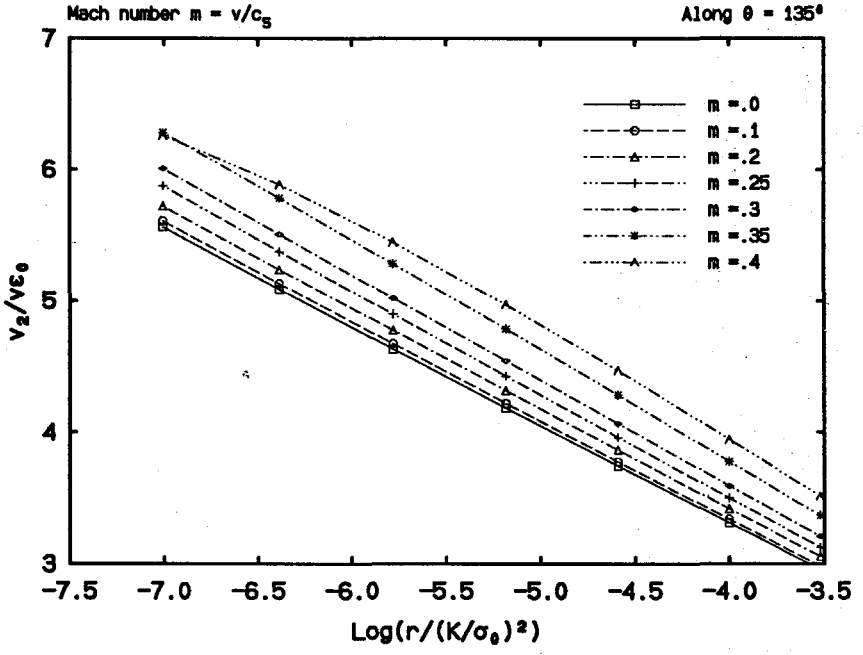

FIGURE 3.3.10b The radial dependence of v_2 in its normalized form plotted against $Log(r/(\frac{K}{\sigma_0})^2)$ along $\theta = 135^0$ for various normalized crack speeds.

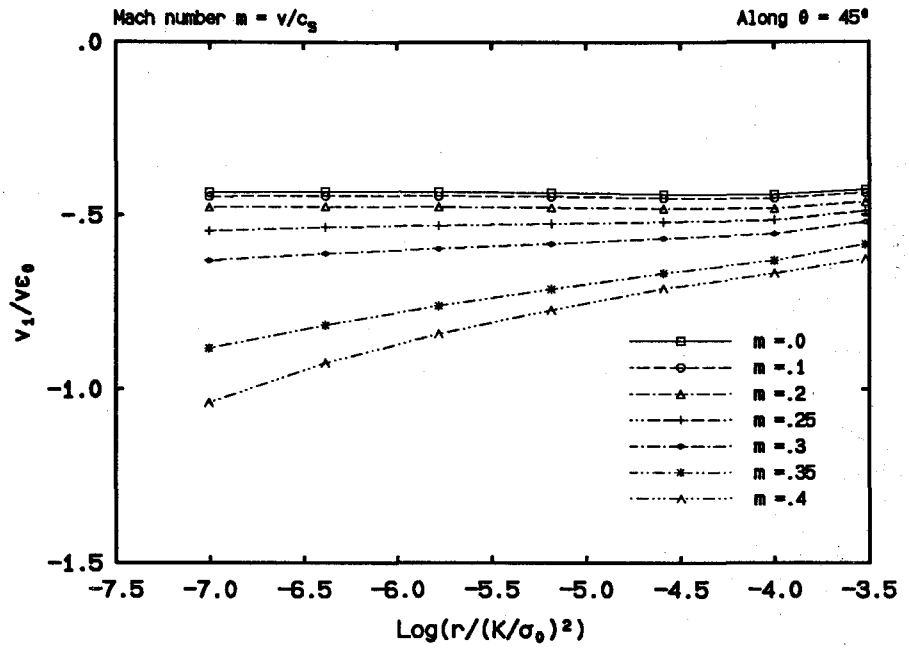

FIGURE 3.3.11a The radial dependence of v_1 in its normalized form plotted against $Log(r/(\frac{K}{\sigma_0})^2)$ along $\theta = 45^0$ for various normalized crack speeds.

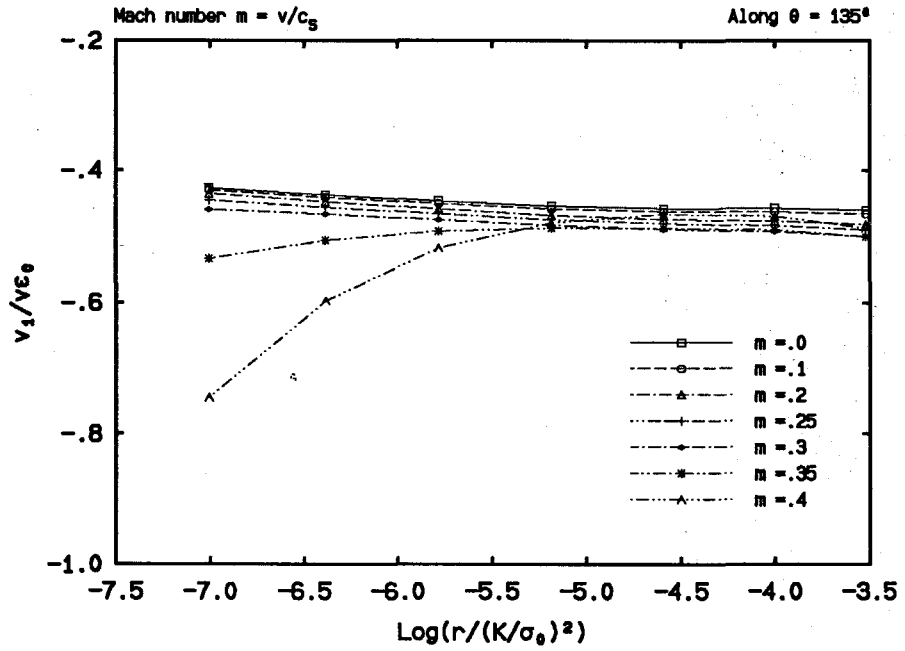

FIGURE 3.3.11b The radial dependence of v_1 in its normalized form plotted against $Log(r/(\frac{K}{\sigma_0})^2)$ along $\theta = 135^0$ for various normalized crack speeds.

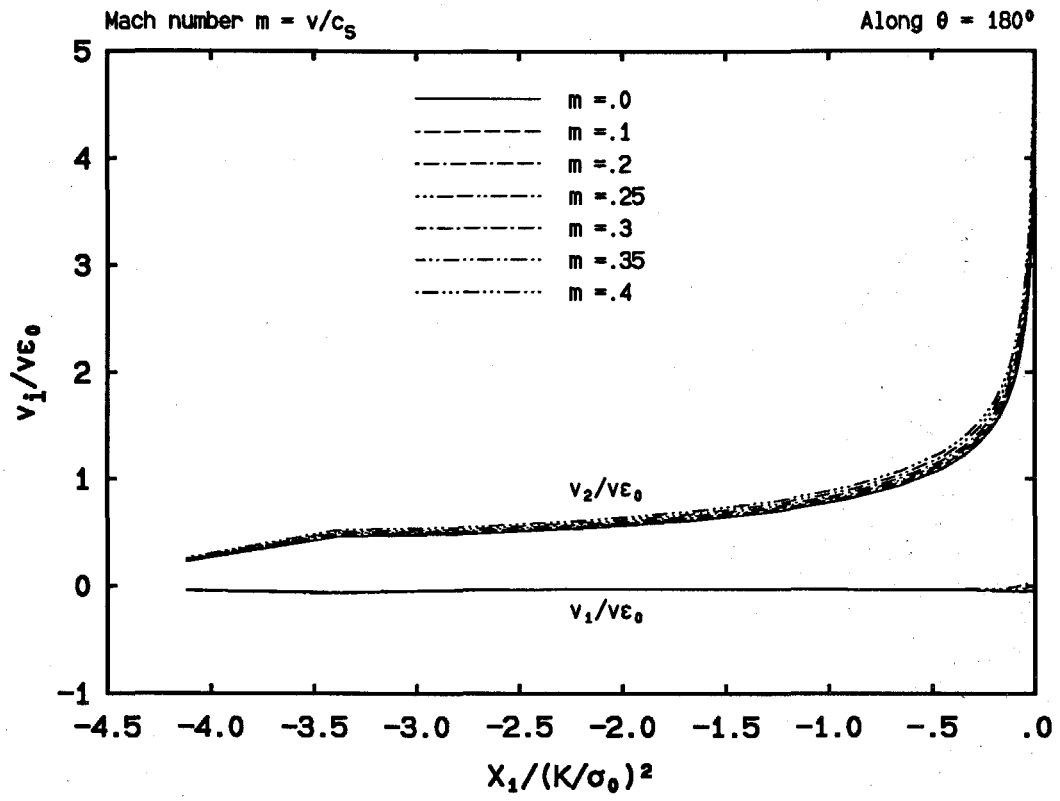

FIGURE 3.3.12 The radial dependence of the velocity components along the crack flank for various normalized crack speeds.

solution. This feature seems contradictory to our numerical findings, which will be explained later in an asymptotic analysis.

Finally we present the results for the crack surface profiles during crack propagation. The global view of the vertical displacement component u_2, which is half the crack opening displacement, is illustrated in Fig. 3.3.13a for different crack speeds. It is noted here that in the normalized coordinates, the magnitude of u_2 increases as m increases.

The question at this point is whether this tendency will reverse, that is, how small r should be in order to see the decrease of u_2 for increasing m. In a similar numerical study for Mode I plane strain crack propagation by Lam and Freund (1985), it is reported that for m values from 0.0 to 0.4, the reversing point is at

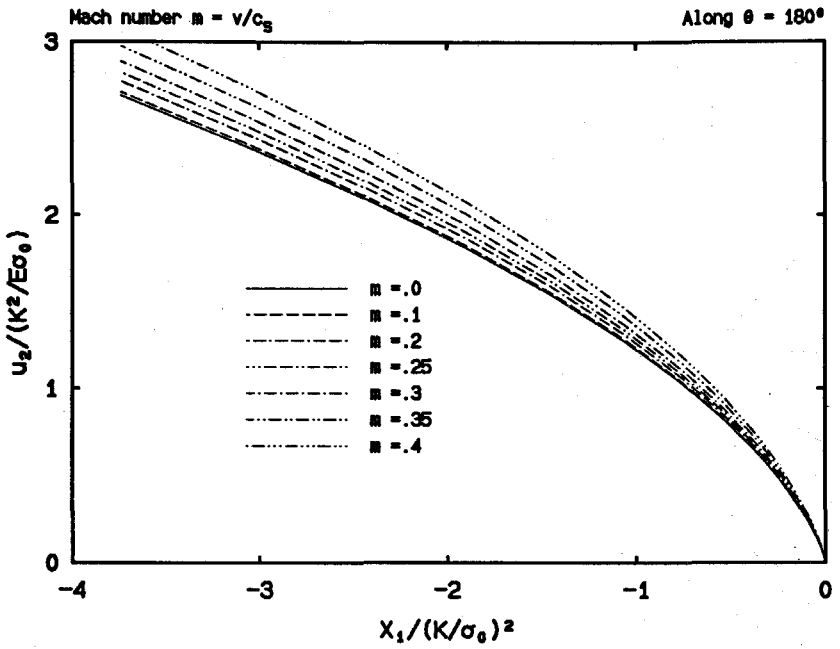

FIGURE 3.3.13a The radial dependence of the displacement component u_2 along the crack flank for various normalized crack speeds.

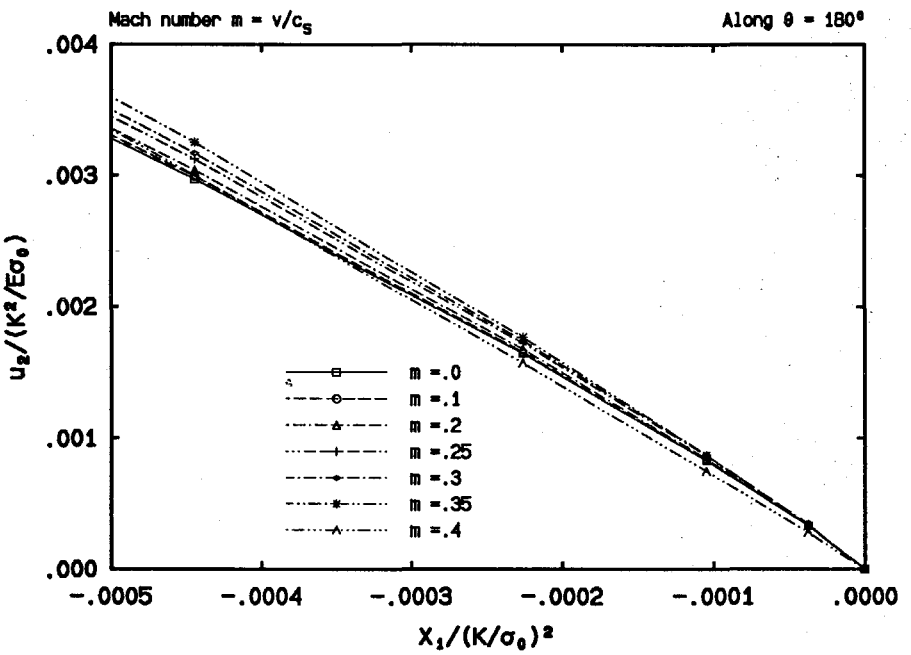

FIGURE 3.3.13b A detailed view of the radial dependence of the displacement component u_2 along $\theta = 180^0$ for various normalized crack speeds.

$r = 0.05(K/\sigma_0)^2$ behind the crack tip. However for the plane stress case, we did not find such an early reversing point. As depicted in Fig. 3.3.13b, no reversing tendency is detected even on a length scale about one one-hundredth smaller than that used by Lam and Freund, except for $m = 0.4$ where a small deviation is noticed.

Now let's pay attention to the slope changes of the crack tip openings for different m values. From Fig. 3.3.13b, it can be seen that while for small m values the opening profiles bend down near the crack tip, they are approximately straight lines for higher m values, whose slopes are actually rather insensitive to the crack speeds. Similar numerical results are also reported for the Mode III case (Douglas, Freund and Parks, 1981). This seems to indicate a tendency that the crack opening displacement possesses a linear radial dependence asymptotically at the tip as the crack speed becomes higher, or as the dynamic effect grows larger.

Asymptotic Analysis

In the above we presented the result of the current finite element study on crack tip stress and deformation fields for dynamic crack propagation in elastic-perfectly plastic solids under conditions of Mode I plane stress, steady state and small-scale yielding. Detailed comparison with the asymptotic solution by Gao (1987) was perfomed.

It was observed that the asymptotic near-tip field by Gao involves many characteristic behaviors often contradictory to the findings of the present full field numerical study. It is noted in Gao's analysis that it is directly assumed that the strain field, and hence the velocity field, possesses lnr-singularities at the crack tip, and that the stresses are bounded and can be treated as functions of θ only. The result of the present finite element solution very near the crack tip seems to confirm the logarithmic behavior of the strain and velocity fields. However, the particular form adopted for the velocity field in Gao's asymptotic analysis implies that only

the velocity component $v_1(r,\theta)$ has lnr-singularity at the crack tip or $r = 0$, whereas the velocity component $v_2(r,\theta)$ is bounded, which seems contrary to our numerical result.

It is our purpose here to discuss a preliminary asymptotic analysis regarding the near-tip radial dependence of the velocity field and of the crack opening displacement. Certain features of the numerically determined crack tip field and differences with Gao's asymptotic solution will be interpreted accordingly. No direct assumptions about the singularity of the velocity field and the boundedness of the stress field will be made, although assumptions of other types are still necessary.

Now suppose a crack is propagating steadily (see Fig. 1.1.1) under Mode I plane stress conditions in an elastic-perfectly plastic solid obeying the von Mises yield criterion and the associated flow rule. From the steady state condition, it is necessary that the crack tip velocity v be a constant and that for any field quantity, say q, its material time derivative be computed from the spatial gradient $-v\partial q/\partial x_1$. For a actively yielded stress state σ_{ij}, the yield condition requires that

$$s_{ij}s_{ij} = \tau_0^2, \tag{3.3.1a}$$

where τ_0 is the yield stress in simple shear and s_{ij} is the deviatoric stress tensor component given by

$$s_{ij} = \sigma_{ij} - \frac{1}{3}\sigma_{kk}\delta_{ij}. \tag{3.3.1b}$$

It is understood here that Latin indices have range one to three while Greek indices have range one and two, and that the standard indicial notation and its associated conventions are used. The plane stress condition simplifies the above equations with

$$\sigma_{3i} = 0. \tag{3.3.2}$$

Immediately from Eq.(3.3.1a), it is seen that s_{ij} must be bounded. Since $\sigma_{33} = 0$, then from Eq.(3.3.1b), $\sigma_{kk} = -3s_{33}$. Hence σ_{kk} is also bounded. Consequently, it can be concluded from Eq.(3.3.1b) that σ_{ij} must be bounded.

To investigate the asymptotic structure of the crack tip field, let's consider a generic sector at the crack tip. Suppose the sector is confined by two straight radial lines from the crack tip. We further assume that all limits taken below exist in this sector such that operations on the order symbols are permissible within this sector.

Next define $\bar{\sigma}_{ij}(\theta)$, a function of θ at the crack tip, as follows

$$\bar{\sigma}_{ij}(\theta) = \lim_{r \to 0} \sigma_{ij}(r, \theta), \tag{3.3.3a}$$

and let

$$\hat{\sigma}_{ij}(r, \theta) = \sigma_{ij}(r, \theta) - \bar{\sigma}_{ij}(\theta). \tag{3.3.3b}$$

Then the stress state $\sigma_{ij}(r, \theta)$ near the crack tip can be expressed as

$$\sigma_{ij}(r, \theta) = \bar{\sigma}_{ij}(\theta) + \hat{\sigma}_{ij}(r, \theta). \tag{3.3.3c}$$

Hence from Eqs.(3.3.3a) and (3.3.3b), it is true that $\lim_{r \to 0} \hat{\sigma}_{ij}(r, \theta) = 0$, or that, using the order symbols (see, for example, the textbook by Erdélyi, 1956), $\hat{\sigma}_{ij}(r, \theta) = o(1)$ as $r \to 0$. Then we must have $\frac{\partial \hat{\sigma}_{ij}}{\partial r} = o(\frac{1}{r})$ as $r \to 0$, since otherwise if $\frac{\partial \hat{\sigma}_{ij}}{\partial r} = O(\frac{1}{r})$ as $r \to 0$, we would have $\hat{\sigma}_{ij}(r, \theta) = O(lnr)$ as $r \to 0$, which violates our original conclusion.

Now it is established that $\frac{\partial \hat{\sigma}_{ij}}{\partial r} = o(\frac{1}{r})$ as $r \to 0$, then $r\frac{\partial \hat{\sigma}_{ij}}{\partial r} = o(1)$ as $r \to 0$ or $\lim_{r \to 0} r\frac{\partial \hat{\sigma}_{ij}}{\partial r} = 0$. Hence from Eq.(3.3.3c), $\lim_{r \to 0} r\frac{\partial \sigma_{ij}}{\partial r} = 0$. Using the above results and the following identities

$$\frac{\partial(\ )}{\partial x_1} = cos\theta \frac{\partial(\ )}{\partial r} - \frac{sin\theta}{r} \frac{\partial(\ )}{\partial \theta}, \tag{3.3.4a}$$

$$\frac{\partial(\ )}{\partial x_2} = sin\theta \frac{\partial(\ )}{\partial r} + \frac{cos\theta}{r} \frac{\partial(\ )}{\partial \theta}, \tag{3.3.4b}$$

it can be proved that

$$\frac{\partial \sigma_{ij}}{\partial x_\alpha} = O(\frac{1}{r}) \quad (\alpha = 1, 2) \quad \text{as } r \to 0. \tag{3.3.5}$$

In order to investigate the singularity of the velocity field $v_\alpha(r,\theta)$ at the crack tip, a study of the basic equations are necessary. Under steady state and plane stress conditions, the equation of motion in the crack tip moving coordinate system will be

$$\frac{\partial \sigma_{\alpha\beta}}{\partial x_\beta} = -v\rho\frac{\partial v_\alpha}{\partial x_1}, \tag{3.3.6}$$

where v is the crack propagation speed and ρ is the mass density of the material. Similarly, the constitutive law can be written as

$$\frac{\partial v_1}{\partial x_1} = -\frac{v}{E}[(1+\nu)\frac{\partial \sigma_{11}}{\partial x_1} - \nu\frac{\partial \sigma_{kk}}{\partial x_1}] + \frac{\dot{\lambda}}{3}(2\sigma_{11} - \sigma_{22}), \tag{3.3.7a}$$

$$\frac{\partial v_2}{\partial x_2} = -\frac{v}{E}[(1+\nu)\frac{\partial \sigma_{22}}{\partial x_1} - \nu\frac{\partial \sigma_{kk}}{\partial x_1}] + \frac{\dot{\lambda}}{3}(2\sigma_{22} - \sigma_{11}), \tag{3.3.7b}$$

$$\frac{\partial v_1}{\partial x_2} + \frac{\partial v_2}{\partial x_1} = -\frac{2v(1+\nu)}{E}\frac{\partial \sigma_{12}}{\partial x_1} + 2\dot{\lambda}\sigma_{12}, \tag{3.3.7c}$$

where E is the Young's modulus, ν is the Poisson ratio, and $\dot{\lambda}$ is the plastic flow factor such that it is zero for an elastic stress state and it is nonnegative for an actively yielded stress state.

From Eqs.(3.3.5) and (3.3.6) it is clear that

$$\frac{\partial v_\alpha}{\partial x_1} = O(\frac{1}{r}) \quad \text{as } r \to 0. \tag{3.3.8a}$$

It is our purpose here to show that

$$\frac{\partial v_\alpha}{\partial x_2} = O(\frac{1}{r}) \quad \text{as } r \to 0, \tag{3.3.8b}$$

for all elastic sectors and for plastic sectors where $\sigma_{22} \neq 2\sigma_{11}$.

First of all, for a sector in an elastic stress state, $\dot{\lambda} = 0$. Then noting Eqs.(3.3.5) and (3.3.8a), it is clear from Eqs.(3.3.7b) and (3.3.7c) that Eq.(3.3.8b) holds.

Secondly, in a plastic sector where $\sigma_{22} \neq 2\sigma_{11}$, it can be shown from Eqs.(3.3.5), (3.3.7a) and (3.3.8a) that $\dot{\lambda} = O(\frac{1}{r})$ as r approaches zero. Substitution of $\dot{\lambda}$ into Eqs.(3.3.7b) and (3.3.7c) will then readily yield Eq.(3.3.8b).

In fact, the results of the present finite element study seem to suggest that the crack tip is surrounded completely by these two types of sectors, as shown in Fig. 3.3.14. Nevertheless, if both Eqs.(3.3.8a) and (3.3.8b) hold, then from the chain rule $\frac{\partial v_\alpha}{\partial r} = \frac{\partial v_\alpha}{\partial x_\beta}\frac{\partial x_\beta}{\partial r}$ and the identities $\frac{\partial x_1}{\partial r} = cos\theta$ and $\frac{\partial x_2}{\partial r} = sin\theta$, it can be concluded that

$$\frac{\partial v_\alpha}{\partial r} = O(\frac{1}{r}) \quad \text{as } r \to 0. \tag{3.3.9}$$

Consequently, $v_\alpha = O(lnr)$ as $r \to 0$. Without loss of generality, v_α can then be written as

$$v_\alpha(r,\theta) = g_\alpha(\theta)lnr + f_\alpha(r,\theta) + h_\alpha(\theta) + o(1), \quad \text{as } r \to 0, \tag{3.3.10}$$

where g_α and h_α are bounded funtions of θ, and f_α is singular at $r = 0$ yet less singular than lnr.

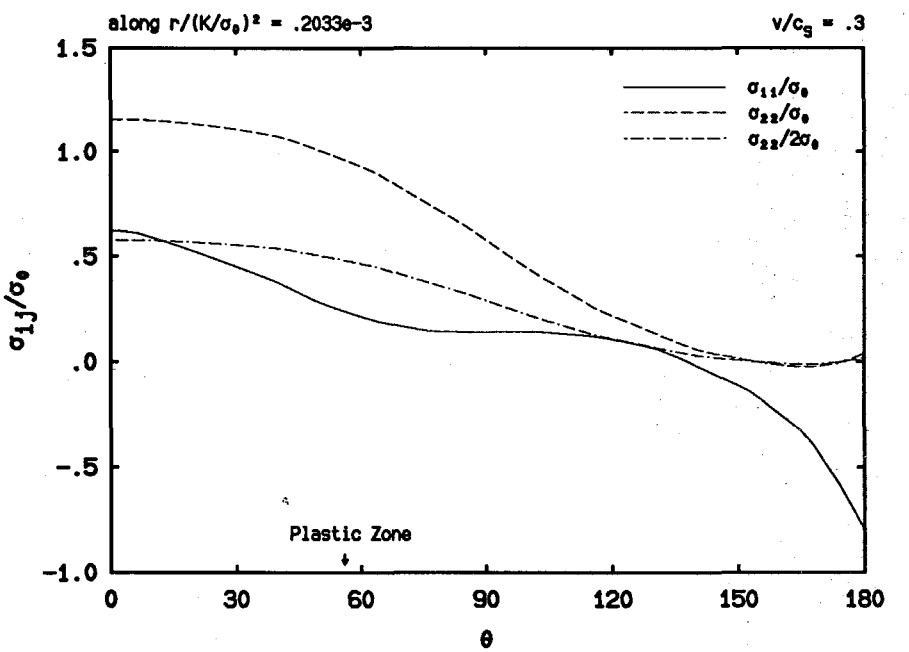

FIGURE 3.3.14 Angular variations of σ_{11}, σ_{22} and $\sigma_{22}/2$ for $v/c_s = 0.3$, normalized by σ_0.

Now it is claimed here that g_α must be a constant and that f_α must be a function of r only. This is true since otherwise from Eqs.(3.3.10) and (3.3.4) we

would have

$$\frac{\partial v_\alpha}{\partial x_1} = -sin\theta \frac{\partial g_\alpha}{\partial \theta} \frac{lnr}{r} - sin\theta \frac{\partial f_\alpha}{\partial \theta} \frac{1}{r} + O(\frac{1}{r}), \qquad (3.3.11a)$$

$$\frac{\partial v_\alpha}{\partial x_2} = cos\theta \frac{\partial g_\alpha}{\partial \theta} \frac{lnr}{r} + cos\theta \frac{\partial f_\alpha}{\partial \theta} \frac{1}{r} + O(\frac{1}{r}), \qquad (3.3.11b)$$

as r approaches zero. Note that $\frac{\partial g_\alpha(\theta)}{\partial \theta} \neq 0$ and that $\frac{\partial f_\alpha(r,\theta)}{\partial \theta}$ is singular at $r = 0$. Hence Eq.(3.3.11) would mean that $\frac{\partial v_\alpha}{\partial x_\beta}$ is more singular than $\frac{1}{r}$ as $r \to 0$, which contradicts Eq.(3.3.8).

At the moment we have showed that if the limits as $r \to 0$ taken in the above deductions exist, if operations on the order symbols are permissible, and if the crack tip is only composed of, as indicated by the results of the present finite element analysis, elastic sectors and those plastic sectors within which $\sigma_{22} \neq 2\sigma_{11}$, then the velocity field can be expressed as

$$v_\alpha(r,\theta) = c_\alpha lnr + f_\alpha(r) + h_\alpha(\theta) + o(1), \quad \text{as } r \to 0, \qquad (3.3.12)$$

where the coeffcients c_1 and c_2 are constants. Further, if velocity continuity is enforced, both c_2 and f_2 would be identically zero as required by the symmetry condition $v_2 = 0$ at $\theta = 0$.

The velocity field expressed in Eq.(3.3.12) with $c_2 = 0$ and f_α excluded is the one essentially assumed in Gao's asymptotic analysis. On the other hand, our finite element results reveal that the velocity component v_2 possesses lnr-singularity, which is apparent from Fig. 3.3.10 at least for $v/c_s \leq 0.35$. An inconsistency seems to exist. To this end, the following explanation is suggested.

First note that in Fig. 3.3.10, there are indeed signs that the lnr-singularity of the velocity component v_2 is dying out as m or v/c_s increases, as evidenced by the tendency of the declining magnitude of slope of the straight lines in Fig. 3.3.10. Secondly, discoveries from Mode III dynamic crack growth have demonstrated that the dominance zone of a first-order dynamic asymptotic solution is very small such

that it decreases rapidly as v/c_s decreases. In other words, characteristics of the leading asymptotic behavior of the crack tip fields can be clearly detected for a certain finite element mesh only at a sufficiently large crack propagation speed. This would mean that the numerical results for $v/c_s \leq 0.35$ (and for $r \geq 0.2033 \times 10^{-3}(K/\sigma_0)^2$) are essentially the solution for quasi-static crack growth or a mixture of both quasi-static and dynamic fields.

Moreover, if Eq.(3.3.12) is taken to be valid and c_2 and f_2 are set to zero in order to satisfy the symmetry conditions at $\theta = 0^0$, then the crack opening displacement (which is twice the vertical displacement u_2 at $\theta = 180^0$), which can be obtained by integrating v_2 with respect to r along $\theta = 180^0$, would be linearly dependent on r or the radial distance to the crack tip. This linear behavior indeed seems to exist for crack propagation speeds higher than certain value (e.g., the curve for $m = 0.4$ in Fig. 3.3.13b).

Recall that for crack propagation at low speeds, no plastic reloading has been detected along the crack flank (see Fig. 3.3.1). At the same time, it is noticed that the slope of the straight lines in Fig. 3.3.11a or the coefficient for the lnr singularity of the velocity component v_1 is approximately zero for small m values. To explain this behavior, it will be demonstrated in the following that the elastic (unloading) sector behind the crack front plastic sectors must be ended (near $\theta = 180^0$) with a trailing plastic sector, or otherwise, the coefficient for the lnr-term in v_1 must be zero.

In fact, suppose the elastic unloading sector extends all the way down to the crack surface. Then, since it is in an elastic sector, Eq.(3.3.7a) becomes

$$\frac{\partial v_1}{\partial x_1} = -\frac{v}{E}[(1+\nu)\frac{\partial \sigma_{11}}{\partial x_1} - \nu\frac{\partial \sigma_{kk}}{\partial x_1}], \tag{3.3.13}$$

which can be integrated with respect to x_1 to yield

$$-\frac{v}{E}[(1+\nu)\sigma_{11} - \nu\sigma_{kk}] = v_1 + P(x_2), \tag{3.3.14}$$

where $P(x_2)$ is a function of x_2 resulted from the integration.

Now from equation Eq.(3.3.12) $v_1(r,\theta) = c_1 lnr + O(1)$ as $r \to 0$. Since it has been shown that the stresses must be bounded, then from Eq.(3.3.14), the quantity $c_1 lnr + P(x_2)$ must bounded. Thus in order to cancel the nonboundedness of this quantity at $r = 0$ due to the lnr-singularity, the function $P(x_2)$ must be such that

$$P(x_2) = -c_1 ln|x_2| + \hat{P}(x_2) = -c_1 lnr - c_1 ln|sin\theta| + \hat{P}(x_2),$$

where $\hat{P}(x_2)$ is bounded. Hence, the quantity $-c_1 ln|sin\theta| + \hat{P}(x_2)$ or $c_1 ln|sin\theta|$ must be bounded since by definition $\hat{P}(x_2)$ is already bounded. This will necessarily require that $c_1 = 0$ since otherwise the whole term will not be bounded due to the fact that $ln|sin\theta| \to \infty$ as $\theta \to 180^0$. This proves the previous claim.

CHAPTER 4

LINEAR HARDENING SOLIDS

4.1 INTRODUCTION

For quasi-static crack growth in isotropic, linear hardening elastic-plastic solids, Amazigo and Hutchinson (1977) performed asymptotic analyses in Mode III and in Mode I plane stress and plane strain through separable form solutions. By assuming the existence of an active plastic zone at the crack front, and by neglecting the possible reverse plastic loading along the traction-free crack surface, they were able to obtain angular variations of the crack tip stress and plastic strain rate fields, and to determine their order of singularities at the crack tip.

The above analyses were generalized in Mode III by Dunayevsky and Achenbach (1982b) for low hardening materials so as to approach the elastic-perfectly plastic solution when hardening disappears, and were extended in Mode III and Mode I plane stress and plane strain to include a secondary plastic zone along the crack flank by Ponte Castañeda (1987a), who also studied the Mode II plane stress and plane strain cases. Ponte Castañeda (1987b) also introduced a novel method for obtaining an approximate amplitude factor of the near-tip singular field and approximate crack tip active plastic zone shapes.

Finite element studies under steady state and small-scale yielding conditions were carried out by Dean and Hutchinson (1980) in Mode III with comparisons to the asymptotic results of Amazigo and Hutchinson (1977), and Dean (1983) in Mode I plane stress. Both of the studies gave explicit results regarding the crack

tip opening displacement variations and the effect of hardening on the shape of the crack tip primary active plastic zone.

For nonisotropic hardening materials, the effect of yield surface vertices was considered by Lo and Peirce (1981) in Mode III, with a phenomenological J_2 corner theory of plasticity (Christoffersen and Hutchinson, 1979). An analysis for Mode I plane strain, steady state quasi-static crack growth was performed by Zhang, Zhang and Hwang (1983) to study Bauschinger-like effects for anisotropic linear hardening solids. Finite element computations for steady state, quasi-static crack growth conducted by Lam (1982) and Lam and McMeeking (1984) in Mode I plane strain also investigated the effect of kinematic hardening with a bilinear stress strain relation.

Under dynamic crack propagation conditions, the asymptotic quasi-static solution of the variable separable type by Amazigo and Hutchinson (1977) were extended for isotropic linear hardening materials to include inertia by Achenbach and Kanninen (1978) in Mode III, and Achenbach, Kanninen and Popelar (1981) in Mode I plane stress and plane strain. It is noted that both of the above studies neglected the possible reverse plastic loading along the crack flank, which may yield large errors when this secondary plastic zone is large.

In the following, we will report the results of a very detailed finite element investigation of the crack tip fields for cracks growing in isotropic, linear hardening solids, under conditions of Mode I plane stress, steady state and small-scale yielding. We will compare the solutions of this study to available asymptotic and numerical counterparts in the literature. Detailed discussions regarding the evolutionary variations of the field quantities with respect to the crack propagation speed and the effect of linear strain hardening on the crack tip fields will be presented. All computations are carried out for the case of the Poisson ratio $\nu = 0.3$. All logarithmic values used in figures are based on the natural number e.

4.2 QUASI-STATIC CRACK GROWTH

Quasi-static crack growth in linear hardening solids under Mode I plane stress and steady state conditions has been investigated through asymptotic analyses using separable solutions of assumed form by Amazigo and Hutchinson (1977) and by Ponte Castañeda (1987a), and through a finite element analysis of the Eulerian type under small-scale yielding conditions by Dean (1983). Explicit results were obtained by Amazigo and Hutchinson and Ponte Castañeda regarding the singularities and angular variations of the crack tip asymptotic stress and velocity fields, and by Dean regarding the shape of the crack tip active plastic zone and the radial dependence of the crack opening profile. In the following subsections, comparisons of the present numerical solution with those mentioned above will be perfomed whenever possible.

The Active Plastic Zones

Approximations for the shapes of the crack tip active plastic zones under small-scale yielding conditions have been given by Dean (1983) and by Ponte Castañeda (1987b). While the approximation by Dean is from a finite element analysis very similar to ours, the one by Ponte Castañeda is the result of matching trial functions to the near-tip elastic-plastic asymptotic fields and to the elastic far-fields, with parameters optimized through the use of a variational compatibility statement. Comparisons with the results of the previous two investigations are shown in Fig. 4.2.1 for $\alpha = 0.25$ and 0.1, where α is the hardening parameter. Note that in Ponte Castañeda's calculation, Poisson ration $\nu = 0.5$ is used, instead of $\nu = 0.3$ which is used by Dean and by the present study. It is seen from Fig. 4.2.1a, as in the case of perfect plasticity discussed in Chapter 3 (see Fig. 3.2.1), Dean's result gives a plastic zone larger than ours. Considering the fact that the current study employed a near-tip finite element mesh much finer than Dean's, it is felt that the current study gives a better approximation for the crack tip active plastic zone.

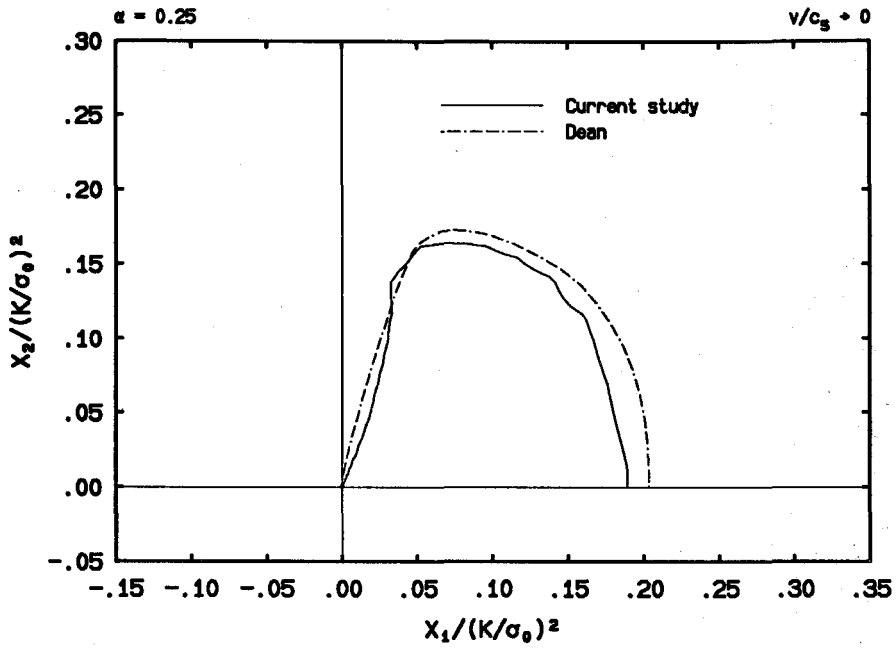

FIGURE 4.2.1a The shape of the crack tip active plastic zone for $\alpha = 0.25$, compared with that of Dean (1983) in normalized coordinates, with the origin located at the crack tip.

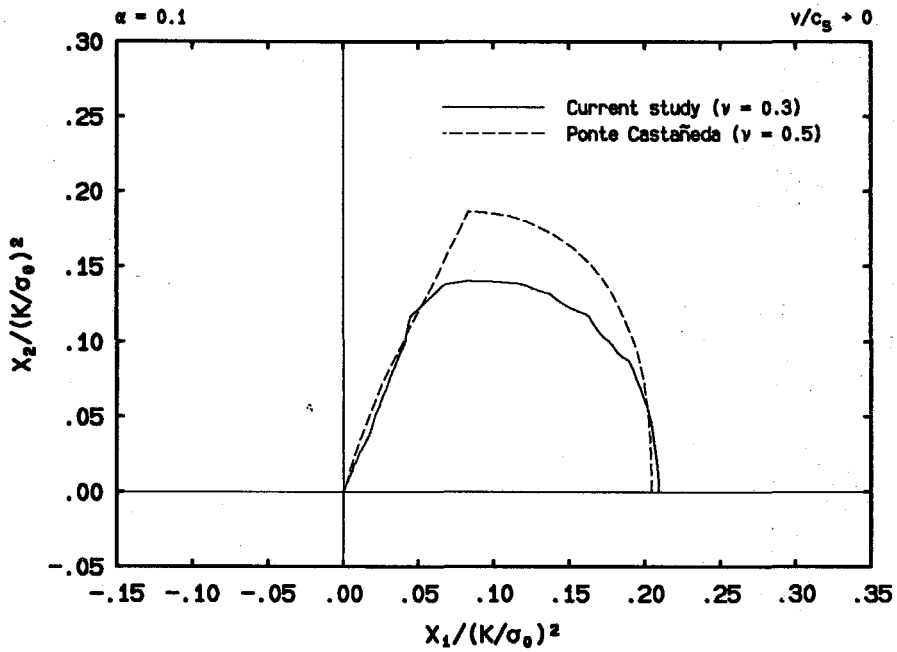

FIGURE 4.2.1b The shape of the crack tip active plastic zone for $\alpha = 0.1$, compared with that of Ponte Castañeda (1987b) in normalized coordinates, with the origin located at the crack tip.

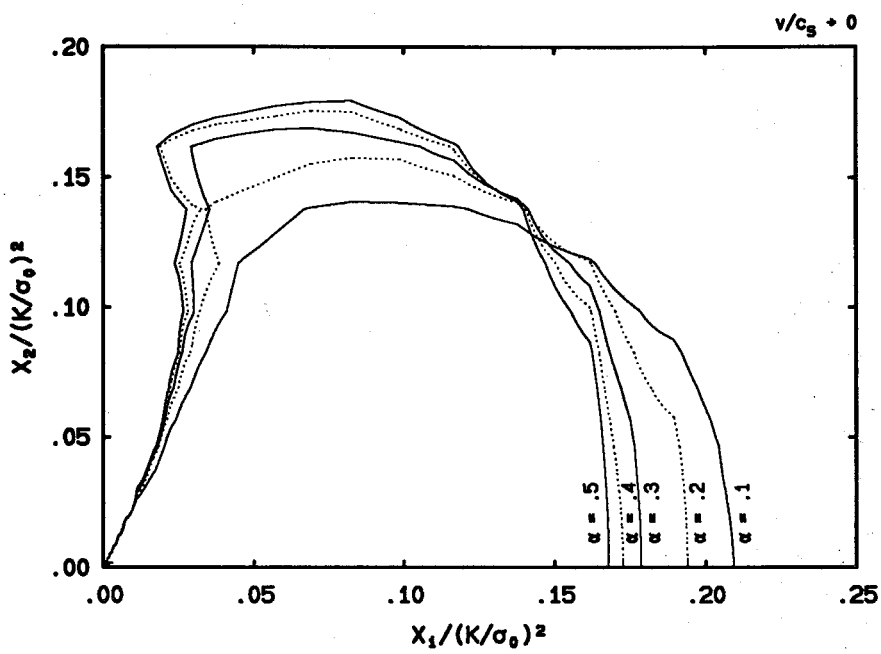

FIGURE 4.2.2 The effect of hardening on the shape of the crack tip active plastic zone in normalized coordinates, with the origin located at the crack tip.

As to the comparison with Ponte Castañeda's result, it is seen from Fig. 4.2.1b that both calculations agree well on the size of the active plastic zone along the prospective crack line, and on the angular extent of the active plastic zone. Yet Ponte Castañeda's approximation estimated a much higher value for the height of the active plastic zone than ours. However it should noted that Ponte Castañeda's result also gave a large plastic zone size in Mode III, but in the horizontal direction rather than in the vertical direction. Nonetheless, due to the use of different Poisson ratio values, it is difficult to draw definite conclusions from the above comparison.

The effect of hardening on the shape of the crack tip active plastic zone is illustrated in Fig. 4.2.2. It is found that as the level of strain hardening decreases (i.e., as the hardening parameter α decreases), the size of the active plastic zone increases from $0.168(K/\sigma_0)^2$ at $\alpha = 0.5$ to $0.209(K/\sigma_0)^2$ at $\alpha = 0.1$ in the horizontal direction, and it decreases from $0.179(K/\sigma_0)^2$ at $\alpha = 0.5$ to $0.140(K/\sigma_0)^2$ at $\alpha = 0.1$ in the vertical direction.

Estimation for the angular extent of the active plastic zone or the angle at which elastic unloading occurs is very sensitive to the contour value used in estimating the shape of the active plastic zone. Consequently, this subject will be temporarily dropped until the angular variation of the stress field is discussed. Moreover, it is worth mentioning that there are no signs of the existence of secondary active plastic zones at the back of the quasi-statically growing crack tip for the hardening parameter values discussed here. This observation will be further studied in the next subsection.

Angular Field Variations

We present the crack tip stress and velocity field variations in this subsection. First of all, a comparison of stress variations is made with the asymptotic solutions of Ponte Castañeda (1987a) which was carried out for the value of the Poisson ratio $\nu = 0.5$. As shown in Fig. 4.2.3, where σ_{rr}, $\sigma_{\theta\theta}$ and $\sigma_{r\theta}$ are the polar stress components, σ_e is the effective stress and σ is the flow stress denoting the current yield surface, the comparison demonstrates very good agreement between the analytical results (for Poisson ratio $\nu = 0.5$) and the finite element results (for $\nu = 0.3$). Furthermore, the asymptotic analysis of Ponte Castañeda predicts that elastic unloading occurs at an angle around 73.65^0 (see Fig. 4.2.3) right at the angular position where the effective stress becomes smaller than the flow stress. On the one hand, this comparison suggests that the Poisson ratio ν has little effect on the stress variation near the crack tip where the elastic part of the strains is negligible compared to its plastic counterpart. On the other hand, this good agreement indicates that the present finite element mesh is fine enough to capture the asymptotic behavior of the crack tip stress and deformation fields. Consequently, the findings of this numerical study can be interpreted with greater confidence.

The effect of hardening on the angular stress variations are demonstrated through the progressive changes of stress components with respect to the linear

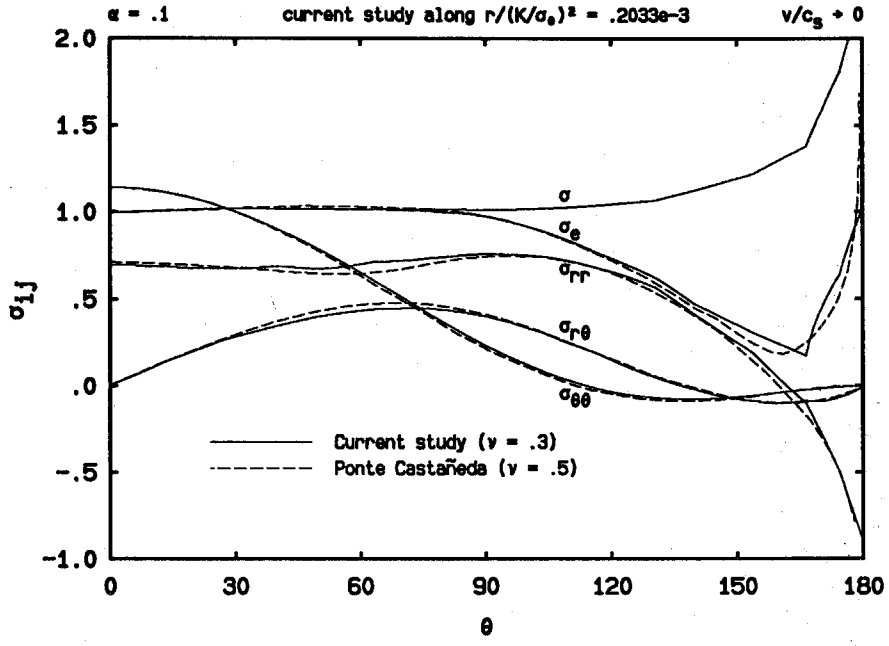

FIGURE 4.2.3 Angular variations of the polar stress components, the effective stress σ_e and the flow stress σ for $\alpha = 0.1$, normalized such that $\sigma_e = 1$ at $\theta = 0^0$, with comparisons to the asymptotic solution by Ponte Castañeda (1987a).

hardening parameter α, as shown in Fig. 4.2.4 where all stress quantities are normalized such that $\sigma_e = 1$ at $\theta = 0^0$. The general tendencies of the stress variations are consistent with the asymptotic solutions by Amazigo and Hutchinson (1977), which was later elaborated by Ponte Castañeda (1987a) as discussed earlier. Moreover, the numerical solution seems to show that the slopes of σ_{rr} at $\theta = 0^0$, and $\sigma_{\theta\theta}$ at $\theta = 0^0$ and 180^0, are very close to zero for all α values computed. Substantial compressive radial stresses behind the crack tip are observed for all α values studied. Consequently, as in the elastic-perfectly plastic case, a tendency of reverse loading exists at the back of the crack tip. However, it is clear from our numerical solution, as indicated by the relative magnitudes of the effective stress σ_e and the flow stress σ, that this tendency is not strong enough for the stress state at the back of the crack tip to regain yielding. This is consistent with existing analytical solutions. For example, according to the asymptotic solution of Ponte Castañeda (1987a), plastic reloading occurs only for $\alpha \leq 0.01$ and at an angle very close to

$\theta = 180^0$. Hence, the plane stress solution by Amazigo and Hutchinson (1977), in which the possibility of plastic reloading behind the crack tip is neglected, is indeed a very accurate approximation. It can be further observed from Fig. 4.2.4 that the value of the circumferential stress component is very close to zero near the crack flank from $\theta = 165^0$ to 180^0. It is noted that the symmetry condition at $\theta = 0^0$ and the traction-free condition at $\theta = 180^0$ are very well satisfied, which is a major sign indicating the convergence of the numerical solution.

It is also worth pointing out that the angular extent of the crack tip active plastic zone or the angle at which elastic unloading occurs can be estimated from the position where the effective stress σ_e deviates from the flow stress σ. To do that numerically, an error tolerance for the relative difference of the effective stress σ_e with respect to the flow stress σ must be specified. For example, we can set the tolerance to be the value such that for $\alpha = 0.1$, the numerically estimated angle value equals the analytically obtained angle value by Ponte Castañeda. It is found that this tolerance is approximately 0.77×10^{-2}. Accordingly, the angle for the active plastic zone is estimated to be 77.9^0 for $\alpha = 0.5$ and 72.4^0 for $\alpha = 0.05$. We have compared these estimations for different α values with those of Ponte Castañeda's asymptotic analysis. Very good agreement is found despite the fact that the present finite element computation is carried out for Poisson ratio $\nu = 0.3$ and the asymptotic solution is for $\nu = 0.5$.

The angular variations of the Cartesian velocity components for $\alpha = 0.1$, with comparisons to the results of Ponte Castañeda (1987a), are shown in Fig. 4.2.5 where the velocity quantities are normalized such that $v_1 = -1$ at $\theta = 0^0$. The comparison between the numerical solution and the analytical solution demonstrates, as in the case of stress variations, that a rather good agreement is achieved. This fact confirms an earlier observation that the angular variations of the stress and deformation fields do not depend strongly on the Poisson ratio at locations very near the crack tip.

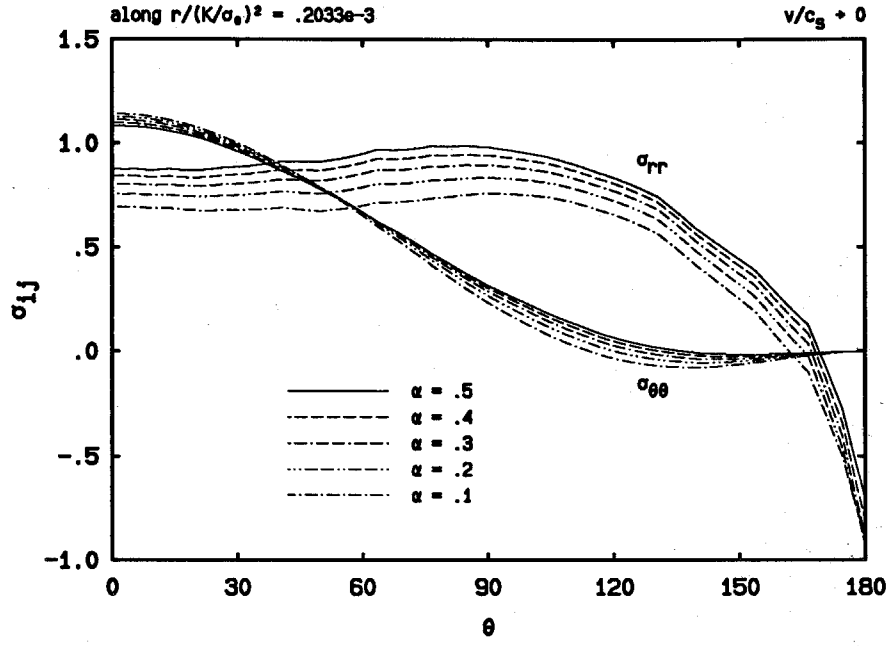

FIGURE 4.2.4a The effect of hardening on the angular variations of the polar stress components σ_{rr} and $\sigma_{\theta\theta}$, normalized such that the effective stress $\sigma_e = 1$ at $\theta = 0^0$.

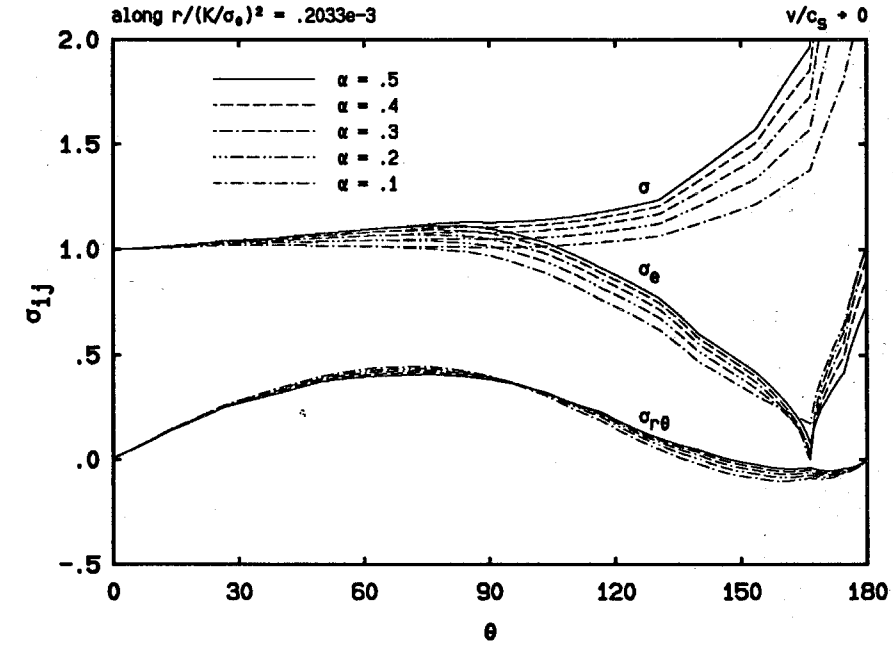

FIGURE 4.2.4b The effect of hardening on the angular variations of the polar stress component $\sigma_{r\theta}$, the effective stress σ_e and the flow stress σ, normalized such that $\sigma_e = 1$ at $\theta = 0^0$.

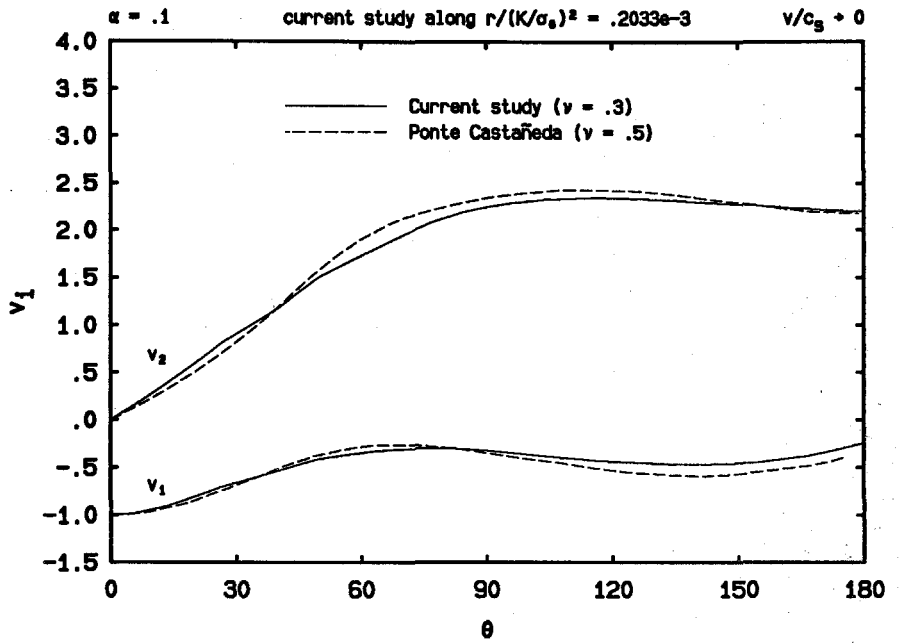

FIGURE 4.2.5 Angular variations of the Cartesian velocity components for $\alpha = 0.1$, normalized such that $v_1 = -1$ at $\theta = 0^0$, with comparisons to the asymptotic solution by Ponte Castañeda (1987a).

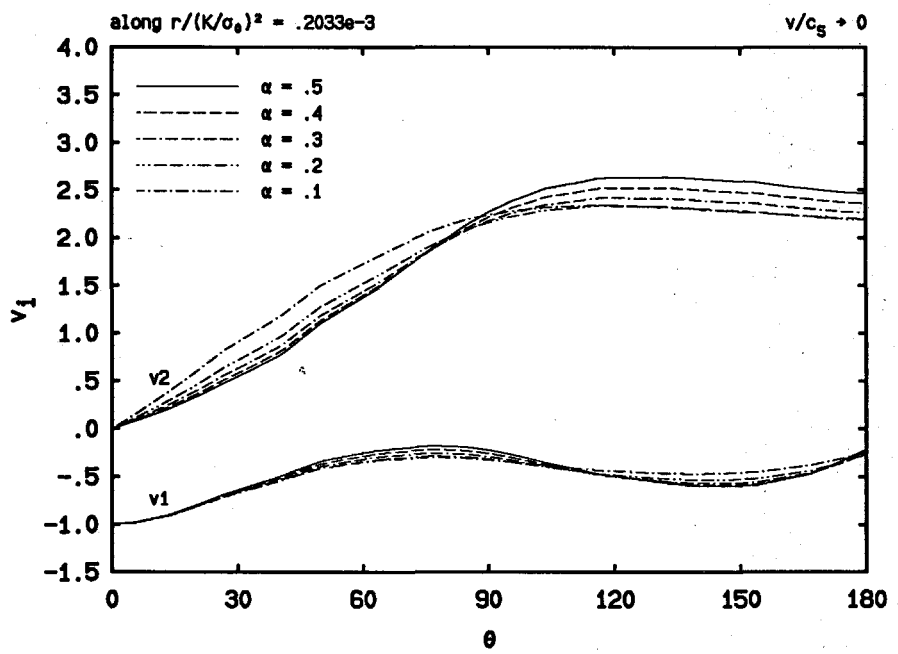

FIGURE 4.2.6 The effect of hardening on the angular variations of the Cartesian velocity components, normalized such that $v_1 = -1$ at $\theta = 0^0$.

The dependence of the angular velocity variations on the linear hardening parameter α is illustrated in Fig. 4.2.6 with normalizations mentioned above. It is observed that v_1 always stays negative whereas v_2 stays positive. At $\theta = 0^0$, the slope of v_2 is found to increase as α decreases. At locations outside the crack tip active plastic zone, i.e., for θ values approximately larger than 70^0, the magnitude of v_2 is always about three times larger than that of v_1.

Radial Field Variations

The radial variations of the stress components are presented here for $\theta = 0^0$, i.e., along the prospective crack line, which are plotted in Fig. 4.2.7 in their original normalized forms and in Fig. 4.2.8 in double-logarithmic coordinates. Note that all data are taken from five elements away from the crack tip and that only one data point is extracted from each element.

It is clear from Fig. 4.2.7 that both σ_{11} and σ_{22} possess strong singularities at the crack tip, and that the magnitudes of the stress distributions decrease as the hardening parameter α decreases. Straight lines are found in Fig. 4.2.8, where the data point on the left is closest to the crack tip. Apparently, it can be concluded from Fig. 4.2.8 that the stresses behave as r^s as $r \to 0$, with the singularity parameter s being negatively valued. Both the absolute value of s, i.e., the slope of a straight line, and the magnitudes of the stress components are found to decrease as α decreases, which means that the crack tip stress field is less singular for materials with less strain hardening. At the same time, it is discovered that the straight lines in Fig. 4.2.8 start to curve up at locations away from the crack tip, especially for smaller α values. In other words, the range of linearity in these plots become smaller as α becomes smaller, which seems to suggest that the dominance zone of the r^s singularity diminishes as hardening disppears. The magnitude of σ_{22} is found to be consistently larger than that of σ_{11}.

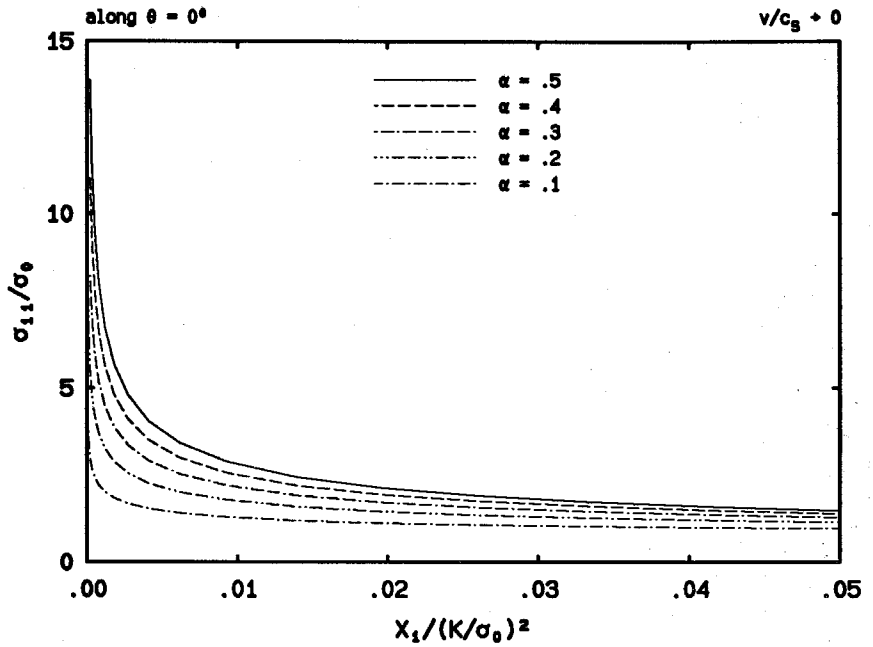

FIGURE 4.2.7a The radial variations of the stress component σ_{11} along the prospective crack line in normalized coordinates.

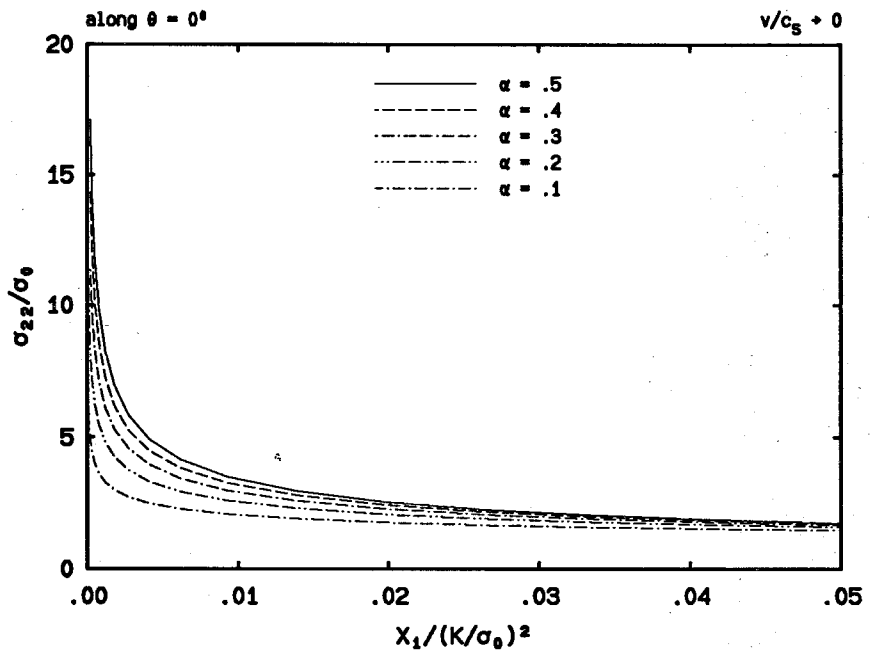

FIGURE 4.2.7b The radial variations of the stress component σ_{22} along the prospective crack line in normalized coordinates.

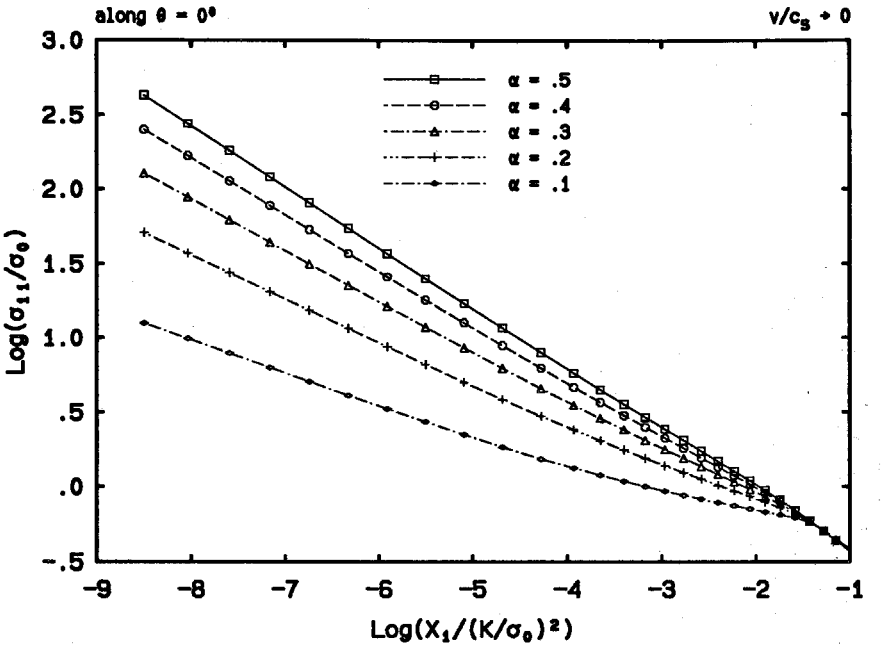

FIGURE 4.2.8a The radial variations of the stress component σ_{11} along the prospective crack line in double-logarithmic coordinates.

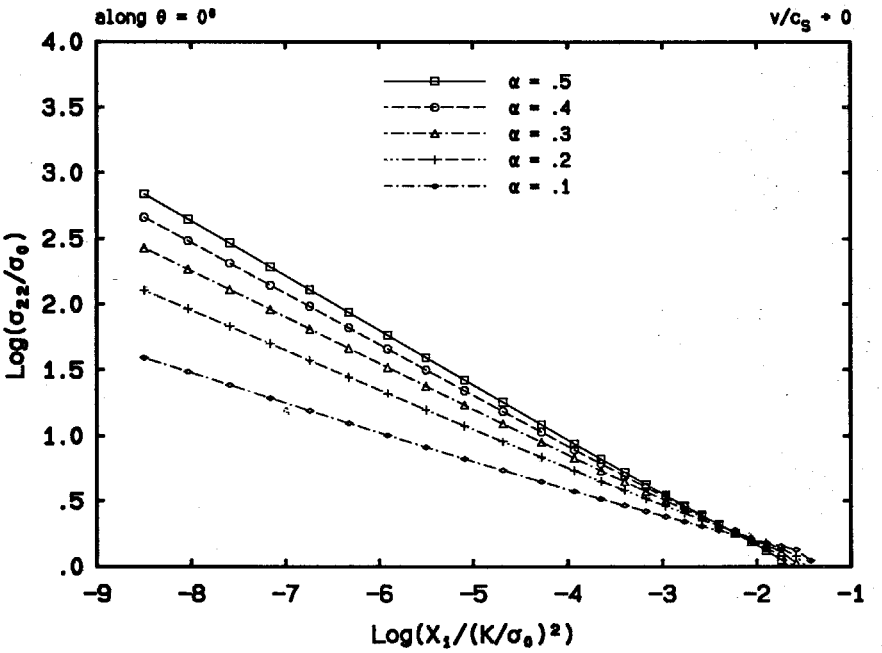

FIGURE 4.2.8b The radial variations of the stress component σ_{22} along the prospective crack line in double-logarithmic coordinates.

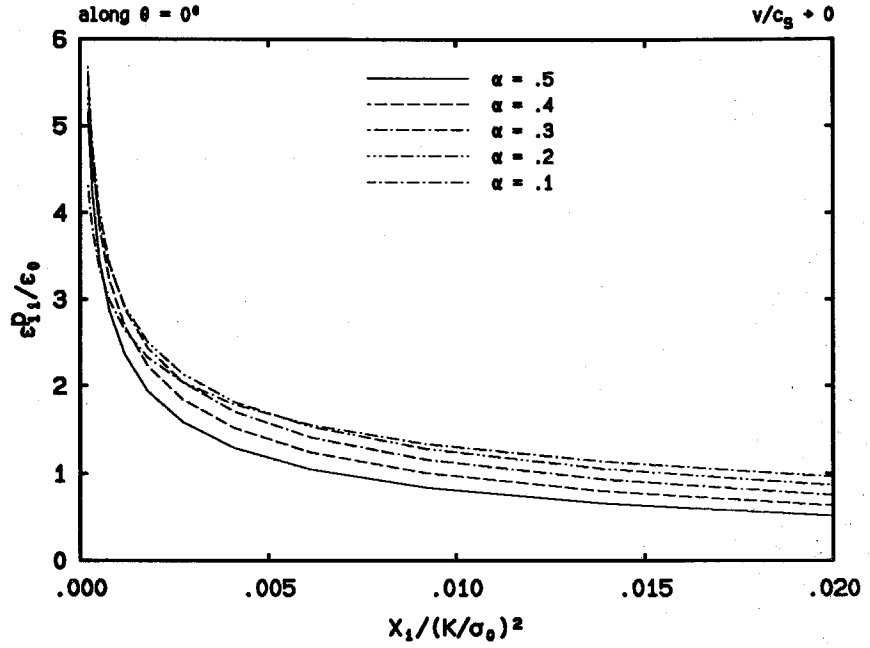

FIGURE 4.2.9a The radial variations of the plastic strain component ε_{11}^p along the prospective crack line in normalized coordinates.

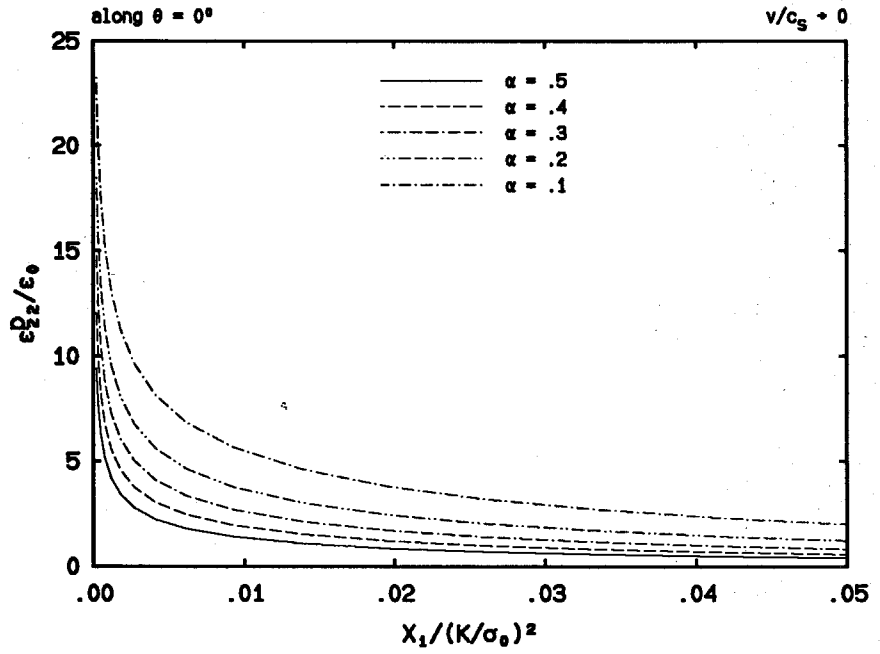

FIGURE 4.2.9b The radial variations of the plastic strain component ε_{22}^p along the prospective crack line in normalized coordinates.

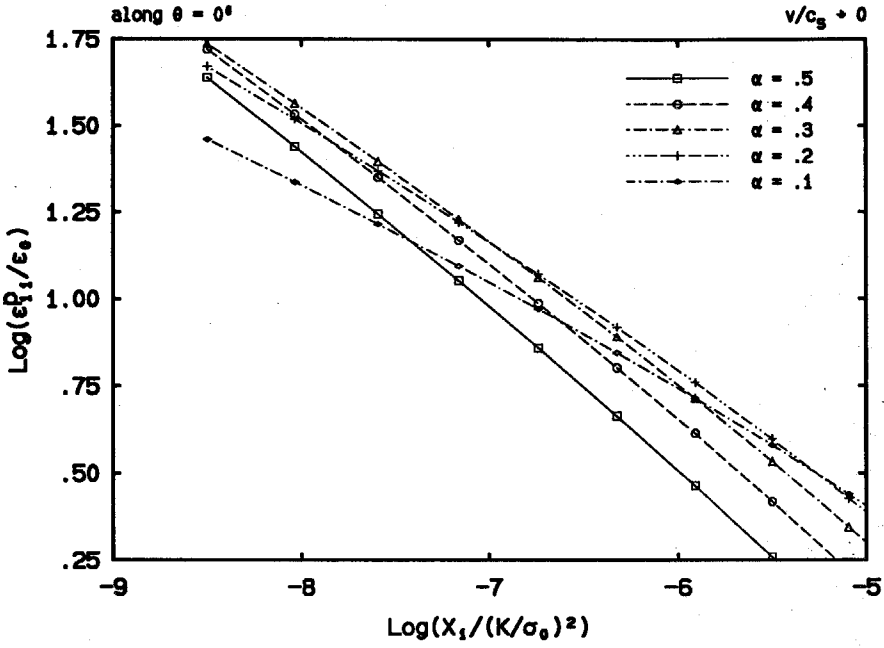

FIGURE 4.2.10a The radial variations of the plastic strain component ε_{11}^{p} along the prospective crack line in double-logarithmic coordinates.

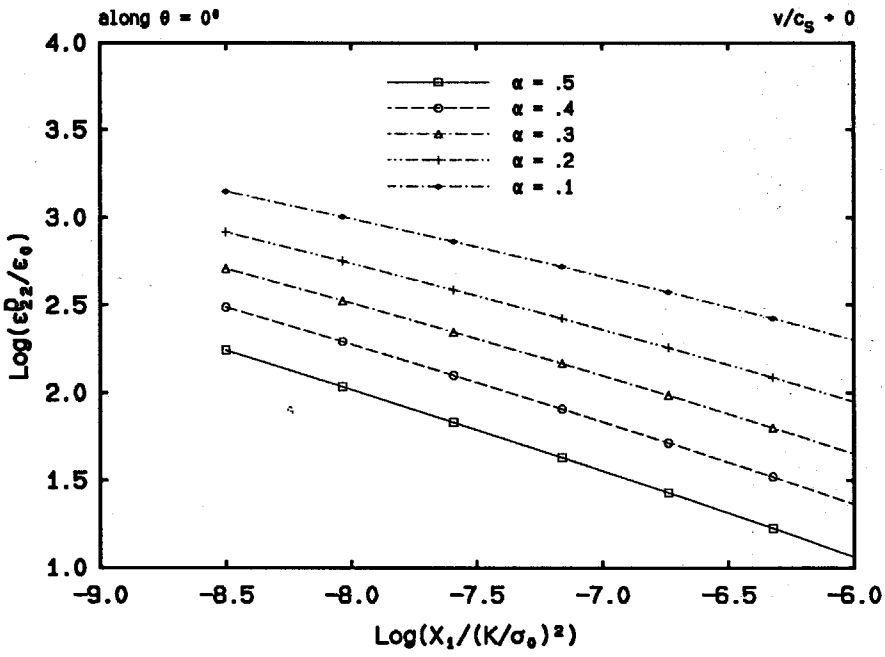

FIGURE 4.2.10b The radial variations of the plastic strain component ε_{22}^{p} along the prospective crack line in double-logarithmic coordinates.

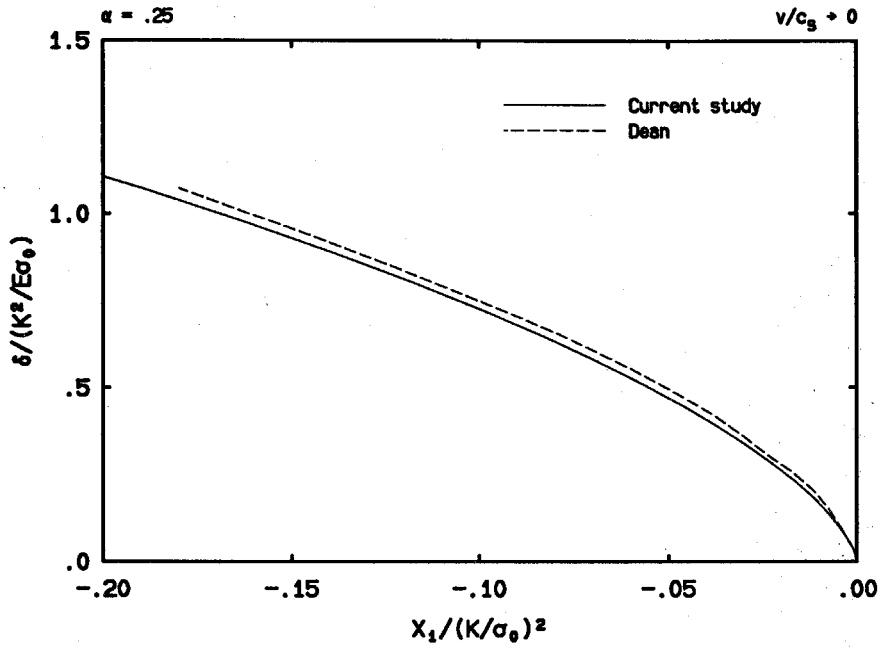

FIGURE 4.2.11 The crack opening displacement δ (twice of the vertical displacement u_2 along the crack surface) in its normalized form, compared with the finite element solution by Dean (1983).

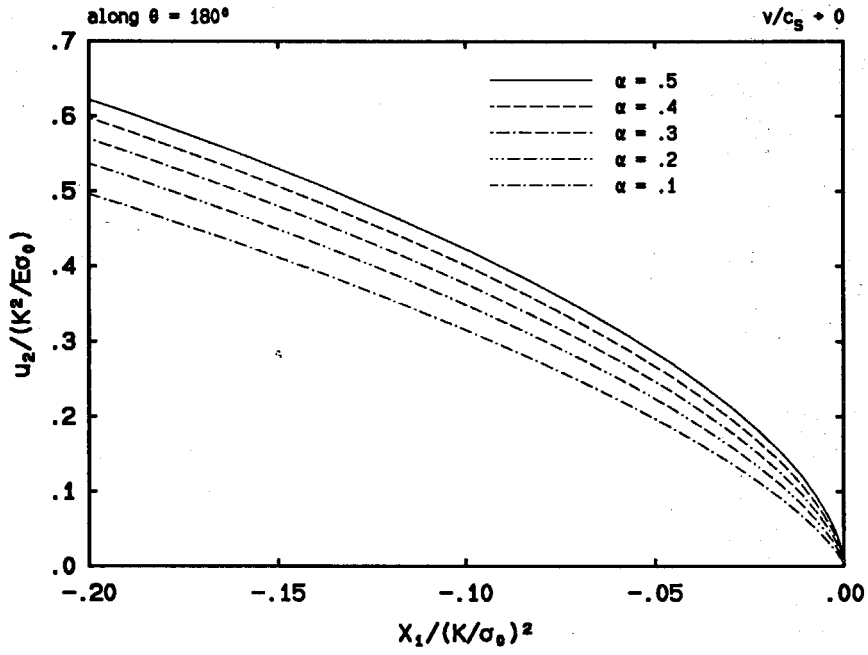

FIGURE 4.2.12 The effect of strain hardening on the radial variation of the vertical displacement u_2 along the crack surface, plotted in its normalized form.

The radial dependence of the plastic strain components along $\theta = 0^0$ is shown in Figs. 4.2.9 and 4.2.10. As in the case of stress variations, the plastic strain components are found to be strongly singular at the crack tip. It is seen from Fig. 4.2.9 that the magnitude of ε_{22}^p is always larger for smaller α values, whereas for ε_{11}^p the opposite seems to show up very near the crack tip. Judging from the tendency illustrated in Fig. 4.2.10a, it seems true that as the crack tip is approached, ε_{11}^P will take on smaller values for smaller α. It is also observed that the magnitude of ε_{22}^p is much larger than that of ε_{11}^p, which is especially true for lower α values. Again, approximately straight lines are observed in Fig. 4.2.10 where the plastic strain variations are plotted in double-logarithmic coordinates, which indicates that plastic strains have the same type of singularities at the crack tip as the stresses, i.e., they behave as r^s $(s < 0)$ as the crack tip is approached. Moreover, the absolute values of the slopes of the straight lines are found to decrease as α decreases, thus confirming our earlier findings from Fig. 4.2.8 that the singularities of the crack tip fields become weaker as α decreases.

As discussed earlier in the introductory section, Amazigo and Hutchinson (1977), and later Ponte Castañeda (1987a), indeed were able to obtain asymptotic solutions with stress and velocity singularities of the form r^s $(s < 0)$. In these investigations, a solution with the above-mentioned singularity was assumed directly. This assumption resulted in a system of ordinary differential equations in θ subject to appropriate boundary and continuity conditions. The ODE system was then solved numerically for the angular variations of the stress and velocity fields and for the value of the singularity.

To compare with the analytical solution regarding the s-values for various α-values, a least square fitting is made to our finite element result at the crack front, with data extracted from the sixth to the tenth elements assuming that the crack tip coincides with the lower-left node of the first element. This type of estimation is performed for each stress component, and the mean value for s is taken to the

final estimation. The comparison is given in Table 4.2.1, where s_1 is the estimation from σ_{11}, s_2 is the estimation from σ_{22}, s_a is the average of s_1 and s_2, and s_r is the reference value for Poisson ratio $\nu = 0.5$ from the asymptotic solution by Ponte Castañeda (1987a), and ϵ is the percentage relative difference of s_a with respect to s_r.

Table 4.2.1 Values of the singularity parameter s at $m = 0.4$

α	s_1	s_2	s_a	s_r	ϵ (%)
.5	-.412	-.416	-.414	-.420	1.4
.3	-.346	-.352	-.349	-.357	2.2
.2	-.297	-.303	-.300	-.310	3.2
.1	-.223	-.228	-.225	-.237	5.1

It can be observed from the table that the differences between the finite element results and the asymptotic results are indeed very small. As to the magnitude of the difference in s, it is seen that as α decreases, the magnitude tends to increase, which somehow reflects the shrinked region of dominance of the leading stress singularity, and hence the increased error by approximating the stress curves as straight lines in the double-logarithmic coordinates.

The size of the r^s stress singularity dominance zone can be estimated by setting a relative error tolerance between the original numerical data and the fitted data. For example, by requiring that the relative error be within 5%, we have obtained such estimations along $\theta = 0^0$, which are shown in Table 4.2.2. In the table, the size of the dominance zone is normalized by the horizontal size of the crack tip active plastic zone. Computation is performed for both of the nonzero stress components and the actual maximum relative error is shown beside each ratio. It can be observed consistently that the stress component σ_{22} has a much larger dominance zone than the stress component σ_{11}. Moreover, the size of the dominance zones for both stress components is found to decrease rapidly as α or the level of strain hardening

decreases. Nonetheless, it seems that the r^s stress singularity has a surprizingly large dominance zone at the crack tip.

Table 4.2.2 Ratio of the r^s stress singularity dominance zone size to the active plastic zone size along $\theta = 0^0$

α	for σ_{11}	$\epsilon(\sigma_{11})$ (%)	for σ_{22}	$\epsilon(\sigma_{22})$ (%)
.5	.640	4.9	1.43	4.4
.3	.234	4.6	.838	4.8
.2	.170	5.0	.467	4.6
.1	.0939	4.4	.247	4.7

Finally we present the results of the crack opening displacement for steady state quasi-static crack growth. For $\alpha = 0.25$, a comparison with that of a similar finite element investigation by Dean (1983) is shown in Fig. 4.2.11. Note that the crack opening displacement δ is twice of the vertical displacement u_2 of the crack surface. It is seen that, as observed for crack growth in elastic-perfectly plastic materials discussed in Chapter 3 (see Fig.3.2.8), the crack opening profile predicted by Dean is slightly larger than that of the current study, which may be due to the fact that a coarser mesh is employed by Dean.

The dependence of the crack opening profile on the linear hardening parameter α is depicted in Fig. 4.2.12. It is discovered, as expected, that the magnitude of u_2 decreases as α decreases, which is apparently due to the fact that as α decreases, the material in question becomes "softer."

4.3 DYNAMIC CRACK PROPAGATION

Dynamic crack propagation in linear hardening solids under Mode I plane stress and steady state conditions has been investigated through asymptotic analyses using separable solutions of assumed form by Achenbach, Kanninen and Popelar (1981), in a manner similar to the one by Amazigo and Hutchinson (1977) for quasi-static

crack growth. Explicit results were obtained regarding the singularities of the crack tip stress and velocity fields, and the asymptotic angular variations of the stress components in the active plastic zone. In the following subsections, comparisons of the present numerical solution with the asymptotic solution of Achenbach et al. will be perfomed whenever possible.

The Active Plastic Zones

Shown in Figs. 4.3.1a and 4.3.1b is the effect of hardening on the shape of the crack tip active plastic zone for $m = 0.3$ and $m = 0.5$, where m is called the Mach number and is defined as the ratio of the speed of crack propagation, v, to that of the elastic shear wave, c_s. It is found that the existence of a secondary active plastic zone behind the crack tip is detected by the present finite element study for $\alpha = 0.05$ at $m = 0.5$, although there is no sign of such a reloading zone for any linear hardening parameter at the lower Mach number $m = 0.3$.

As in the case of quasi-static crack growth (see Fig. 4.2.2), it is found that as the linear hardening parameter α decreases, the active plastic zone elongates in the direction of crack propagation, and it shrinks slightly in the direction perpendicular to that of crack propagation at $v/c_s = 0.5$. For example, at $v/c_s = 0.3$, the width and height of the active plastic zone change, respectively, from $0.177(K/\sigma_0)^2$ and $0.202(K/\sigma_0)^2$ at $\alpha = 0.5$ to $0.221(K/\sigma_0)^2$ and $0.164(K/\sigma_0)^2$ at $\alpha = 0.1$.

Moreover, it is observed from Fig. 4.3.1a that at $v/c_s = 0.3$, the near-tip angular extent of the crack front active plastic zone almost remains the same as α or the level of strain hardening decreases. Recall that in the case of quasi-static crack growth (see Fig. 4.2.2), the situation is very similar. However, at $v/c_s = 0.5$ which is the highest crack speed we have investigated, it can be seen clearly from Fig. 4.3.1b that as α decreases, the angular extent of the crack fron active plastic zone is actually increasing.

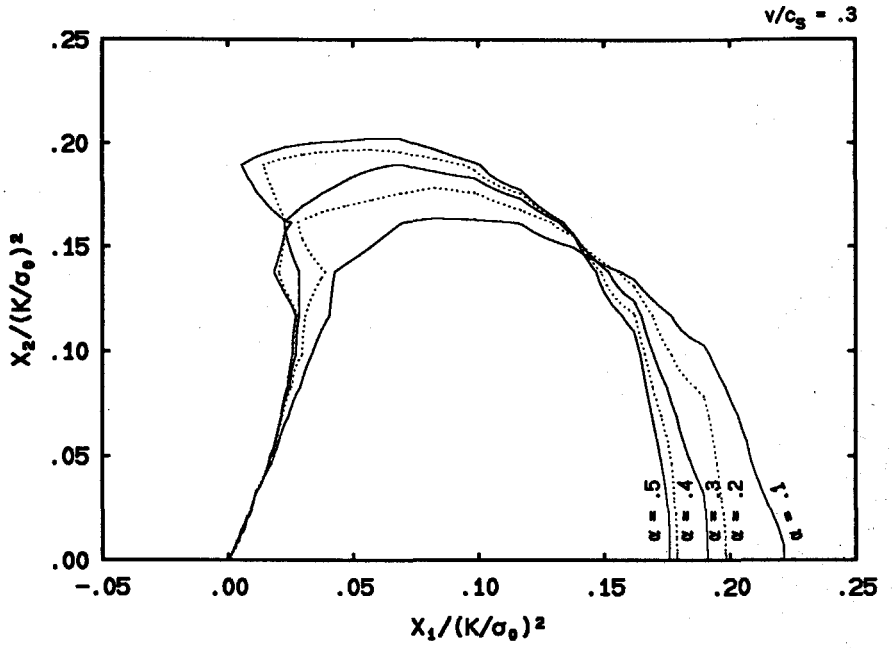

FIGURE 4.3.1a The effect of hardening on the shape of the crack tip active plastic zone at $v/c_s = 0.3$, plotted in normalized coordinates with the origin located at the crack tip.

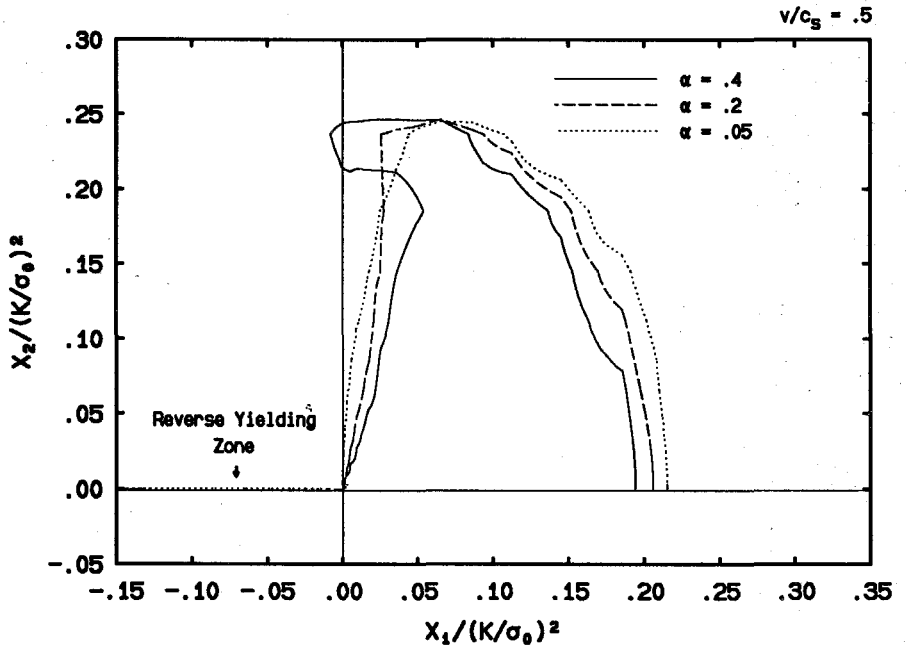

FIGURE 4.3.1b The effect of hardening on the shape of the crack tip active plastic zone at $v/c_s = 0.5$, plotted in normalized coordinates with the origin located at the crack tip.

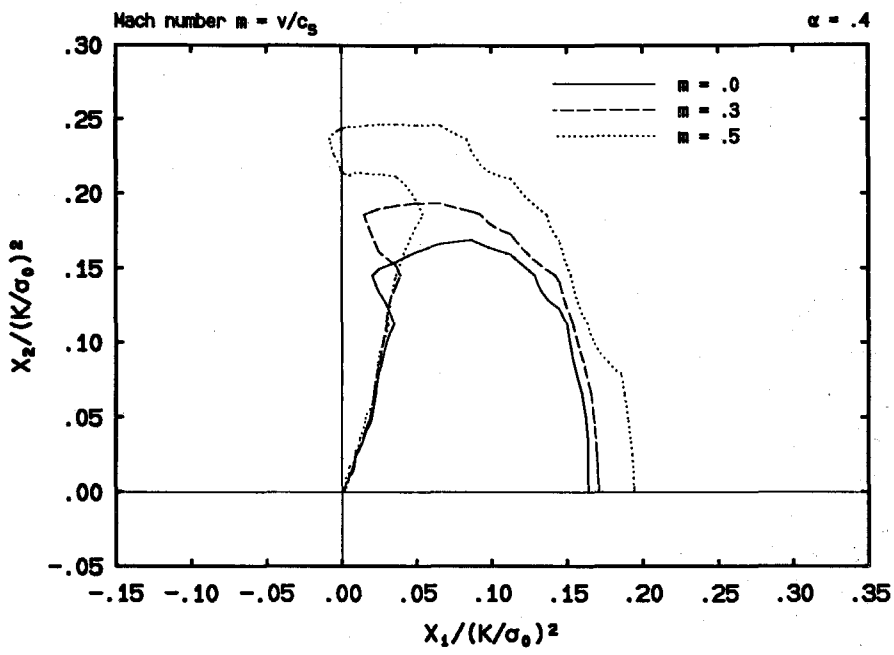

FIGURE 4.3.2a The effect of crack propagation speed on the shape of the crack tip active plastic zone for $\alpha = 0.4$, plotted in normalized coordinates, with the origin located at the crack tip.

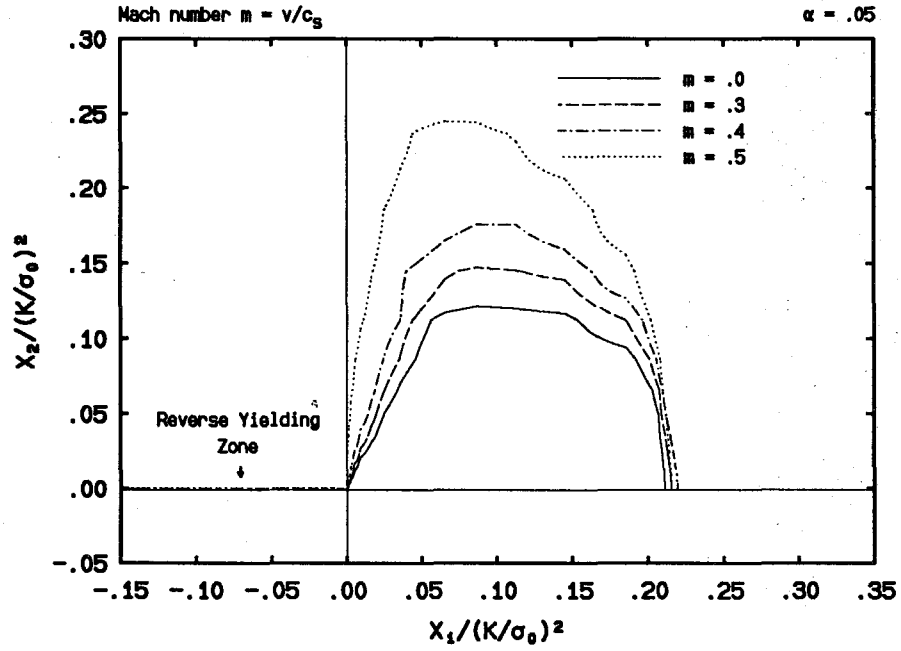

FIGURE 4.3.2b The effect of crack propagation speed on the shape of the crack tip active plastic zone for $\alpha = 0.05$, plotted in normalized coordinates, with the origin located at the crack tip.

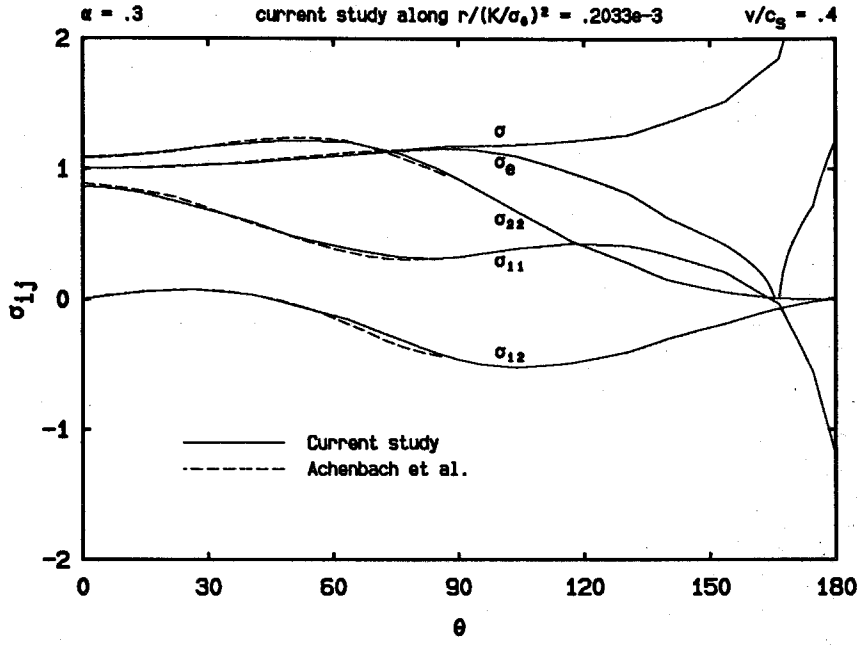

FIGURE 4.3.3 Angular variations of the polar stress components, the effective stress and the flow stress for $\alpha = 0.3$ and $v/c_s = 0.4$, normalized such that the effective stress $\sigma_e = 1$ at $\theta = 0^0$, with comparisons to the asymptotic solution by Achenbach, Kanninen and Popelar (1981).

As explained previously for quasi-static crack growth, the determination of the angle separating the active plastic zone and the elastic unloading zone is very sensitive to the contour value employed in estimating the shape of the active plastic zone. Nontheless, a rough estimation of the unloading angle can be made from the angular variation of the stress field which is to be discussed.

The evolutionary variations of the crack tip active plastic zone with respect to the crack propagation speed is illustrated in Fig. 4.3.2a for $\alpha = 0.4$ and in Fig. 4.3.2b for $\alpha = 0.05$. It is seen that for $\alpha = 0.4$, a typical value for materials with relatively high level of strain hardening, the active plastic zone expands at the crack front as m increases, whereas in the limiting case of $\alpha = 0$ (i.e., for elastic-perfectly plastic materials), the plastic zone actually shrinks, although slightly, at the crack front (see Fig. 3.3.1a). In fact, this tendency is already evident for the low-hardening case of $\alpha = 0.05$ shown in Fig. 4.3.2b, where it is observed that as m

increases, the size of the active plastic zone along the crack line first increases and then decreases. As to the height and the angular extent of the active plastic zone, the same tendency is exhibited for all the cases, namely that as m increases, both the height and the angular extent increase, except that the percentage of increase is much higher for lower hardening materials.

Another feature of the active plastic zone worth mentioning is that, at higher crack propagation speeds and for lower levels of strain hardening, for example, at $m = 0.4$ and 0.5 for $\alpha = 0.05$ (see Fig. 4.3.2b), secondary active plastic zones are indeed detected by the present finite element solution. It is noted, however, that reversed plastic reloading is limited to an area very close to the crack flank. The same feature is discovered for elastic-perfectly plastic solids (see Fig.3.3.1).

Angular Field Variations

In Fig. 4.3.3 the angular variations of the Cartesian stress components, σ_{ij} $(i, j = 1, 2)$, the effective stress σ_e and the flow stress σ for $\alpha = 0.3$ and $m = v/c_s = 0.4$ are plotted against the angular position θ. Shown in the same figure are the results of an asymptotic analysis by Achenbach, Kanninen and Popelar (1981) for the same linear hardening values yet for $m \approx 0.403$ (or $\beta = 0.25$ in their paper). For comparison purposes, all stress quantities are normalized such that $\sigma_e = 1$ at $\theta = 0^0$. It is clear that the two solutions agree very well in the angular variations of the stress field. The solution by Achenbach et al. stops at the angle at which elastic unloading takes place, which is found by them to be around 85.8^0. In the numerical solution, as discussed for the quasi-static case, this angle should be determined from the angular position where σ_e deviates from σ. Using the error tolerance 0.77×10^{-2}, it is estimated to be around 81^0, which is slightly smaller than the one predicted by Achenbach et al.. However, if one recalls that a slightly higher m value is used by Achenbach et al., and considers the fact that the elastic unloading angle increases as m increases (see Fig. 4.3.2), it can be concluded that the estimate from the present

numerical solution is reasonable.

Using the same error tolerance, the effect of hardening and inertia on the angular extent of the crack tip active plastic zone can be estimated. For example, at crack propagation speed $v/c_s = 0.3$, it is found that the angle changes slightly from 78^0 for $\alpha = 0.5$ to 80^0 for $\alpha = 0.05$. Whereas at $v/c_s = 0.5$, it changes from 82^0 for $\alpha = 0.4$ to 92^0 for $\alpha = 0.05$. On the other hand, for the strain hardening level $\alpha = 0.4$, the angle is estimated to be 76^0 at $v/c_s = 0$ and 82^0 at $v/c_s = 0.5$.

The effect of hardening on the angular stress variations are demonstrated in Fig. 4.3.4 for $v/c_s = 0.3$ and in Fig. 4.3.5 for $v/c_s = 0.5$. It can be seen that at the lower crack propagation speed, the stress variations are not much different from their quasi-static counterparts (refer to Fig. 4.2.4). However, at the higher crack propagation speed, and for $\alpha = 0.1$ and 0.05, which correspond to very low strain hardening, the variations develop a feature distinct from both of their quasi-static counterparts and their higher hardening counterparts.

It is clear from Fig. 4.3.5 that kinks, or in other words, strong signs of slope discontinuities in the stress components σ_{rr} and $\sigma_{r\theta}$, appear at locations approximately where elastic unloading takes place. This feature has also been observed for dynamic crack propagation in elastic-perfectly plastic solids at high speeds (see Fig. 3.3.2 of the present study and the asymptotic solution of Gao, 1987). This observed discontinuity in the slopes of the stresses, if not attributed to numerical errors, may probably explain an interesting situation encountered by Achenbach, Kanninen and Popelar (1981). In carrying out the integration of a set of ordinary differential equations in their asymptotic analysis, they reported that for different values of the hardening parameter α, there exist corresponding different limiting crack speeds above which their numerical integration algorithm failed to converge.

In connection with the existence of a secondary active plastic zone behind the crack tip, it is apparent from Fig. 4.3.5b that for the linear hardening parameter

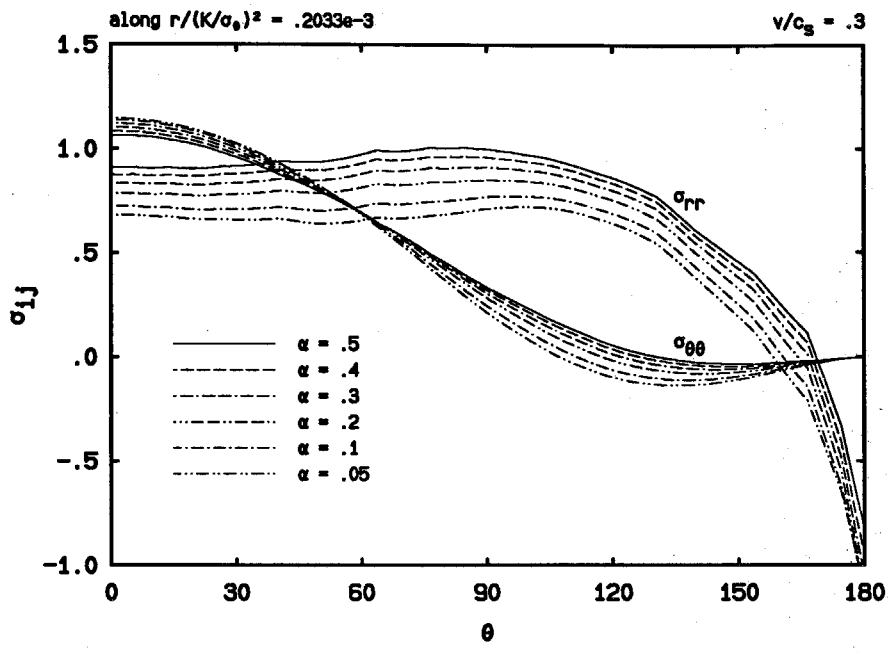

FIGURE 4.3.4a The effect of hardening on the angular variations of the polar stress components σ_{rr} and $\sigma_{\theta\theta}$ for $v/c_s = 0.3$, normalized such that the effective stress $\sigma_e = 1$ at $\theta = 0^0$.

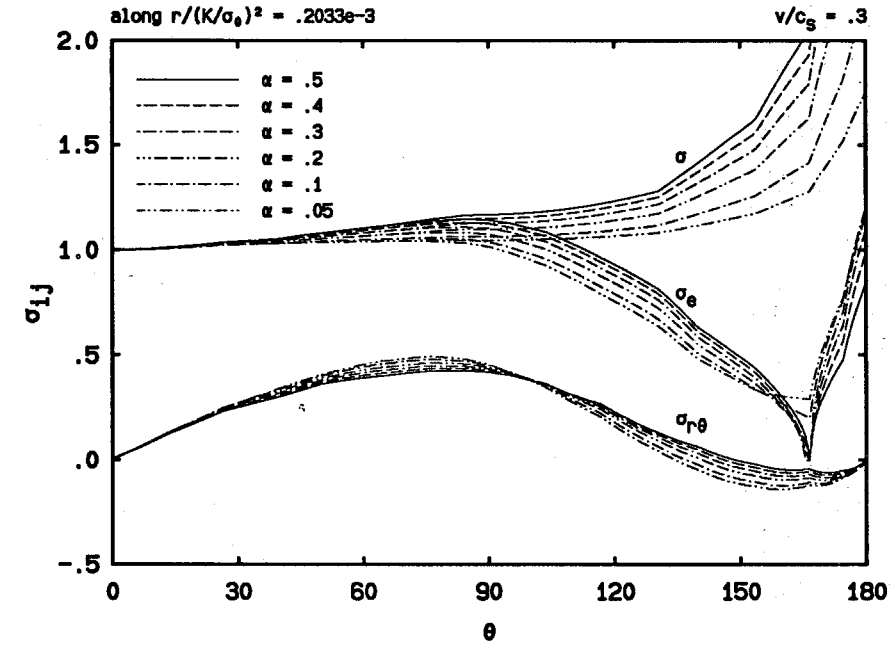

FIGURE 4.3.4b The effect of hardening on the angular variations of the polar stress component $\sigma_{r\theta}$, the effective stress σ_e and the flow stress σ for $v/c_s = 0.3$, normalized such that $\sigma_e = 1$ at $\theta = 0^0$.

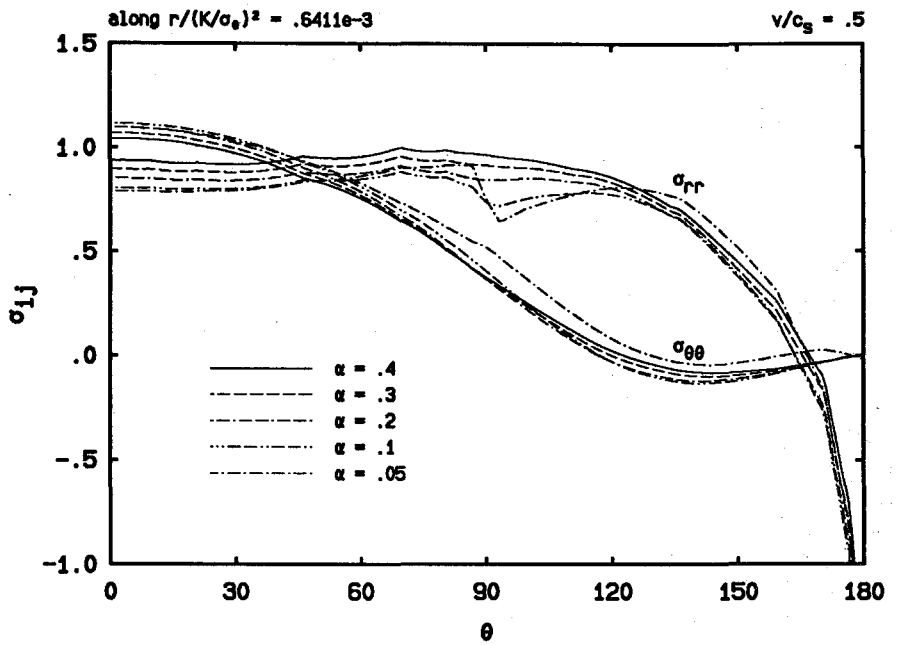

FIGURE 4.3.5a The effect of hardening on the angular variations of the polar stress components σ_{rr} and $\sigma_{\theta\theta}$ for $v/c_s = 0.5$, normalized such that the effective stress $\sigma_e = 1$ at $\theta = 0^0$.

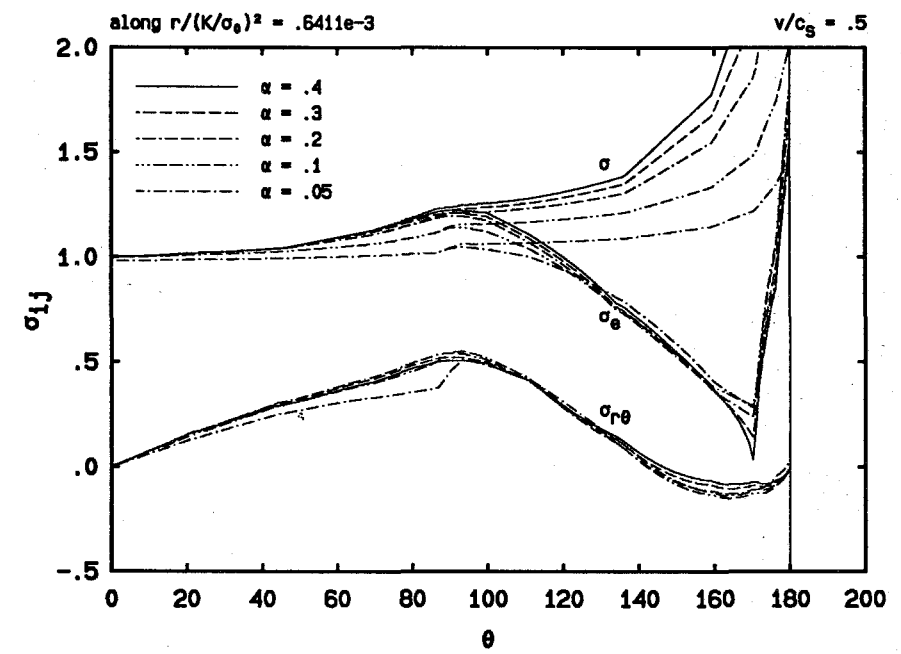

FIGURE 4.3.5b The effect of hardening on the angular variations of the polar stress component $\sigma_{r\theta}$, the effective stress σ_e and the flow stress σ for $v/c_s = 0.5$, normalized such that $\sigma_e = 1$ at $\theta = 0^0$.

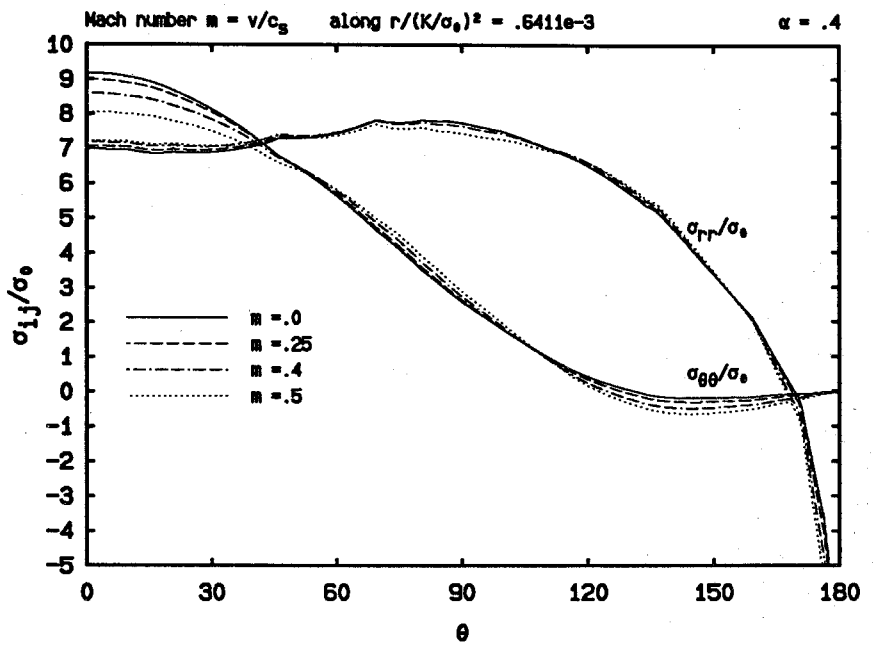

FIGURE 4.3.6a The effect of crack speed on the angular variations of the polar stress components σ_{rr} and $\sigma_{\theta\theta}$ for $\alpha = 0.4$, plotted in normalized form.

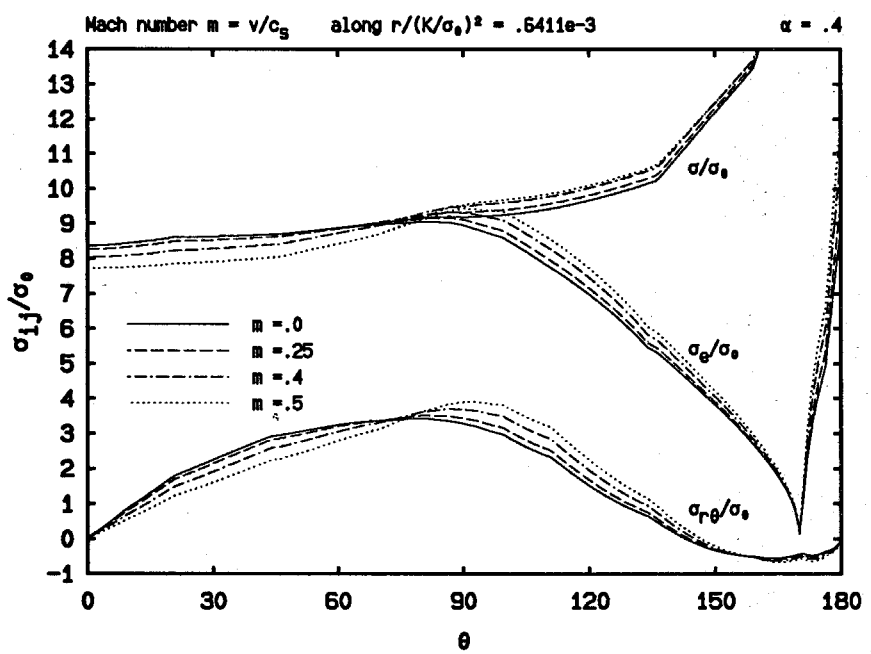

FIGURE 4.3.6b The effect of crack speed on the angular variations of the polar stress component $\sigma_{r\theta}$, the effective stress σ_e and the flow stress σ for $\alpha = 0.4$, plotted in normalized form.

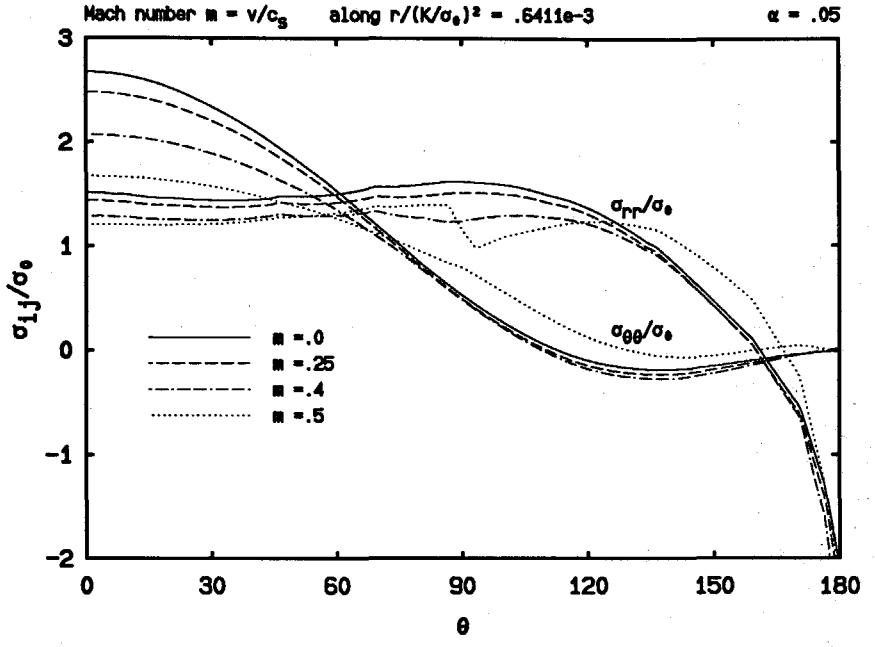

FIGURE 4.3.7a The effect of crack speed on the angular variations of the polar stress components σ_{rr} and $\sigma_{\theta\theta}$ for $\alpha = 0.05$, plotted in normalized form.

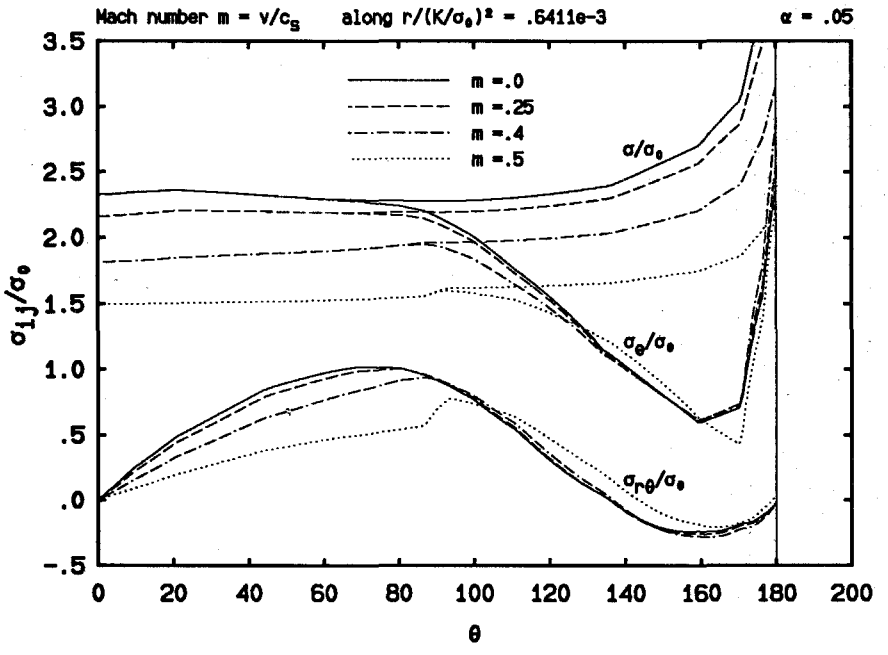

FIGURE 4.3.7b The effect of crack speed on the angular variations of the polar stress component $\sigma_{r\theta}$, the effective stress σ_e and the flow stress σ for $\alpha = 0.05$, plotted in normalized form.

$\alpha = 0.05$ at the crack speed $v/c_s = 0.5$, the effective stress σ_e rises up at $\theta \approx 180^0$ and joins the curve for the flow stress σ, which means reversed plastic loading there.

Shown in Fig. 4.3.6 and Fig. 4.3.7 are the dependence of the angular stress variations on the crack propagation speed for, respectively, $\alpha = 0.4$ and 0.05. A very interesting phenomenon can be observed at $\theta = 0^0$. From Fig. 4.3.6a, in which $\alpha = 0.4$, it is seen that, as m increases, σ_{rr} *increases* and $\sigma_{\theta\theta}$ decreases. However, from Fig. 4.3.7a, in which $\alpha = 0.05$, it is seen that, as m increases, σ_{rr} *decreases* although $\sigma_{\theta\theta}$ still decreases. Yet from our discussions for the limiting case of $\alpha = 0$, i.e., for crack propagation in elastic-perfectly plastic solids, the tendency discussed above in the case of $\alpha = 0.4$ is observed again (see Figs. 3.3.2b and 3.3.5b, c).

The angular variations of the crack tip velocity field for various strain hardening levels and crack propagation speeds are presented in Fig. 4.3.8 with normalizations such that $v_1 = -1$ at $\theta = 0^0$ for each value of α, and in Fig. 4.3.9 with the standard normalization defined in Chapter 2 such that the relative magnitudes of the velocity components at different crack propagation speeds can be observed.

For $v/c_s = 0.3$ (see Fig. 4.3.8a), it is seen that the variations of the Cartesian velocity components are very much the same as those for quasi-static crack growth (see Fig. 4.2.6). Yet for $v/c_s = 0.5$ (see Fig. 4.3.8b), for which dynamic effects are expected to be stronger, it is observed that the angular variations undergo large changes, especially for very lower hardening materials. Specifically, the velocity curves tend to deviate from the general trends exhibited by the quasi-static solution. For example, the transition of the curve for the v_2 component from the actively yielded plastic zone, where its slope is positive, to the elastic unloading zone, where its slope is closer to zero or slightly negative, becomes more abrupt, or in other words, better defined.

This observation can be further demonstrated from the evolutionary changes of the velocity field with respect to the speed of crack propagation, for two typical

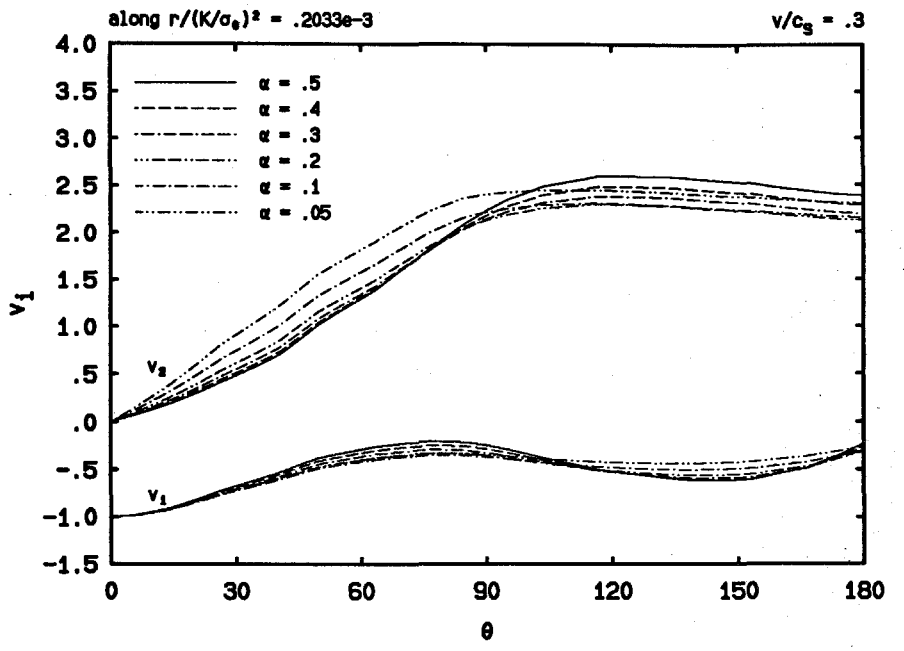

FIGURE 4.3.8a The effect of hardening on the angular variations of the Cartesian velocity components for $v/c_s = 0.3$, normalized such that $v_1 = -1$ at $\theta = 0^0$.

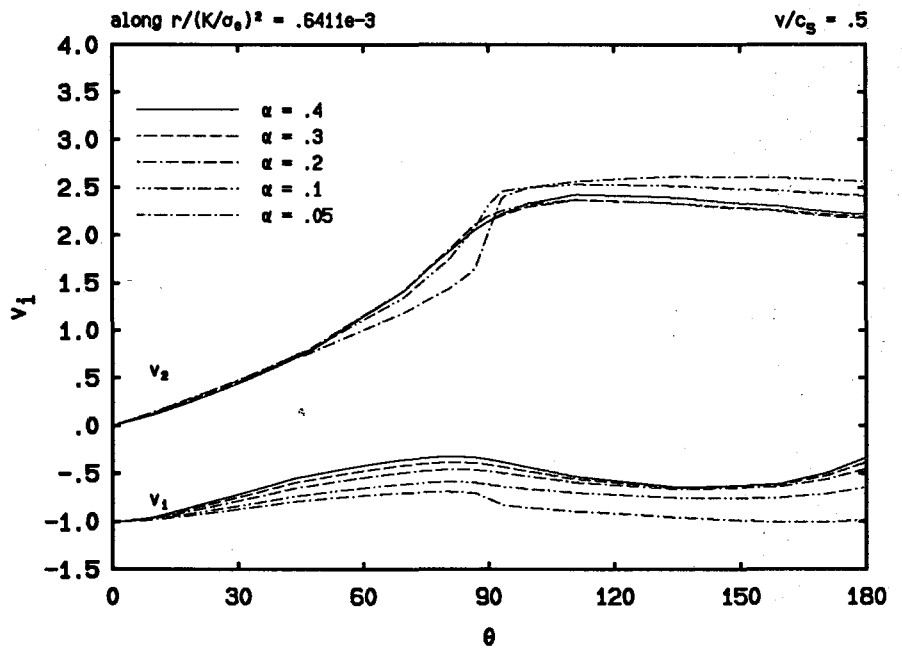

FIGURE 4.3.8b The effect of hardening on the angular variations of the Cartesian velocity components for $v/c_s = 0.5$, normalized such that $v_1 = -1$ at $\theta = 0^0$.

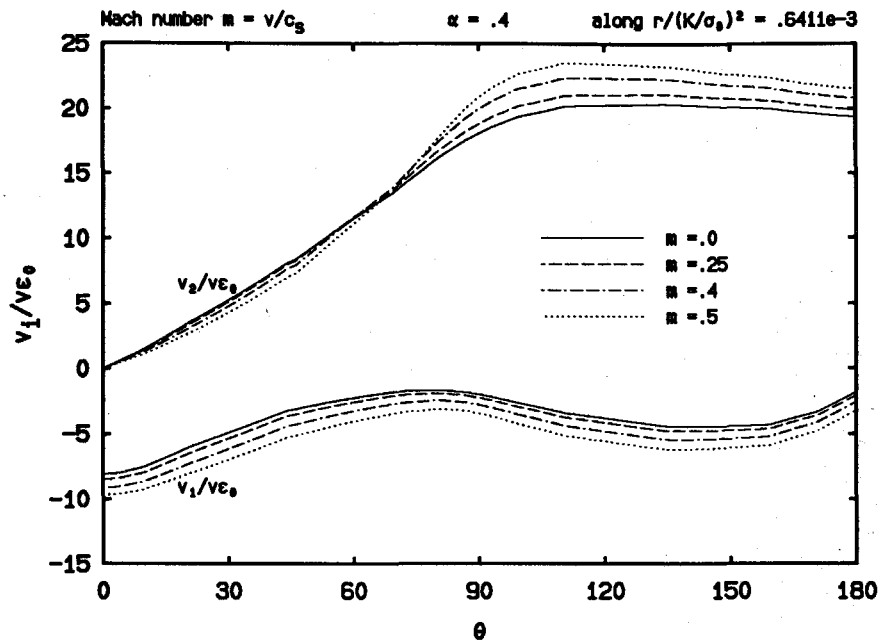

FIGURE 4.3.9a The crack speed dependence of the angular variations of the Cartesian velocity components for $\alpha = 0.4$, plotted in normalized form.

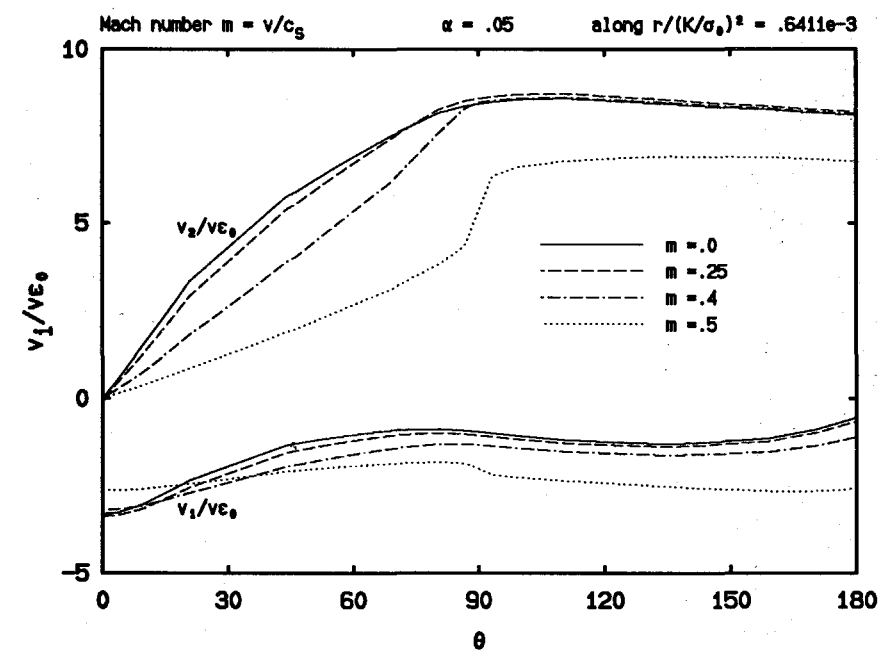

FIGURE 4.3.9b The crack speed dependence of the angular variations of the Cartesian velocity components for $\alpha = 0.05$, plotted in normalized form.

hardening parameter values $\alpha = 0.4$ and $\alpha = 0.05$, shown respectively in Figs. 4.3.9a and 4.3.9b. It is found for both α values that the values of v_1 and v_2 are, respectively, consistently negative and nonnegative for the complete range of θ values, and that as m increases, the slope of v_2 at $\theta = 0^0$ decreases, and the magnitude of v_1 at $\theta = 180^0$ increases. However, although for $\alpha = 0.4$ the magnitude of v_1 at $\theta = 0^0$ and that of v_2 at $\theta = 180^0$ respectively decreases and increases as m increases, the trend seems to reverse for $\alpha = 0.05$ and for m values larger than a certain value.

Radial Field Variations

The effect of hardening on the radial variations of the stress field along the prospective crack line are illustrated in Fig. 4.3.10 and Fig. 4.3.12 for $v/c_s = 0.3$ and 0.5, respectively. It is observed that, as α decreases, the magnitudes of σ_{11} and σ_{22} decrease. Moreover, as r approaches zero, where r is the radial distance to the crack tip, the stresses are found to rise rapidly. These observations strongly indicate that the stresses are singular at the crack tip yet the singularity decreaes as α decreases. In fact, the double-logarithmic plots in Fig. 4.3.11 and Fig. 4.3.13 reveals approximate straight lines near $r = 0$, which strongly suggests crack tip stress singularities of the type r^s with $s < 0$. Meanwhile, there are signs that as α increases, some of the straight lines in the double-logarithmic plots become curved, which can be viewed as an evidence of the shrinkage of the range of dominance of the r^s stress singularities. Nevertheless, this r^s-singularity region is found to exist for α even as low as 0.05 and for v/c_s as high as 0.5.

More interesting features of the stress variations at the crack front can be discovered from the influence of crack propagation speed on those quantities. First of all, it it can be seen from Figs. 4.3.14 and 4.3.15 for $\alpha = 0.4$ and from Figs. 4.3.16 and 4.3.17 for $\alpha = 0.05$ that, as $m = v/c_s$ increases, the magnitude of σ_{22} decreases. Whereas, as already observed from the angular variations of the stress field, the magnitude of σ_{11} increases for $\alpha = 0.4$, yet it decreases for $\alpha = 0.05$.

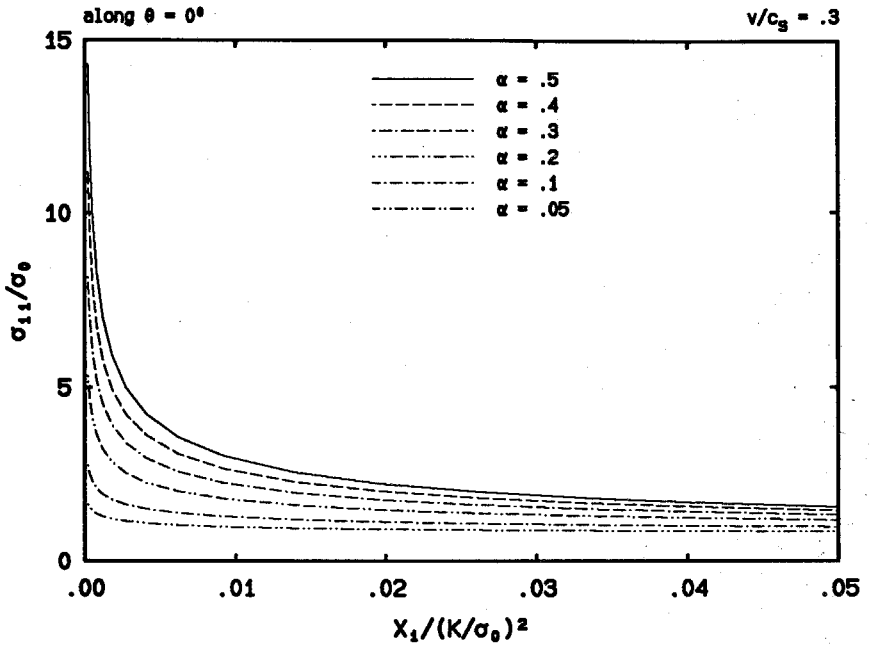

FIGURE 4.3.10a The radial variations of the stress component σ_{11} for $v/c_s = 0.3$, along the prospective crack line in the normalized coordinates.

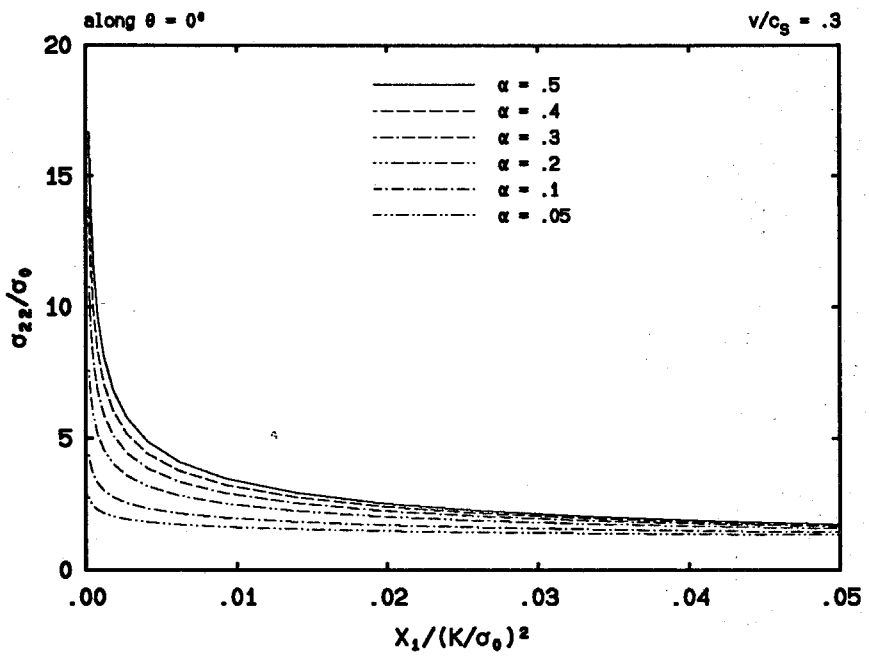

FIGURE 4.3.10b The radial variations of the stress component σ_{22} for $v/c_s = 0.3$, along the prospective crack line in the normalized coordinates.

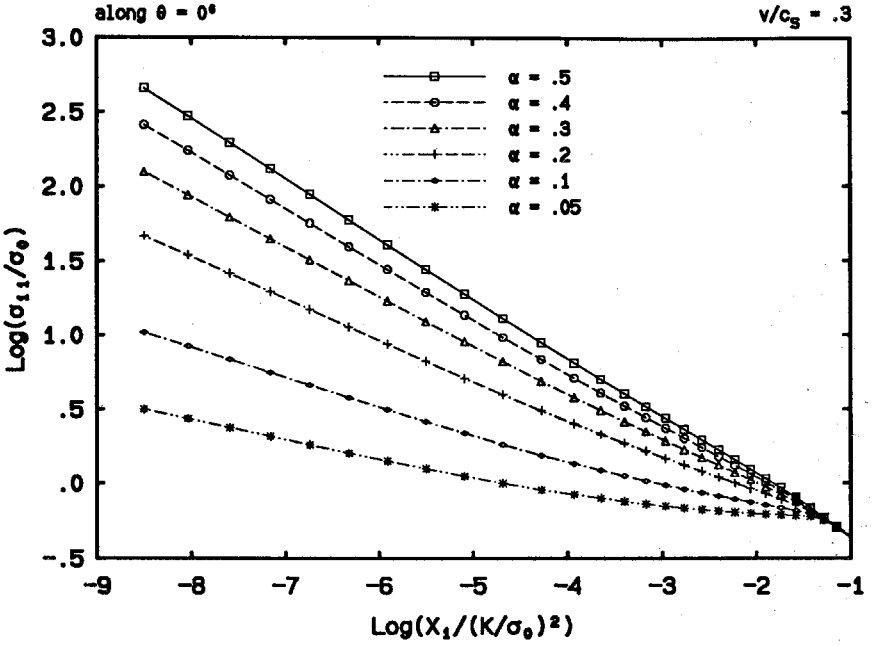

FIGURE 4.3.11a The radial variations of the stress component σ_{11} for $v/c_s = 0.3$, along the prospective crack line in normalized double-logarithmic coordinates.

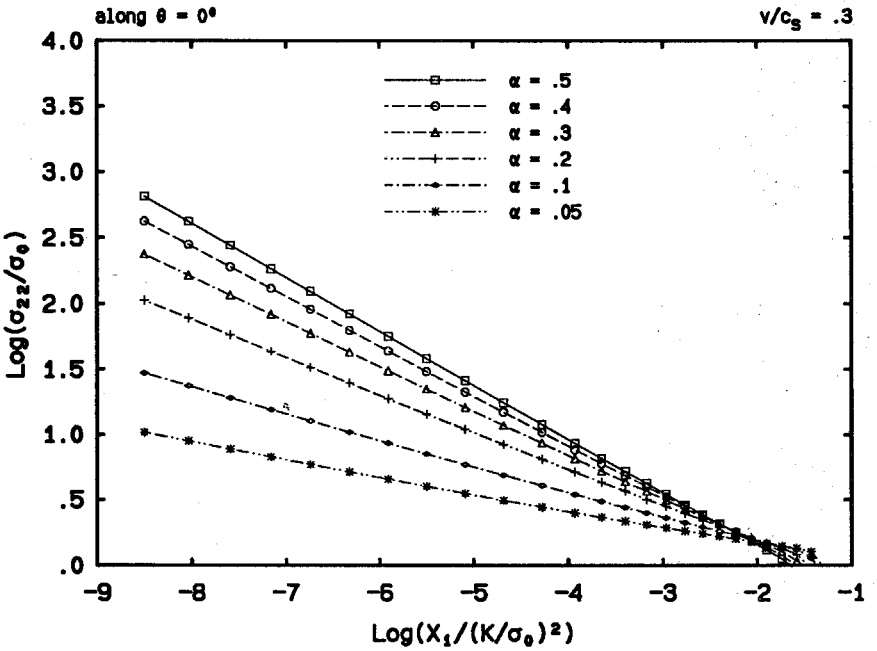

FIGURE 4.3.11b The radial variations of the stress component σ_{22} for $v/c_s = 0.3$, along the prospective crack line in normalized double-logarithmic coordinates.

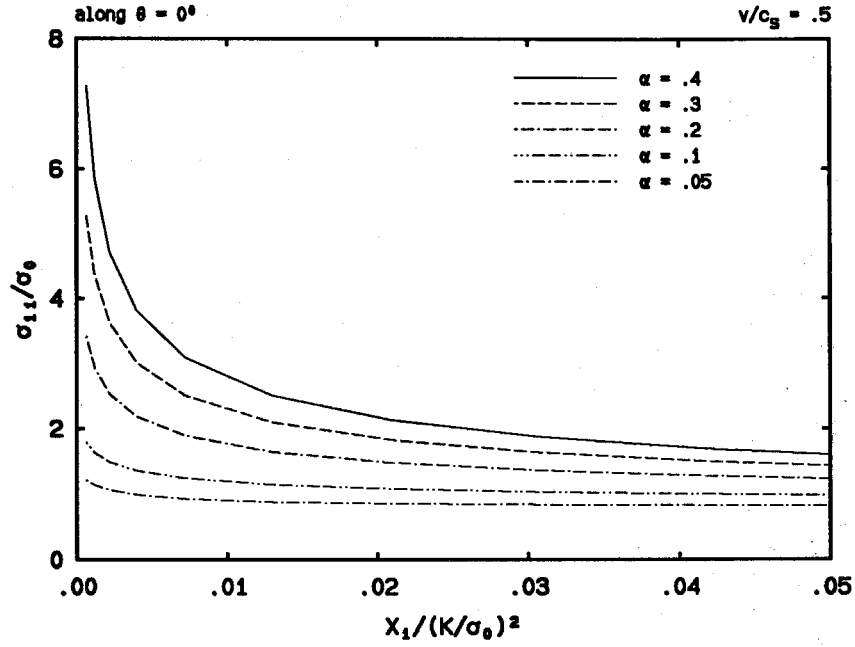

FIGURE 4.3.12a The radial variations of the stress component σ_{11} for $v/c_s = 0.5$, along the prospective crack line in the normalized coordinates.

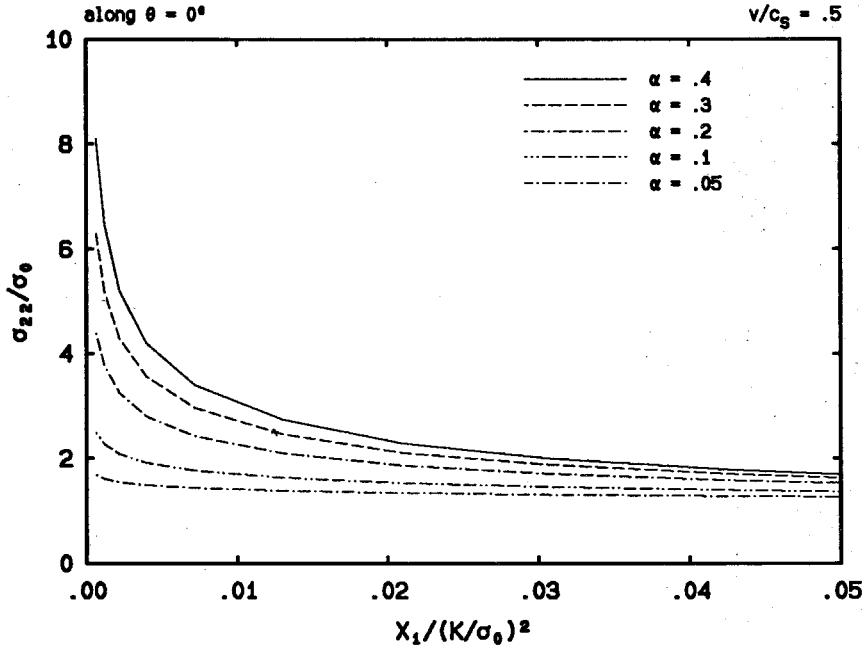

FIGURE 4.3.12b The radial variations of the stress component σ_{22} for $v/c_s = 0.5$, along the prospective crack line in the normalized coordinates.

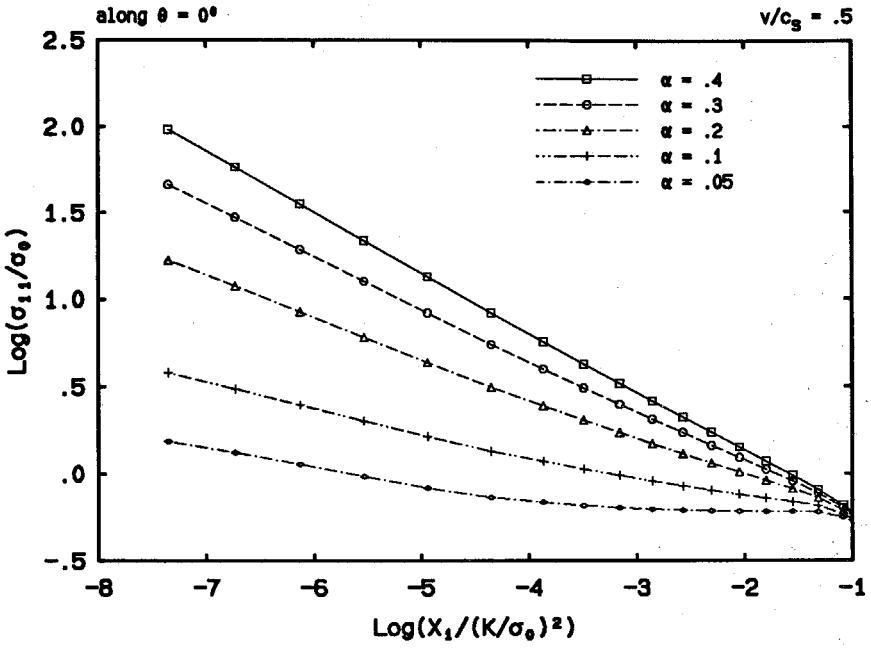

FIGURE 4.3.13a The radial variations of the stress component σ_{11} for $v/c_s = 0.5$, along the prospective crack line in normalized double-logarithmic coordinates.

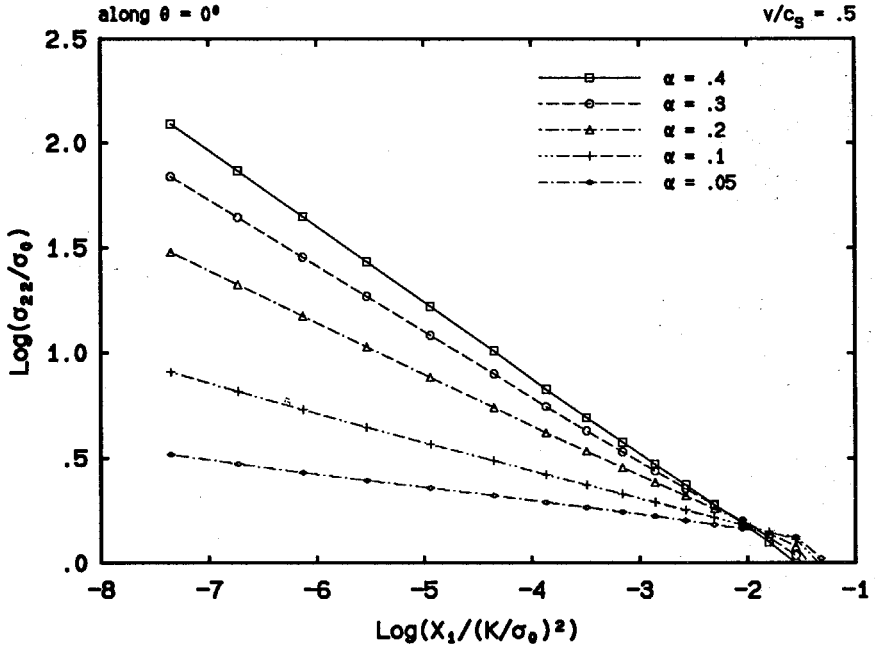

FIGURE 4.3.13b The radial variations of the stress component σ_{22} for $v/c_s = 0.5$, along the prospective crack line in normalized double-logarithmic coordinates.

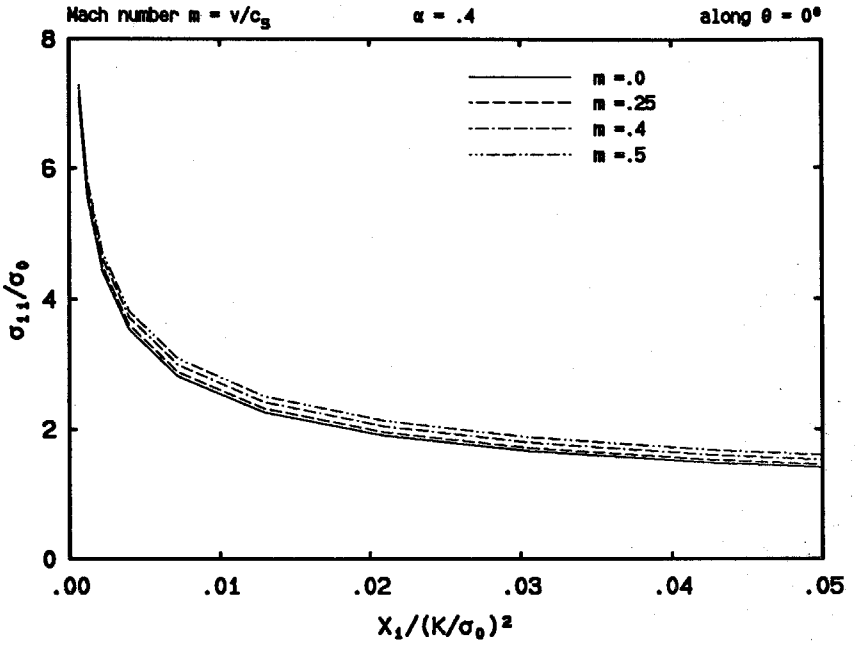

FIGURE 4.3.14a The radial variations of the stress component σ_{11} for $\alpha = 0.4$, along the prospective crack line in the normalized coordinates.

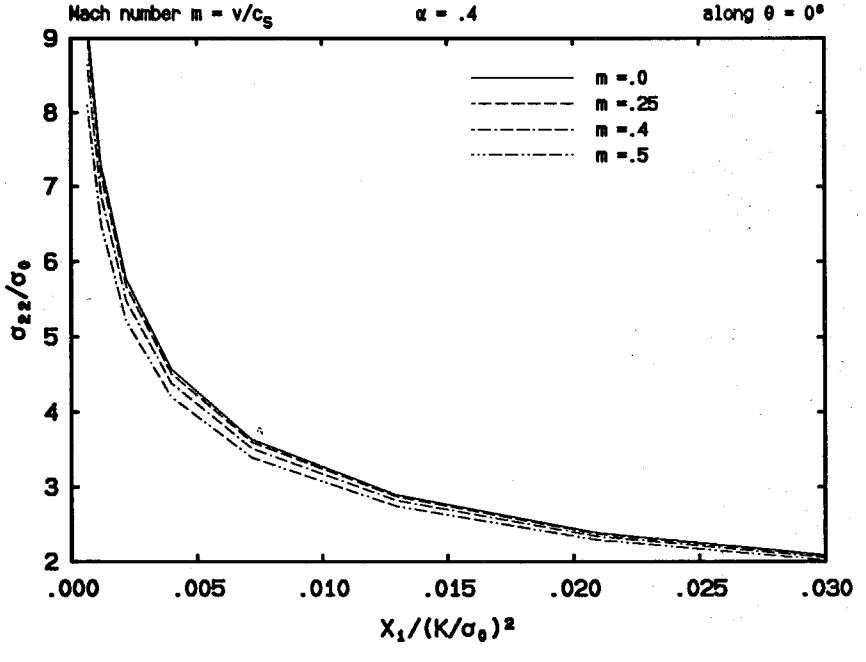

FIGURE 4.3.14b The radial variations of the stress component σ_{22} for $\alpha = 0.4$, along the prospective crack line in the normalized coordinates.

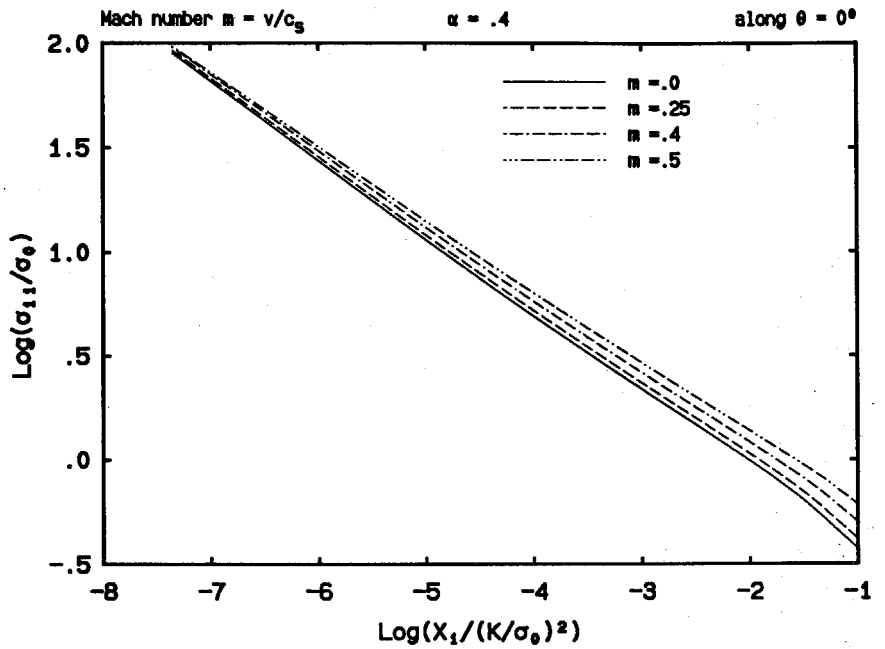

FIGURE 4.3.15a The radial variations of the stress component σ_{11} for $\alpha = 0.4$, along the prospective crack line in normalized double-logarithmic coordinates.

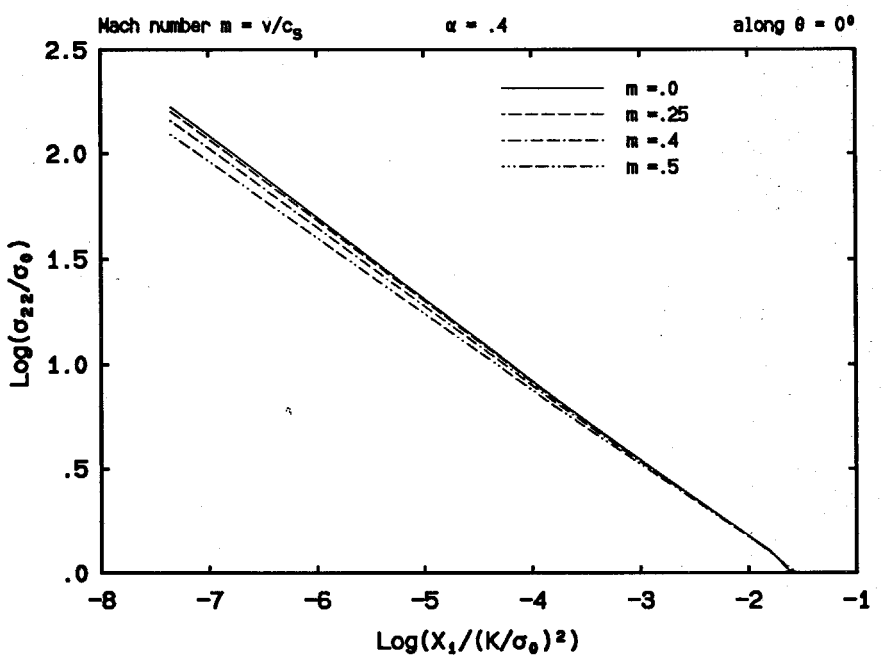

FIGURE 4.3.15b The radial variations of the stress component σ_{22} for $\alpha = 0.4$, along the prospective crack line in normalized double-logarithmic coordinates.

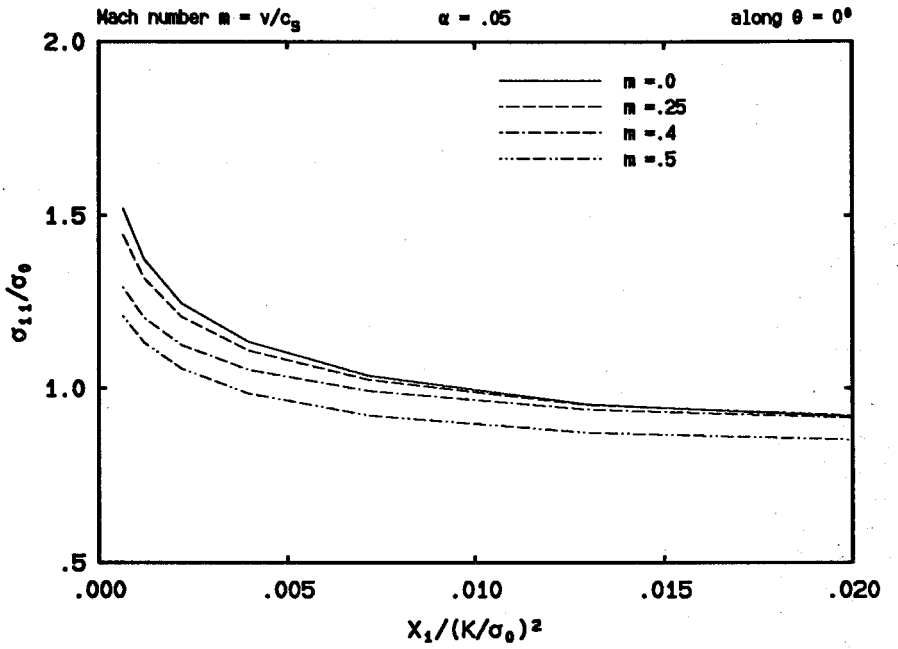

FIGURE 4.3.16a The radial variations of the stress component σ_{11} for $\alpha = 0.05$, along the prospective crack line in the normalized coordinates.

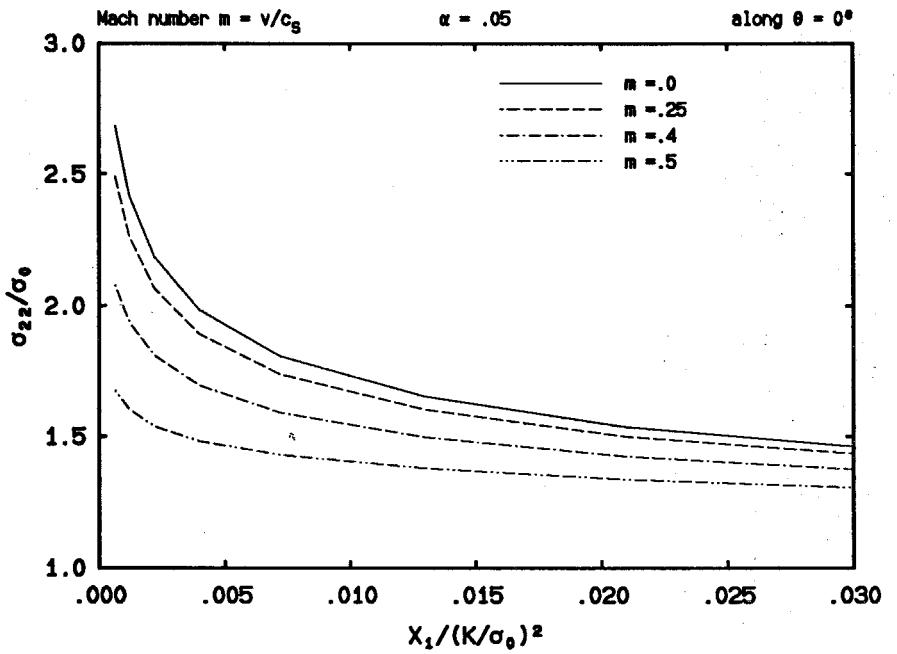

FIGURE 4.3.16b The radial variations of the stress component σ_{22} for $\alpha = 0.05$, along the prospective crack line in the normalized coordinates.

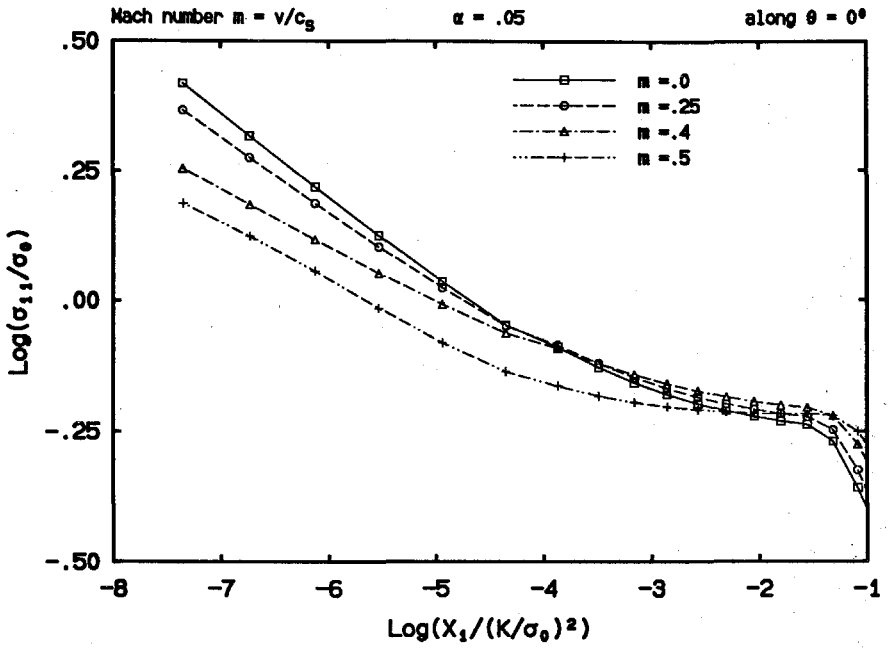

FIGURE 4.3.17a The radial variations of the stress component σ_{11} for $\alpha = 0.05$, along the prospective crack line in normalized double-logarithmic coordinates.

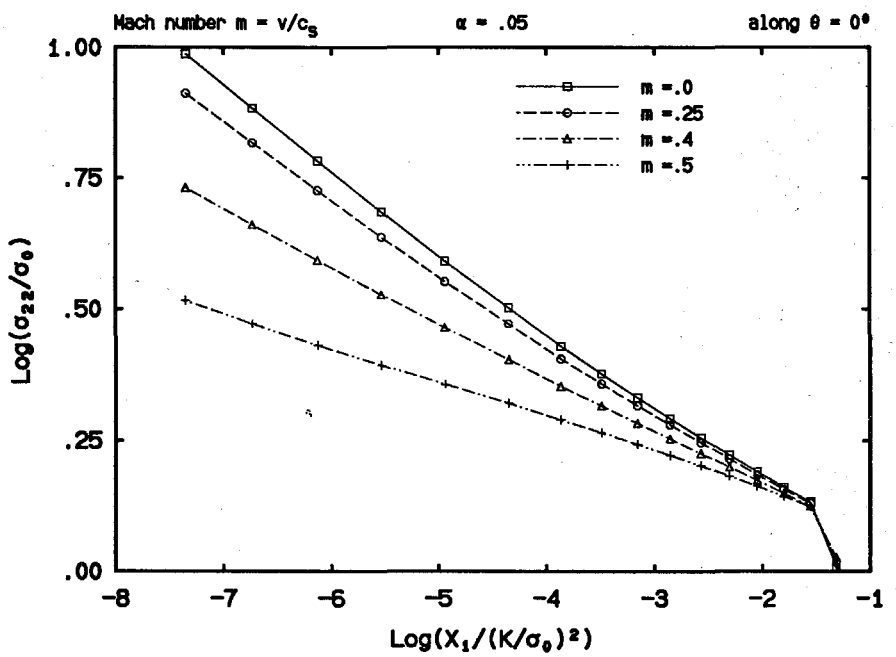

FIGURE 4.3.17b The radial variations of the stress component σ_{22} for $\alpha = 0.05$, along the prospective crack line in normalized double-logarithmic coordinates.

However, in the limiting case of $\alpha = 0$, the magnitude of σ_{11} increases again as m increases (see Fig. 3.3.5b), as discussed in Chapter 3. Moreover, by comparing the double-logarithmic plots in Fig. 4.3.15a and with those in Fig. 4.3.17a, it can be concluded that both the hardening parameter α and the Mach number $m = v/c_s$ affect the singularity and its range of dominance of the crack tip stress field. It seems that, as α decreases and as m increases, the range of dominance for the r^s-type stress singularity shrinks, and at the limit $\alpha = 0$, as demonstrated by results presented in Chapter 3 for elastic-perfectly plastic solids, stress singularity disappears or stresses are bounded (see Fig. 3.3.5).

As discussed earlier, the current problem is also studied asymptotically by Achenbach, Kanninen and Popelar (1981), who assumed *a priori* that both the stress and the velocity fields possess r^s ($s < 0$) singularities at the crack tip. A solution of this kind was indeed obtained by solving a system of ordinary differential equations resulting from a separable form of solution with the assumed r^s-dependence.

Table 4.3.1 Values of the singularity parameter s at $m = 0.4$

α	s_1	s_2	s_a	s_r	ϵ (%)
.5	-.402	-.406	-.404	-.411	1.7
.3	-.328	-.333	-.331	-.339	2.4
.2	-.271	-.276	-.274	-.282	2.8

To compare with the above analytical solution regarding the s-values for various α-values, a least square fitting is made to our finite element result at the crack front, with data extracted from the sixth to the tenth elements if the crack tip is supposed to reside at the lower-left corner of the first element. This type of estimation is performed for each stress component, and the mean value for s is taken to be the final estimation. The comparison is given in Table 4.3.1, where s_1 is the estimation from σ_{11}, s_2 is the estimation from σ_{22}, s_a is the average of s_1 and s_2, s_r is the reference value from the asymptotic solution of Achenbach, Kanninen and Popelar, and ϵ is the relative difference of s_a with respect to s_r in percentage.

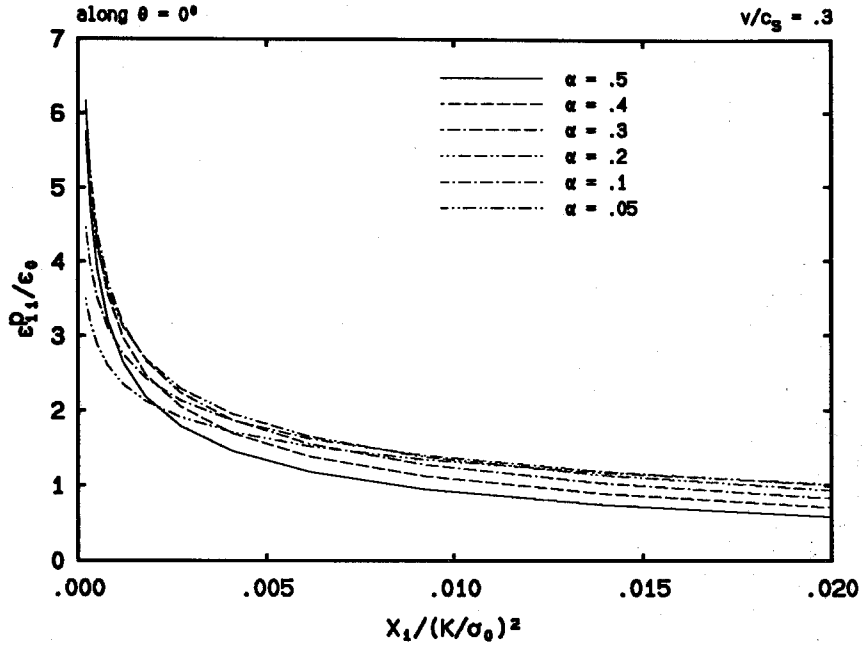

FIGURE 4.3.18a The radial variations of the plastic strain component ε_{11}^p for $v/c_s = 0.3$, along the prospective crack line in the normalized coordinates.

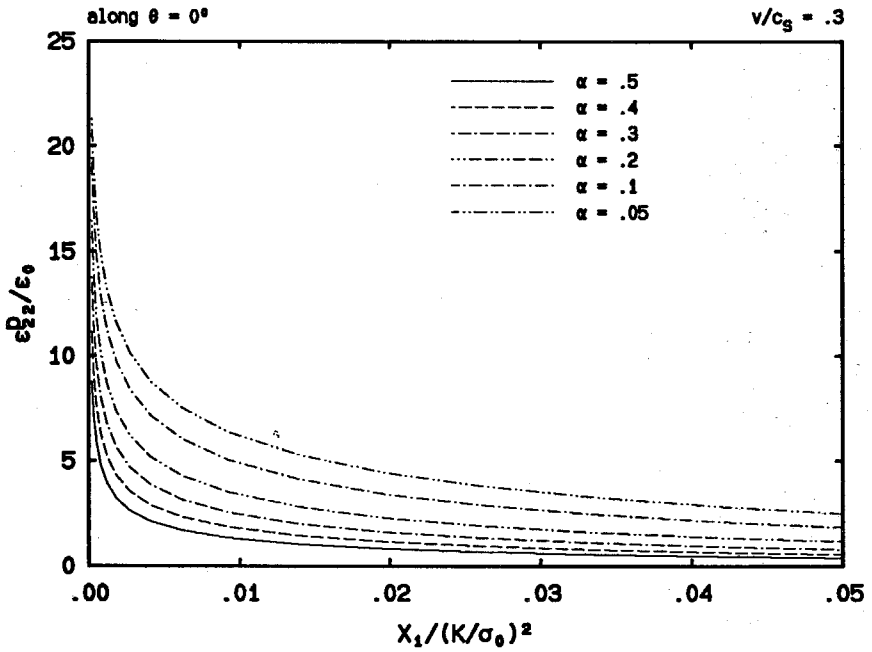

FIGURE 4.3.18b The radial variations of the plastic strain component ε_{22}^p for $v/c_s = 0.3$, along the prospective crack line in the normalized coordinates.

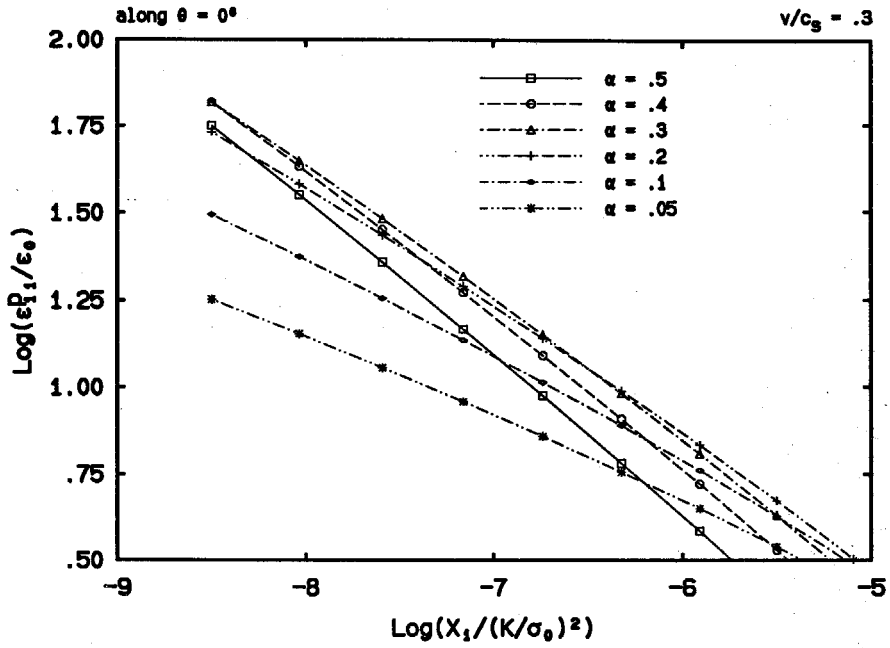

FIGURE 4.3.19a The radial variations of the plastic strain component ε_{11}^p for $v/c_s = 0.3$, along the prospective crack line in double-logarithmic coordinates.

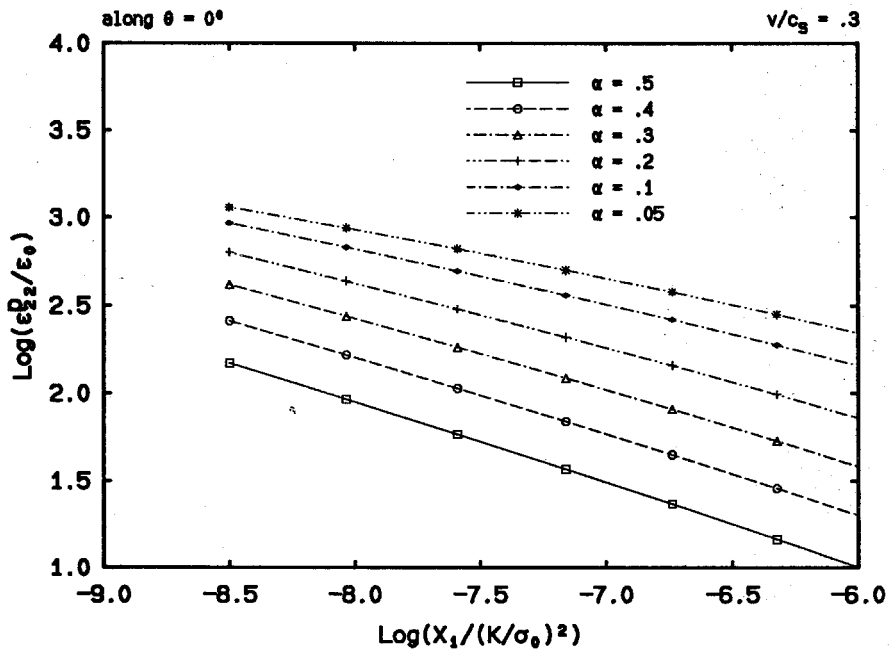

FIGURE 4.3.19b The radial variations of the plastic strain component ε_{22}^p for $v/c_s = 0.3$, along the prospective crack line in double-logarithmic coordinates.

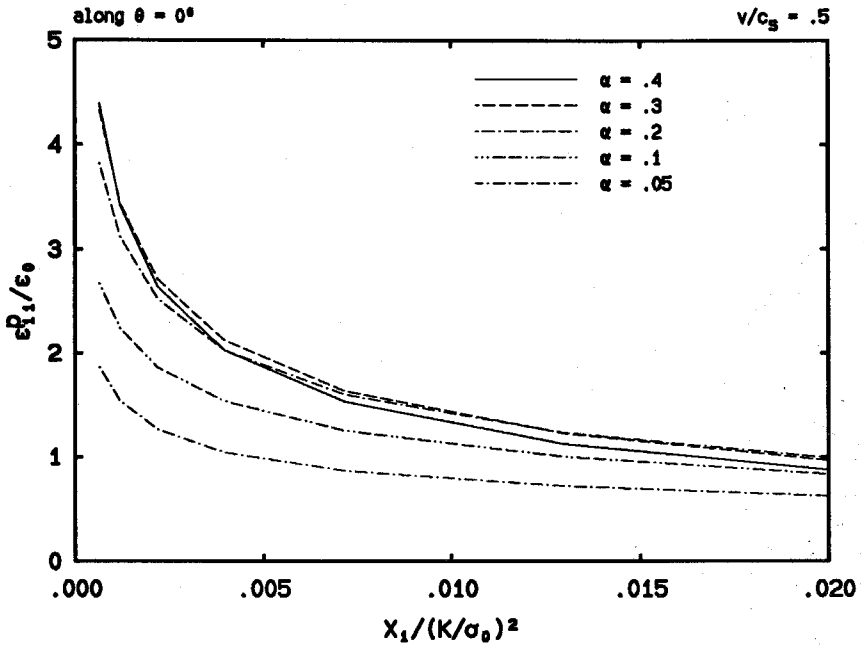

FIGURE 4.3.20a The radial variations of the plastic strain component ε_{11}^p for $v/c_s = 0.5$, along the prospective crack line in the normalized coordinates.

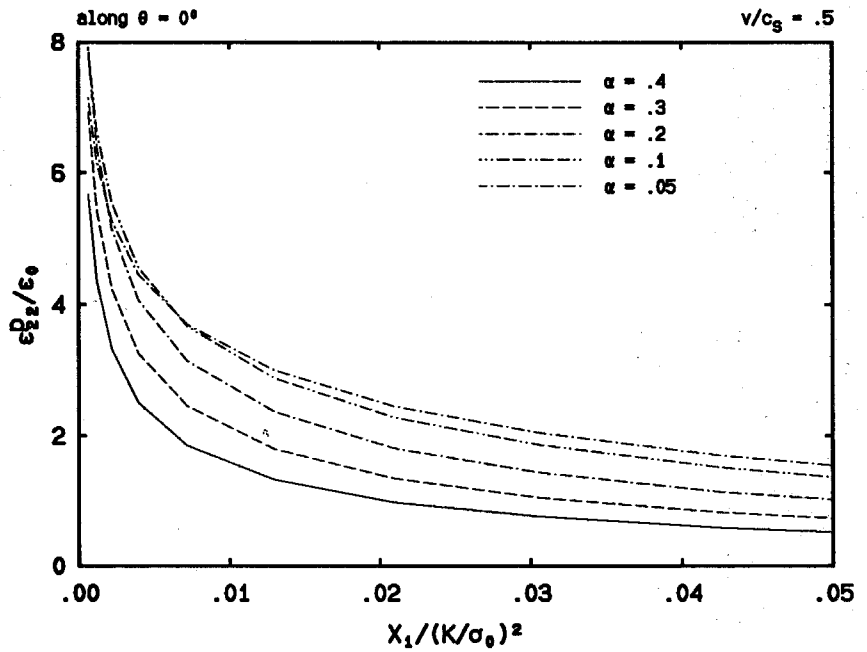

FIGURE 4.3.20b The radial variations of the plastic strain component ε_{22}^p for $v/c_s = 0.5$, along the prospective crack line in the normalized coordinates.

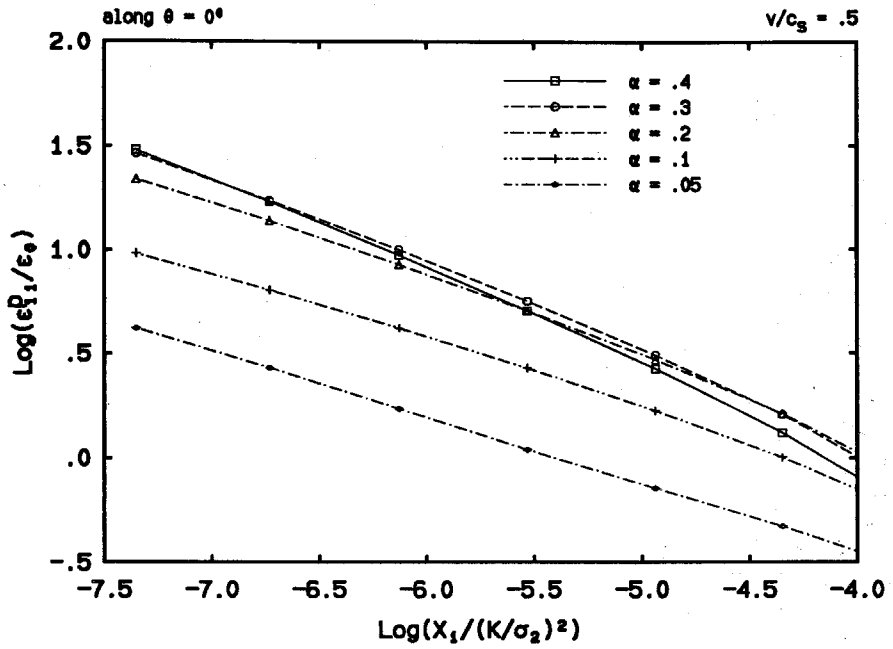

FIGURE 4.3.21a The radial variations of the plastic strain component ε_{11}^p for $v/c_s = 0.5$, along the prospective crack line in double-logarithmic coordinates.

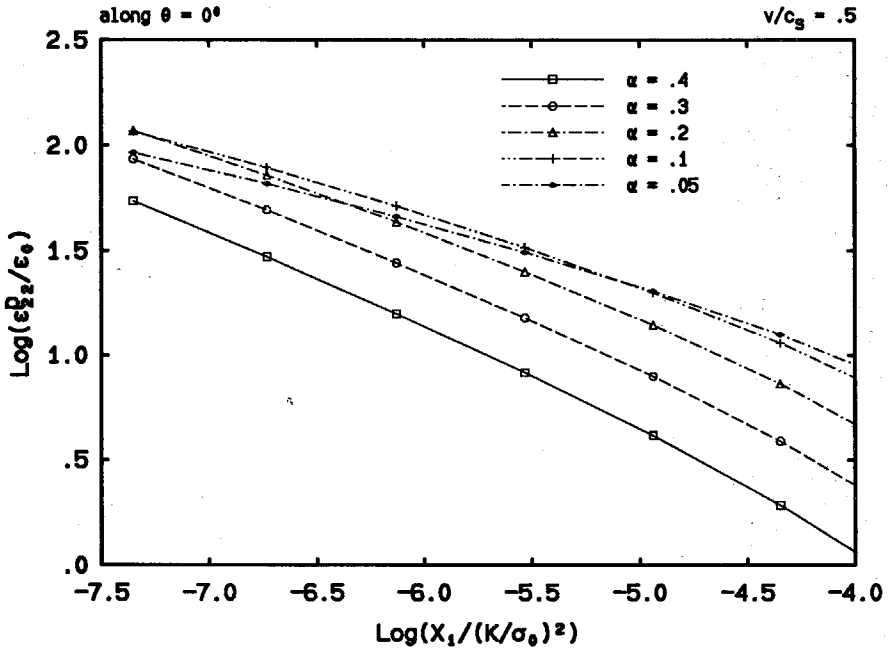

FIGURE 4.3.21b The radial variations of the plastic strain component ε_{22}^p for $v/c_s = 0.5$, along the prospective crack line in double-logarithmic coordinates.

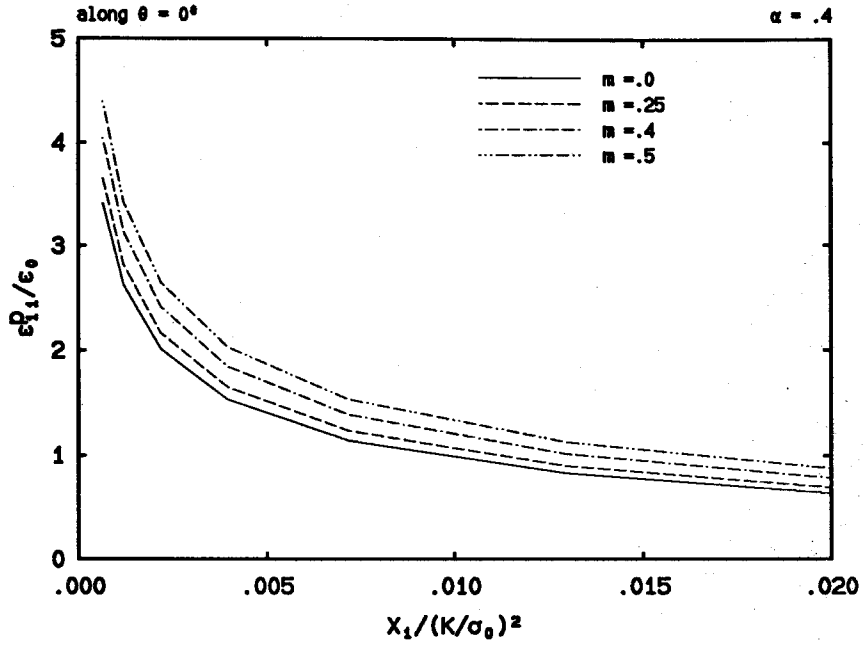

FIGURE 4.3.22a The radial variations of the plastic strain component ε^p_{11} for $\alpha = 0.4$, along the prospective crack line in the normalized coordinates.

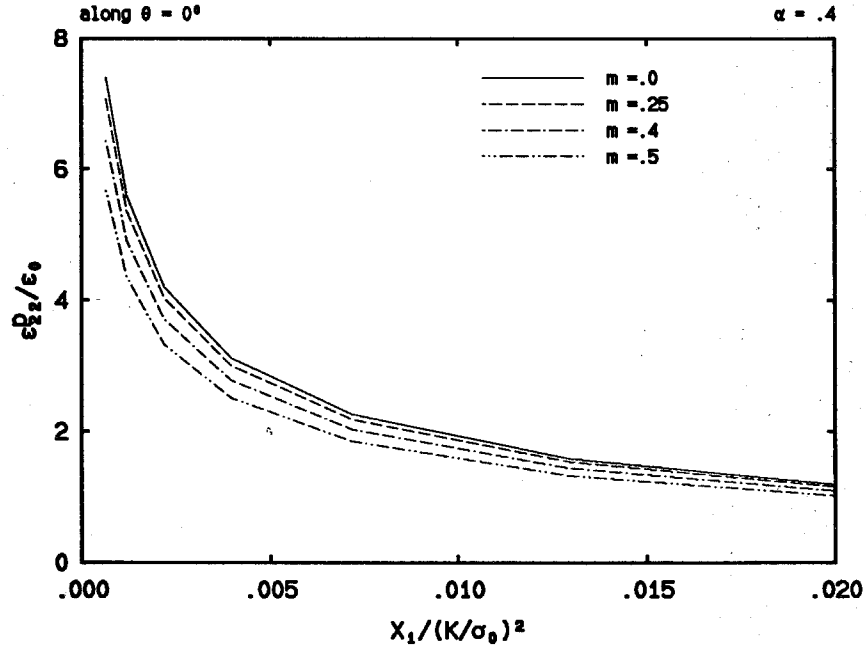

FIGURE 4.3.22b The radial variations of the plastic strain component ε^p_{22} for $\alpha = 0.4$, along the prospective crack line in the normalized coordinates.

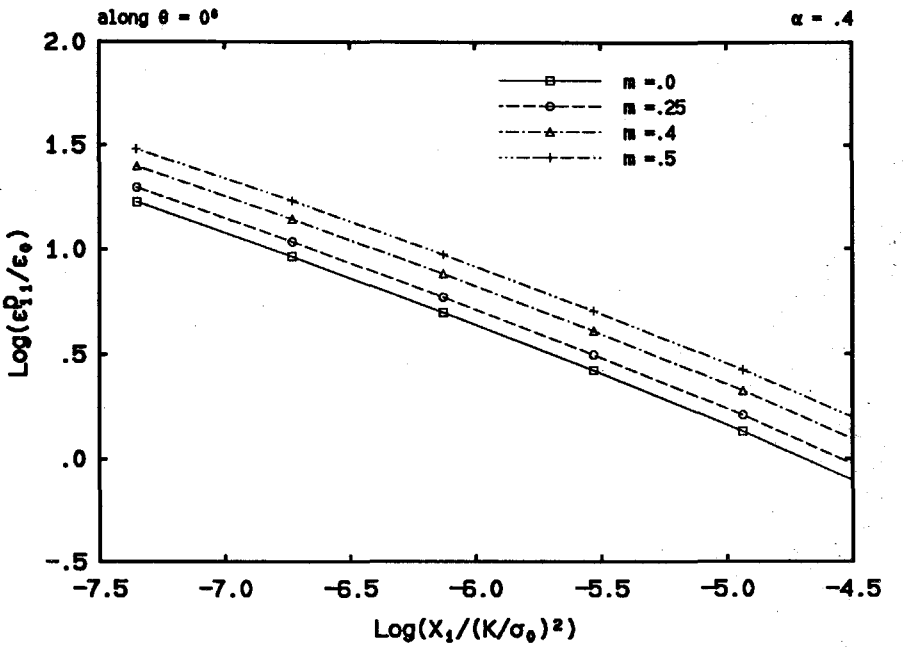

FIGURE 4.3.23a The radial variations of the plastic strain component ε_{11}^p for $\alpha = 0.4$, along the prospective crack line in double-logarithmic coordinates.

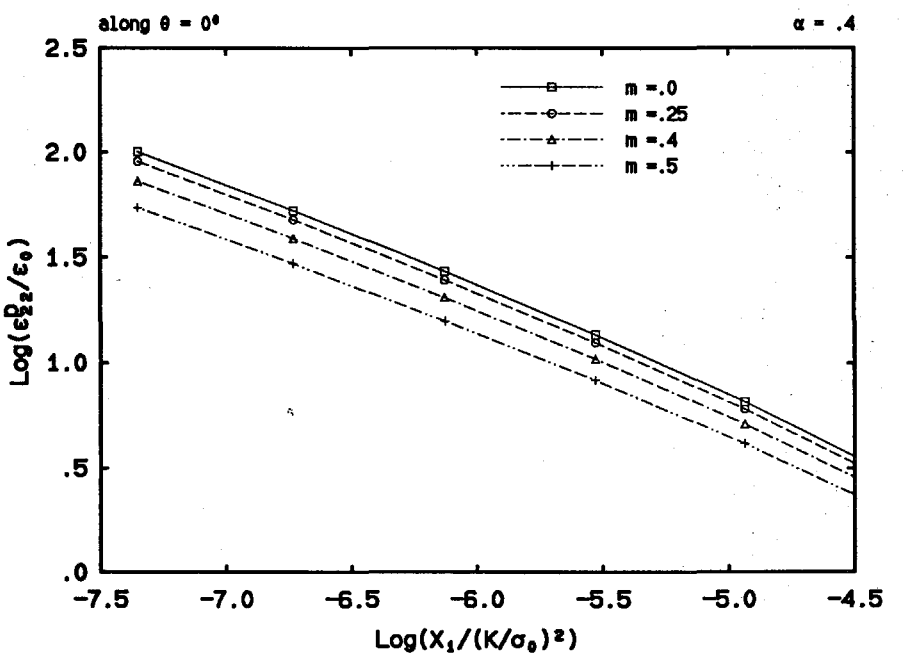

FIGURE 4.3.23b The radial variations of the plastic strain component ε_{22}^p for $\alpha = 0.4$, along the prospective crack line in double-logarithmic coordinates.

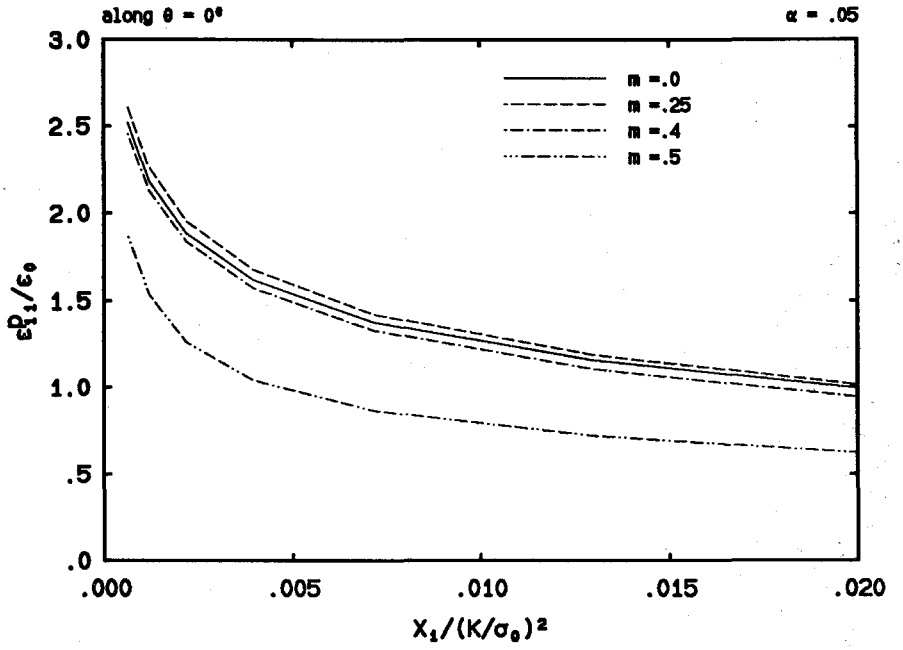

FIGURE 4.3.24a The radial variations of the plastic strain component ε^p_{11} for $\alpha = 0.05$, along the prospective crack line in the normalized coordinates.

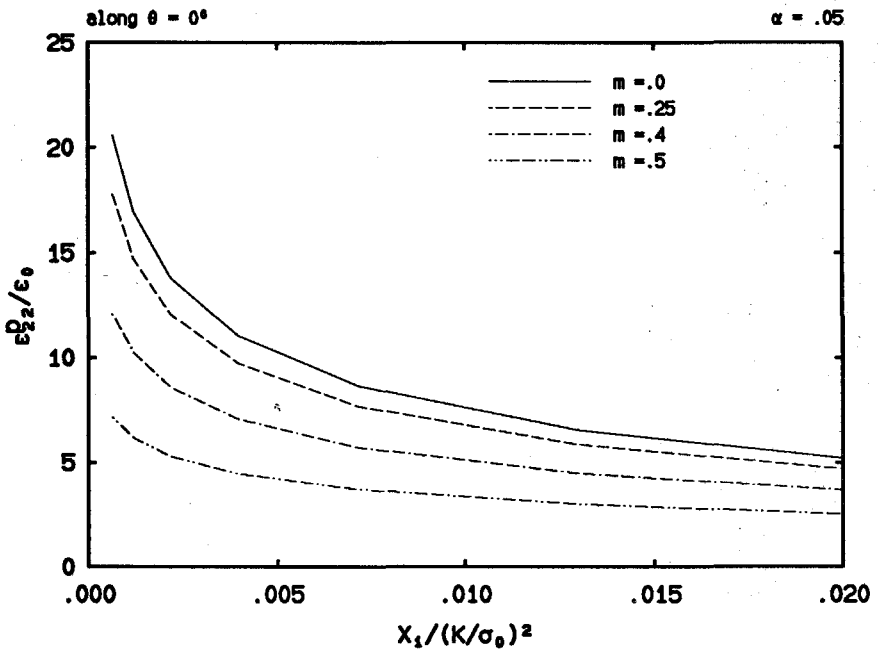

FIGURE 4.3.24b The radial variations of the plastic strain component ε^p_{22} for $\alpha = 0.05$, along the prospective crack line in the normalized coordinates.

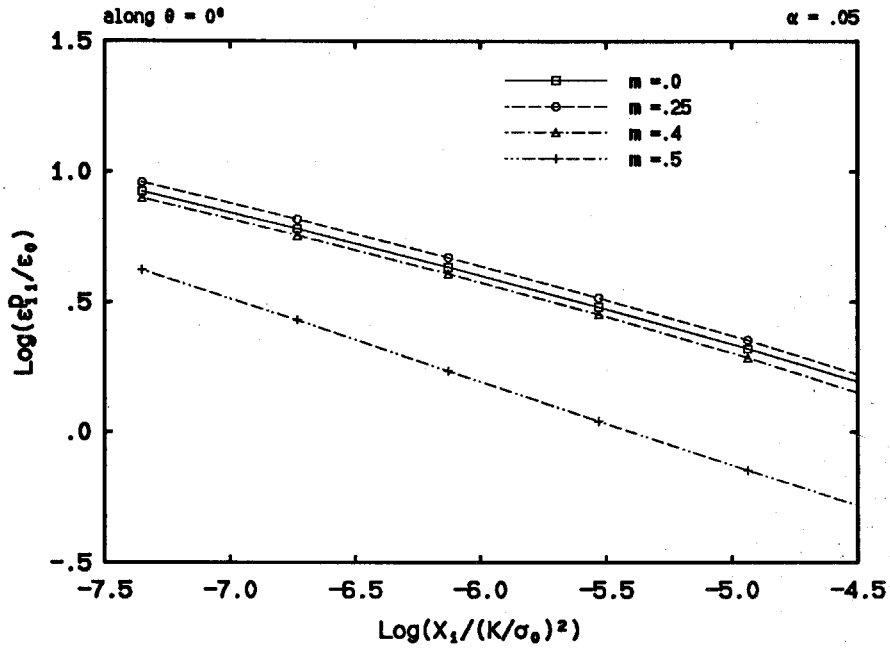

FIGURE 4.3.25a The radial variations of the plastic strain component ε_{11}^{p} for $\alpha = 0.05$, along the prospective crack line in double-logarithmic coordinates.

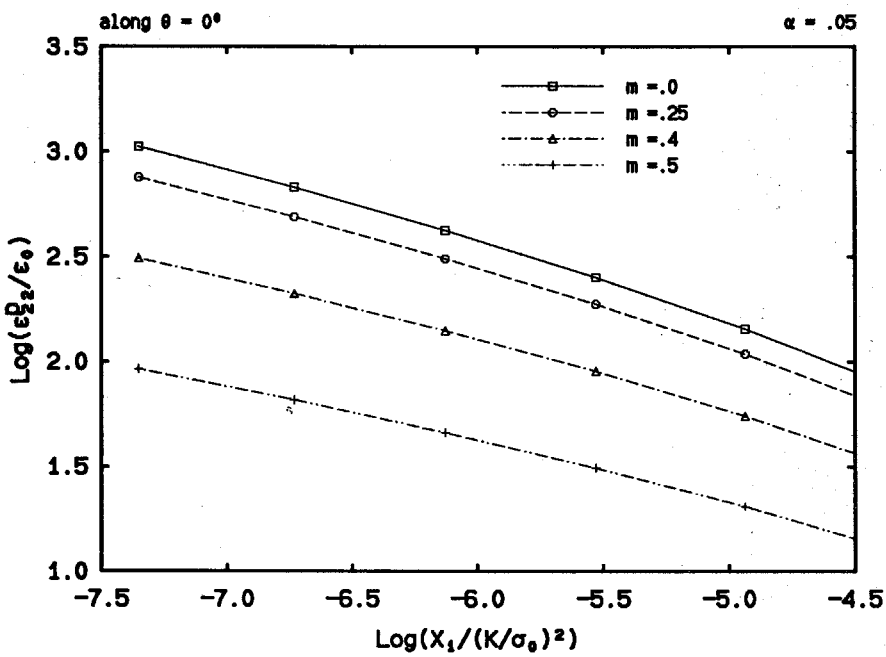

FIGURE 4.3.25b The radial variations of the plastic strain component ε_{22}^{p} for $\alpha = 0.05$, along the prospective crack line in double-logarithmic coordinates.

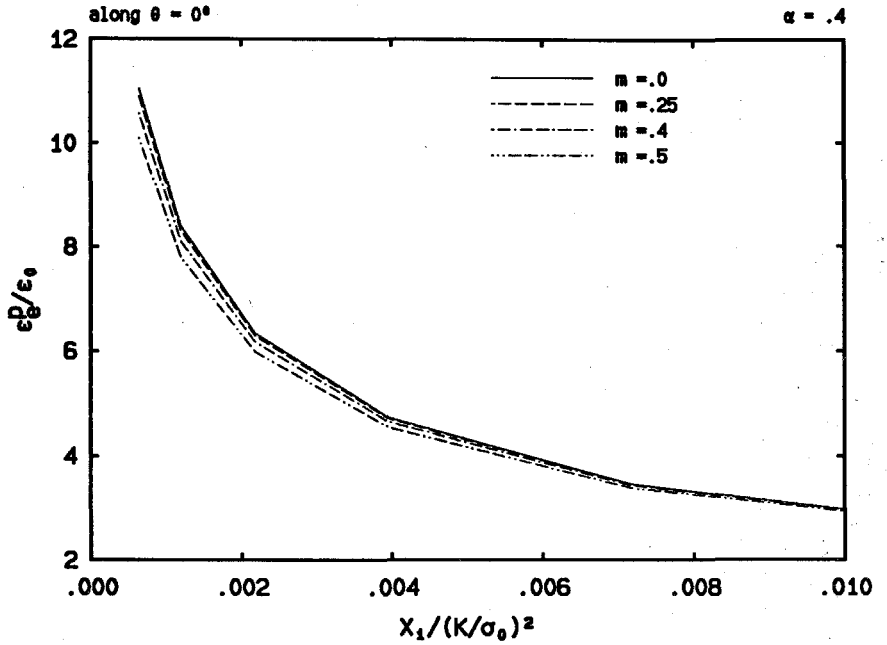

FIGURE 4.3.26a The radial variations of the effective plastic strain ε_e^p for $\alpha = 0.4$, along the prospective crack line in the normalized coordinates.

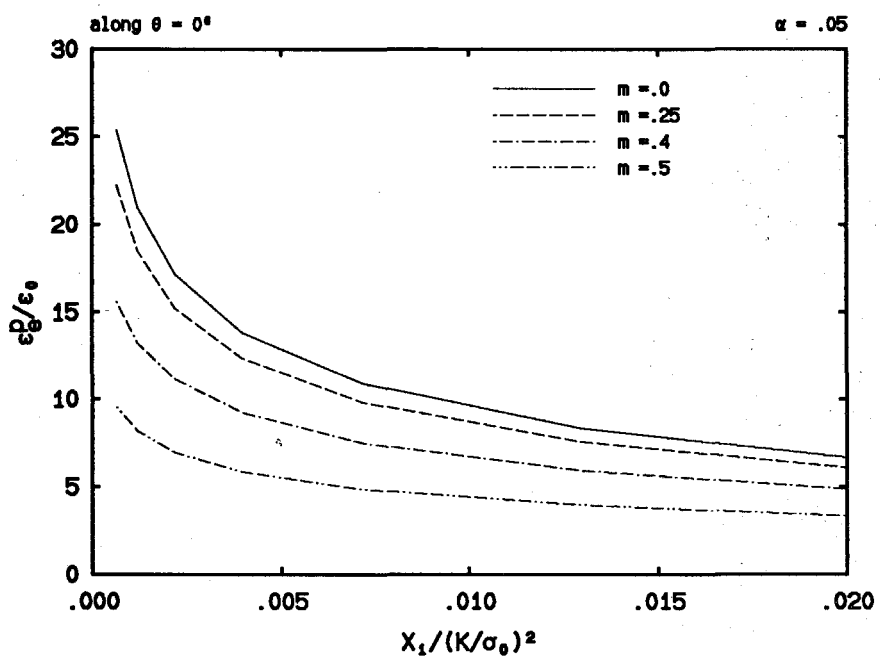

FIGURE 4.3.26b The radial variations of the effective plastic strain ε_e^p for $\alpha = 0.05$, along the prospective crack line in the normalized coordinates.

It can be observed from the table that the differences between the finite element results and the asymptotic results are small. It is observed that as α decreases, the relative difference between the numerical estimation and the analytical value tends to increase. This is reasonable since as α increases, the region of dominance of the asymptotic solution shrinks, and the error in approximating the stress curves by straight lines in the double-logarithmic coordinates increases.

As discussed in the case of quasi-static crack growth, the size of the r^s stress singularity dominance zone can be estimated by setting a relative error tolerance between the original numerical data and the fitted data. For example, by requiring that the relative error be within 5%, we have obtained such estimations along $\theta = 0^0$, which is shown in Table 4.3.2. In the table, the size of the dominance zone is normalized by the horizontal size of the crack tip active plastic zone. The computation is performed for both of the nonzero stress components and the actual maximum relative error is shown beside each ratio. It can be observed consistently that the stress component σ_{22} has a much larger dominance zone than the stress component σ_{11}. Moreover, the size of the dominace zones for both stress components is found to decrease rapidly as α or the level of strain hardening decreases. Nonetheless, it seems that the r^s stress singularity has a surprizingly large dominance zone at the crack tip.

Table 4.3.2 Ratio of the r^s stress singularity dominance zone size to the active plastic zone size along $\theta = 0^0$ at $m = 0.4$

α	for σ_{11}	$\epsilon(\sigma_{11})$ (%)	for σ_{22}	$\epsilon(\sigma_{22})$ (%)
.5	.997	4.9	1.36	4.3
.3	.321	4.7	1.23	4.0
.2	.199	4.4	.605	4.7

Plastic strain variations along ray $\theta = 0^0$ are discussed in the following, as shown in Figs. 4.3.18 through 4.3.25, regarding the singularities of the plastic strain components at the crack tip and the effects of strain hardening and crack

propagation speed on the magnitude of those components.

First of all, just like in the case of stress variations, it is generally observed that as the distance to the crack tip approaches zero, the magnitudes of the plastic strain components rise up rapidly, which suggests the existence of strain singularities at the crack tip. Further, the straight lines observed from the double-logarithmic plots strongly indicate that the plastic strains have the same type of singularities as the stresses. That is, as $r \to 0$, the plastic strains behave as r^s with $s < 0$, where r is the distance to the crack tip.

Moreover, it is consistently seen that, for the same α and v/c_s values and at the same normalized distance to the crack tip, the 2-2 plastic strain component, ε^p_{22}, is predominantly larger than the 1-1 component, ε^p_{11}, although the magnitude of relative dominance seems to decrease as α increases or as v/c_s increases.

For dynamic crack propagation at a typical intermediate speed $v/c_s = 0.3$, it is clear from Figs. 4.3.18a and 4.3.19a that at locations very close to the crack tip, the magnitude of ε^p_{11} tends to become smaller as α decreases, and that further away from the crack tip, it tends to becomes larger for smaller α values. It is also found that the 2-2 plastic strain component always has higher values near the crack tip for lower α values. However, at the higher crack speed $v/c_s = 0.5$, judging from the tendencies shown in Figs. 4.3.20 and 4.3.21, it seems that both ε^p_{11} and ε^p_{22} will have smaller magnitudes as α decreases.

The effect of crack propagation speed on the plastic strain field is illustrated below. For all cases investigated, it is discovered that as m or v/c_s increases, the magnitude of ε^p_{22} is seen to decrease (see Figs. 4.3.22b through 4.3.25b). At the same time, it is found that as m increases, although the magnitude of ε^p_{11} for $\alpha = 0.4$ also increases (see Figs. 4.3.22a and 4.3.23a), it reverses this tendency at a certain m value for $\alpha = 0.05$ (see Figs. 4.3.24a and 4.3.25a). However, since ε^p_{22} is always much larger than ε^p_{11} near the crack tip, the effective plastic strain, by definition, would

be dominated by, and hence behave as ε_{22}^{p}. That is, as the crack speed increases, the level of effective plastic strain will decrease (see Fig. 4.3.26). Thus, just like in the case of dynamic crack propagation in elastic-perfectly plastic solids discussed in Chapter 3, this behavior can be used to explain experimental observations on many metallic materials, namely that at a higher crack propagation speed, the material resistance to fracture is higher. Hence, we can interpret the above behavior as follows. At a certain fixed load level characterized by the value of the far-field stress intensity factor K, the level of plastic straining represented by the effective plastic strain is lower for higher crack propagation speeds at the same location ahead of the crack tip. In order for the level of plastic straining at a higher crack speed to be the same as that at a lower crack speed, the loading level for the former must be raised. Consequently, continued fracture will occur at a higher loading level for a higher crack speed, if fracture is characterized by the attainment of a critical plastic strain level at a certain distance ahead of the crack tip.

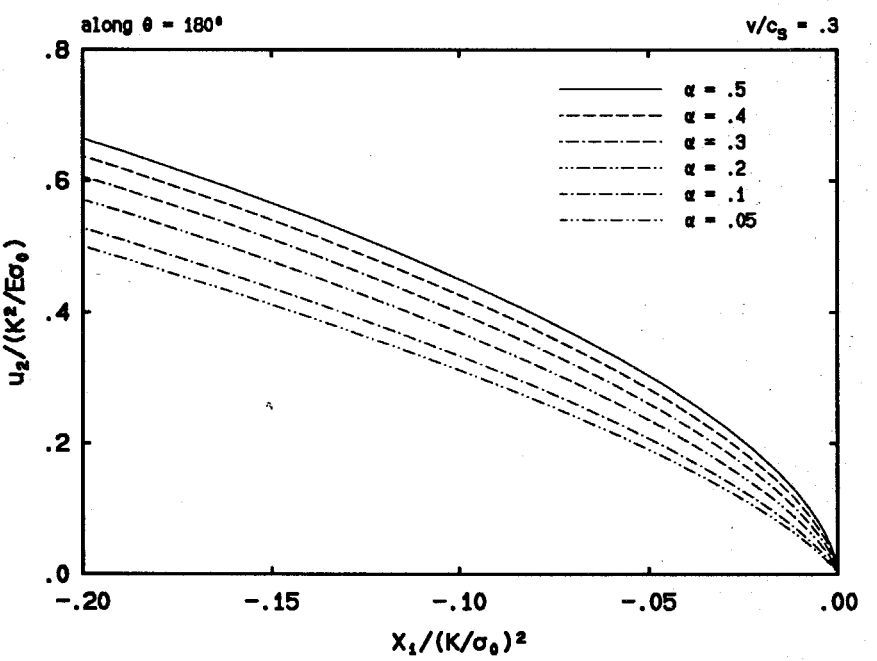

FIGURE 4.3.27a The effect of strain hardening on the radial variation of the vertical displacement u_2 along the crack surface for $v/c_s = 0.3$, plotted in its normalized form.

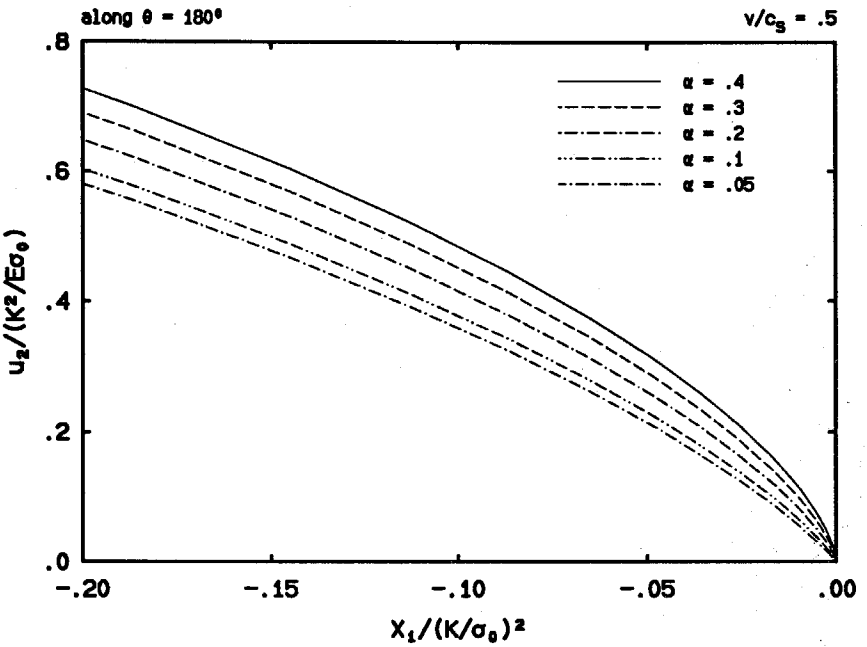

FIGURE 4.3.27b The effect of strain hardening on the radial variation of the vertical displacement u_2 along the crack surface for $v/c_s = 0.5$, plotted in its normalized form.

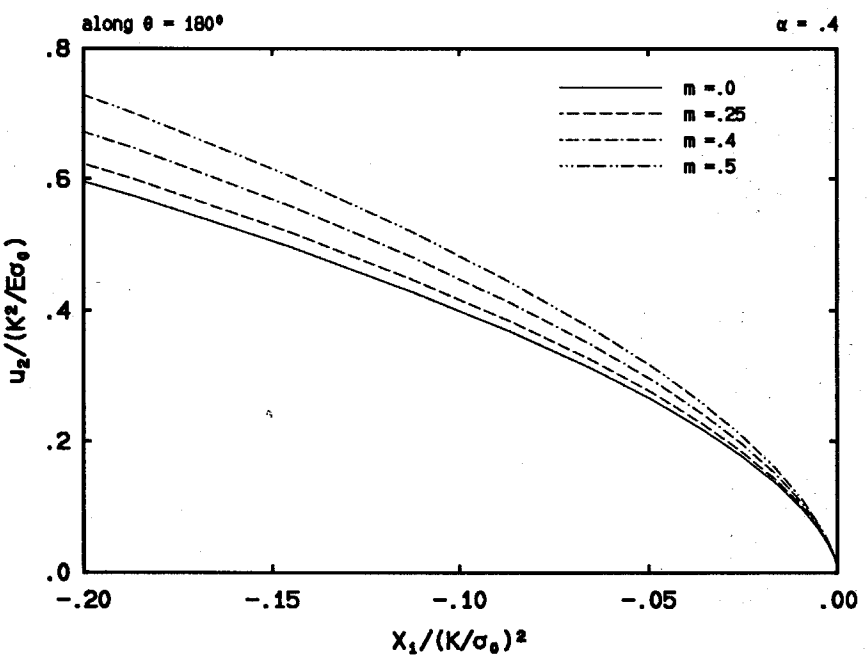

FIGURE 4.3.28a The effect of crack propagation speed on the radial variation of the vertical displacement u_2 along the crack surface for $\alpha = 0.4$, plotted in its normalized form.

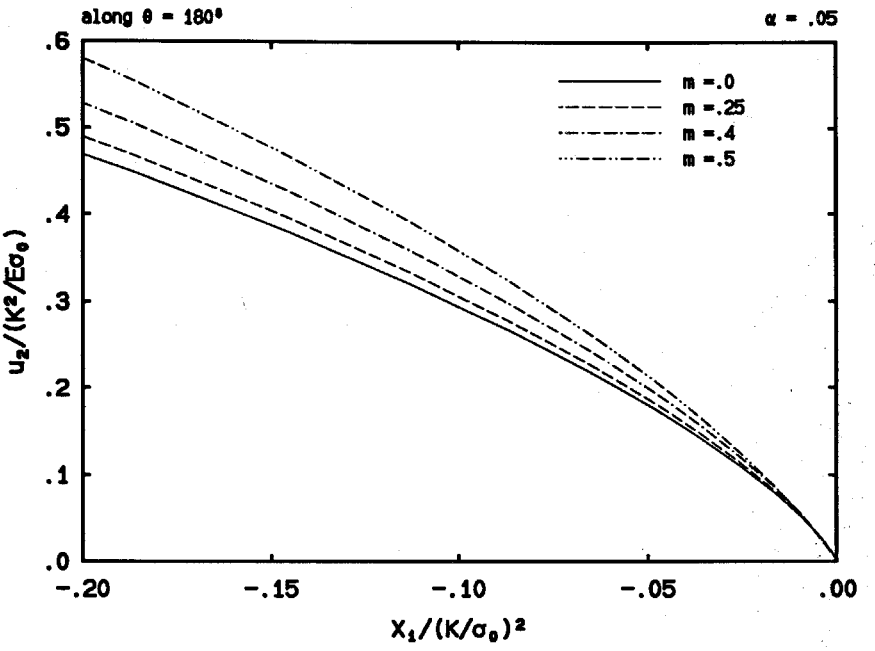

FIGURE 4.3.28b The effect of crack propagation speed on the radial variation of the vertical displacement u_2 along the crack surface for $\alpha = 0.05$, plotted in its normalized form.

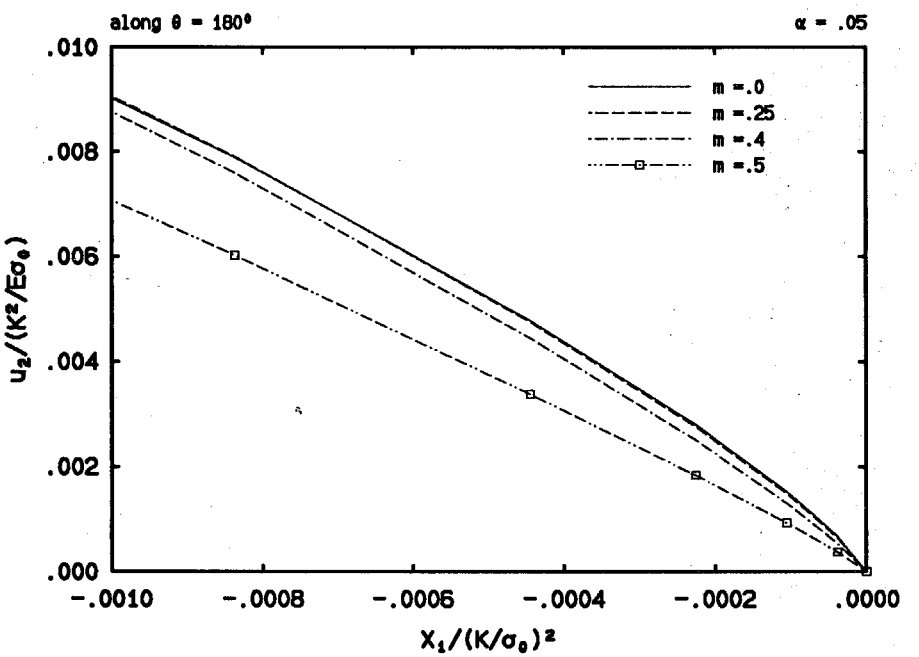

FIGURE 4.3.28c A detailed view of the effect of crack propagation speed on the radial variation of the vertical displacement u_2 along the crack surface for $\alpha = 0.05$, plotted in its normalized form.

Finally we present the results of the present finite element study regarding the effects of strain hardening and crack propagation speed on the crack opening displacement. As in the case of quasi-static crack growth, it is found that the magnitude of the vertical displacement component u_2 in the normalize coordinates decreases as α decreases for all the crack speeds we investigated (see Fig. 4.3.27). Moreover, for a typical high hardening material, e.g., for $\alpha = 0.4$, it is discovered that the magnitude of u_2 increases as the crack speed increases (see Fig. 4.3.28a). However, for a low hardening material, e.g., for $\alpha = 0.05$, the previous tendency, although it still holds far away from the crack tip as shown in Fig. 4.3.28b, is reversed very near the crack tip, as can be seen clearly from Fig. 4.3.28c. This feature has been more clearly observed in Mode I plane strain for elastic-perfectly plastic materials by Lam and Freund (1985) even at a distance about one-hundred times larger than the present one. As will be discussed in Chapter 6, by using this behavior and a critical crack tip opening angle criterion, they were able to explain the phenomenon of increased material resistance to continued crack propagation at higher speeds. Note that they were able to detect this feature by the same finite element method as used here from a near-tip mesh much coarser than the one employed here, with which, as discussed in Chapter 3 (see Fig. 3.3.13) we were not able to conclusively make a similar statement for elastic-perfectly plastic materials in Mode I plane stress. However, if this feature is an inherent characteristic of the dynamic crack tip fields (which, in fact, should be true if crack growth is to be achieved when a constant critical opening angle is retained, and if the material fracture toughness is to increase if the crack propagation speed is increased), then perhaps it can be more clearly revealed in plane stress for higher hardening materials and for elastic-perfectly plastic materials using a mesh much finer than the present one.

CHAPTER 5
POWER-LAW HARDENING SOLIDS

5.1 INTRODUCTION

For isotropic power hardening solids, asymptotic analyses for steady state, quasi-static crack growth were given by Gao and Hwang (1981b) in Mode III, and by Gao, Zhang and Hwang (1983) in Mode I plane strain. After exploring the possibilities of series solutions with logarithmic expansion as well as with power expansion, they concluded that the near-tip stress and plastic strain singularities are of the logarithmic type. Specifically, if the hardening exponent is n ($n \geq 1$), then the stresses are as singular as $[ln(R_0/r)]^{2/(n-1)}$ in Mode III, and as singular as $[ln(R_0/r)]^{1/(n-1)}$ in Mode I plane strain. As to strains, their singularities are of the order $[ln(R_0/r)]^{(n+1)/(n-1)}$ for the x_1-component and $[ln(R_0/r)]^{2n/(n-1)}$ for the x_2-component in Mode III, and of the order $[ln(R_0/r)]^{n/(n-1)}$ for all components in Mode I plane strain, where R_0 is a length scaling parameter which is not obtainable through asymptotic analyses. It is noted however that no quasi-static asymptotic solutions in Mode I plane stress are available.

For dynamic crack propagation in isotropic power hardening solids, similar steady state asymptotic analyses were conducted by Gao and Nemat-Nasser (1983b) in modes I and II plane strain (for incompressible materials only) and in Mode III, and by Zhang and Gao (1988) in Mode I plane stress. By assuming a certain form of displacement expansions, they were able to derive the same stress and strain singularities as for Mode I plane strain quasi-static crack growth. Moreover, they argued that angular stress and strain field variations in Mode I and Mode II for hardening materials are the same as those for elastic-perfectly plastic materials.

On the other hand, full field numerical investigations regarding crack tip stress and deformation field singularities and angular field variations for crack growth in power hardening materials are rare.

For quasi-static crack growth in Mode III and Mode I plane strain, finite element studies were performed by Dean and Hutchinson (1980) under steady state and small-scale yielding conditions, and for isotropic hardening materials obeying the J_2 flow theory and for nonisotropic hardening materials obeying the J_2 corner theory (Christoffersen and Hutchinson, 1979). Results were reported for the shape of the crack tip active plastic zone, for the variation of the crack opening displacement behind the crack tip, and for the distribution of the strains at the crack front.

A more detailed finite element investigation of crack tip stress and strain fields for steady state, quasi-static crack growth in Mode I plane strain was later conducted by Lam (1982). Angular variations of the stress and plastic strain fields, as well as the radial variations of the hoop stress, are described in this study.

Under Mode I plane stress conditions, a similar analysis for steady state, quasi-static crack growth was provided by Luo, Zhang and Hwang (1984). Explicit results for isotropic power hardening solids are reported for the shape changes of the crack tip active plastic zones with respect to the hardening exponent.

While in the above finite element studies the Eulerian-type formulation initiated by Dean and Hutchinson (1980) was employed, a nodal release procedure (Sorensen, 1978) was adopted in a more recent finite element analysis performed by Narasimhan, Rosakis and Hall (1987b). In their study, crack tip fields for quasi-static crack growth in Mode I plane stress under small-scale yielding conditions are investigated with a fracture criterion assumed *a priori*. In particular, numerical results are given for the shape of the crack tip active plastic zone, for crack opening displacements, for angular stress variations, for radial stress distributions at the

crack front, and also for certain plastic strain distributions at the crack front.

Hence, it is seen that, as far as the crack tip fields are concerned, no numerical analyses for dynamically propagating cracks are available as of today. It is the purpose of this chapter to report the results of a detailed finite element study, under conditions of steady state, Mode I plane stress and small-scale yielding, for isotropic power hardening materials obeying the J_2 flow theory of plasticity.

It is worth pointing out that, due to lack of well-established fracture criteria as well as special difficulties involved in such finite element computations, numerical studies of crack tip fields are usually performed under small-scale yielding conditions, which is also true of the present investigation.

In this chapter, results of the present study are presented both for quasi-static crack growth and for dynamic crack propagation, with comparisons to or discussions about available asymptotic and numerical solutions. The effects of hardening and inertia on crack tip fields are addressed in detail. All computations are carried out for the case of the Poisson ratio $\nu = 0.3$. All logarithmic values used in figures are based on the natural number e.

5.2 QUASI-STATIC CRACK GROWTH

The Active Plastic Zones

We begin our discussion on crack tip active plastic zones with a comparison to the result of a finite element study by Narasimhan, Rosakis and Hall (1987b) for $n = 5$, where n is the hardening parameter. It is noted that the plastic zone from the solution of Narasimhan, Rosakis and Hall for stable crack growth is obtained (from a nodal release procedure) at the twentieth nodal release and is found in an approximate steady state, hence comparable with our steady state solution. Shown in Fig. 5.2.1 are the active plastic zone shapes from the current study and from that

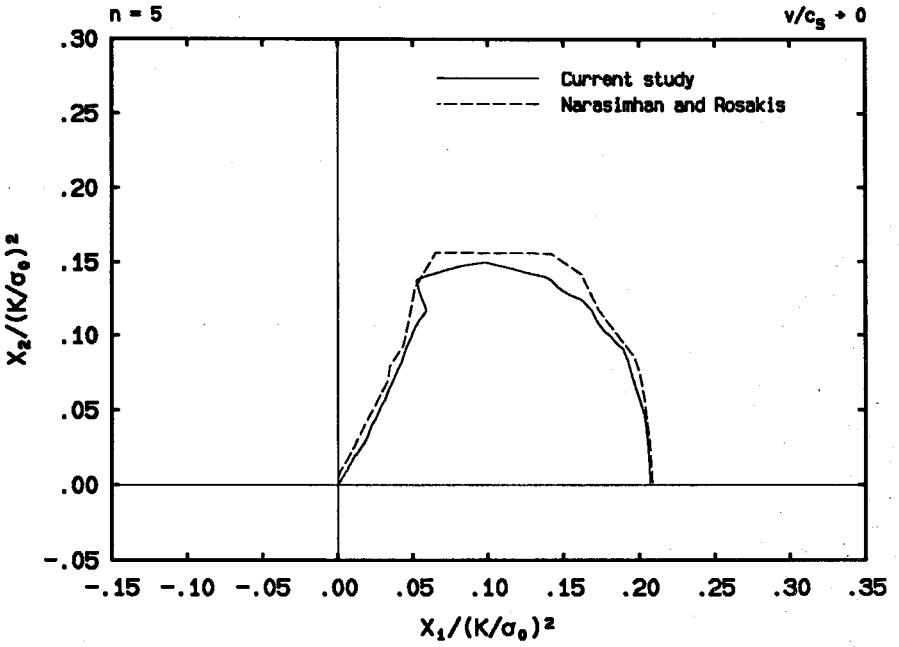

FIGURE 5.2.1 The shape of the crack tip active plastic zone for $n = 5$, compared with that by Narasimhan, Rosakis and Hall (1987b) in normalized coordinates, with the origin located at the crack tip.

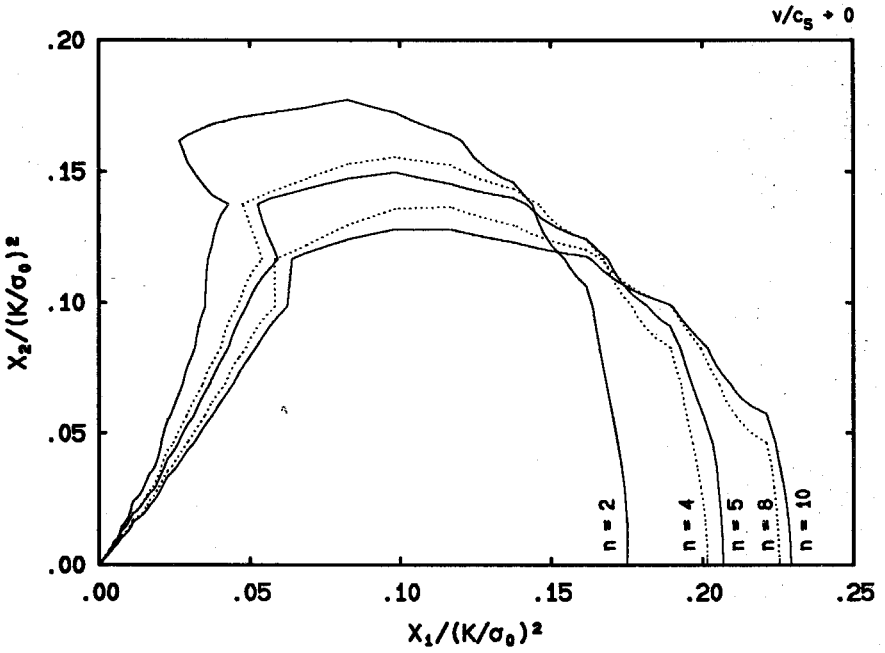

FIGURE 5.2.2 The effect of hardening on the shape of the crack tip active plastic zone in normalized coordinates, with the origin located at the crack tip.

of Narasimhan, Rosakis and Hall which was reproduced from their original plot. A good agreement is observed.

The progressive changes of the crack tip active plastic zone with respect to the power hardening parameter n for quasi-static crack growth is illustrated in Fig. 5.2.2 in a normalized coordinate. As the level of strain hardening decreases (i.e., as n increases), the plastic zone is seen to expand in the direction of crack growth and to shrink in the direction perpendicular to crack growth. Specifically, its horizontal size changes from $0.175(K/\sigma_0)^2$ at $n = 2$ to $0.229(K/\sigma_0)^2$ at $n = 10$, whereas its vertical size changes from $0.177(K/\sigma_0)^2$ at $n = 2$ to $0.128(K/\sigma_0)^2$ at $n = 10$. It is observed that the angular extent of the active plastic zone decreases as n increases (we will discuss this point further in the next subsection). No secondary active plastic zone is found behind the crack tip.

Angular Field Variations

We present the crack tip stress and velocity field variations in this subsection. First of all, as shown in Fig. 5.2.3, a comparison of stress variations for $n = 5$ is made with the finite element solution of Narasimhan, Rosakis and Hall from a nodal release procedure. Since the stress values from the two solutions are taken at different distances from the crack tip, all stress quantities are normalized such that the effective stress σ_e equals one at $\theta = 0^0$ in order to minimize differences due to strong radial dependence. It is noted that although the overall tendencies of the two solutions are similar, the actual magnitudes of the angular variations are quite different, which can be explained as follows. First note that for hardening materials, as will be discussed later, stresses are singular at the crack tip. Hence, numerical values must be extracted from locations along circular paths around the crack tip in order to reveal any realistic angular variations. To this end, it is worth pointing out that while data from the present study are obtained along a circular path, those from that of Narasimhan, Rosakis and Hall are from a *rectangular path* which will

certainly introduce radial dependence into the angular variations. Recall that in the case of crack growth in elastic-perfectly plastic solids, as discussed in Chapter 3 (see Fig. 3.2.2a), a similar comparison with Narasimhan, Rosakis and Hall's study shows very good agreement, it seems that this strong radial dependence introduced in Narasimhan, Rosakis and Hall's solution is a major factor responsible for the disagreement in the present comparison.

Secondly, it is noted that the present study is much more detailed than the other one in the sense that the present study employed a mesh with the ratio of the active plastic zone size to that of the smallest near-tip element on the order of 16,000, whereas the study by Narasimhan, Rosakis and Hall used a mesh with the ratio only on the order of 385. Moreover, the data of the present study are taken from locations very close to the crack tip, specifically, from a distance about $0.2 \times 10^{-3}(K/\sigma_0)^2$ away from the crack tip, while those from that of Narasimhan, Rosakis and Hall are from a distance of about $0.2 \times 10^{-1}(K/\sigma_0)^2$ away from the crack tip. In this light, we believe that the result of the present study is a better approximation for the crack tip fields. The advantage of a very detailed finite element mesh near the crack tip will be elaborated further when we discuss the radial dependence of the crack tip fields.

The effect of hardening on the angular stress variations are demonstrated through the progressive changes of stress components with respect to the power hardening parameter n, as shown in Fig. 5.2.4 where all stress quantities are normalized such that $\sigma_e = 1$ at $\theta = 0^0$. The overall variations are very similar to those for linear hardening materials which are presented in Chapter 4. It is seen that the slopes of σ_{rr} at $\theta = 0^0$, and $\sigma_{\theta\theta}$ at $\theta = 0^0$ and 180^0 are very close to zero. Large compressive radial stresses behind the crack tip (see Fig. 5.2.4a) are observed for all n values investigated, which indicates a tendency of reverse plastic loading there. However, judging from the relative magnitudes of the effective stress σ_e and the flow stress σ (see Fig. 5.2.4b), it is clear that this tendency is not strong

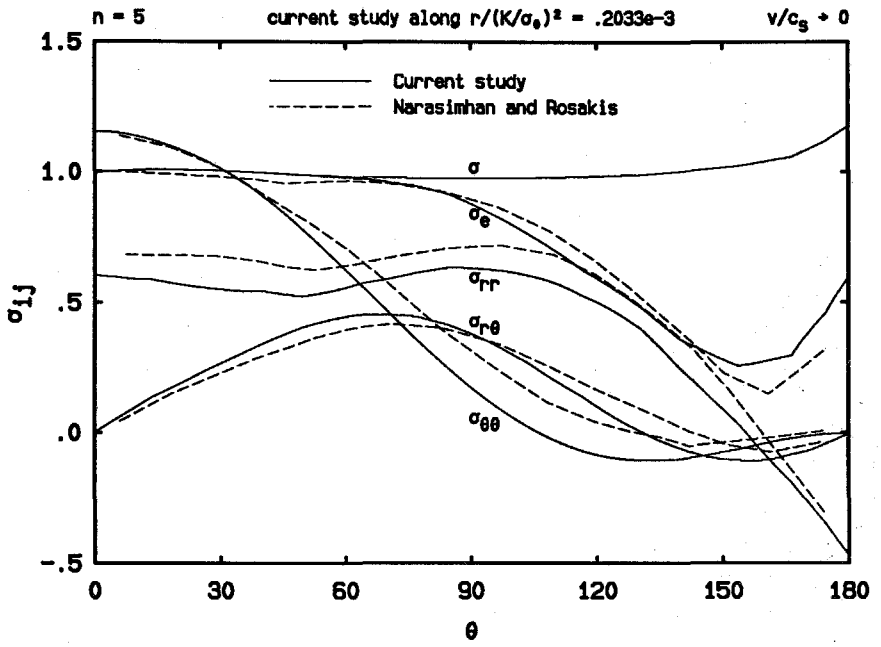

FIGURE 5.2.3 Angular variations of the polar stress components, the effective stress σ_e and the flow stress σ for $n = 5$, normalized such that $\sigma_e = 1$ at $\theta = 0^0$, with comparisons to the solution by Narasimhan, Rosakis and Hall (1987b).

enough to reach yielding. Of course, this may also suggest that if yielding is actually achieved in a region along the crack flank, it must be extremely small such that the present numerical solution (although already very detailed) is not able to detect its existence.

We would like to point out that the traction-free condition $\sigma_{\theta\theta} = 0$ and $\sigma_{r\theta} = 0$ at $\theta = 180^0$ and the symmetry condition $\sigma_{r\theta} = 0$ at $\theta = 0^0$ are very well satisfied by our numerical solution, which is a major sign of its convergence. In fact, it is seen that $\sigma_{\theta\theta}$ is close to zero along the crack flank for quite an angular range.

By definition, the angular extent of the crack tip active plastic zone or the angle at which elastic unloading occurs can be estimated from the position where the effective stress σ_e deviates from the flow stress σ. To do that, as discussed in Chapter 4 for the case of linear hardening, an error tolerance must be specified for the relative difference of σ_e with respect to σ. For example, using the error tolerance

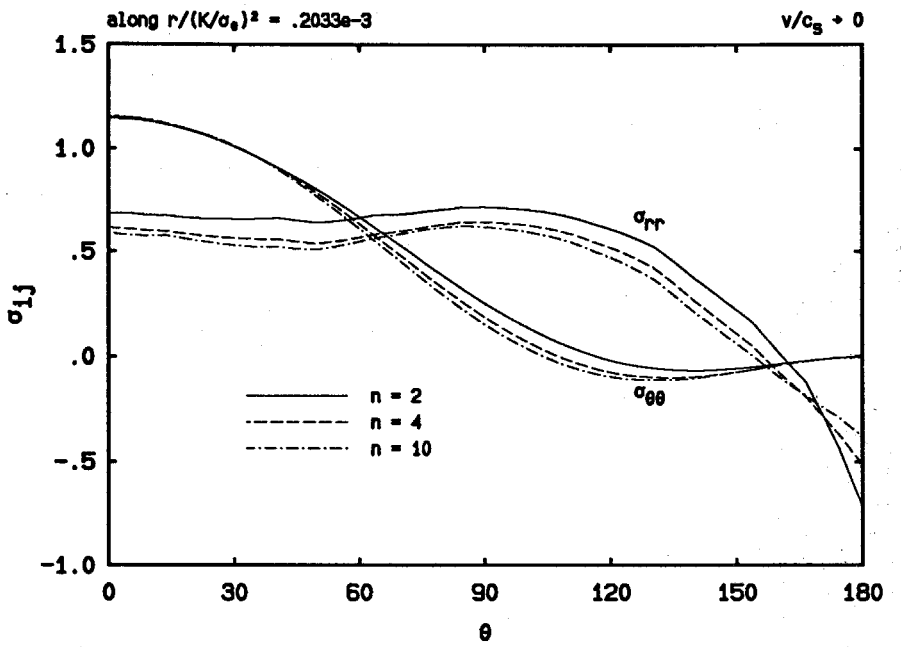

FIGURE 5.2.4a The effect of hardening on the angular variations of the polar stress components σ_{rr} and $\sigma_{\theta\theta}$, normalized such that the effective stress $\sigma_e = 1$ at $\theta = 0^0$.

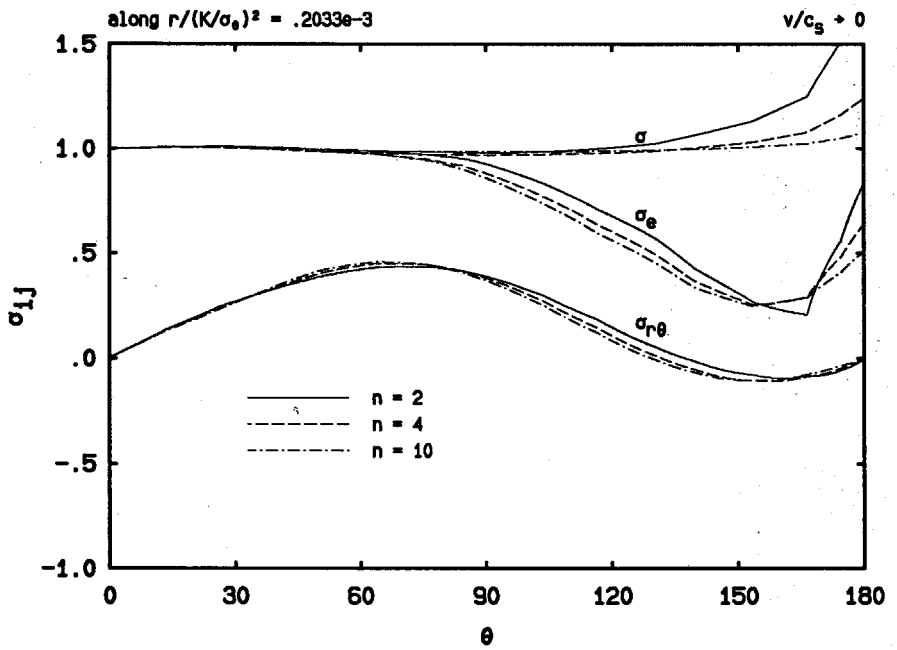

FIGURE 5.2.4b The effect of hardening on the angular variations of the polar stress component $\sigma_{r\theta}$, the effective stress σ_e and the flow stress σ, normalized such that $\sigma_e = 1$ at $\theta = 0^0$.

0.77×10^{-2} from Chapter 4, it is found that this angle changes from 70^0 for $n = 2$ to 55^0 for $n = 10$.

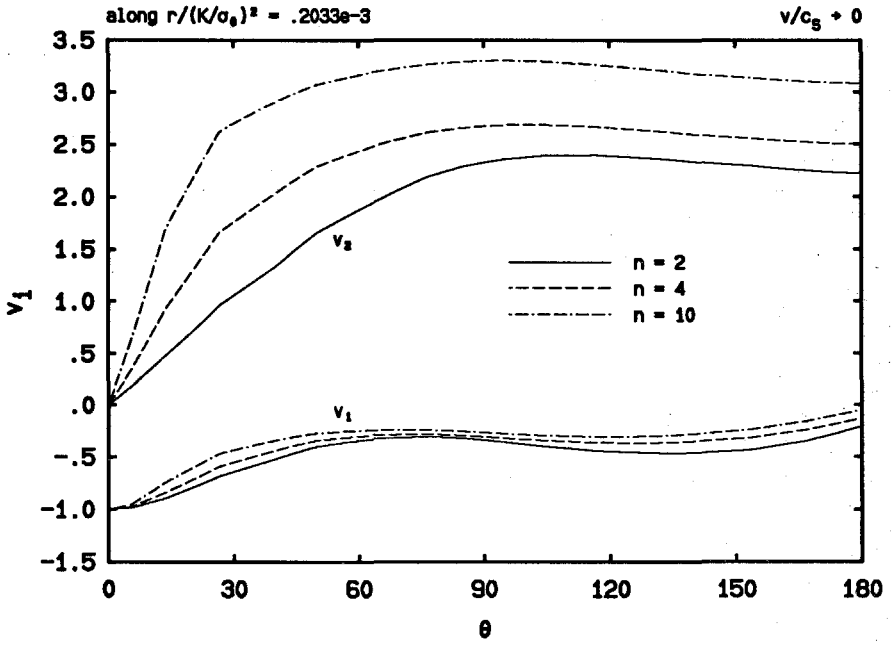

FIGURE 5.2.5 The effect of hardening on the angular variations of the Cartesian velocity components, normalized such that $v_1 = -1$ at $\theta = 0^0$.

The effect of power-law strain hardening on the angular variations of the velocity field is demonstrated in Fig. 5.2.5 where the velocity components are normalized such that $v_1 = -1$ at $\theta = 0^0$. It is found that, just like the case of linear hardening, the slope of the velocity component v_2 at $\theta = 0^0$ becomes larger as the level of hardening becomes smaller or as the power hardening parameter n becomes larger. Besides, it is observed that the value of v_1 is always negative while that of v_2 is always positive. In the elastic unloading sector which begins, for example for $n = 2$, at approximately $\theta = 55^0$, the magnitude of v_2 is consistently about three times greater than that of v_1.

Radial Field Variations

The radial variations of the stress components are presented here for $\theta = 0^0$,

i.e., along the prospective crack line, which are plotted in Fig. 5.2.6 in their original normalized forms and in Fig. 5.2.7 in special logarithmic coordinates. Note that all data are taken from five elements away from the crack tip and that only one data point is extracted from each element.

It can be seen that while the rapid changes of the magnitudes of the stress components (see Fig. 5.2.6, especially for lower n values or for higher hardening materials), indicate the existence of stress singularities at the crack tip, the approximate straight lines observed in Fig. 5.2.7 strongly suggest that the singularities are of the type $[ln(R_0/r)]^s$ $(s > 0)$, where R_0 is a length scaling parameter. It is also found that as n increases, both the value of s or the slope of the straight lines and the magnitude of the stress components decrease, which simply means that stress singularities at the crack tip are weaker for materials with less strain hardening. In any case, the magnitude of σ_{22} is found to be larger than that of σ_{11}.

At this moment we would like to make more comparisons with the solution of Narasimhan, Rosakis and Hall and demonstrate the need of a detailed finite element mesh near the crack tip. Shown in Figs. 5.2.8a and 5.2.8b are the comparisons for the radial dependence of stress components σ_{11} and σ_{22}, and the radial dependence of the plastic strain component ε^p_{22}, respectively, along the ray $\theta = 0^0$. It is clear from the comparisons that the solution of Narasimhan, Rosakis and Hall, for example, for the variation of σ_{11}, missed the characteristic singular feature of the near-tip field, although its agreement with the present study at locations away from the crack tip is very good. This again confirms our earlier explanations regarding angular stress variations that the disagreement is caused by the singular radial dependence of the stress components and the use of a rectangular path for the sample data points in the solution by Narasimhan, Rosakis and Hall. In fact, in the case of ideal plasticity (see Fig. 3.2.5b) when the stresses are bounded at the crack tip, the solution of Narasimhan, Rosakis and Hall does agree very well with that of the present study.

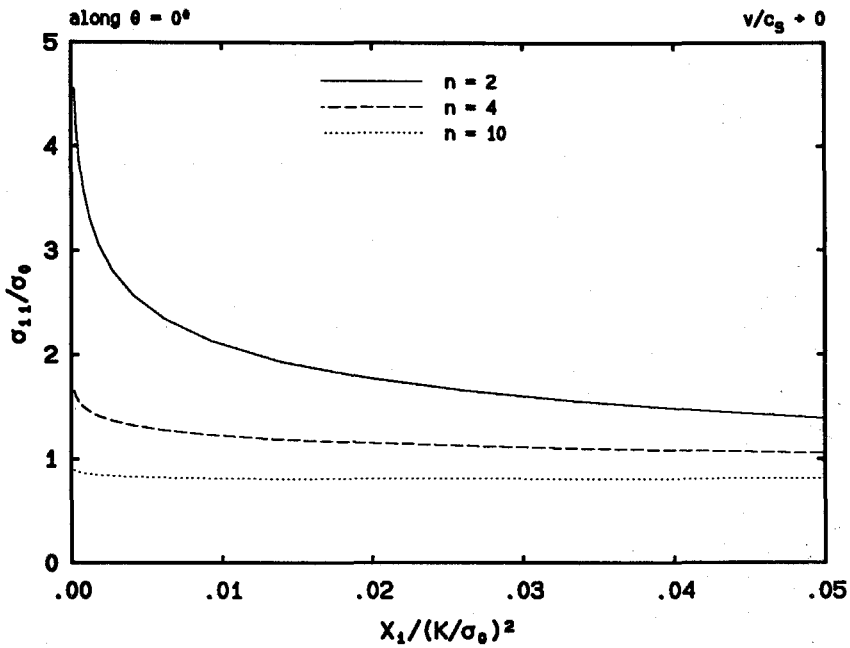

FIGURE 5.2.6a The radial variations of the stress component σ_{11} along the prospective crack line in normalized coordinates.

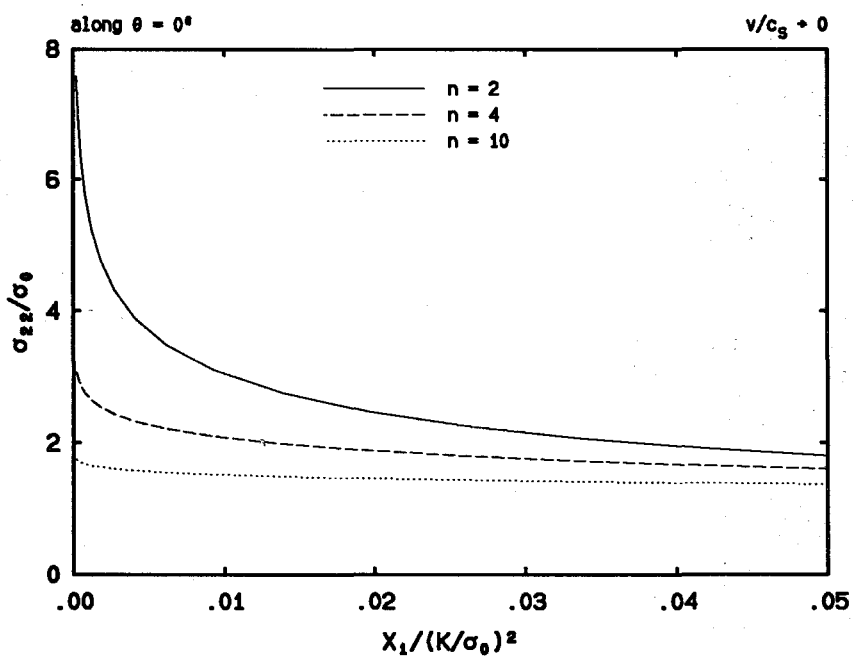

FIGURE 5.2.6b The radial variations of the stress component σ_{22} along the prospective crack line in normalized coordinates.

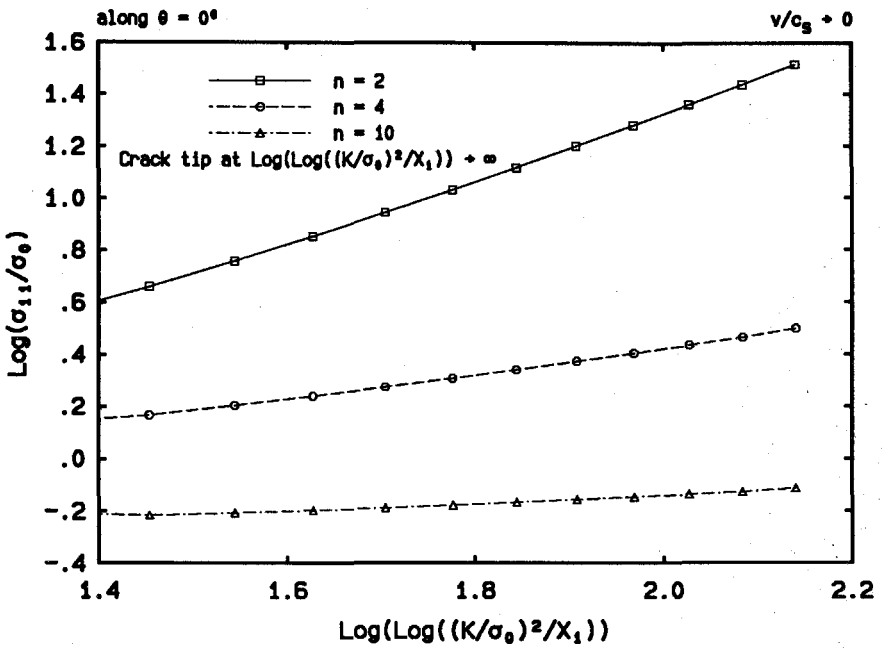

FIGURE 5.2.7a The radial variations of the stress component σ_{11} along the prospective crack line in special logarithmic coordinates.

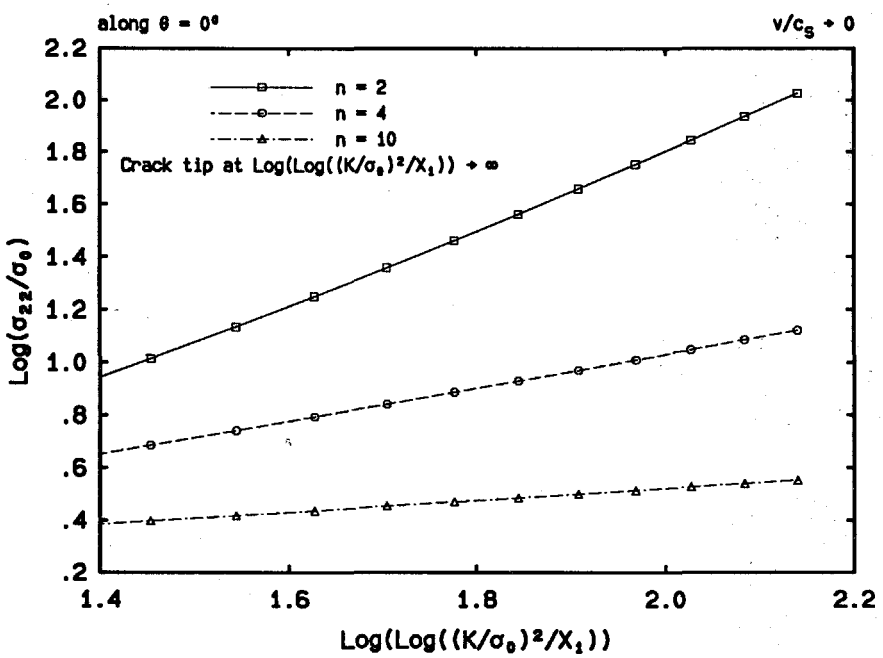

FIGURE 5.2.7b The radial variations of the stress component σ_{11} along the prospective crack line in special logarithmic coordinates.

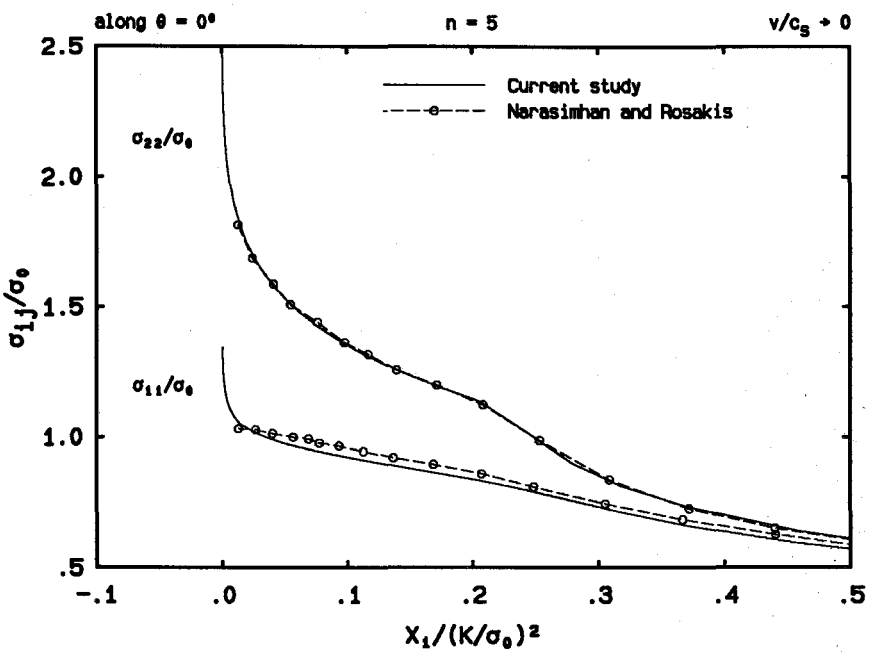

FIGURE 5.2.8a The radial variations of stress components σ_{11} and σ_{22} along the prospective crack line for $n = 5$, compared with the solution of Narasimhan, Rosakis and Hall (1987b).

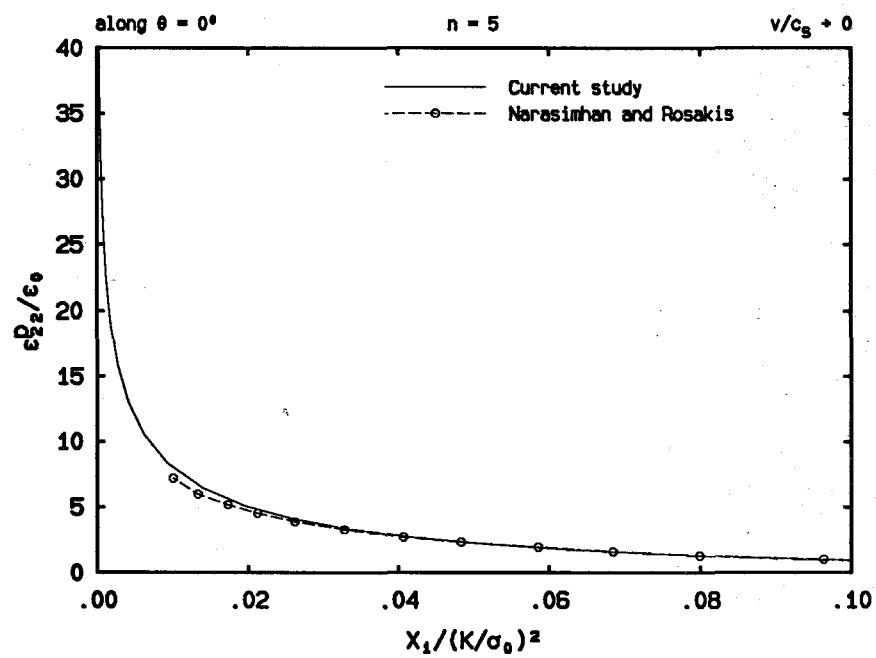

FIGURE 5.2.8b The radial variations of the plastic strain component ε_{22}^p along the prospective crack line for $n = 5$, compared with the solution of Narasimhan, Rosakis and Hall (1987b).

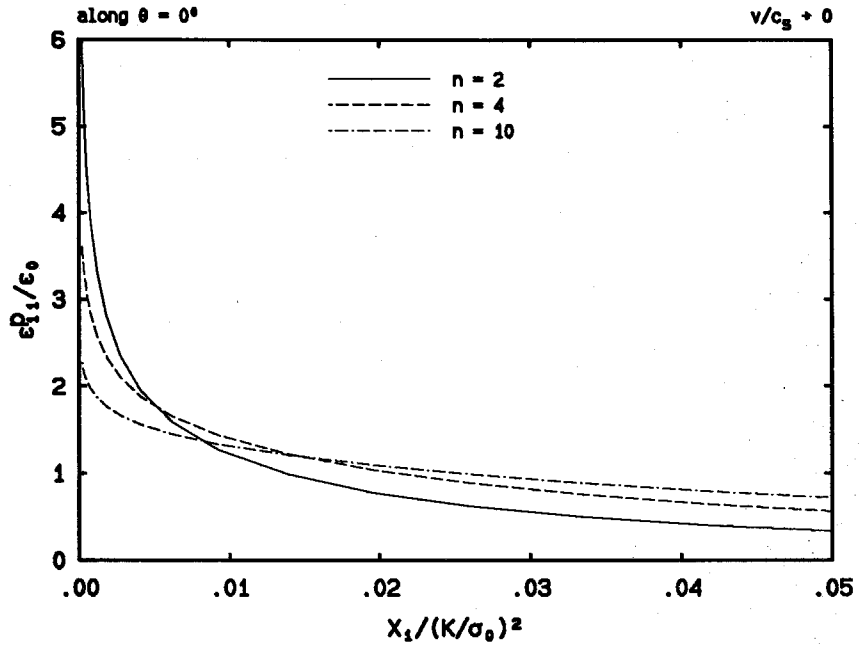

FIGURE 5.2.9a The radial variations of the plastic strain component ε_{11}^p along the prospective crack line in normalized coordinates.

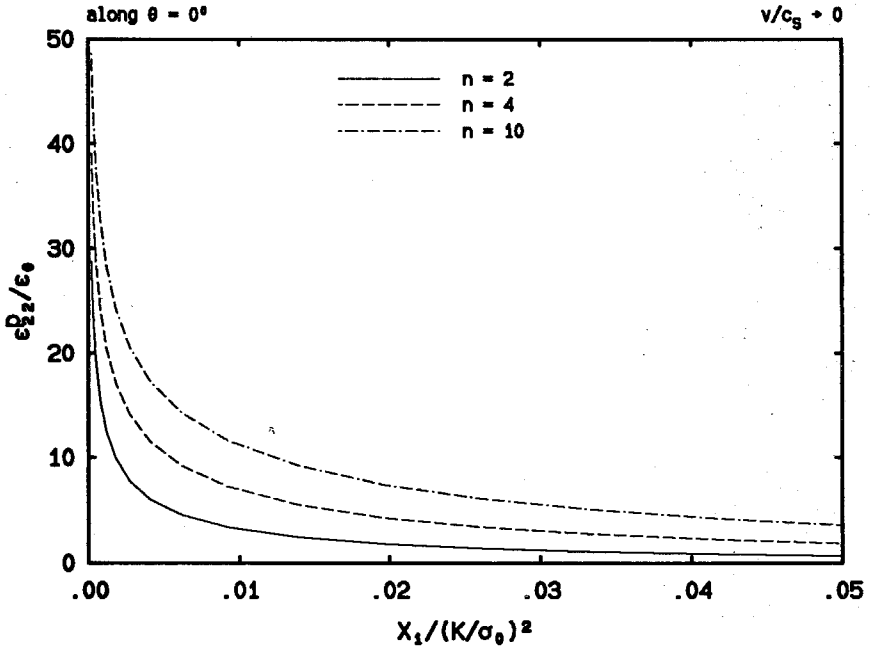

FIGURE 5.2.9b The radial variations of the plastic strain component ε_{22}^p along the prospective crack line in normalized coordinates.

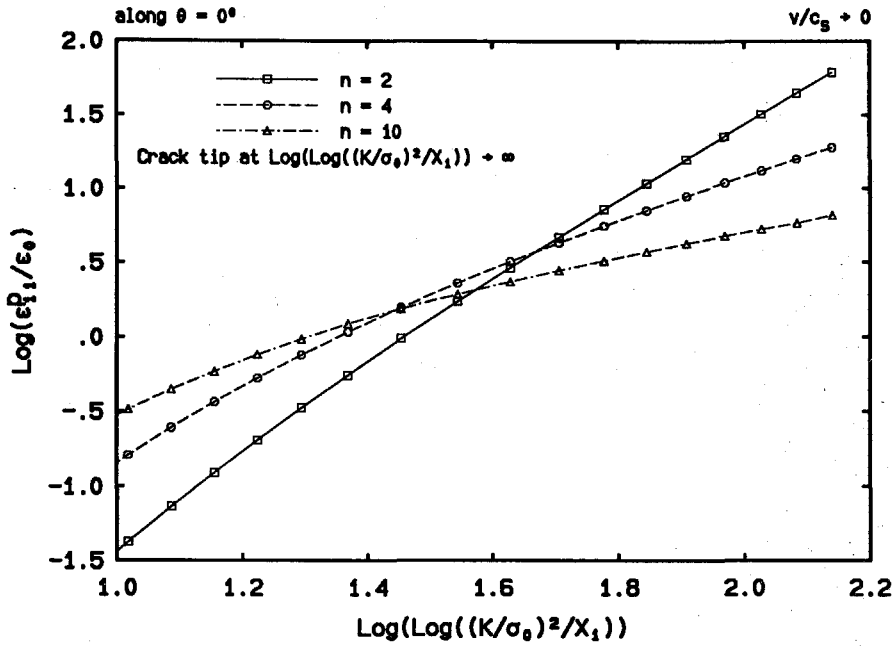

FIGURE 5.2.10a The radial variations of the plastic strain component ε_{11}^p along the prospective crack line in special logarithmic coordinates.

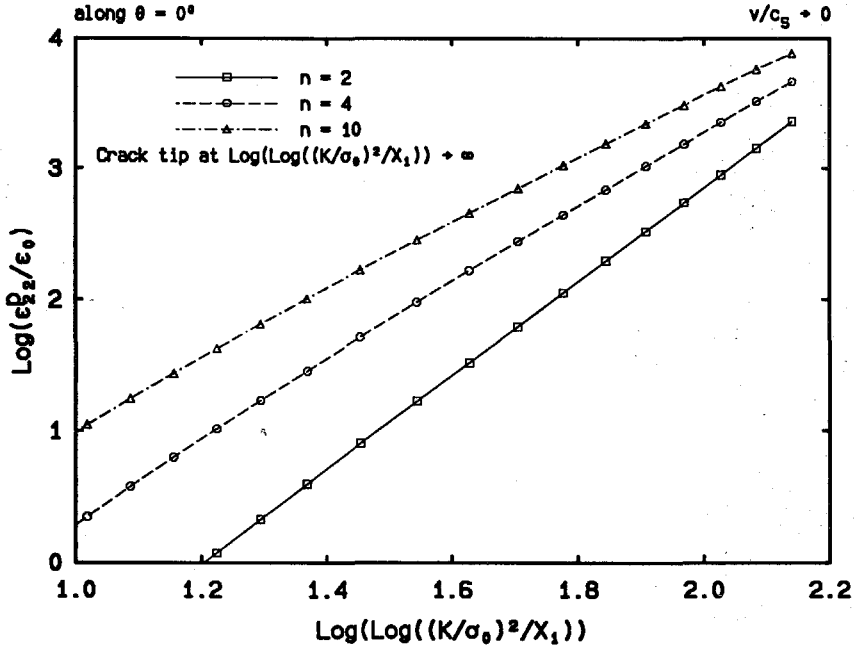

FIGURE 5.2.10b The radial variations of the plastic strain component ε_{22}^p along the prospective crack line in special logarithmic coordinates.

The effect of hardening on the radial dependence of the plastic strain components are shown in Figs. 5.2.9 and 5.2.10 for the case of $\theta = 0^0$. Just like stress variations, it is seen from Fig. 5.2.9 that the plastic strain components behave singularly as the crack tip is approached. Further, fairly straight lines are observed in Fig. 5.2.10 where special logarithmic coordinates are employed, which strongly indicates strain singularities of the type $[lnr(R_0/r)]^s$ $(s > 0)$ at the crack tip $r = 0$, where R_0 is a length scaling parameter and the exponent s for strain singularities are in general different from that for stress singularities. It is clear that s decreases as n increases, which means that strain singularities at the crack tip become weaker for materials with weaker level of strain hardening.

Moreover, from Fig. 5.2.9 alone, it seems that very near the crack tip, the magnitude of ε_{11}^p decreases as n increases, whereas that of ε_{22}^p increases. However, tendencies demonstrated by the straight lines in Fig. 5.2.10 suggest that both plastic strain components will take smaller values very near the crack tip as n increases. It is also clear from the figures that the magnitude of ε_{22}^p is always much larger than that of ε_{11}^p.

As discussed earlier in the introductory section, some investigators indeed were able to obtain asymptotic solutions with assumed singularities of the type $[ln(R_0/r)]^s$ $(s > 0)$ for quasi-static crack growth although not under Mode I plane stress conditions. For example, it is found that stresses and strains behave, respectively, as $[ln(R_0/r)]^{1/(n-1)}$ and $[ln(R_0/r)]^{n/(n-1)}$ in Mode I plane strain, which gives explicit values of the exponents for stresses and strains.

It is recalled here that in the case of linear hardening, we have numerically estimated the values of the exponent for stress singularities of the type r^s $(s > 0)$ for different levels of strain hardening, and we have compared those values to available asymptotic approximations with satisfying agreement. Unfortunately, we are not able to repeat the same calculation here for power hardening materials.

This is because, for a singularity of the form $[ln(R_0/r)]^s$, a numerically estimated value of s, for example, calculated from the slope of the straight line in logarithmic coordinates (see Fig. 5.2.10b), will in general depend on the value of the unknown parameter R_0, although theoretically the value of s is independent of the choice of R_0. This numerical difficulty is not encountered in the case of linear hardening when singularities are of the form r^s $(s < 0)$.

Table 5.2.1 Values of the Length Scaling Parameter R_0

	$R_0/(K/\sigma_0)^2$			
n	for σ_{11}	for σ_{22}	for ε^p_{11}	for ε^p_{22}
2	.165	.0769	.205	.0416
4	.0814	.0312	.520	.0233
5	.0793	.0281	.945	.0220
8	.0892	.0265	5.34	.0216
10	.0990	.0259	13.2	.0219

On the other hand, if s is known, say, from an asymptotic analysis, then we can estimate the value of R_0 from a numerical solution. However, due to the fact that practically a numerical solution cannot be obtained at arbitrarily small distances from the crack tip, estimations of R_0 from data for different stress and plastic strain components will be different. Nonetheless, we have computed, for each nonzero stress and plastic strain component at $\theta = 0^0$, an estimation of R_0 from data taken from the sixth to tenth elements if the element at the crack tip is considered as the first one. Since, to the author's best knowledge, no asymptotic study for quasi-static crack growth in power hardening solids is available in Mode I plane stress, we will assume that the asymptotic result for Mode I plane strain can be applied here. Hence, s is set to $1/(n-1)$ for stress singularities and to $n/(n-1)$ for plastic strain singualrities, where n being the power hardening parameter. Results of this calculation are shown in Table 5.2.1.

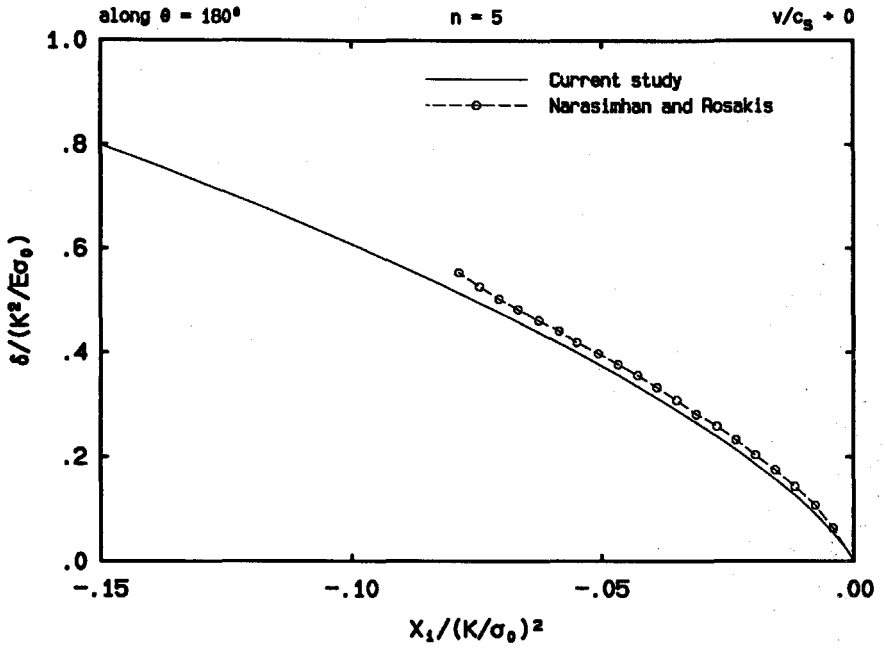

FIGURE 5.2.11 The crack opening displacement δ (twice of the vertical displacement u_2 along the crack surface) in its normalized form, compared with the finite element solution by Narasimhan, Rosakis and Hall (1987b).

Finally we would like to present results regarding radial variations of the crack opening displacement δ, which is twice of the value of the vertical displacement u_2 along the crack surface. For $n = 5$, a comparison is performed as shown in Fig. 5.2.11. As in the case of linear hardening when a comparison is made with that of Dean (see Fig. 4.2.11), the current comparison with the result of Narasimhan, Rosakis and Hall shows again that the crack opening profile predicted by the present study is slightly smaller. Once again we think that this difference is mainly due to the fact that a much finer mesh is employed in the present study and hence the present solution gives a better approximation.

Shown in Fig. 5.2.12 is the radial dependence of the vertical displacement along the crack surface for various hardening levels. It is seen that the radial variation of u_2 takes similar forms for different values of n. Moreover, as n increases, the crack opening is found to decrease accordingly.

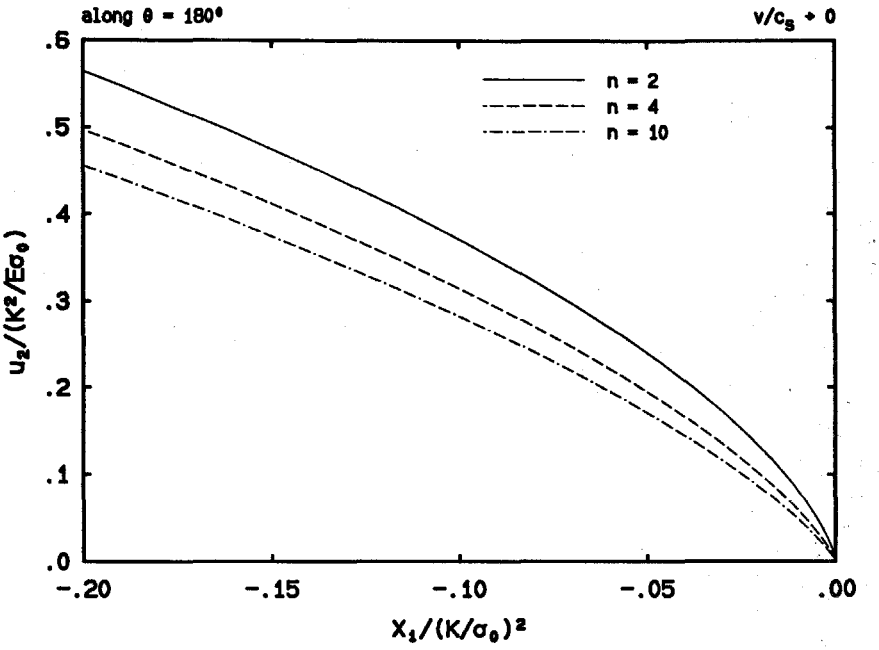

FIGURE 5.2.12 The effect of strain hardening on the radial variation of the vertical displacement u_2 along the crack surface, plotted in its normalized form.

5.3 DYNAMIC CRACK PROPAGATION

The Active Plastic Zones

Shown in Figs. 5.3.1a and 5.3.1b are the progressive variations of the crack tip active plastic zone with respect to the hardening parameter n in normalized coordinates, for the case of dynamic crack propagation at speeds $v = 0.3c_s$ and $0.4c_s$, respectively, where c_s is the elastic shear wave speed of the material. It is found that secondary active plastic zones along the crack flank are detected by the present numerical study at $v/c_s = 0.4$ for both $n = 4$ and 10, although no such reverse yielding zone is observed for any hardening level we studied at $v/c_s = 0.3$.

Similar to the case of quasi-static crack growth, it can be seen that as n increases, the crack tip active plastic zone elongates horizontally or in the direction of crack propagation, and it shortens vertically or in the direction perpendicular to that of crack propagation. For example, at $v/c_s = 0.3$, it is found that the size of

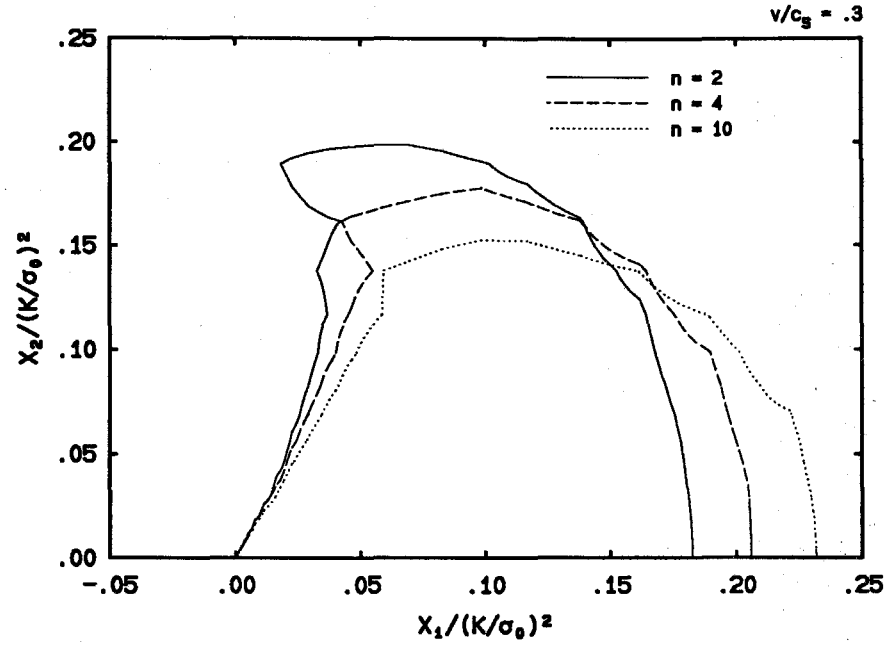

FIGURE 5.3.1a The effect of hardening on the shape of the crack tip active plastic zone at $v/c_s = 0.3$, plotted in normalized coordinates with the origin located at the crack tip.

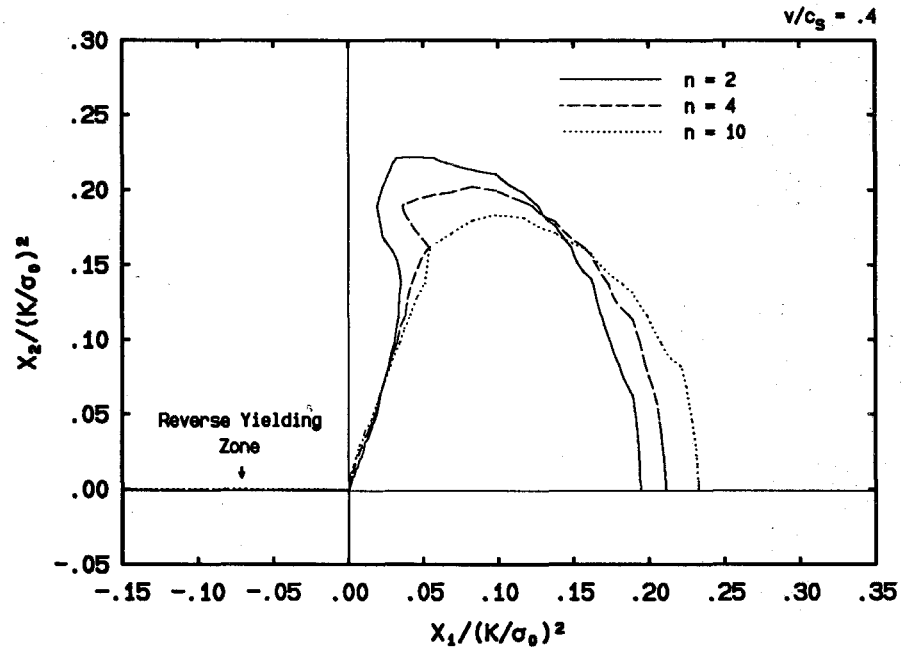

FIGURE 5.3.1b The effect of hardening on the shape of the crack tip active plastic zone at $v/c_s = 0.4$, plotted in normalized coordinates with the origin located at the crack tip.

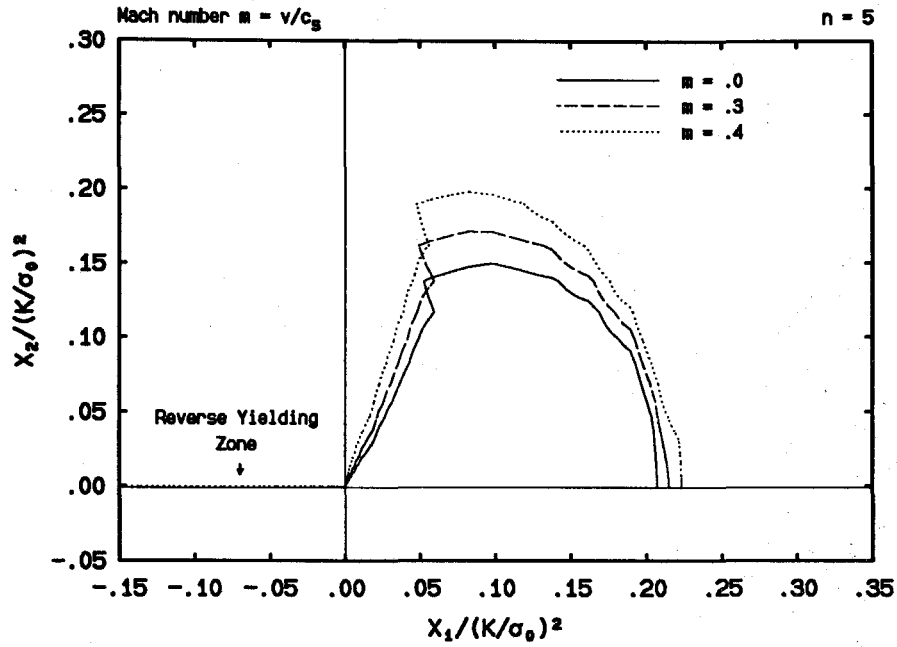

FIGURE 5.3.2a The effect of crack propagation speed on the shape of the crack tip active plastic zone for $n = 5$, plotted in normalized coordinates, with the origin located at the crack tip.

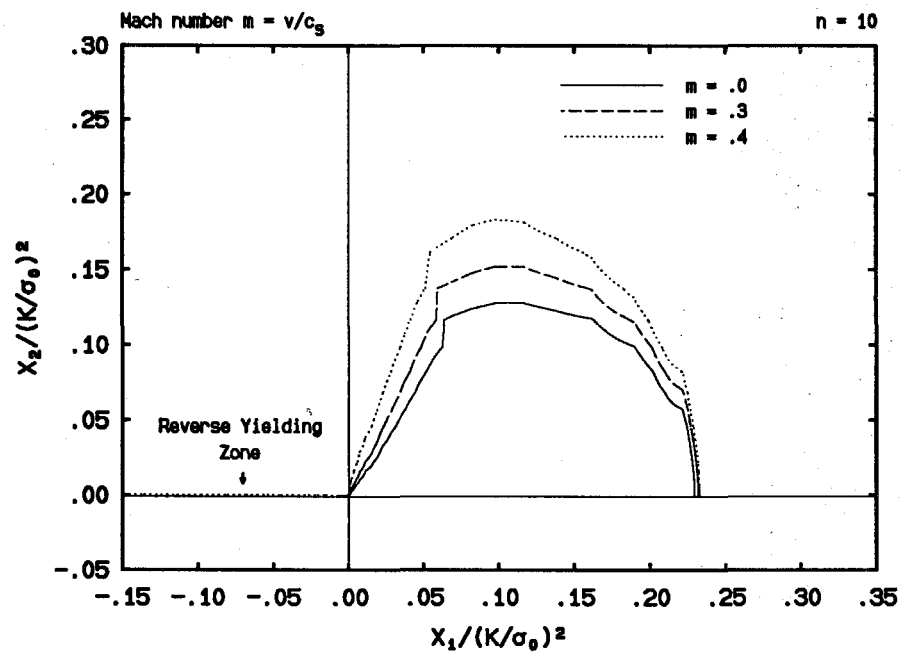

FIGURE 5.3.2b The effect of crack propagation speed on the shape of the crack tip active plastic zone for $n = 10$, plotted in normalized coordinates, with the origin located at the crack tip.

the crack front active plastic zone changes horizontally from about $0.182(K/\sigma_0)^2$ for $n = 2$ to about $0.232(K/\sigma_0)^2$ for $n = 10$, and vertically from about $0.187(K/\sigma_0)^2$ for $n = 2$ to about $0.152(K/\sigma_0)^2$ for $n = 10$.

Moreover, at $v/c_s = 0.3$, the near-tip angular extent of the plastic zone is found to decrease as n increases, which is basically the same as in the case of quasi-static crack growth. However, at $v/c_s = 0.4$ when inertia due to high-speed crack propagation is strong, the tendency described above is reversed. In fact, it can be seen from Fig. 5.3.1b that as n increases, this near-tip elastic unloading angle also increases, although slightly. This point will be further noted when we try to give an estimation of this angle from angular variations of near-tip stress quantities.

The effect of inertia or crack propagation velocity on the shape of the crack tip active plastic zone is illustrated in Fig. 5.3.2a for $n = 5$ and in Fig. 5.3.2b for $n = 10$. It is first noted that a secondary active plastic zone or reverse yield zone is detected by the present finite element solution at Mach number $m = 0.4$ ($m = v/c_s$) for both $n = 5$ and 10, which can be viewed as a sign of stronger dynamic effect at a higher crack speed.

Recall that in the case of ideal plasticity (refer to Fig. 3.3.1a of Chapter 3), the size of the crack front active plastic zone slightly shrinks along the prospective crack line as m increases. However, this is not the case for hardening materials. Just like for linear hardening materials, the crack front plastic zone for crack propagation in power hardening materials expands both horizontally and vertically as m increases. Yet it can be seen that the extent of its horizontal expansion diminishes (see Fig. 5.3.2b) as n increases or as the elastic-perfectly plastic limit is approached.

Angular Field Variations

Angular variations of the polar stress components, the effective stress and the flow stress are plotted in Fig. 5.3.3 for $v/c_s = 0.3$ and in Fig. 5.3.4 for $v/c_s = 0.4$

with normalizations such that $\sigma_e = 1$ at $\theta = 0^0$. At the lower crack propagation velocity $v/c_s = 0.3$, the variations are not very much different from those for quasi-static crack growth. It is seen that although relatively high compressive σ_{rr} values are found behind the crack tip (see Fig. 5.3.3a), reverse plastic yielding is not detected which is clear from the gap between σ_e and σ (see Fig. 5.3.3b). However, at the higher crack speed $v/c_s = 0.4$ when stronger inertia effect is expected, features not observed from quasi-static fields begin to show up as the level of hardening decreases or as n increases. First of all, it is clear from Fig. 5.3.4a that a sudden change of slope or a kink has developed in σ_{rr} for $n = 10$ at a location where approximately σ_e deviates from σ or where elastic unloading first takes place (see Fig. 5.3.4b). In fact a sign of kinking can already be seen for $n = 4$. Besides, corresponding to the appearance of the kink near the elastic-plastic interface, a secondary active plastic zone is also developed along the crack flank, which can be seen from the fact that $\sigma_e = \sigma$ near $\theta = 180^0$ for $n = 4$ and 10 (see Fig. 5.3.4b). The existence of this reverse loading zone behind the crack tip has been discussed earlier (see Fig. 5.3.2).

In the first-order asymptotic analysis of Zhang and Gao (1988), it is concluded that angular field variations do not depend on the power hardening parameter n since very near the crack tip the values of the plastic strains are so high that the effective stress and strain relationship are basically that of an elastic-perfectly plastic material. Hence, they argued that the angular field variations should be the same as those for elastic-perfectly plastic materials. To this end, we would mention that there is only one such first-order asymptotic analysis for elastic-perfectly plastic materials available as of today, which was given by Gao (1987) and has been discussed in Chapter 3. In this asymptotic analysis for steady state dynamic crack growth, a kink indeed exists at the elastic-plastic interface in the angular stress variations, which we have observed in our numerical solutions at high crack propagation speeds for elastic-perfectly plastic materials (see Fig. 3.3.2b), for low-level linear harden-

ing materials (see Fig. 4.3.7) and for the above discussed low-level power hardening materials (see Fig. 5.3.4).

However, there seem to be more differences than similarities between the results of the present study and those of the asymptotic analysis of Gao in regard to angular stress variations. In the case of ideal plasticity, we attributed the differences to the lack of enough dominance zone of first-order dynamic asymptotic solution at low crack propagation speeds, which was first discovered by Freund and Douglas (1982). Naturally, if this was the right reason, it will also hold for hardening materials with a low level of hardening since then the materials are expected to show characteristics similar to those of nonhardening materials. Yet, in the present case where the asymptotic analysis of Zhang and Gao has suggested that the angular field variations be the same for power hardening and nonhardening materials, the lack of enough dominance zone at a high level of strain hardening for the effective stress strain relation to be approximated by that of a nonhardening material may be another major factor. Theoretically speaking, this approximation is valid only at the limit the effective plastic strain approaches infinity, or at the limit $r = 0$ assuming strain singularities exist at the crack tip.

As in the case of linear hardening, the angle at which elastic unloading takes place may be founded by estimating the location where the effective stress σ_e deviates from the flow stress σ. By taking the same error tolerance in the inequality $\sigma_e < \sigma$ as in the case of linear hardening, i.e., 0.77×10^{-2}, the following estimations can be made. At crack speed $v/c_s = 0.3$, the elastic unloading angle is calculated to be, respectively, 76.9^0 and 72.4^0 for $n = 2$ and 10, from which we see the angle decreases as n increases. However, at $v/c_s = 0.4$, the angle is found to be, respectively, 82.3^0 and 85.9^0 for $n = 2$ and 10. That is, as n increases, the angle also increases, which confirms our earlier observation on this point (see Fig. 5.3.1b).

The effect of inertia or crack propagation speed on the angular stress variations

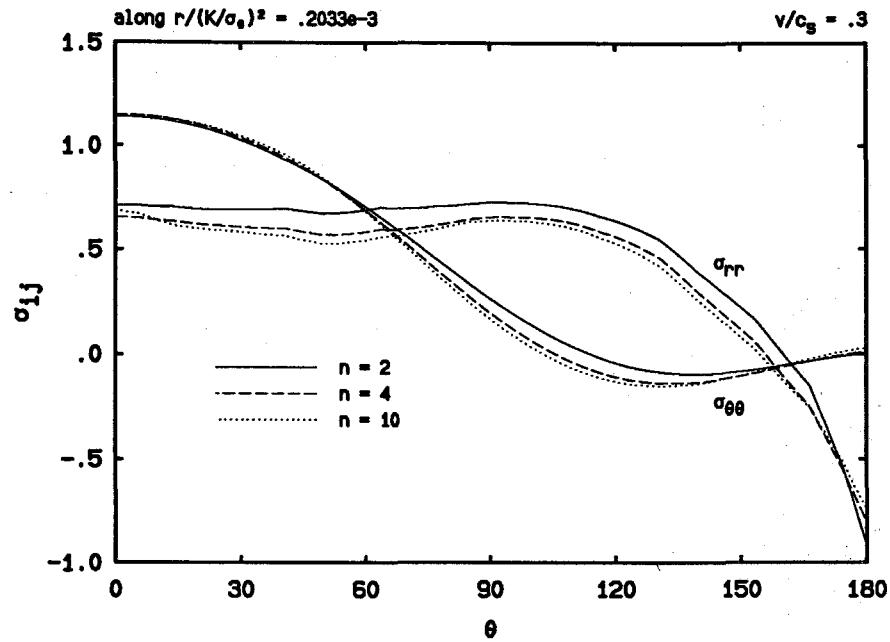

FIGURE 5.3.3a The effect of hardening on the angular variations of the polar stress components σ_{rr} and $\sigma_{\theta\theta}$ for $v/c_s = 0.3$, normalized such that the effective stress $\sigma_e = 1$ at $\theta = 0^0$.

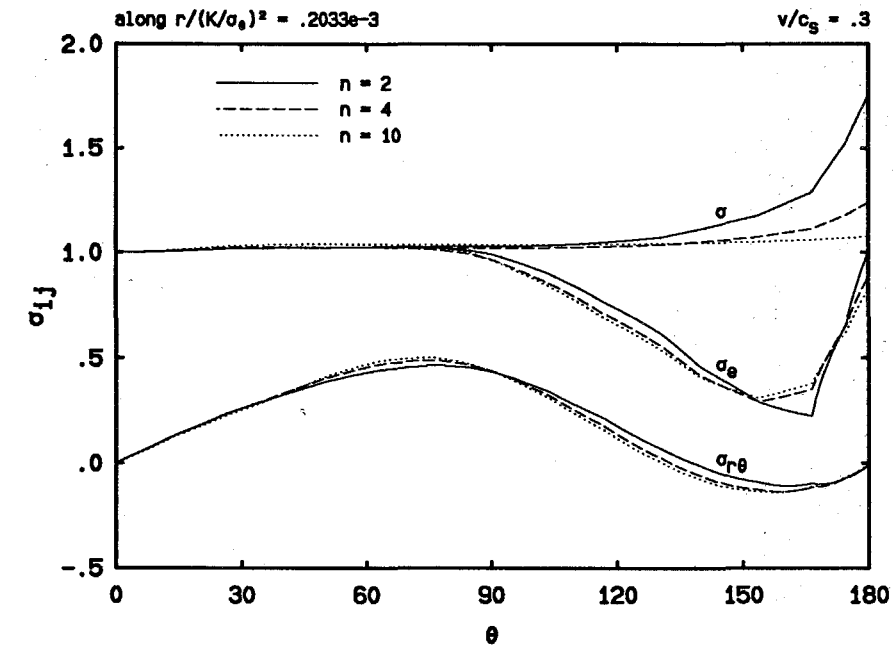

FIGURE 5.3.3b The effect of hardening on the angular variations of the polar stress component $\sigma_{r\theta}$, the effective stress σ_e and the flow stress σ for $v/c_s = 0.3$, normalized such that $\sigma_e = 1$ at $\theta = 0^0$.

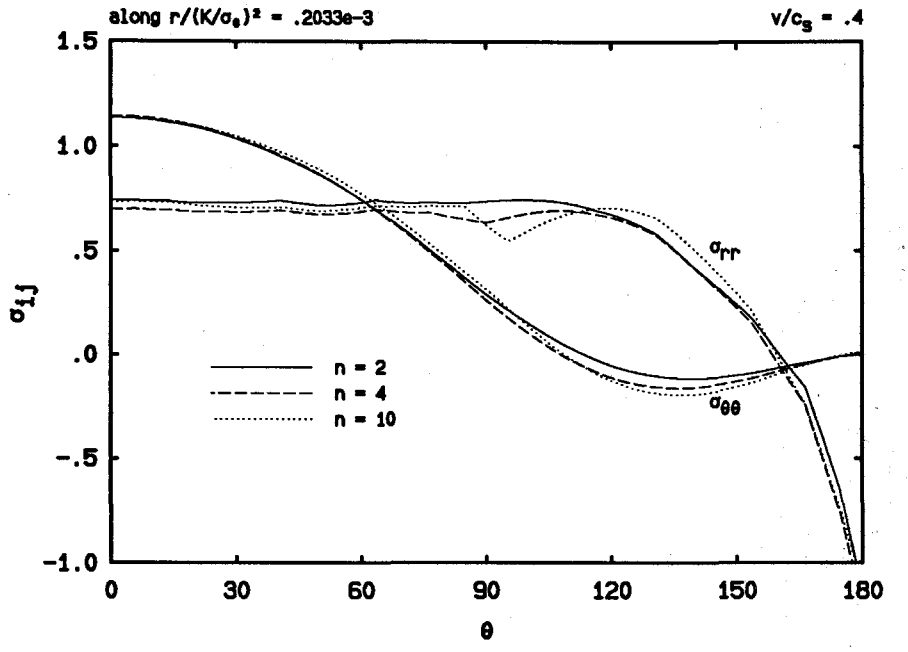

FIGURE 5.3.4a The effect of hardening on the angular variations of the polar stress components σ_{rr} and $\sigma_{\theta\theta}$ for $v/c_s = 0.4$, normalized such that the effective stress $\sigma_e = 1$ at $\theta = 0^0$.

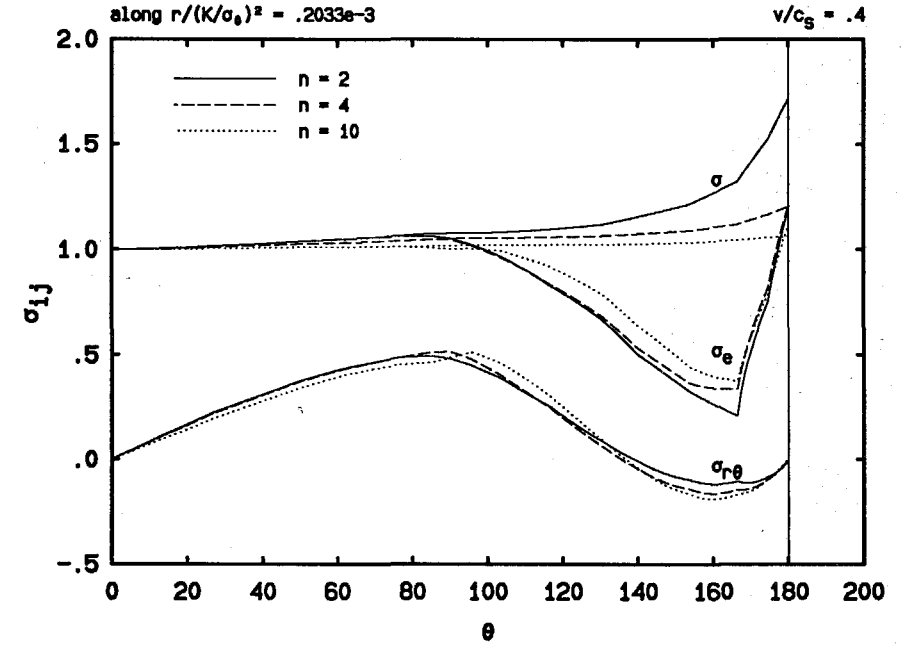

FIGURE 5.3.4b The effect of hardening on the angular variations of the polar stress component $\sigma_{r\theta}$, the effective stress σ_e and the flow stress σ for $v/c_s = 0.4$, normalized such that $\sigma_e = 1$ at $\theta = 0^0$.

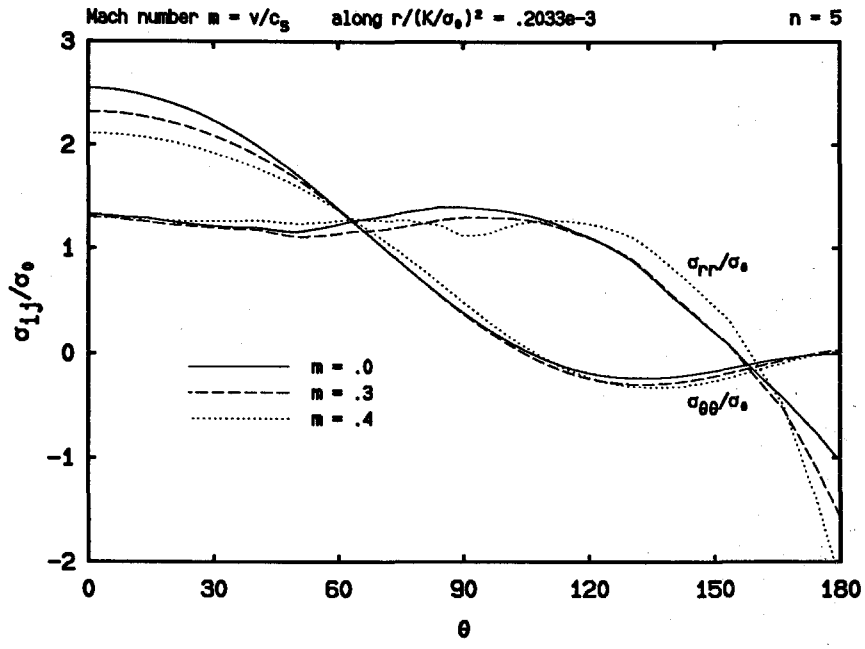

FIGURE 5.3.5a The effect of crack speed on the angular variations of the polar stress components σ_{rr} and $\sigma_{\theta\theta}$ for $n = 5$, normalized such that the effective stress $\sigma_e = 1$ at $\theta = 0^0$.

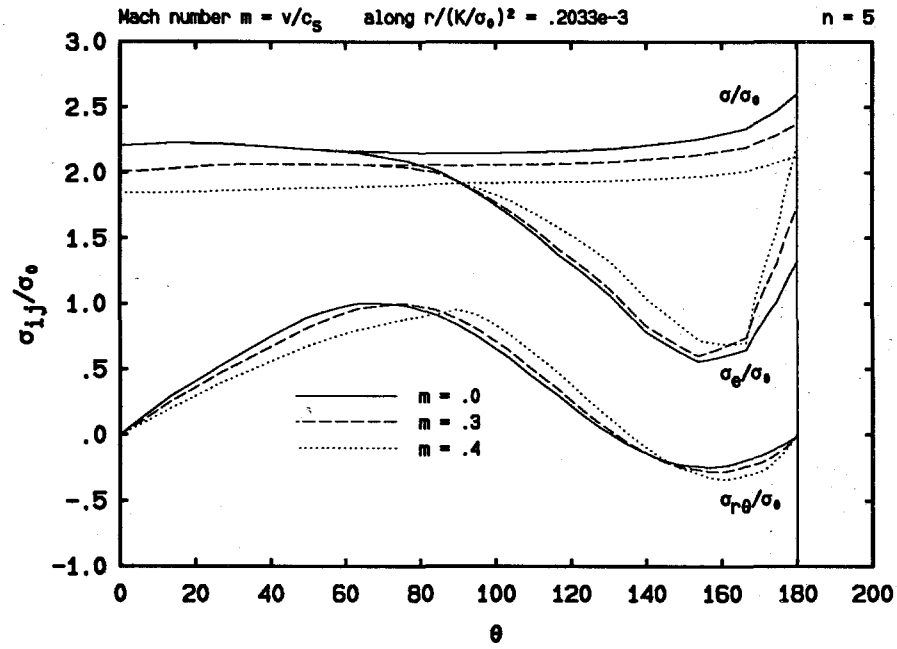

FIGURE 5.3.5b The effect of crack speed on the angular variations of the polar stress component $\sigma_{r\theta}$, the effective stress σ_e and the flow stress σ for $n = 5$, normalized such that $\sigma_e = 1$ at $\theta = 0^0$.

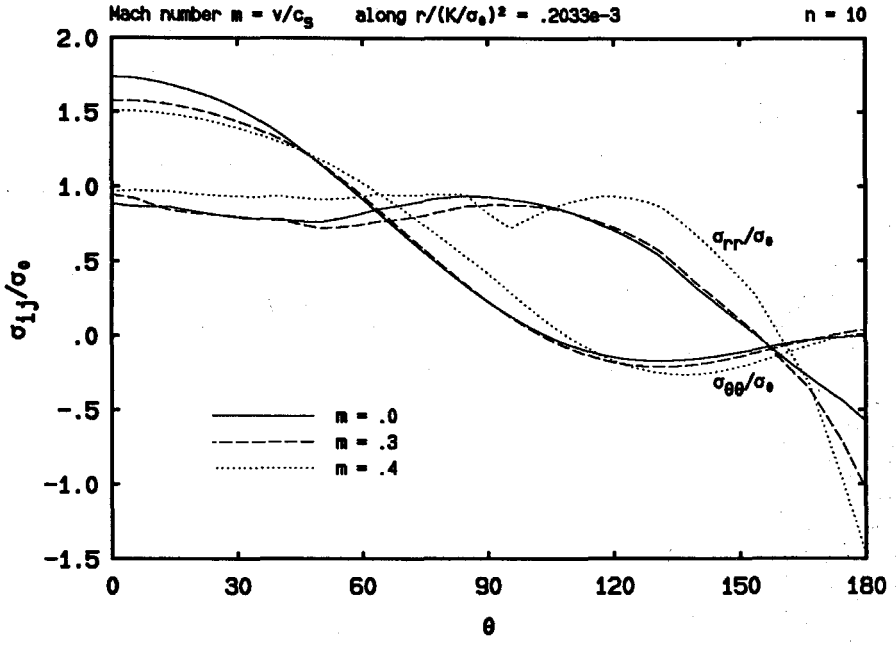

FIGURE 5.3.6a The effect of crack speed on the angular variations of the polar stress components σ_{rr} and $\sigma_{\theta\theta}$ for $n = 10$, normalized such that the effective stress $\sigma_e = 1$ at $\theta = 0^0$.

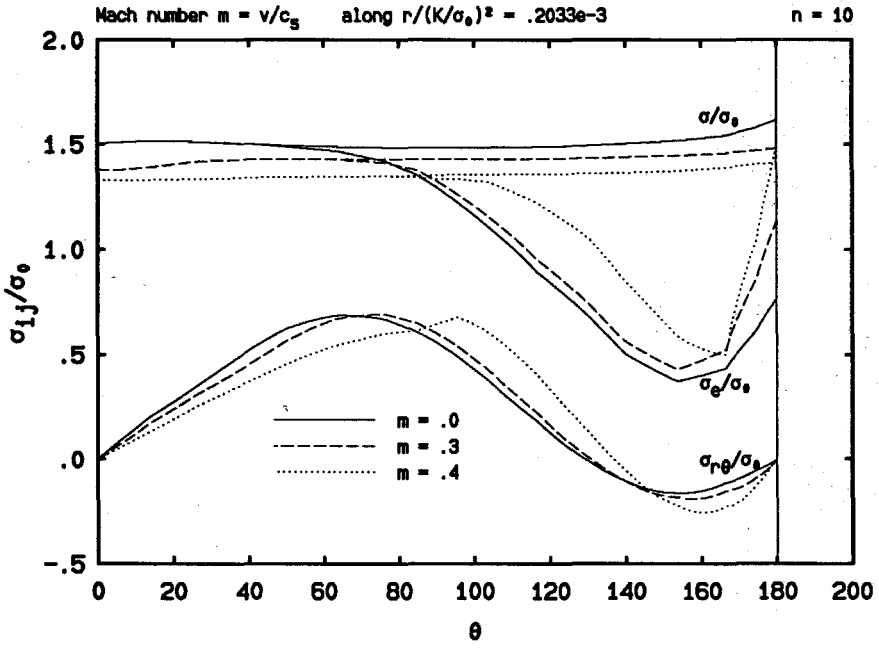

FIGURE 5.3.6b The effect of crack speed on the angular variations of the polar stress component $\sigma_{r\theta}$, the effective stress σ_e and the flow stress σ for $n = 10$, normalized such that $\sigma_e = 1$ at $\theta = 0^0$.

can be more clearly seen from Fig. 5.3.5 for $n = 5$ and Fig. 5.3.6 for $n = 10$. Note that all stress quantities are normalized by the initial yield stress σ_0. Hence, comparisons between magnitudes of stress quantities corresponding to different m values can be performed. For example, as m increases, σ is found to decrease for all θ values. At the same time, the magnitude of the compressive radial stress σ_{rr} near $\theta = 180^0$ also increases such that σ_e, at at $m = 0.4$, reaches the value of σ behind the crack tip, resulting in the observed reverse plastic loading.

The angular variations of the crack tip velocity field for various strain hardening levels and crack propagation speeds are illustrated in Fig. 5.3.7 with normalizations such that $v_1 = -1$ at $\theta = 0^0$, and in Fig. 5.3.8 with the standard normalization so that the magnitudes of the velocity components at different crack speeds can be compared.

At the crack speed $v/c_s = 0.3$ (see Fig. 5.3.7a), it is seen that the variations of the Cartesian velocity components are very much the same as in the case of quasi-static crack growth (see Fig. 4.2.5). Yet at $v/c_s = 0.4$ when dynamic effect is expected to be stronger, it is obsesrved that the angular variations show very different features (see Fig. 5.3.7b). For example, the transition of the curve for the v_2 component from the actively yielded plastic zone, where its slope is positive, to the elastic unloading zone, where its slope is closer to zero or slightly negative, becomes more abrupt or better defined. This behavior is more clearly demonstrated in Figs. 5.3.8a and 5.3.8b for $n = 5$ and 10, respectively.

Nevertheless, the following observations can be made for all cases studied. First of all, throughout the angular range, v_2 stays positive while v_1 stays negative. Secondly, the velocity curves tend to rise up in the angular range corresponding to the active plastic zone, and they tend to flatten out in the angular range corresponding to the elastic unloading zone. Thirdly, as n and v/c_s increase, both the slopes of the velocity curves tend to become zero. Finally, the magnitude of v_2 is about three

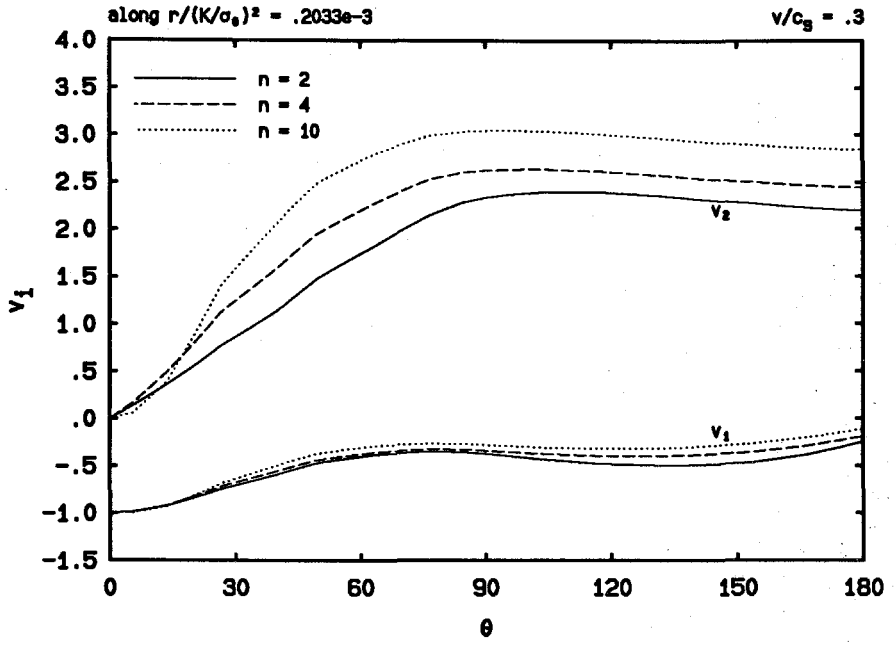

FIGURE 5.3.7a The effect of hardening on the angular variations of the Cartesian velocity components for $v/c_s = 0.3$, normalized such that $v_1 = -1$ at $\theta = 0^0$.

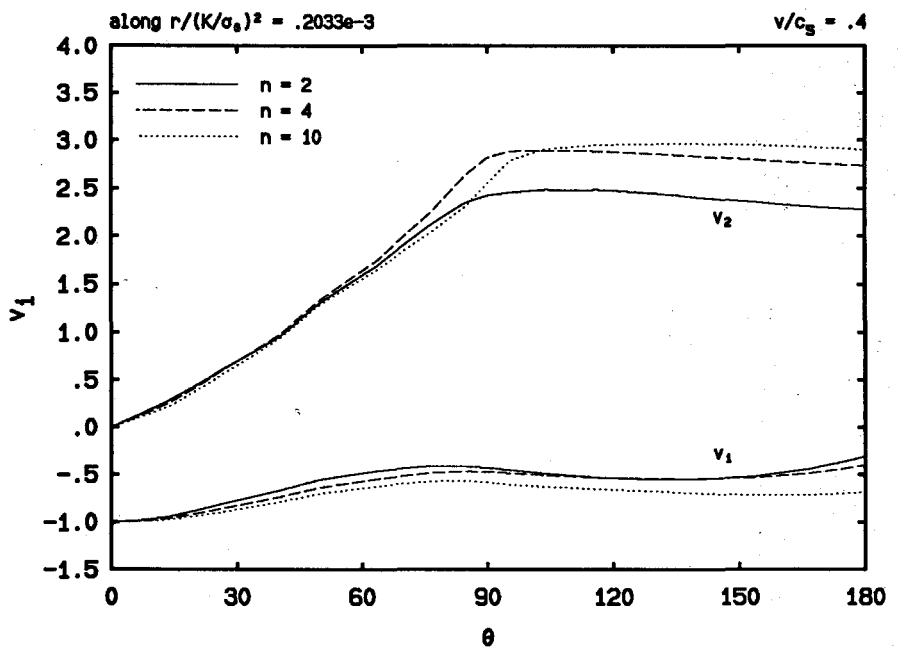

FIGURE 5.3.7b The effect of hardening on the angular variations of the Cartesian velocity components for $v/c_s = 0.4$, normalized such that $v_1 = -1$ at $\theta = 0^0$.

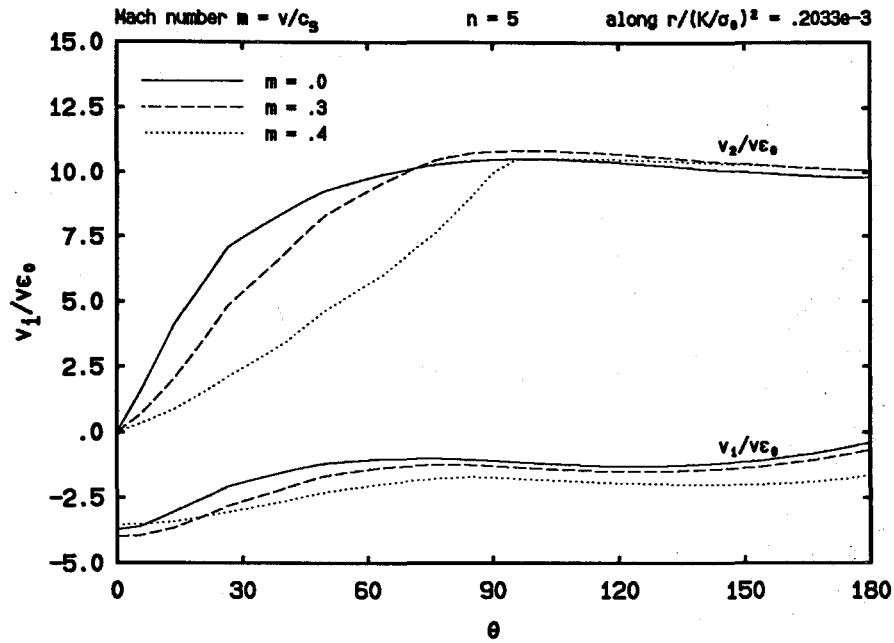

FIGURE 5.3.8a The crack speed dependence of the angular variations of the Cartesian velocity components for $n = 5$, normalized such that $v_1 = -1$ at $\theta = 0^0$.

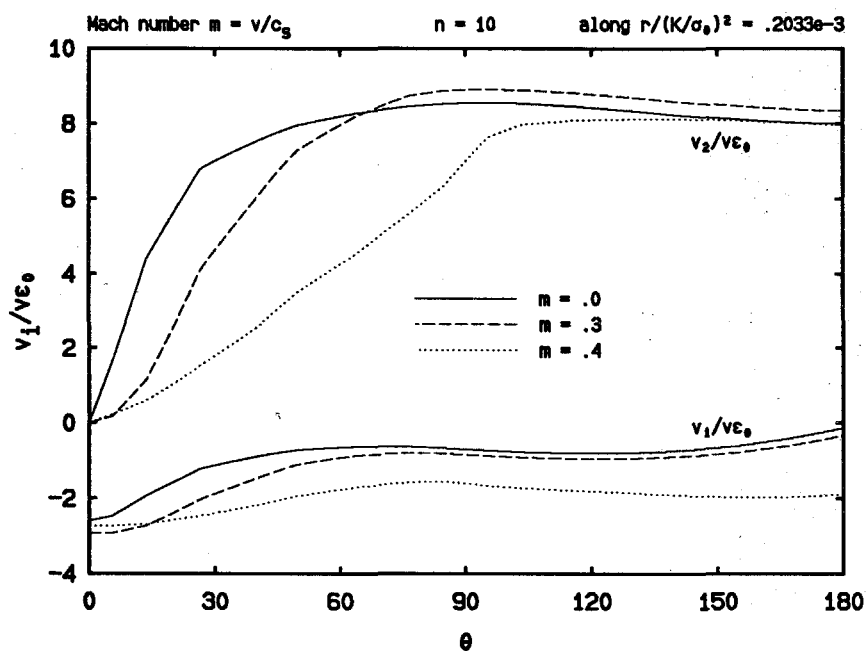

FIGURE 5.3.8b The crack speed dependence of the angular variations of the Cartesian velocity components for $n = 10$, normalized such that $v_1 = -1$ at $\theta = 0^0$.

times larger than that of v_1 most of the time.

Radial Field Variations

The effect of hardening on the radial variations of the stress field along the prospective crack line is illustrated in Fig. 5.3.9 for $v/c_s = 0.3$ and in Fig. 5.3.11 for $v/c_s = 0.4$. It can be seen that, as n increases or as the level of hardening decreases, the magnitudes of σ_{11} and σ_{22} decrease. Moreover, as r approaches zero, where r is the radial distance to the crack tip, the stresses are found to rise rapidly. These observations strongly indicate that the stresses are singular at the crack tip, yet the singularity decreases as n increases. In fact, when the stress variations are plotted in special logarithmic coordinates, as shown in Figs. 5.3.10 and 5.3.12, the stress curves appear to be straight lines. This suggests that the crack tip stress singularities are of the type $[ln(R_0/r)]^s$ $(s > 0)$, where R_0 is a length scaling parameter.

It is worth pointing out again that any asymptotic expression at $r = 0$ with leading singularity term of the type $[ln(R_0/r)]^s$ is ill-conditioned. This comes from the fact that when r approaches zero, the choice of R_0 is in fact not unique or it can be any length scale. To state it more precisely, for any given length scale R, a range for r near zero can be found such that the leading singularity in the asymptotic expression can be changed from $[ln(R_0/r)]^s$ to $[ln(R/r)]^s$. This ill-conditioning may result in complicated and confusing numerical problems.

For example, in Figs. 5.3.10 and 5.3.12, r is normalized by $(K/\sigma_0)^2$ which may not be the right length scaling parameter. If the scaling parameter R_0 corresponding to the correct singularity power s for the range of numerical data being processed is very different from the one we used, we would then observe curved lines, although the curved lines resulted from such a bad choice of length scaling do not change the fact that the singularity is still given by $[ln(R_0/r)]^s$.

Furthermore, as briefly mentioned in the case of quasi-static crack growth, if we have a set of data representing a behavior of the form $[ln(R_0/r)]^s$ and try to estimate s or the slope of the straight line in special logarithmic coordinates (see, for example, Fig. 5.3.10b), we will find that the slope will strongly depend on the choice of R_0 if the range of r for the set of data is not close enough to zero such that the effect of R_0 can be neglected.

More features of the radial variations of stress components at the crack front can be discovered by examing their dependence on the crack propagation speed. At $n = 5$, it can be seen from Fig. 5.3.13, that very close to the crack tip the magnitudes of σ_{11} and σ_{22} both decrease as m increases. Whereas at $n = 10$, the magnitude of the stress component σ_{11} increases as m increases, which resembles the feature found in the case of ideal plasticity (see Fig.3.3.5b).

Some inconsistent behaviors of the stress component σ_{11} can be observed from Fig. 5.3.14a and especially from Fig. 5.3.16a, where it is seen that the stress lines are curved for $n = 5$ (although slightly), and particularly for $n = 10$ at $m = 0.3$ and 0.4. There are several possibilities for these unusual behaviors. Besides numerical errors occurring in the finite element computation, they may be due to the normalization we used, which, for the range of distance to the crack tip, may not correctly represent the leading asymptotic term as discussed earlier. There may also be a lack of enough dominance zone near the crack tip.

Shown in Figs. 5.3.17 through 5.3.20 are the variations of the plastic strain components along the prospective crack line for some typical values of the power hardening parameter n.

First of all, as in the case of radial stress variations, it can be generally observed that the magnitudes of the plastic strain components rise up rapidly as the distance to the crack tip approaches zero, which suggests the existence of strain singularities at the crack tip. Further, the straight lines shown in the special logarithmic

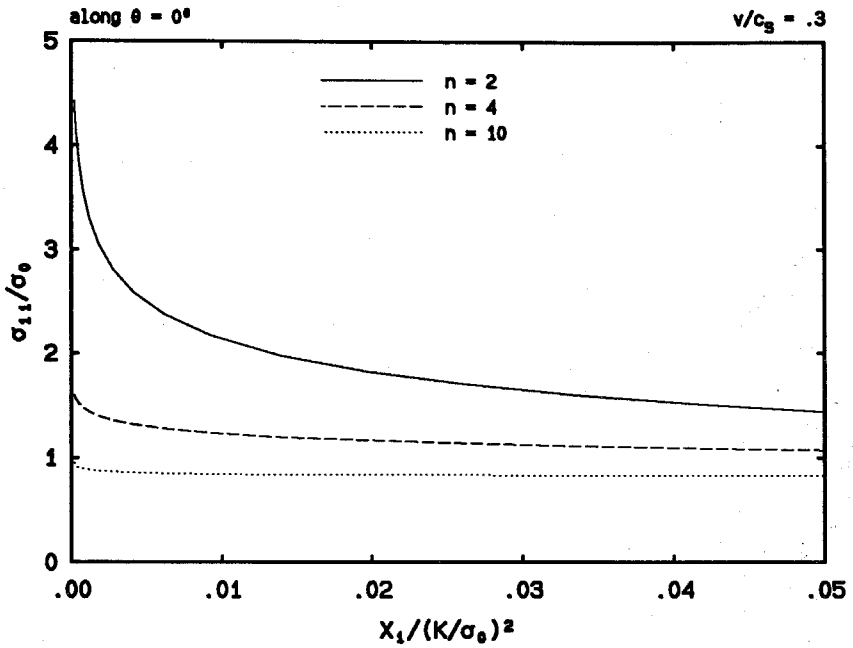

FIGURE 5.3.9a The radial variations of the stress component σ_{11} for $v/c_s = 0.3$, along the prospective crack line in the normalized coordinates.

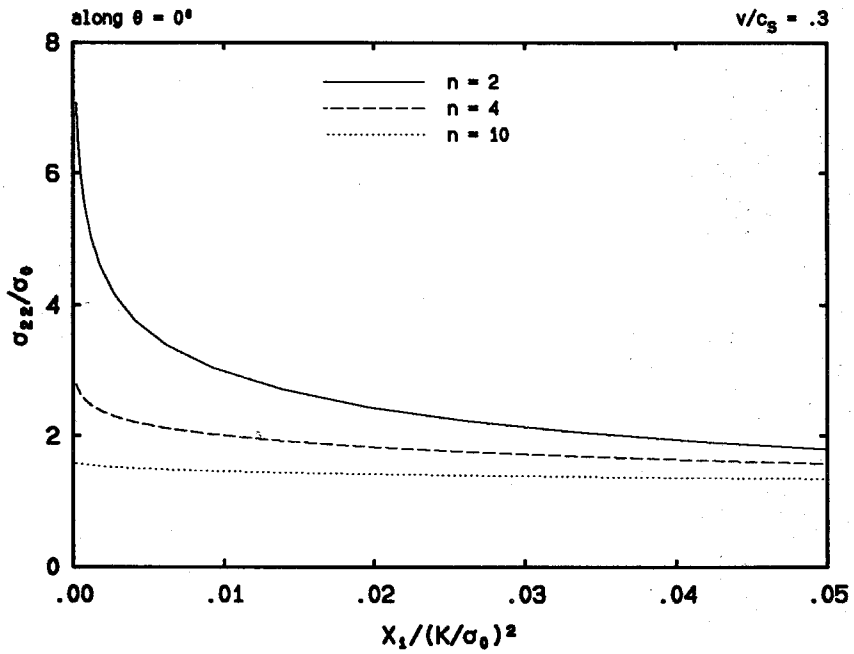

FIGURE 5.3.9b The radial variations of the stress component σ_{22} for $v/c_s = 0.3$, along the prospective crack line in the normalized coordinates.

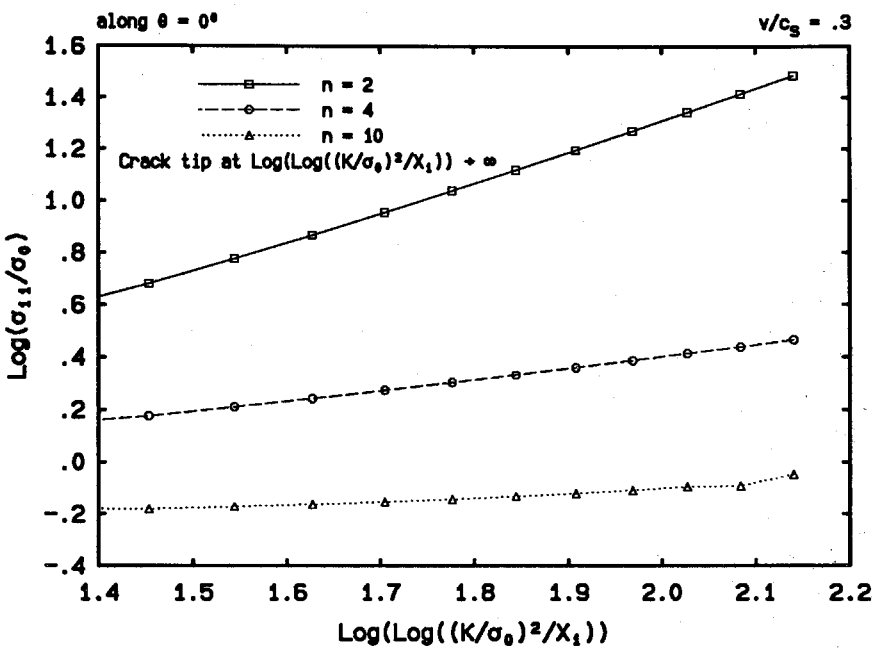

FIGURE 5.3.10a The radial variations of the stress component σ_{11} for $v/c_s = 0.3$, along the prospective crack line in special logarithmic coordinates.

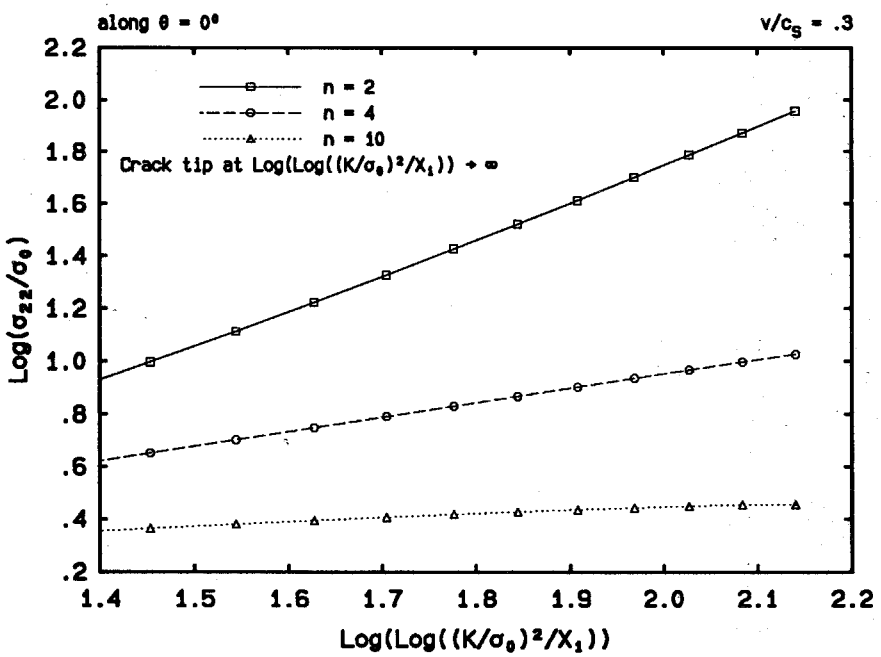

FIGURE 5.3.10b The radial variations of the stress component σ_{22} for $v/c_s = 0.3$, along the prospective crack line in special logarithmic coordinates.

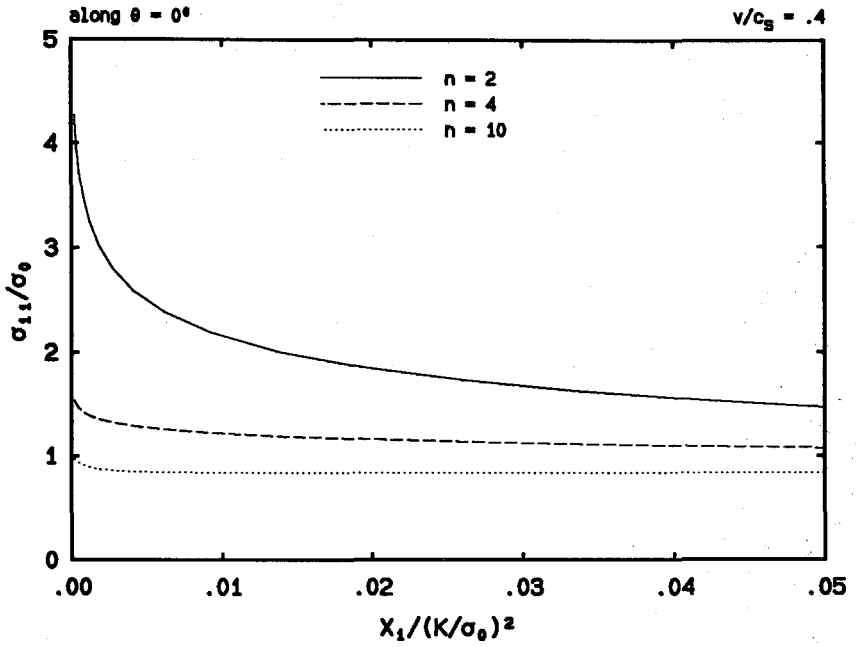

FIGURE 5.3.11a The radial variations of the stress component σ_{11} for $v/c_s = 0.4$, along the prospective crack line in the normalized coordinates.

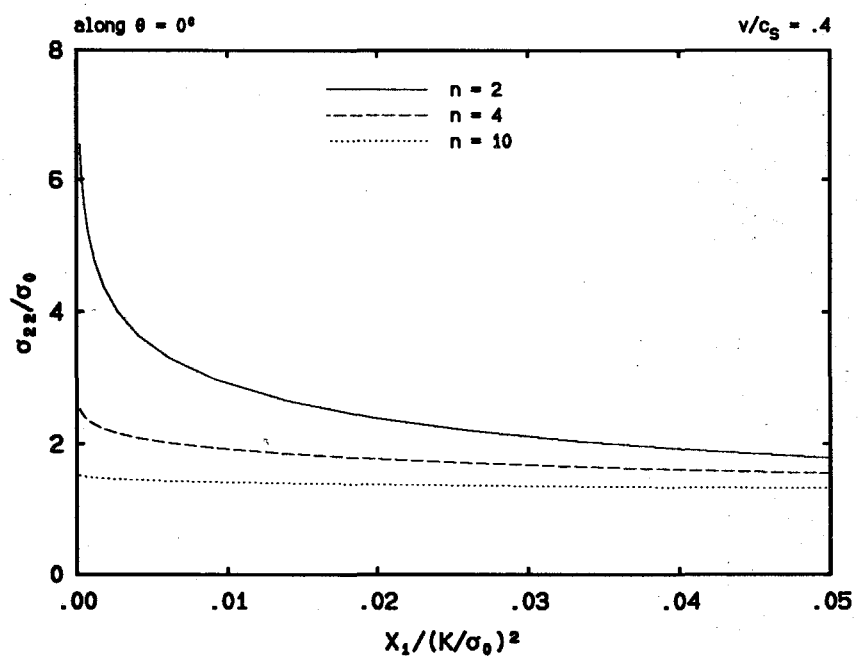

FIGURE 5.3.11b The radial variations of the stress component σ_{22} for $v/c_s = 0.4$, along the prospective crack line in the normalized coordinates.

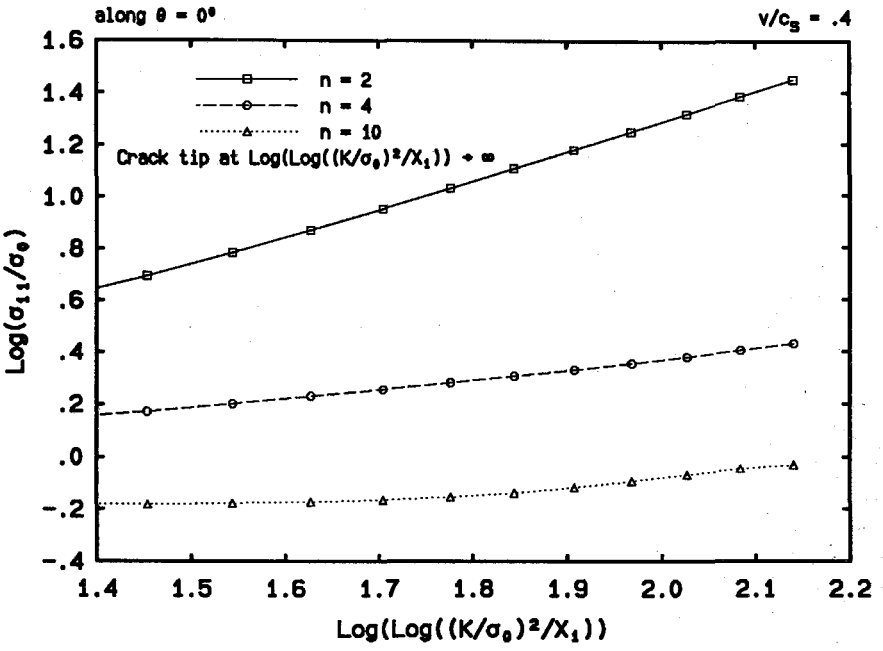

FIGURE 5.3.12a The radial variations of the stress component σ_{11} for $v/c_s = 0.4$, along the prospective crack line in special logarithmic coordinates.

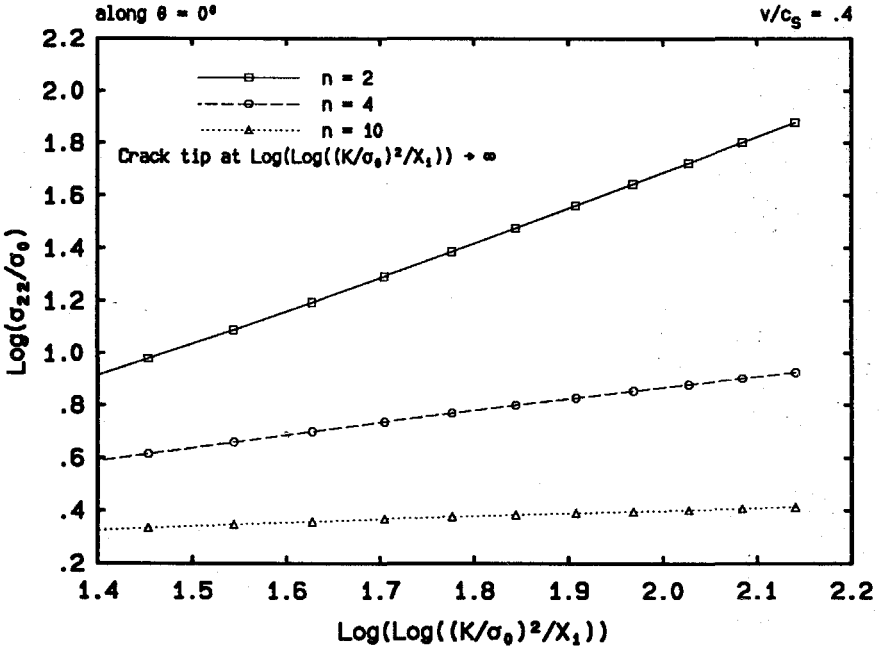

FIGURE 5.3.12b The radial variations of the stress component σ_{22} for $v/c_s = 0.4$, along the prospective crack line in special logarithmic coordinates.

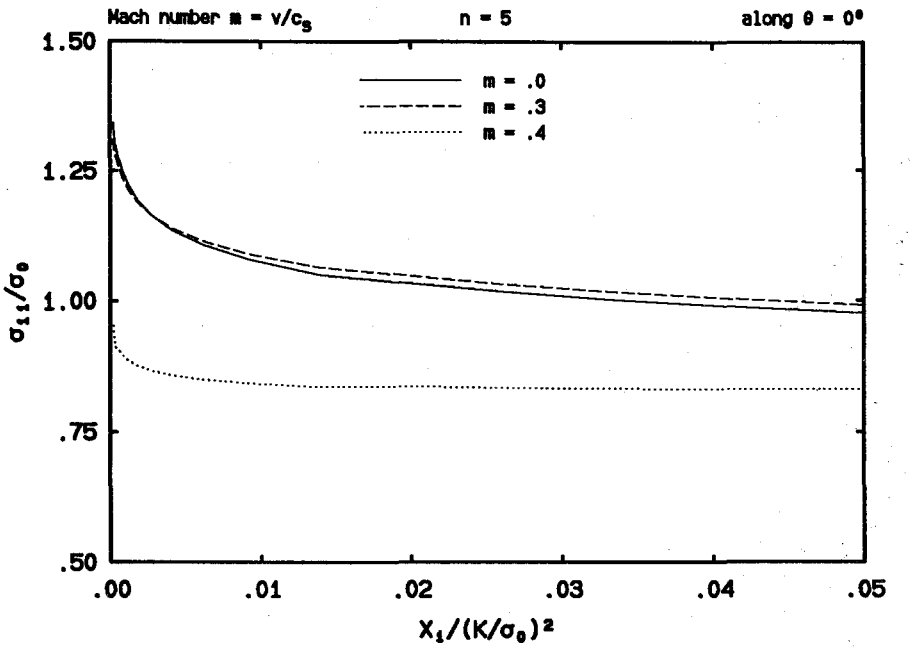

FIGURE 5.3.13a The radial variations of the stress component σ_{11} for $n = 5$, along the prospective crack line in the normalized coordinates.

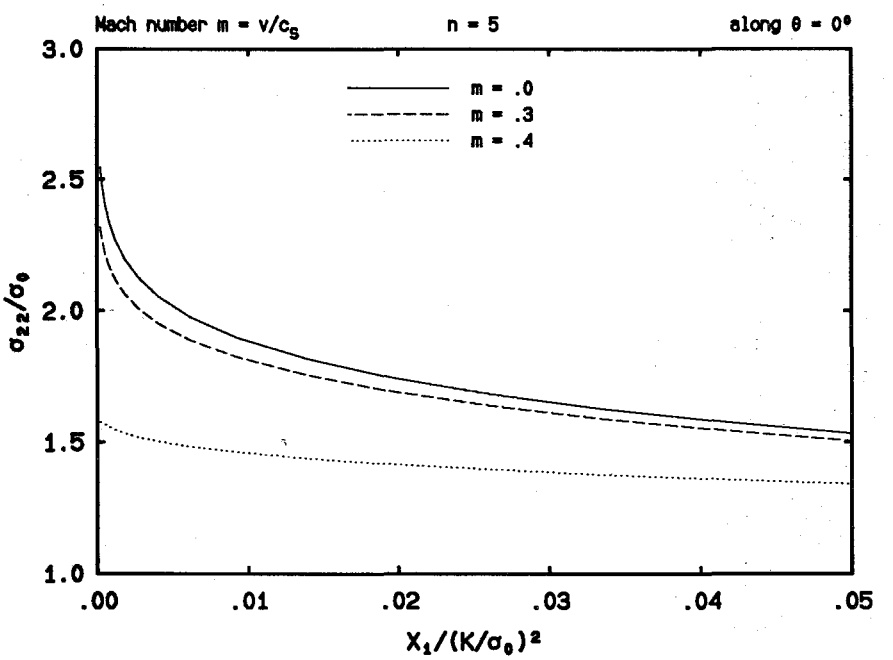

FIGURE 5.3.13b The radial variations of the stress component σ_{22} for $n = 5$, along the prospective crack line in the normalized coordinates.

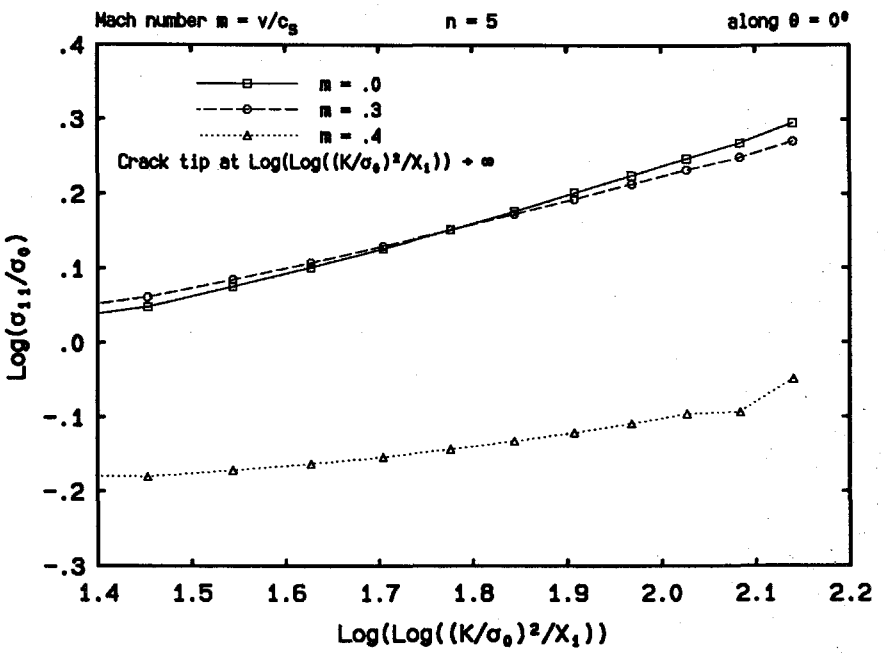

FIGURE 5.3.14a The radial variations of the stress component σ_{11} for $n = 5$, along the prospective crack line in special logarithmic coordinates.

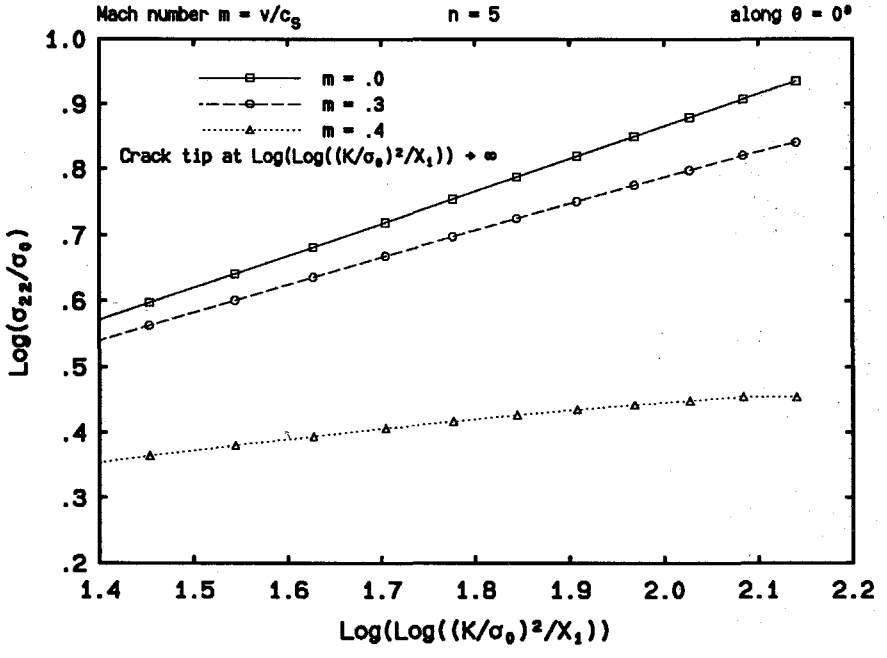

FIGURE 5.3.14b The radial variations of the stress component σ_{22} for $n = 5$, along the prospective crack line in special logarithmic coordinates.

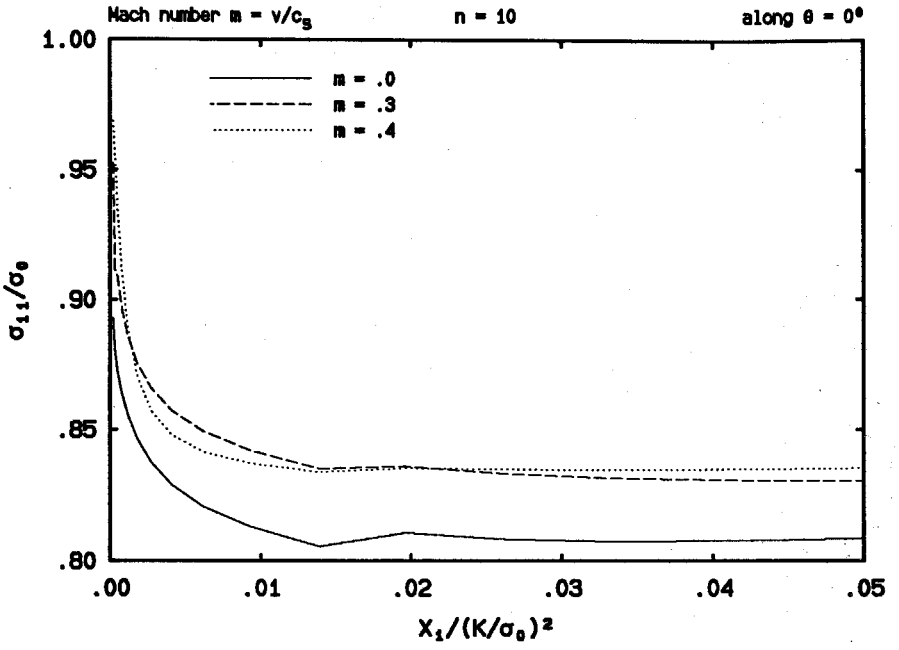

FIGURE 5.3.15a The radial variations of the stress component σ_{11} for $n = 10$, along the prospective crack line in the normalized coordinates.

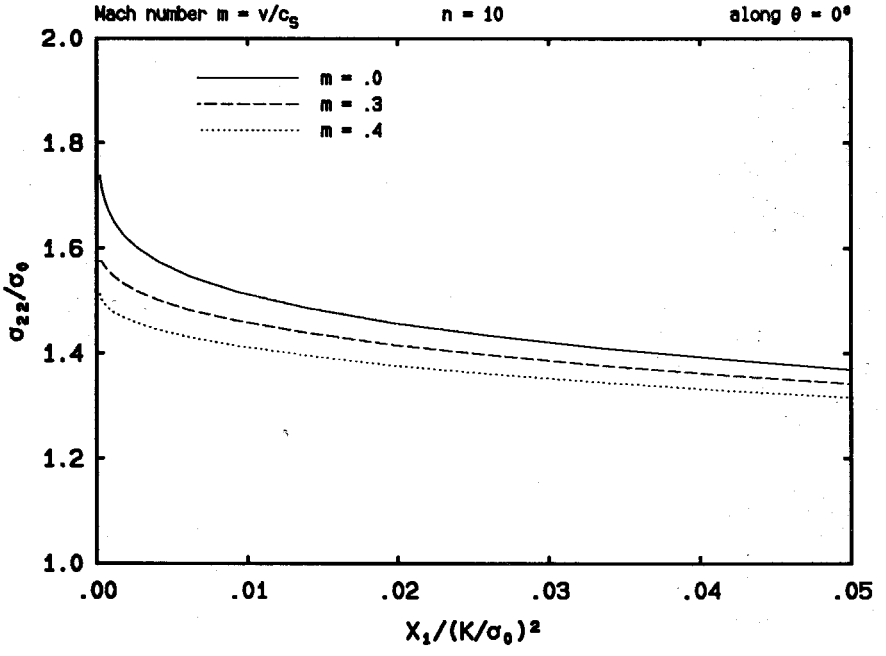

FIGURE 5.3.15b The radial variations of the stress component σ_{22} for $n = 10$, along the prospective crack line in the normalized coordinates.

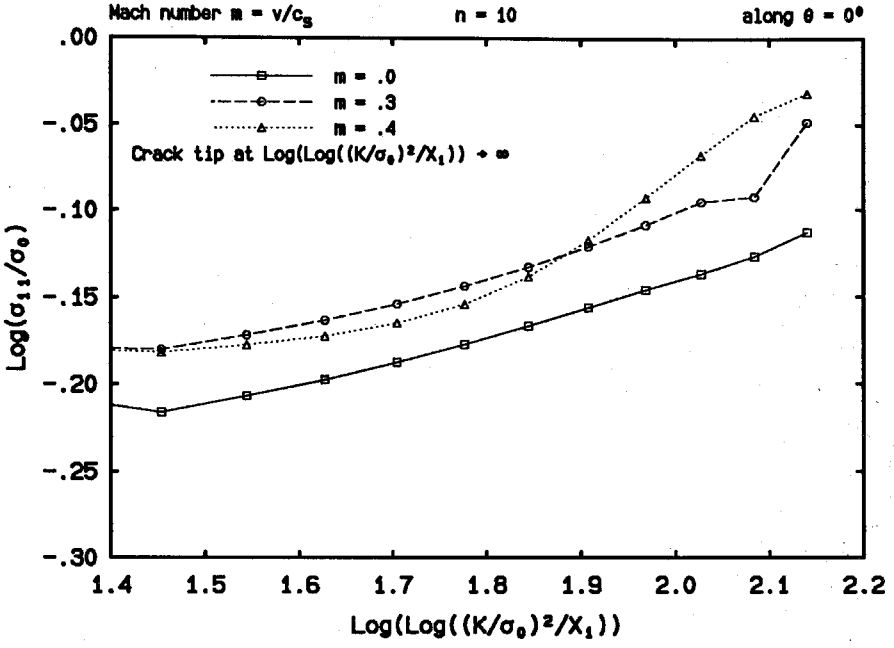

FIGURE 5.3.16a The radial variations of the stress component σ_{11} for $n = 10$, along the prospective crack line in special logarithmic coordinates.

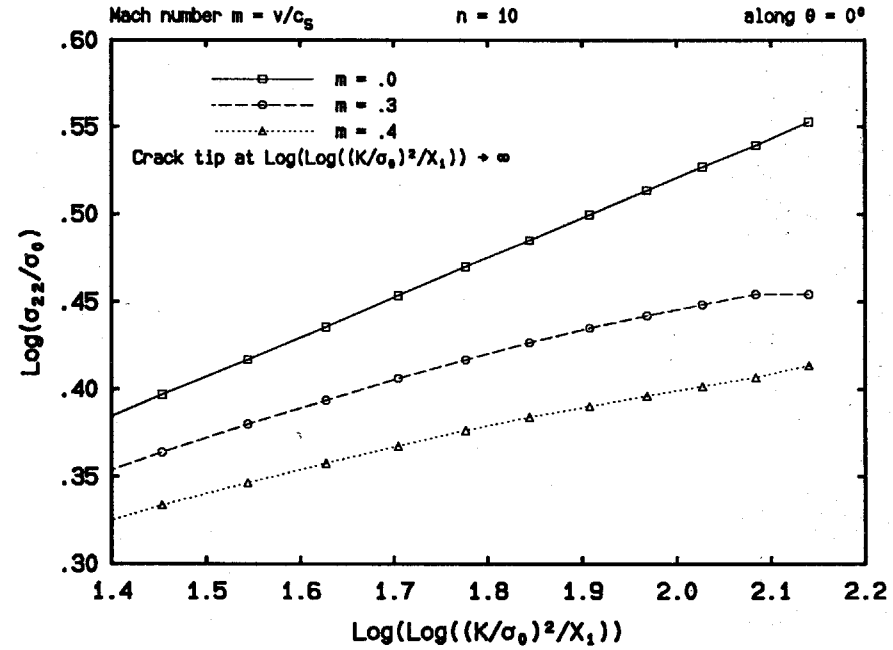

FIGURE 5.3.16b The radial variations of the stress component σ_{22} for $n = 10$, along the prospective crack line in special logarithmic coordinates.

coordinates in Figs. 5.3.18 and 5.3.20 strongly indicate that the plastic strains have the same type of singularities as the stresses. That is, as $r \to 0$, the plastic strains behave as $[ln(R_0/r)]^s$ $(s > 0)$, where r is the distance to the crack tip and R_0 is a length scaling parameter.

Moreover, it is consistently seen that, for the same values of the hardening parameter n and the normalized crack propagation velocity v/c_s, the magnitude of the plastic strain component ε^p_{22} is always much larger than that of the strain component ε^p_{11}, especially at lower v/c_s values.

From the tendencies demonstrated in the figures, especially those plotted in special logarithmic coordinates, it can be seen that at locations very close to the crack tip, the magnitudes of both ε^p_{11} and ε^p_{22} tend to decrease as n increases. Whereas further away from the crack tip, the opposite is observed.

As discussed earlier, a first-order asymptotic analysis for steady state dynamic crack propagation in Mode I plane stress has been given by Zhang and Gao (1988). Using series expansions, they were indeed able to obtain a solution with stress and strain singularities of the type indicated by our full field numerical solution, namely $[ln(R_0/r)]^s$ $(s > 0)$. They have also explicitly given the value of s in terms of the power hardening parameter n, which is $1/(n-1)$ for all stress components and $n/(n-1)$ for all strain components. Note that the length scaling parameter R_0 is not obtainable from an asymptotic analysis. In fact, as we argued earlier, the choice for R_0 is not unique. Unfortunately, for the same reason, it seems that one cannot determine the values of R_0 and s from numerical fitting, since to do so would require that any numerical or experimental data be obtained at distances arbitrarily close to the crack tip, which in reality is not feasible.

The effect of crack propagation speed on the plastic strain field will be discussed below. For all cases investigated, it was discovered that as m or v/c_s increases, the magnitude of ε^p_{22} is seen to decrease (see Figs. 5.3.21b through 5.3.24b). Whereas

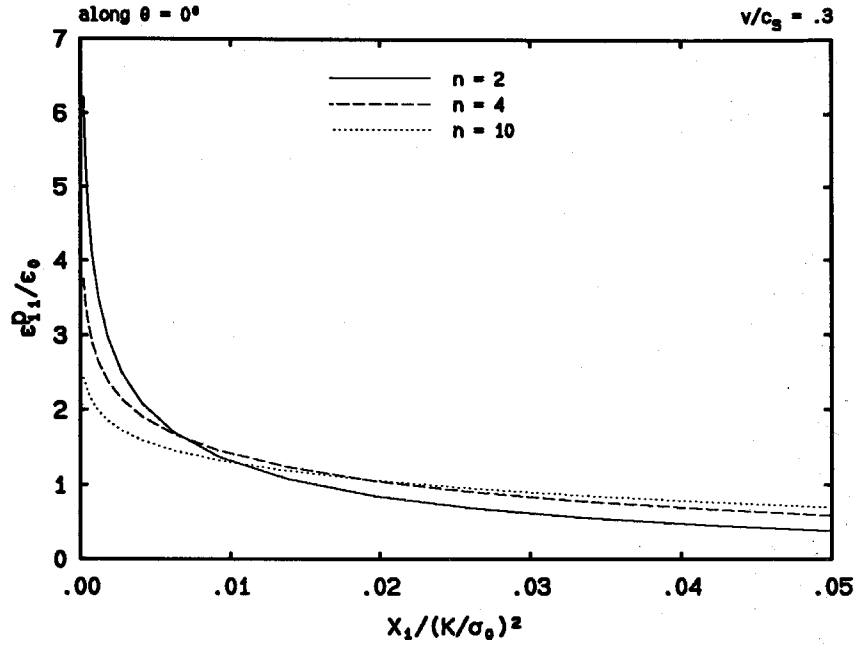

FIGURE 5.3.17a The radial variations of the plastic strain component ε_{11}^p for $v/c_s = 0.3$, along the prospective crack line in the normalized coordinates.

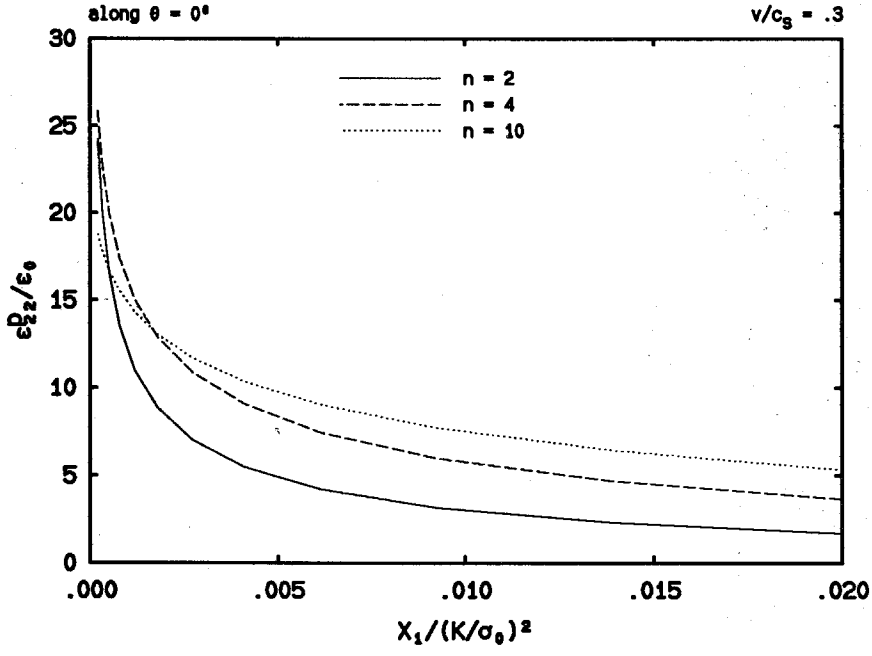

FIGURE 5.3.17b The radial variations of the plastic strain component ε_{22}^p for $v/c_s = 0.3$, along the prospective crack line in the normalized coordinates.

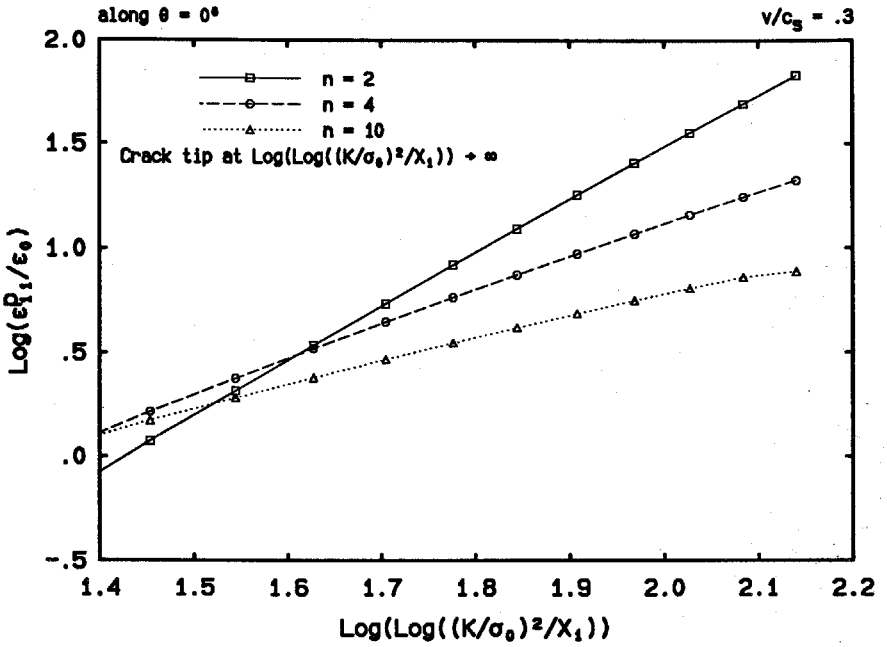

FIGURE 5.3.18a The radial variations of the plastic strain component ε_{11}^p for $v/c_s = 0.3$, along the prospective crack line in special logarithmic coordinates.

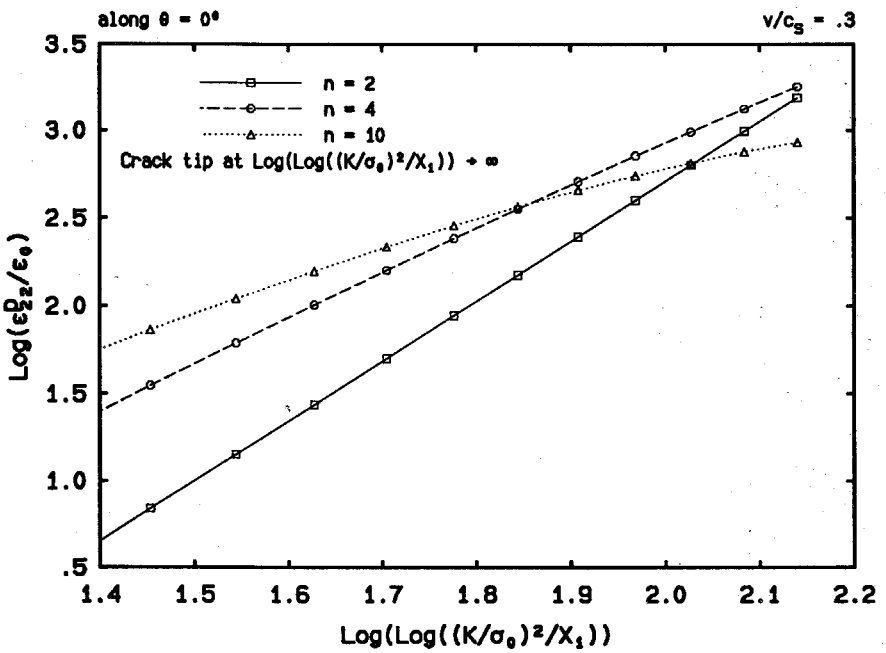

FIGURE 5.3.18b The radial variations of the plastic strain component ε_{22}^p for $v/c_s = 0.3$, along the prospective crack line in special logarithmic coordinates.

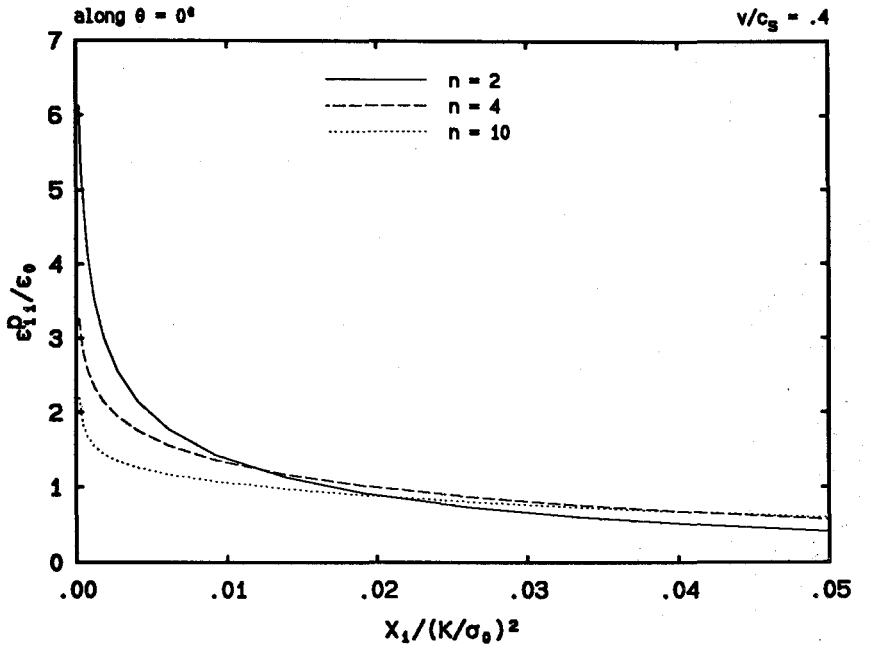

FIGURE 5.3.19a The radial variations of the plastic strain component ε_{11}^p for $v/c_s = 0.4$, along the prospective crack line in the normalized coordinates.

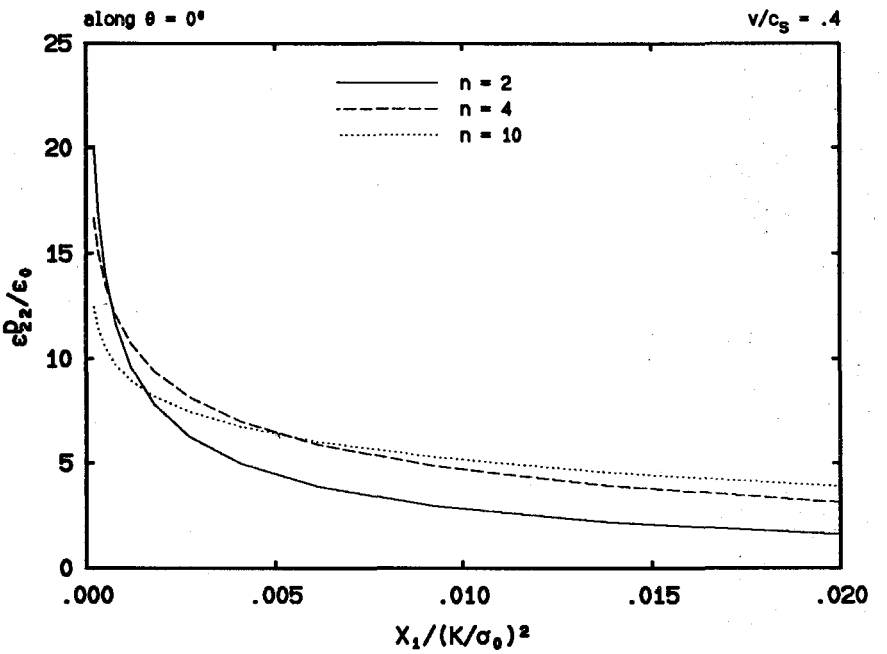

FIGURE 5.3.19b The radial variations of the plastic strain component ε_{22}^p for $v/c_s = 0.4$, along the prospective crack line in the normalized coordinates.

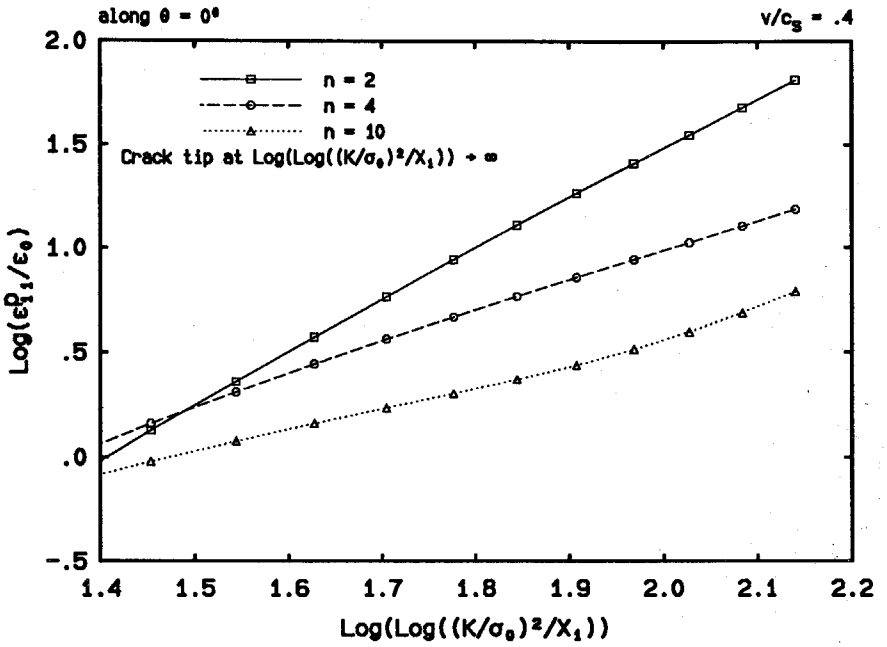

FIGURE 5.3.20a The radial variations of the plastic strain component ε_{11}^p for $v/c_s = 0.4$, along the prospective crack line in special logarithmic coordinates.

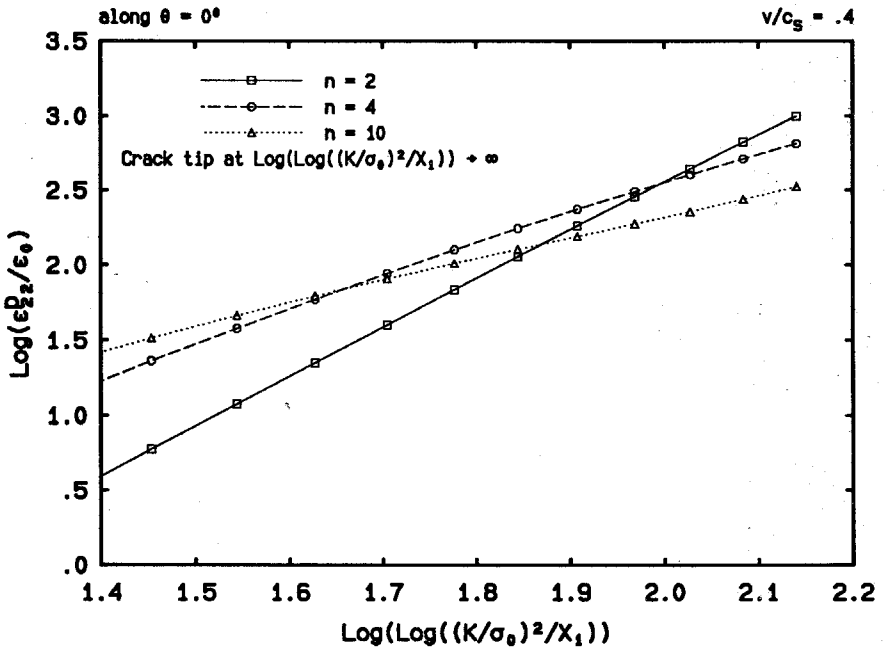

FIGURE 5.3.20b The radial variations of the plastic strain component ε_{22}^p for $v/c_s = 0.4$, along the prospective crack line in special logarithmic coordinates.

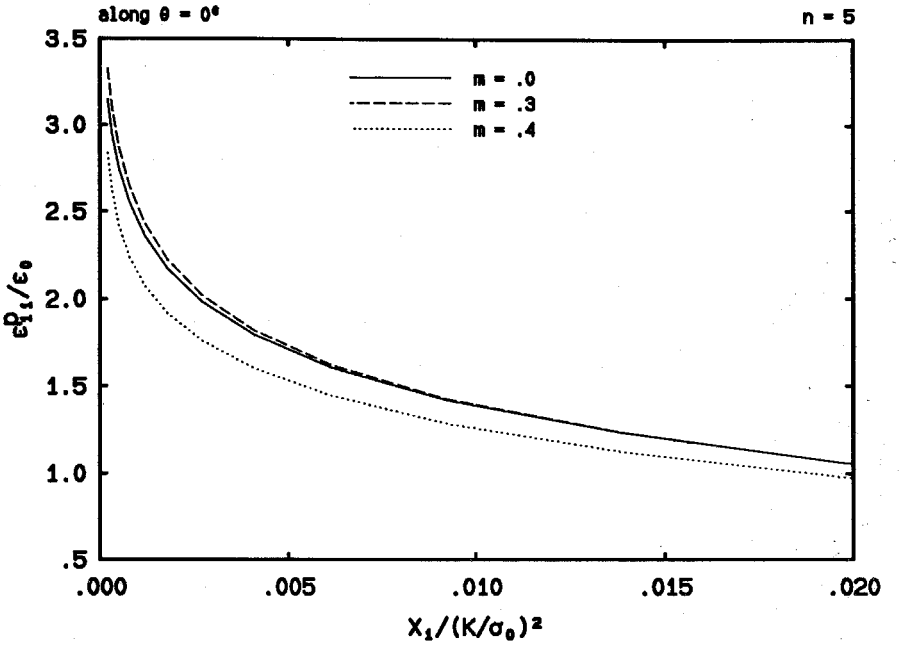

FIGURE 5.3.21a The radial variations of the plastic strain component ε^p_{11} for $n = 5$, along the prospective crack line in the normalized coordinates.

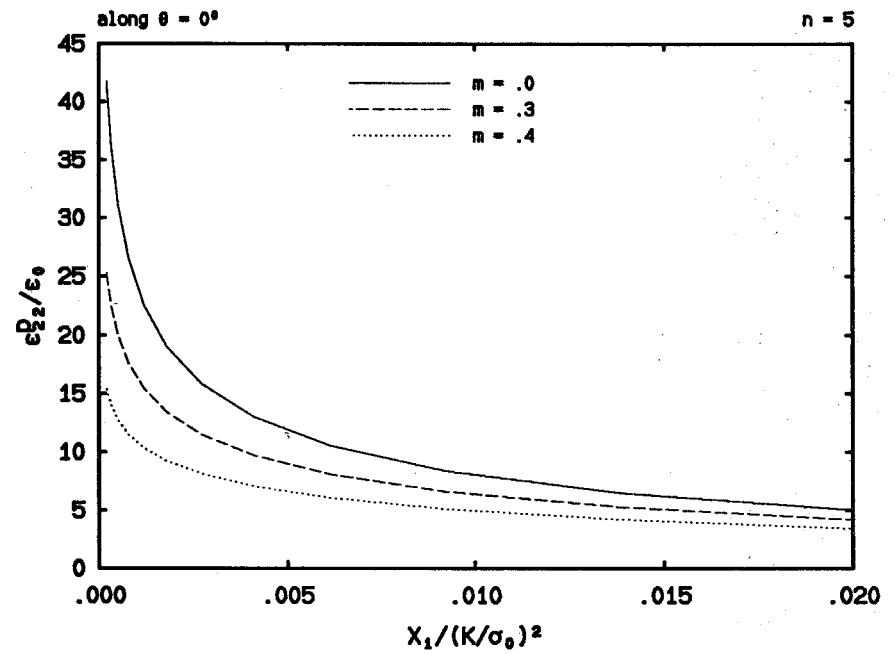

FIGURE 5.3.21b The radial variations of the plastic strain component ε^p_{22} for $n = 5$, along the prospective crack line in the normalized coordinates.

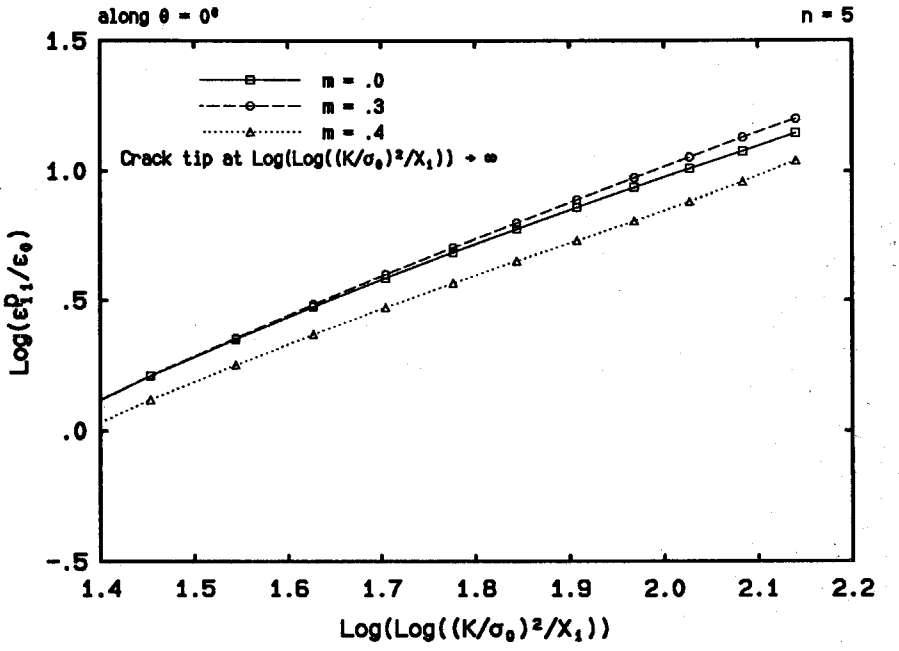

FIGURE 5.3.22a The radial variations of the plastic strain component ε_{11}^p for $n = 5$, along the prospective crack line in special logarithmic coordinates.

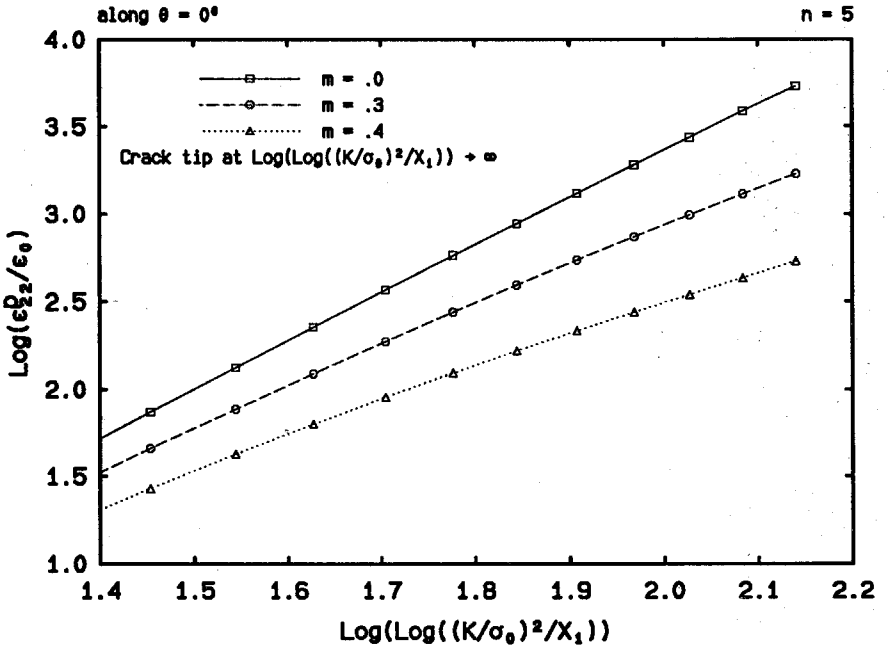

FIGURE 5.3.22b The radial variations of the plastic strain component ε_{22}^p for $n = 5$, along the prospective crack line in special logarithmic coordinates.

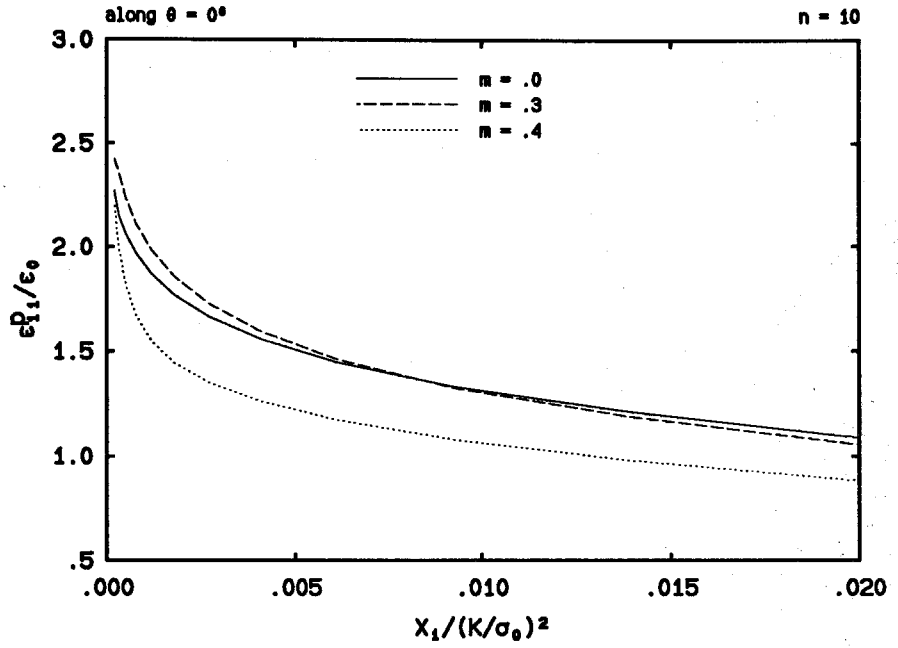

FIGURE 5.3.23a The radial variations of the plastic strain component ε^p_{11} for $n = 10$, along the prospective crack line in the normalized coordinates.

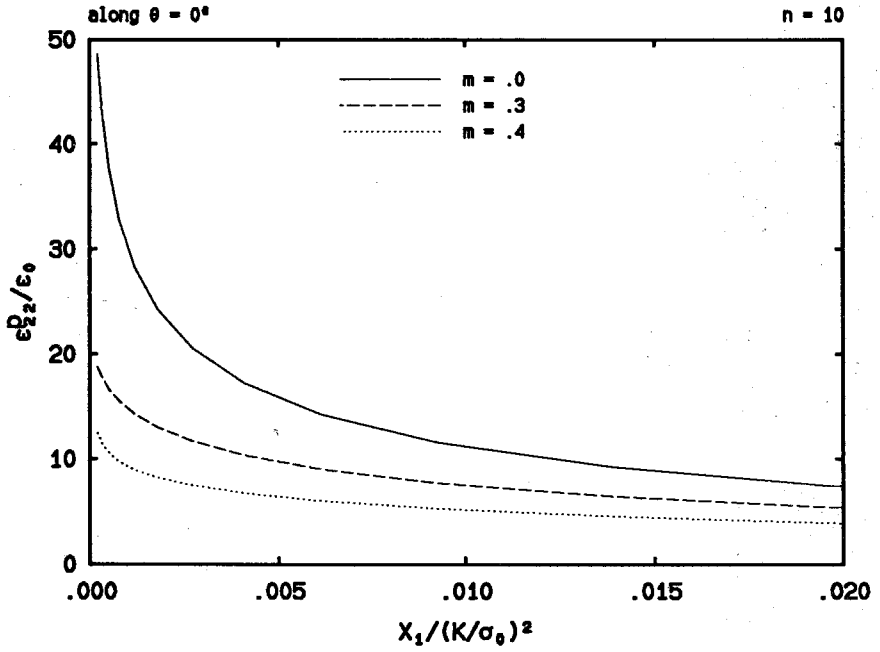

FIGURE 5.3.23b The radial variations of the plastic strain component ε^p_{22} for $n = 10$, along the prospective crack line in the normalized coordinates.

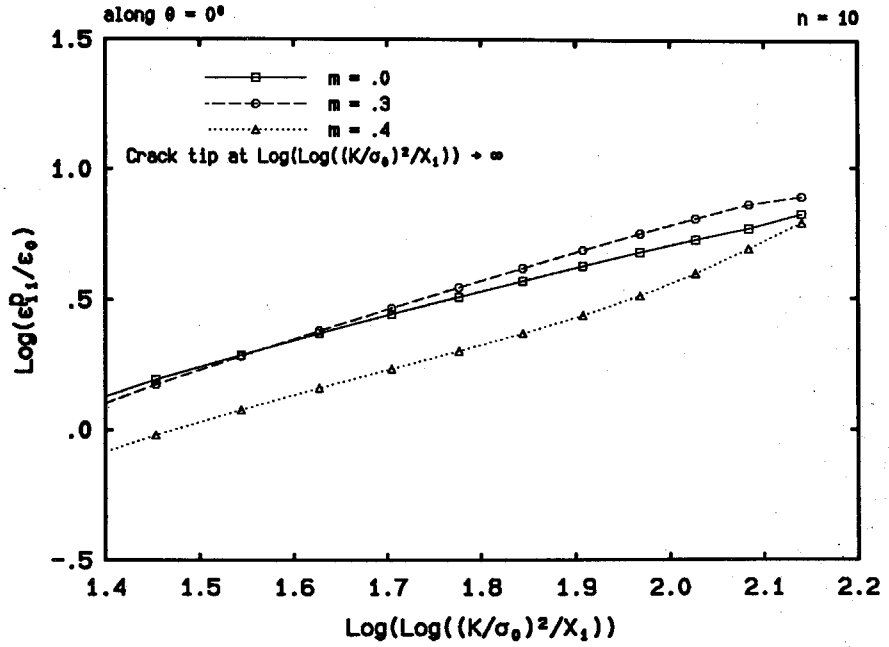

FIGURE 5.3.24a The radial variations of the plastic strain component ε_{11}^p for $n = 10$, along the prospective crack line in special logarithmic coordinates.

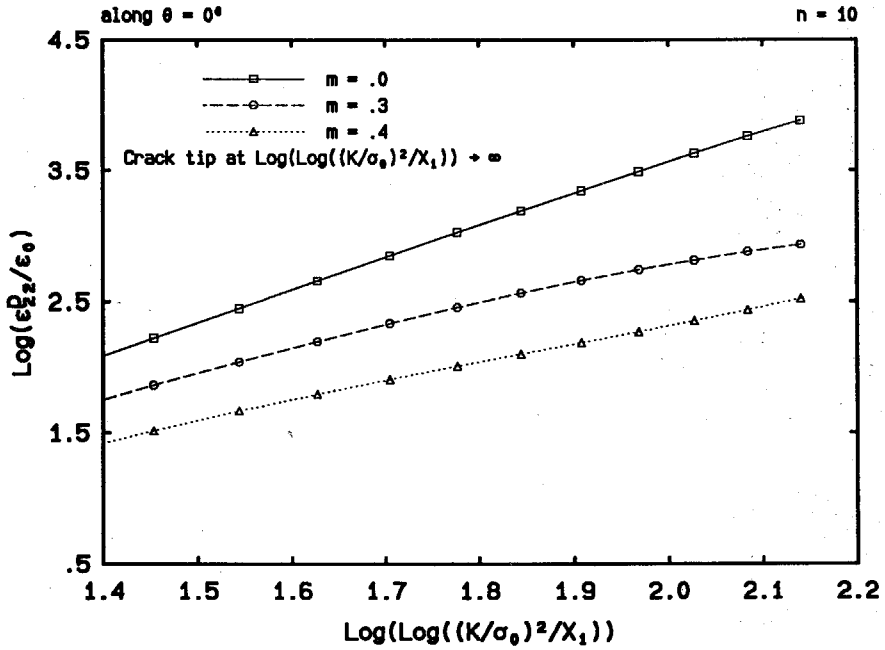

FIGURE 5.3.24b The radial variations of the plastic strain component ε_{22}^p for $n = 10$, along the prospective crack line in special logarithmic coordinates.

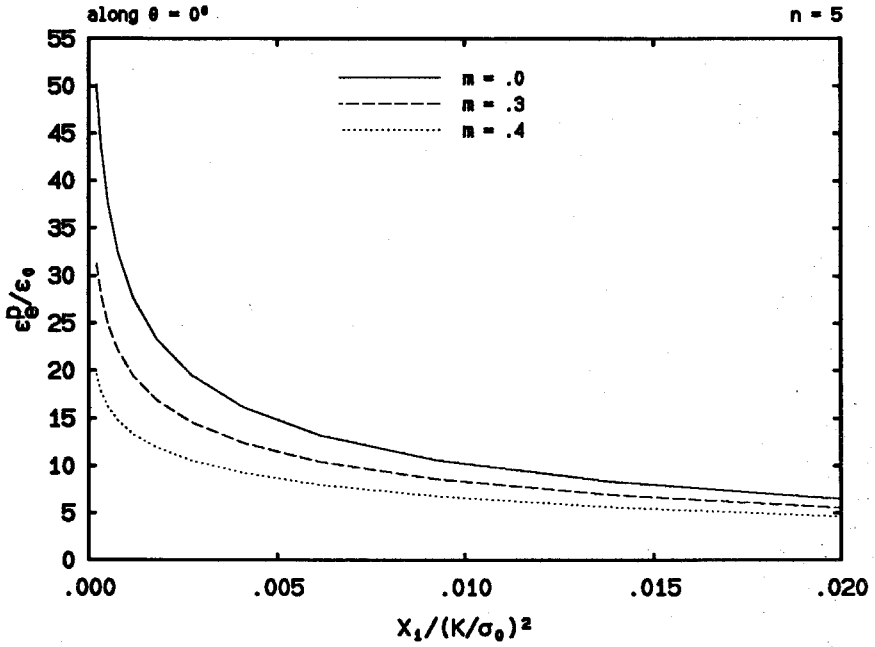

FIGURE 5.3.25a The radial variations of the effective plastic strain ε_e^p for $n = 5$, along the prospective crack line in the normalized coordinates.

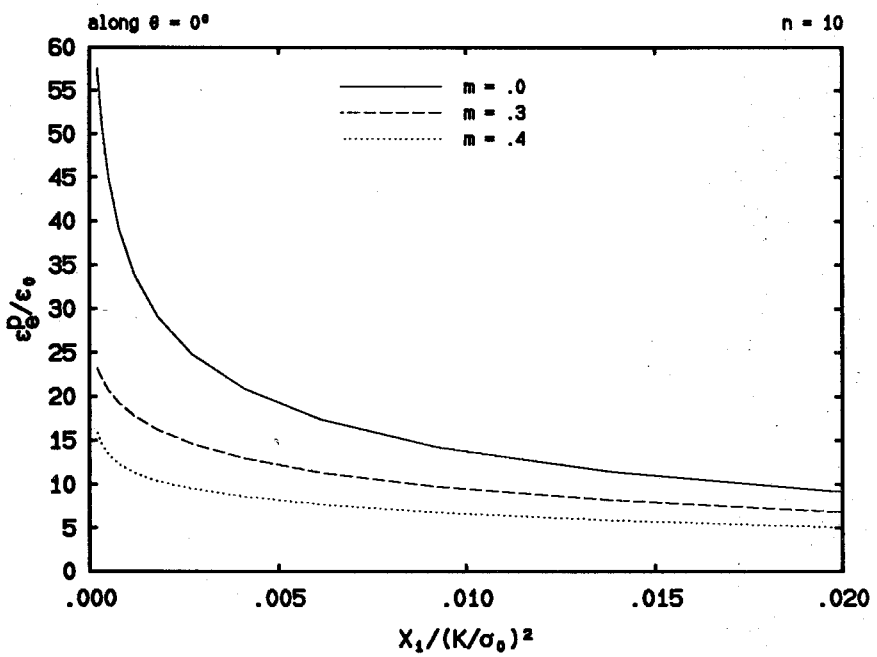

FIGURE 5.3.25b The radial variations of the effective plastic strain ε_e^p for $n = 10$, along the prospective crack line in the normalized coordinates.

at the same time, it is found that as m increases, the magnitude of ε_{11}^p first increases and then at a certain m value it decreases (see Figs. 5.3.21a through 5.3.24a). However, since ε_{22}^p is always much larger than ε_{11}^p near the crack tip, the effective plastic strain, by definition, would be dominated by, and thus behave as ε_{22}^p. That is to say, as the crack speed increases, the level of effective plastic strain will decrease (see Fig. 5.3.25). Hence, as in the case of dynamic crack propagation in elastic-perfectly plastic solids discussed in Chapter 3, this behavior can be utilized to explain experimental observations on many metal specimens, namely that at a higher crack propagation speed, the material resistance to fracture is higher. Thus the above behavior can be interpreted as follows. At a certain fixed load-level characterized by the value of the far-field stress intensity factor K, the level of plastic straining represented by the effective plastic strain is lower for higher crack propagation speeds at the same location ahead of the crack tip. In order for the level of plastic straining at a higher crack speed to be the same as that at a lower crack speed, the loading level for the former must be raised. Consequently, continued fracture will occur at a higher loading level at a higher crack speed, if fracture is characterized by the attainment of a critical plastic strain level at a certain distance ahead of the crack tip.

Finally we present the results of the present finite element study regarding the effects of strain hardening and crack propagation speed on the crack opening displacement. As in the case of quasi-static crack growth, it is found that the magnitude of the vertical displacement component u_2 in the normalized coordinates decreases as n increases for all crack speeds we investigated (see Fig. 5.3.26). Moreover, for typical power hardening materials, e.g., for $n = 5$ and 10, it is found that the magnitude of u_2 becomes larger as m increases (see Fig. 5.3.27) at distances far away from the crack tip. Whereas at locations very near the crack tip, the previous tendency does not hold any longer. Instead, it is seen that the above tendency begins to reverse, that is, as m increases, the magnitude of u_2 tends to

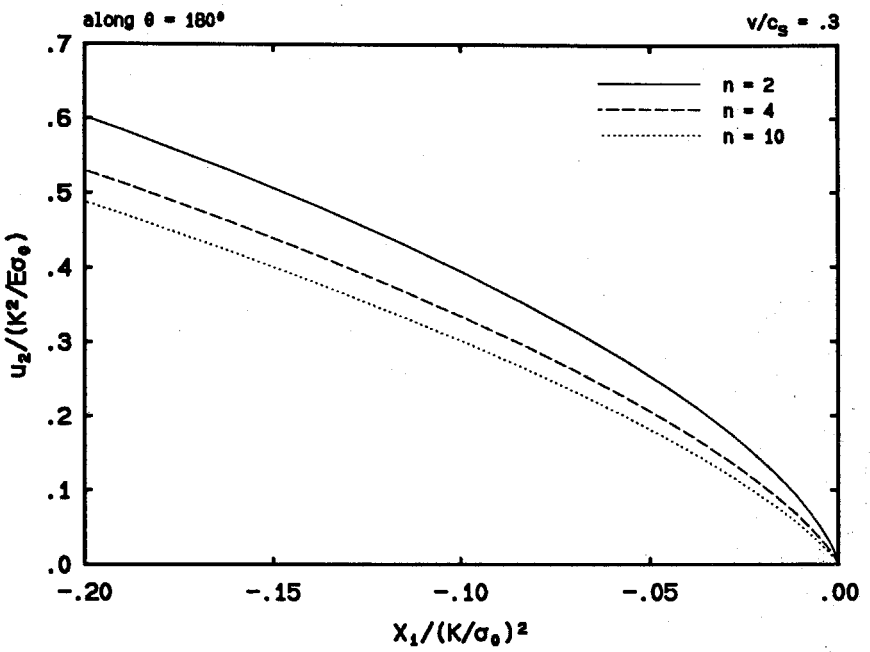

FIGURE 5.3.26a The effect of strain hardening on the radial variation of the vertical displacement u_2 along the crack surface for $v/c_s = 0.3$, plotted in its normalized form.

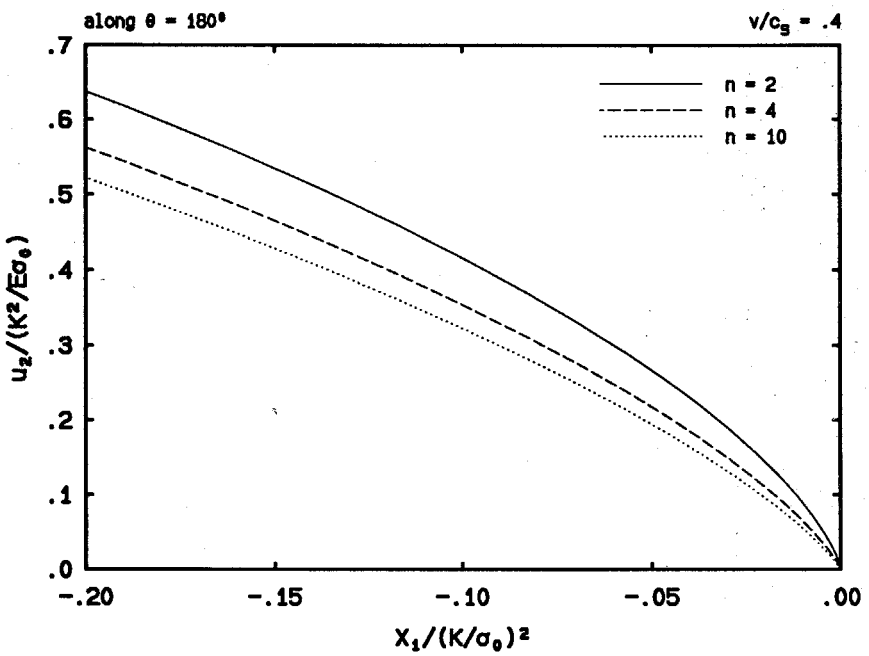

FIGURE 5.3.26b The effect of strain hardening on the radial variation of the vertical displacement u_2 along the crack surface for $v/c_s = 0.4$, plotted in its normalized form.

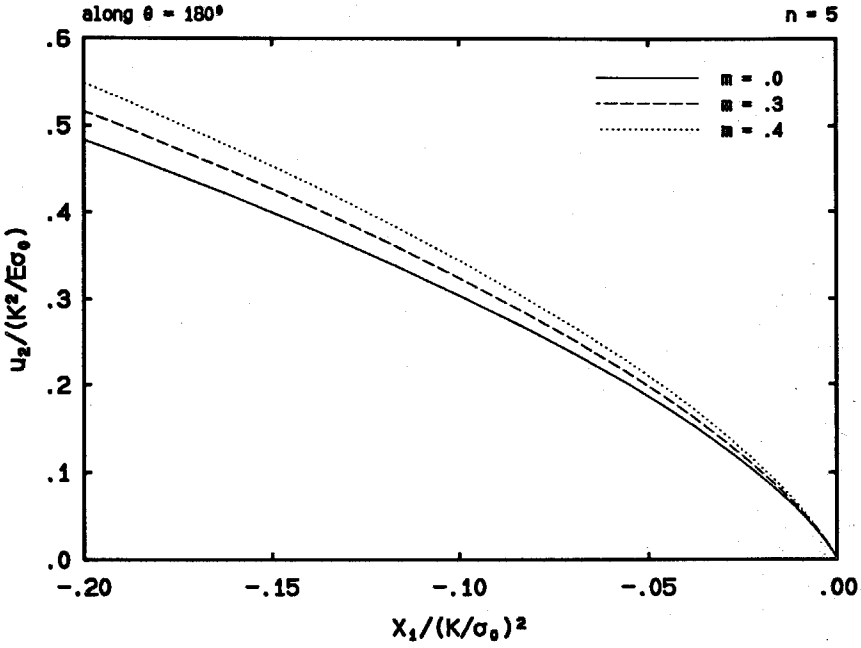

FIGURE 5.3.27a The effect of crack propagation speed on the radial variation of the vertical displacement u_2 along the crack surface for $n = 5$, plotted in its normalized form.

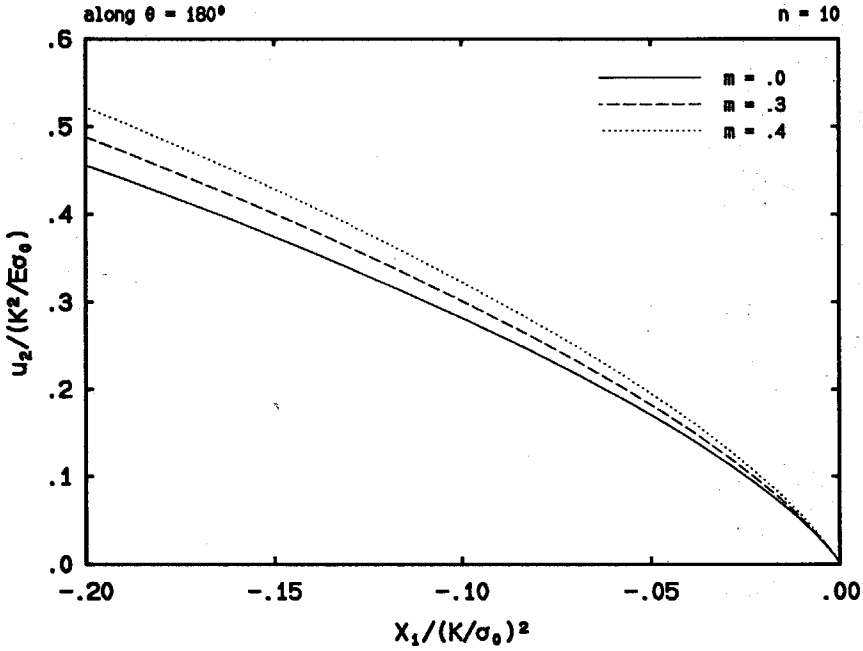

FIGURE 5.3.27b The effect of crack propagation speed on the radial variation of the vertical displacement u_2 along the crack surface for $n = 10$, plotted in its normalized form.

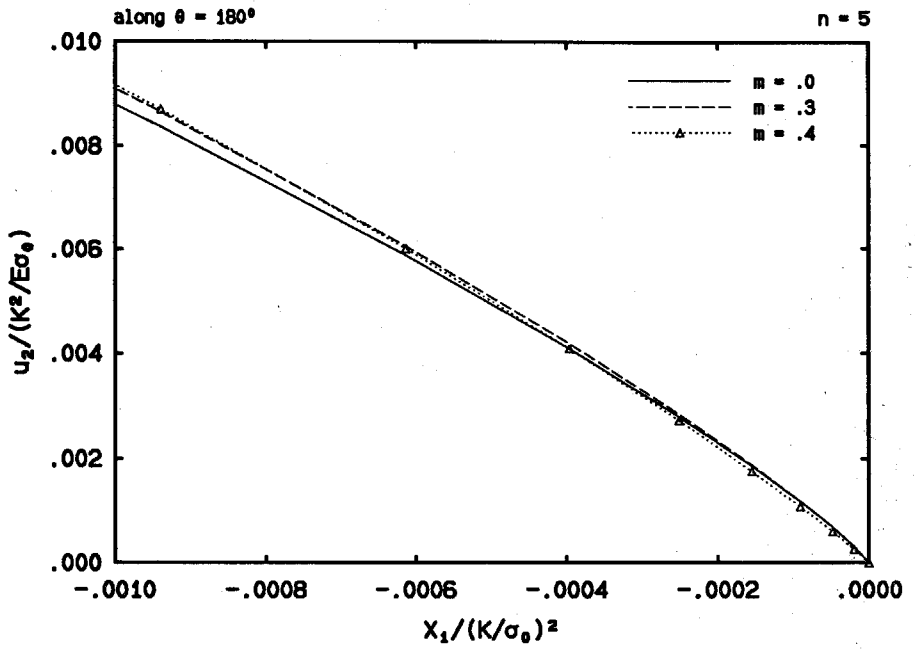

FIGURE 5.3.28a A detailed view of the effect of crack propagation speed on the radial variation of the vertical displacement u_2 along the crack surface for $n = 5$, plotted in its normalized form.

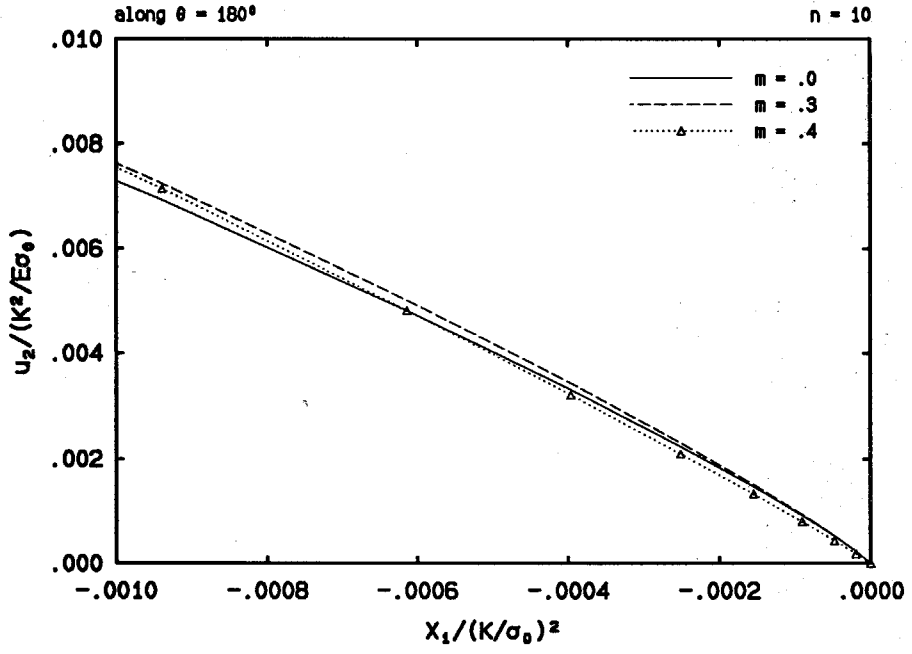

FIGURE 5.3.28b A detailed view of the effect of crack propagation speed on the radial variation of the vertical displacement u_2 along the crack surface for $n = 10$, plotted in its normalized form.

decrease (see Fig. 5.3.28), which has also been observed for linear hardening solids (see Fig.4.3.28c). This feature has been more clearly observed in Mode I plane strain for elastic-perfectly plastic materials by Lam and Freund (1985) even at a location about one-hundred times farther away from the crack tip than the present one. As discussed in Chapter 6, by using this behavior and a critical crack tip opening angle criterion, they were able to explain the phenomenon of increased material resistance to continued crack propagation at higher speeds. Note that they were able to detect this feature by the same finite element method as used here from a near tip mesh much coarser than the one employed here, with which, as discussed in Chapter 3 (see Fig. 3.3.13) we were not able to conclusively make a similar statement for elastic-perfectly plastic materials in Mode I plane stress. However, if this feature is an inherent characteristic of the dynamic crack tip fields (which, in fact, should be true if crack growth is to be achieved when a constant critical opening angle is retained, and if the material fracture toughness is to increase if the crack propagation speed is increased), then perhaps it can be revealed in plane stress for higher hardening materials and for elastic-perfectly plastic materials using a mesh much finer than the present one.

CHAPTER 6

FRACTURE CRITERIA

6.1 INTRODUCTION

It is fair to say that the history of fracture mechanics is a history of searching for fracture criteria. Griffith (1920, 1924), in his pioneering work on the rupture of brittle materials such as glass and quartz, stated that fracture would occur when the released elastic strain energy from a cracked system, due to an infinitesimal crack growth, compensates the surface energy needed for the creation of the new crack surface. It is well known that the appearance of this Griffith energy criterion marks the beginning of fracture mechanics.

The Griffith criterion is, however, applicable to ideally elastic materials only. This very fact hindered its use on metals for almost 30 years, until Irwin (1948) and Orowan (1949) independently modified this criterion to include work done in plastic deformation at the crack tip.

The energy balance criterion is, however, only a necessary condition for fracture initiation. Its satisfaction merely means that it is energetically favorable for the crack to grow, but whether the crack grows or not depends on whether the stress and deformation states in the immediate neighborhood of the crack tip permit such crack growth. To this end, the Griffith criterion is not sufficient, which may also be one of the main factors for the long silence of research activities in fracture mechanics.

Fracture mechanics began to prosper when Irwin (1956) defined the concept of a strain energy release rate, or a crack extension force. This strain energy release rate, which is usually denoted by G, differs from the Griffith's elastic strain energy release in that it is determined from the stress and displacement fields in the vicinity of the crack tip, rather than from a global energy consideration. Since, as observed by Irwin, the value of G measures the intensity of the crack tip stress field, so long as the influence of plastic deformations accompanying fracture extension is limited to the close neighborhood of the crack tip, it is expected that when G reaches a critical value, G_c, crack extension occurs, which is the strain energy release rate criterion, or simply the *G-criterion.*

The G-criterion is further substantiated by the general analyses of Irwin (1957) and Williams (1957) on the crack tip stress and strain fields for elastic materials. It is found that the near-tip singular fields are uniquely characterized by a loading parameter K, the so-called stress intensity factor, and that G is proportional to the square of K. Due to the wide availability of handbooks and testing methods on stress intensity factors, a fracture criterion based on K, or the *K-criterion*, is now in vast application. Naturally, it is noted, that the G-criterion and the K-criterion are equivalent.

Although the concept of energy balance is universally valid, the G-criterion and hence the K-criterion are applicable only to problems where plasticity is localized in the crack tip area. This necessitates the search for alternate fracture criteria.

A fracture criterion, which holds for even larger scale plastic deformations, is established through the discoveries of a path-independent integral, the so-called J-integral (Rice, 1968b), and the HRR-singularity (Hutchinson, 1968a; and Rice and Rosengren, 1968). For nonlinear elastic power-law solids or elastic-plastic solids under proportional loading conditions, where the deformation theory of plasticity can be employed, the HRR-singularity states that the stress and deformation fields

at the crack tip are uniquely determined by the value of the J-integral. Under conditions of monotonic loading and small-scale yielding, it is shown that $J{=}G$ by virtue of the path-independence of the J-integral. This fact rationalizes the use of G and hence K as fracture-controlling parameters, since G and hence K, through J, still measure the intensity of the crack tip stress and strain fields under the specified conditions. The generality of the J-integral warrants the popular applications (for the onset of crack extension) of the fracture criterion based J (see Broberg, 1971; Begley and Landes, 1972; and Landes and Begley, 1972).

It is a well-established fact that a phase of stable crack growth in elastic-plastic solids exists in many applications following the onset of crack extension (see, for example, Broek, 1968; Rice, 1975; and Broberg, 1975). Fracture control for such cases is accomplished by means of fracture criteria used in fracture initiation, through the concept of Resistance-Curves (ASTM STP 527, 1974). Under small-scale yielding conditions, there are the *K_R-curves* and *G_R-curves*, which characterize the increase of material resistance to continued crack extension. Fracture conditions under which such stable crack extensions occur are usually termed the *K-controlled*, or the *G-controlled* conditions. Similarly, *J-controlled* fracture conditions also exist. It is observed (Paris, Tada, Zahoor and Ernst, 1977; Hutchinson and Paris, 1979; and Hutchinson, 1979, 1983) that under certain restrictions, a short range of J-controlled slow stable crack growth exists in an approximate sense, although as a crack extends materials near the crack tip experience nonproportional plastic deformation, which renders inappropriate the deformation theory of plasticity, and hence the HRR-singularity and the path-independence of the J-integral.

The aforementioned fracture criteria, when used for the onset of crack growth in elastic-plastic solids under proper constraints, or for continued crack growth in ideally brittle solids, have clear physical meanings and sound theoretical bases. Under elastic-plastic stable crack growth conditions, however, these criteria themselves do not tell the sources of increased material resistance to continued fracture. Be-

sides, these criteria cannot be extended without more fundamental studies to cases beyond their limits, such as cases involving dynamic crack propagation.

There is as yet no universal fracture criterion for crack growth in elastic-plastic solids, i.e., fracture criteria in such instances are, broadly speaking, problem-specific. In the case of dynamic crack propagation, in particular, a generally accepted fracture criterion does not even exist, although a criterion based on the dynamic stress intensity factor has been proposed. Besides, as discussed later, different fundamental criteria have to be used for Mode I plane strain, and for Mode I plane stress and Mode III, the anti-plane strain case.

In this chapter, two types of fracture criteria for continued crack growth in elastic-plastic solids are discussed, namely the ones based on the plastic strains at the crack front, and the ones based on the crack opening displacements behind the tip. These criteria make use of the stress and deformation field quantities very near the crack tip. Therefore, the use of these criteria depends on the availability of solutions of the crack tip elastic-plastic fields, which raises some mathematical and experimental difficulties. The common problem with this type of criteria is that the critical values for crack growth to occur do not allow calculations of fracture stress or critical crack size. But at the same time, it is theoretically advantageous to assume criteria of these kind, since these criteria are based on local crack tip fields, and hence they are more fundamental than criteria based on indirect quantities such as the stress intensity factor K or the J-integral.

6.2 CRITERIA BASED ON PLASTIC STRAINS

Orowan was the first to suggest a fracture criterion based on plastic strains at a crack front. He stated that for ductile fracture "the simplest assumption is that the crack propagates if the plastic strain at its tip reaches a critical magnitude."(Orowan, 1949.) However such a over-simplified criterion will not work

because of the existence of theoretical singularities of plastic strains at the crack tip in elastic-plastic solids.

A fracture criterion, which avoids the difficulties associated with the strain singularity at the crack tip, was proposed by McClintock (1956, 1958) and McClintock and Irwin (1964). It is suggested that fracture would occur when the crack front plastic strain level at a characteristic distance away from the crack tip reaches a critical value. The characteristic distance is on the order of grain or subgrain size and should be determined experimentally.

This critical plastic strain criterion has its bearings from micromechanical experimental observations. As discussed by Puttick (1959), Glennie (1972), Cox and Low (1974), and Andersson (1977), ductile fracture, where fibrous and shear-type fractography is observed, is always accompanied by void growth and coalescence within the crack front fracture process zone. These micromechanical activities are grossly reflected as measurable large strains in the region adjacent to the fracture process zone. Thus the critical strain criterion has sound physical grounds.

Due to experimental difficulties, the McClintock-Irwin criterion is not employed frequently in practical applications. For example, it is impossible to actually measure the critical value of the plastic strain corresponding to the separation of material, at least not with current experimental techniques and facilities. However, its theoretical potentials should not be overlooked. In fact, this criterion has been used successfully to study the effects of inertia on a rapidly moving crack (Freund and Douglas, 1982). When combined with numerical methods, this criterion offers many advantageous properties over those based on crack tip opening displacements (see discussions later).

6.3 CRITERIA BASED ON DISPLACEMENTS

Fracture criteria based on displacements were first introduced for the initiation

of crack growth in the presence of large plastic deformation. It was proposed by Wells (1961, 1963, 1965) that crack growth in elastic-perfectly plastic solids occurs when the crack tip opening displacement δ, usually known as CTOD or COD, reaches a critical value δ_c, where δ_c is a material constant which may depend on the environment and the thickness of the plate in question.

This fracture criterion is consistent with the theoretical discoveries that δ is nonzero at a stationary crack tip for an elastic-perfectly plastic solid (see, for example, Rice, 1967, 1968a), and with the experimental observations of crack tip blunting. Under conditions where the J-integral is applicable, it can also be shown that J is directly proportional to δ. For example, in the case of Mode I plane stress, the application of the Dugdale model (Dugdale, 1960), the Tresca yield criterion and the path-independency of the J-integral, would readily produce that $J = \sigma_0 \delta$, where σ_0 is the initial yield stress in tension.

Problems arise when the above defined criterion is used for hardening materials, simply because δ at the crack tip is zero for such materials, as shown by the HRR-field (Hutchinson, 1968a; and Rice and Rosengren, 1968). An extension of the *δ-criterion* was then proposed by Rice (see Tracey, 1976), through an properly redefined δ value at the crack tip.

For continued crack extension, it has been proposed (Andersson, 1973; and de Koning, 1977) that the slope of the crack tip opening profile, or the crack tip opening angle which is usually termed CTOA, be used as a parameter characterizing the fracture process. In fact it is observed (for example, see Kanninen, Popelar and Broek, 1981) that CTOA is approximately a material constant during stable crack growth.

Theoretically, however, it can be shown that for advancing cracks the crack surface intersects the crack tip at a right angle, which renders the above-defined CTOA meaningless. A modification of the critical crack tip opening angle criterion

was suggested by Rice and Sorensen (1978). They assumed that fracture initiation and continued crack growth can occur if a critical opening $\delta = \delta_c$ is maintained at a small characteristic distance r_m behind the tip, where r_m is a micromechanical length scale. This criterion is found to be very useful in interpreting theoretical asymptotic results (see discussions later).

There also exists a different modification of the CTOA criterion. Known as the critical opening angle criterion, or COA in short, the criterion assumes that continued crack growth is realized when a certain averaged crack tip opening angle is maitained at a constant level (see Shih, deLorenzi and Andrews, 1979; and Kanninen et al., 1979).

Methods based on fracture criteria of the CTOD, CTOA, or COA types are now in broad application, especially where large-scale yielding is involved. Yet there are still many important issues remaining to be answered. A practical difficulty, as we noted, is the definition of these quantities. Later we will also point out more difficulties encountered when a criterion of this kind is used in conjunction with numerical results. Our emphasis here is, however, on the micromechanical aspects of those criteria. As we know, a critical plastic strain criterion at the crack front would in a gross sense represent the micromechanical activities in the fracture process zone, namely the activities of void nucleation, growth and coalescence. But what is the connection between the crack tip opening profile and those micromechanical behaviors at the crack front?. Although there is yet no complete answer to this key-note question, we would like to draw attention to an argument offered by Rice (1968a) and Rice and Johnson (1969).

It is observed for stationary cracks that, in contrast to the cases of Mode III and Mode I plane stress, maximum strain concentrations for elastic-plastic materials do not occur directly ahead of a Mode I plane strain crack tip (see Rice, 1967, 1968a). This situation is more pronounced for nonhardening materials, where sin-

gular strains appear only in the centered fan sector, which is 45^0 away from the prospective crack line, whereas at the crack front strains are bounded. In fact this phenomenon is typical of Mode I elastic-plastic fields around plane strain, sharp crack tips, including growing cracks (see Drugan, Rice, and Sham, 1982). A question then arises as to how ductile fracture occurs if there is no strain concentration at the crack front. This paradox was investegated by Rice (1968a), and Rice and Johnson (1969), who attributed this to the negligence of crack tip blunting due to finite strain effect during progressive loading. They argued that, a crack tip blunting of size δ_t, the discrete or nonzero crack tip opening displacement, would modify the near-tip slip line network, so as to produce an intensive straining region, spreading ahead over a length scale about twice that of δ_t. It then seems plausible that crack growth would occur when the size of the intensive straining region, and hence the crack tip opening displacement, reaches a critical value. In this light, a ductile fracture criterion based on the local crack opening profile, rather than on crack front strains, seems more appropriate for Mode I plane strain problems. However there are no similar analyses for growing cracks.

6.4 THEORETICAL K_{Ic}^d vs. v CURVES

There are many issues regarding the use of K as a fracture-characterizing parameter for dynamic crack propagation, not only due to experimental discrepancies, as discussed in the introductory chapter, but also due to the fact that K, under small-scale yielding conditions, no longer holds its many fine properties as in the case of fracture initiation. Because of the existence of residual plastic wake behind the crack tip, K loses its simple relation to the energy release rate G, which is somehow the physical ground for the K-criterion for fracture initiation. Also because of the plastic wake, the singular K-field will not exactly surround the crack tip elastic-plastic zone, and it is not clear whether K still characterizes the fracture behavior at the crack tip. To summarize, directly assuming the validity of

the K-criterion for dynamic crack propagation in elastic-plastic materials has no solid theoretical ground. However, as we know, there have been vast investments in developing and standardizing K-measurement techniques and instruments, and well documented data are widely available. It is therefore of vital importance to carefully investigate the validity of the K-criterion from a more fundamental point of view, and to properly assess its accuracy and reliability as a practical fracture criterion.

It is our purpose in this section to demonstrate, instead of directly assuming, the legitimacy of the K-criterion for dynamic crack propagation in solids which fail in a locally ductile manner through the use of more fundamental fracture criteria such as those discussed earlier. In particular, we will utilize the McClintock-Irwin critical plastic strain criterion to extract theoretical K_{Ic}^d vs. v curves from our numerical full field solutions for Mode I plane stress crack tip fields in elastic-perfectly plastic solids, where K_{Ic}^d is the critical dynamic stress intensity factor, and v is the speed of crack propagation. Good agreement with experimental results on 4340 steel will be demonstrated. We will also point out the source of difficulty, or impossibitity to be more accurate in some circumstances, to extract such a K_{Ic}^d vs. v relation from a crack tip opening displacement based fracture criterion. Theoretical implications of this phenomenon will be addressed.

As mentioned in the previous sections, fracture criteria based on G, K, or J alone cannot explain the source of increased material resistance to contined fracture. And hence it is impossible to theoretically generate resistance curves, such as $G_R(\Delta a)$, $K_R(\Delta a)$, and $J_R(\Delta a)$ curves (Δa being the amount of crack growth), using these criteria without invoking more fundamental assumptions.

The δ-based fracture criterion is usually used in plane strain where, as discussed before, the crack tip plastic straining is not, according to the small strain theory, concentrated directly at the crack front. Under contained yielding conditions, it

has been a long endeavor to correlate the crack tip opening profile $\delta(r)$ to the value of the J-integral, and to predict stable crack growth theoretically, where r is the distance to the crack tip. Note that J is defined here in the elastic region surrounding the crack tip plastic zone and is, under small-scale yielding conditions, related to K through

$$J = \frac{K^2}{E'}, \tag{6.4.1}$$

with $E' = E$ for Mode I plane stress and $E' = E/(1-\nu^2)$ for Mode I plane strain, where E is the Young's modulus. It is shown by the asymptotic analysis of Rice, Drugan and Sham (1980) for elastic-perfectly plastic materials that the relation between $\delta(r)$ and J can be described in the following rate form during crack growth:

$$\dot{\delta} = \alpha \dot{J}/\sigma_0 + \beta \dot{a}(\sigma_0/E) ln(R/r), \tag{6.4.2}$$

where $\dot{a}$ is the crack speed, β is a constant known from the asymptotic analysis ($\beta = 5.462$ for $\nu = 0.3$, for example), α is a dimensionless quantity, and R is a length scale undetermined by the asymptotic analysis, but can be approximately obtained from a full field finite element analysis. For a continuously growing crack (i.e., when dJ/da is finite), Eq.(6.4.2) can be integrated to get the profile very near the tip as

$$\delta = (\alpha r/\sigma_0) dJ/da + (\beta r \sigma_0/E) ln(eR/r), \tag{6.4.3}$$

where $e = 2.718$ is the natural number or the base of the natural logarithm. It is clear from Eq.(6.4.3) that $\delta = 0$ at $r = 0$ for a advancing crack, and that the crack faces meet the tip at a right angle with the crack line. Hence the crack growth criteria based on the crack tip opening displacement at $r = 0$, or on the crack tip opening angle at $r = 0$, cannot be used here, rather, a criterion based on a critical value of δ at $r \neq 0$ must be adopted. Rice and Sorensen (1978) proposed such a criterion by assuming that fracture initiation and continued crack growth can occur if a critical opening $\delta = \delta_c$ is maintained at a small characteristic distance r_m behind the tip, which can be viewed as a critical crack opening angle criterion. Thus from

Eq.(6.4.3), it is required that

$$\frac{\delta_c}{r_m} = \frac{\alpha}{\sigma_0}\frac{dJ}{da} + \beta\frac{\sigma_0}{E}ln(\frac{eR}{r_m}). \tag{6.4.4}$$

It was noted by Rice, Drugan and Sham (1980) that the critical crack opening angle criterion can be rephrased in a manner which makes no reference to the "microscale" parameters r_m and δ_c. This was done by rearranging Eq.(6.4.3) into the form

$$\delta = \beta r\frac{\sigma_0}{E}ln(\frac{\rho}{r}), \quad \text{as } r \to 0 \tag{6.4.5}$$

where

$$\rho = Re^{(1+\alpha T/\beta)}, \tag{6.4.6}$$

with $T = (E/\sigma_0^2)dJ/da$ being the tearing modulus (Paris, Tada, Zahoor, and Ernst, 1977). Thus, equivalently, the criterion for crack growth with a geometrically similar profile very near the tip is that ρ, after attaining its critical value ρ_c at the onset of crack extension, remains constant during stable crack growth.

A relation between δ_c and J of the type in Eq.(6.4.4), which is extracted from asymptotic analyses and crack growth criteria, can be used to describe the process of stable crack growth. The description is, however, not complete without the values of α and R, which are obtainable only through a full field analysis, such as a finite element computation. For example, under small-scale yielding conditions, it is observed from finite element calculations (Sham, 1979, 1983; Dean and Hutchinson 1980; and Parks, Lam and McMeeking, 1981) that

$$R = sEJ/\sigma_0^2, \tag{6.4.7}$$

where s is obtained from crack opening profile through numerical fitting. Unfortunately, s is found to vary widely in the range of $0.11 \sim 0.78$ from one study to another. We believe that this somewhat random behavior is mainly due to the inevitably large crack tip discretization errors, especially for the Eulerian-type finite element formulations employed by the latter two investigators. Nonetheless

if Eq.(6.4.7) is assumed, stable crack growth under small-scale yielding conditions would yield from Eq.(6.4.6)

$$dJ/da = (\beta/\alpha)(\sigma_0^2/E)ln[\rho\sigma_0^2/(seEJ)], \tag{6.4.8}$$

with ρ determined from its constancy

$$\rho = seEJ_{Ic}/\sigma_0^2, \tag{6.4.9}$$

where J_{Ic} is the critical J value at crack initiation. Eq.(6.4.8) is the governing equation for stable crack growth under small-scale yielding. Its prediction that J increases with continued fracture agrees with experimental observations.

The Rice-Sorensen critical crack tip opening angle criterion is more recently applied to extract theoretical K_{Ic}^d vs. v curves for Mode I plane strain dynamic crack propagation by Lam and Freund (1985). Under steady state and small-scale yielding conditions, they employed the Eulerian-type finite element formulation originally proposed by Dean and Hutchinson (1980) for quasi-static crack extension. From crack opening results very near the crack tip, they were able to generate the crack speed dependence of the critical dynamic stress intensity factor, which are qualitatively very similar to the experimental findings of Rosakis, Duffy, and Freund (1984).

The application of this criterion to our Mode I plane stress case is however not successful. Data for the critical dynamic stress intensity, or the dynamic fracture toughness K_{Ic}^d, obtained from laboratory tests performed on thin metal plates, which fracture in a locally ductile manner, exhibit a monotonic rising tendency as the crack speed v increases (see, for example, Rosakis, Duffy, and Freund, 1984; and Zehnder and Rosakis, 1990a). In order to predict such a tendency with the Rice-Sorensen criterion, it is necessary for the so-defined crack tip opening angle $\delta(r)/r$, when plotted against the normalized toughness value K_{Ic}^d/K_{ss} with K_{ss} being the quasi-static steady state value, to have lower values for higher crack speeds when

the normalized toughness is fixed. Another requirement is that when the same plot is used, the quantity K_{Ic}^{d}/K_{ss} should have lower values for lower crack speeds when the opening angle is fixed. We notice that such a tendency is indeed observed for Mode I plane strain (see Fig. 6 of the paper by Lam and Freund, 1985). Yet this is not the case in Mode I plane stress for elastic-perfectly plastic materials, although our finite element mesh is much finer than that employed by Lam and Freund. In fact, we did not observe such a tendency even on a scale about one-hundredth finer than that of the previous two authors. The same situation is also reported by Douglas, Freund and Parks (1981) for Mode III.

The difficulty in applying the critical crack tip opening angle criterion to Mode III and Mode I plane stress can in one way be attributed to numerical errors accumulated near the crack tip. One such error is simply due to the lack of enough spatial resolution near the crack tip. This leads to the usual finite element discretization error which alone would blur the real behavior of the crack tip opening profile. To this end, it is emphasized here that the mesh we employed has a ratio of plastic zone size to the smallest element size on the order of 1.6×10^4, which is already a very high resolution. Another source of numerical error is somewhat peculiar to the Eulerian formulation in which updated stresses are obtained through numerical integrations of the incremental constitutive law from crack front to crack back. This integration, after sweeping the crack tip, carries large discretization errors to the areas behind the crack tip, which is most significant immediately near the tip. The crack tip opening profile, which is to be used in a fracture criterion, happens to be most inaccurate there.

Another factor contributing to this difficulty may come from the asymptotic nature of the crack tip fields in Mode I plane stress and Mode III. Take the Mode III case for example, the asymptotic solution for dynamic crack propagation by Slepyan (1976) predicts a crack tip opening as expressed in Eq.(3.1.3). It was pointed out in the introduction section in Chapter 3 that the asymptotic result, which although

it gives the desired property that $\delta(r)/r$ decreases as the crack speed (normalized by the shear wave speed) increases, was not confirmed by the full field numerical solution of Douglas, Freund and Parks (1981). Recall the discovery of Freund and Douglas (1982) that the region of dominance of the dynamic asymptotic solution decreases rapidly as the crack speed goes to zero, it is very possible that the region in which the desired property of the crack opening displacement exists in order to apply the critical angle criterion is extremely small such that no numerical study of reasonable cost can detect such a presence. Considering the similarities between Mode III fracture and the fracture in Mode I plane stress, and the fact that we have already used a very fine finite element mesh near the crack tip, it is believed that this difficulty, or impossibility , to use the critical crack opening angle criterion to extract K_{Ic}^{d} vs. v curves is due to the asymptotic nature of the Mode I dynamic plane stress crack tip fields. In fact, when the crack speed is higher, i.e., when the dominance zone of the dynamic asymptotic crack tip field is larger, the above-mentioned desirable crack opening property is indeed observed (see Figs. 3.3.13b, 4.3.28 and 5.3.28), which somewhat verifies our previous belief.

The aforementioned difficulty thus leaves us only one choice, that is to use the plastic strain based fracture criterion, or the McClintock-Irwin critical plastic strain criterion to be more specific. In light of this, we would like to recall some consistent observations regarding the change of magnitudes of plastic strains from various solutions discussed in Chapter 3.

It is observed by many that for stationary cracks, strains have $\frac{1}{r}$ singularity at the crack tip for all three fracture modes. For advancing cracks, the singularity changes at crack front from $ln^2(r)$ for quasi-static crack growth to $ln(r)$ for dynamic crack propagation in Mode III. In Mode I plane strain for the case of Poisson ratio $\nu = 0.5$, plastic strains possess logarithmic singularity at least in the centered fan sector for quasi-static crack growth, yet they are less singular for rapid crack extension. Thus it may be concluded that crack growth reduces the level of plastic

straining at the crack tip if the same load level is maintained.

Likewise in Mode I plane stress, as depicted in Figs.3.3.8a and 3.3.9a, the magnitudes of plastic strains at the crack front decreases as the crack speed increases if the stress intensity factor is fixed at the same level. In other words, to maintain the same strain level at the same point ahead of the crack, greater stress intensity factors must be maintained for higher crack speeds, which is the behavior observed in Mode I fracture for many metals. Note that since strain rate sensitivity is not considered in the above dynamic analyses, inertia alone is expected to be responsible for such behaviors.

Thus under small-scale yielding conditions, monotonically rising K_{Ic}^{d} vs. v curves can be obtained from a full field, or simply a crack line solution, if the critical plastic strain criterion is assumed. The first successful application of this criterion was performed by Freund and Douglas (1982) for Mode III dynamic crack propagation in elastic-perfectly plastic solids. Their theoretical curves are qualitatively very similar to the findings of Rosakis, Duffy, and Freund (1984) from experiments conducted on thin, high strength steel plates and assuming generalized plane stress conditions. From both theoretical and practical points of view, it would then be very interesting to observe such a good correlation between theory and experiments under approximately the same type of constraints, basically the plane stress or generalized plane stress conditions.

The radial dependence of the effective plastic strain at the front of a Mode I plane stress crack tip is illustrated in the usual normalized form in Fig. 6.4.1 in much detail for crack velocities ranging from zero to forty percent of the elastic shear wave speed of the elastic-perfectly plastic material. We note that the effective plastic strain ε_e^p is normalized by ε_0, the initial yield strain in tension, and that the radial distance X_1 along the prospective crack line is normalized by $(K/\sigma_0)^2$, where K is the generic critical dynamic stress intensity factor and σ_0 is the initial

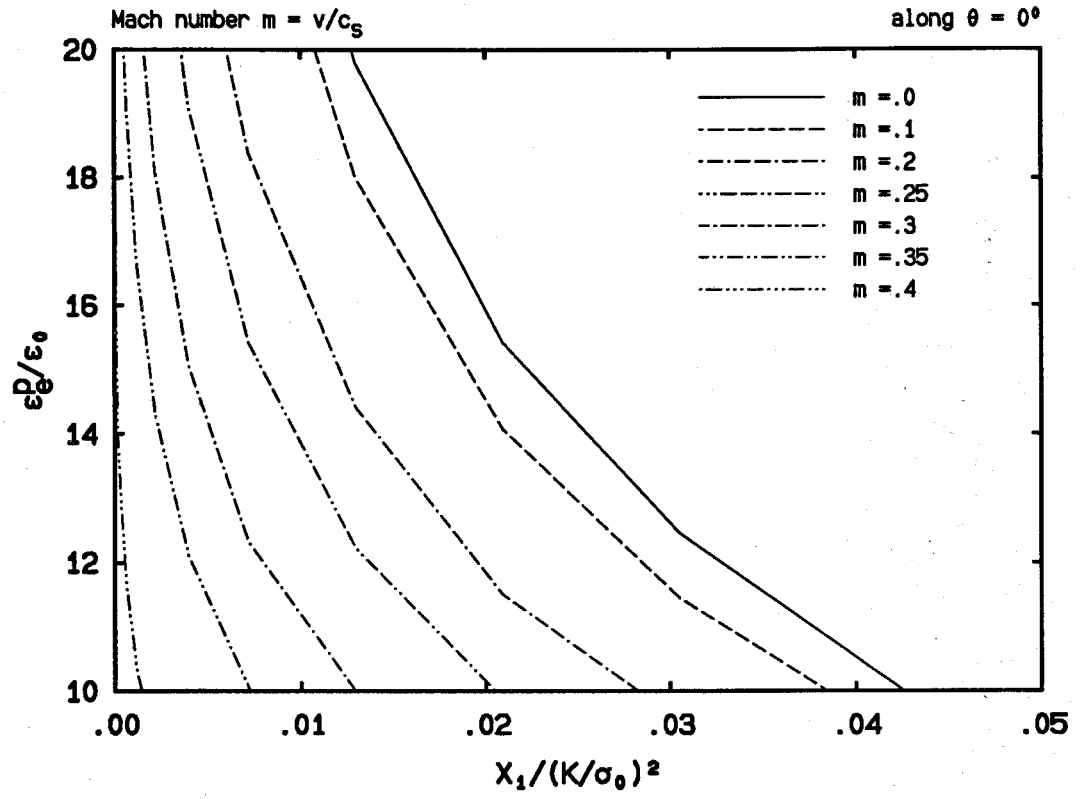

FIGURE 6.4.1 The radial dependence of the effective plastic strain at the crack front along the prospective crack line.

yield stress in tension. The procedure we used to extract the K_{Ic}^d vs. v curves from numerical results is outlined as follows. First a critical plastic strain value is chosen and a horizontal line corresponding to this value is drawn on the plot, which intersects the various effective plastic strain distribution curves at different normalized radial locations. If we denote the intersection location for the quasi-static curve by $X_1/(K_{ss}/\sigma_0)^2$, where K_{ss} is the critical stress intensity factor for steady state quasi-static crack growth, and denote the intersection location for a generic m value (m being the ratio of crack tip speed to the shear wave speed) by $X_1/(K_{Ic}^d/\sigma_0)^2$, where K_{Ic}^d is the critical dynamic stress intensity factor corresponding to Mach number m, we would obtain for each m the ratio of $(K_{Ic}^d)^2$ to $(K_{ss})^2$, and hence the value K_{Ic}^d/K_{ss}, by dividing the second location by the first, since it is assumed that the critical plastic strain value is achieved at the same physical location X_1 for

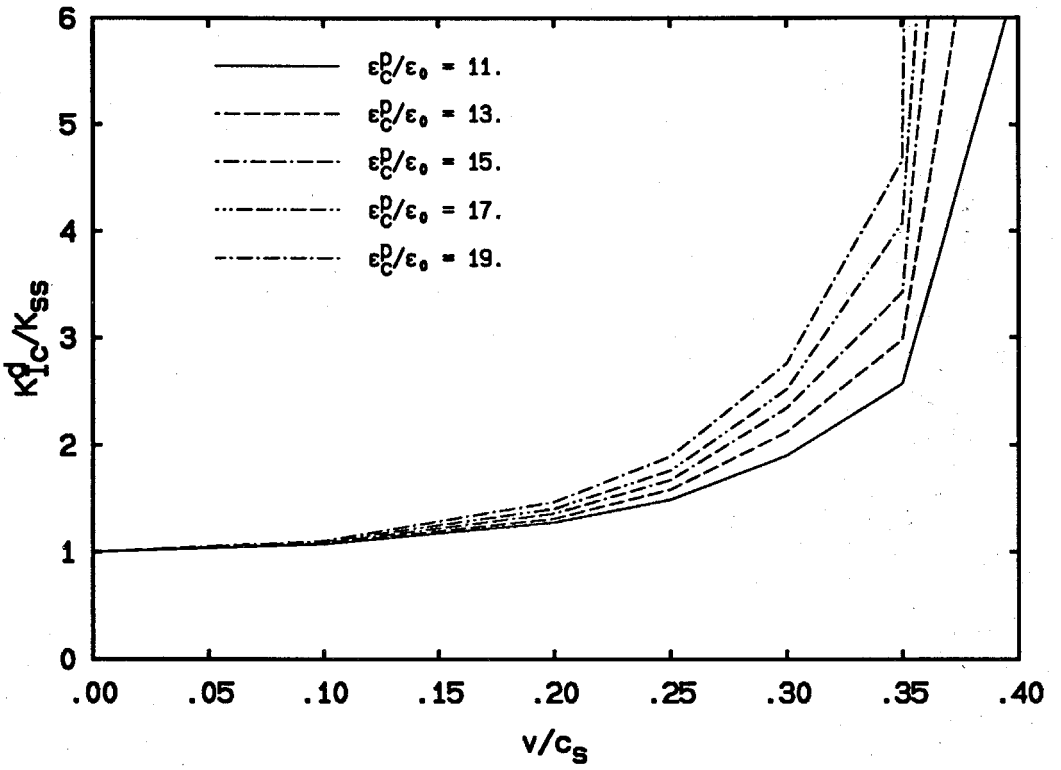

FIGURE 6.4.2 Theoretical K_{Ic}^d vs. v curves in their normalized forms for various critical plastic strain levels.

all m.

We would like to point out at this stage that the procedure we discussed above is different from the one employed by Freund and Douglas. Specifically, their procedure needs to use results for stationary cracks (which may not always be available), whereas ours doesn't. Another advantage of the present procedure is that comparisons with dynamic experimental results are made easier and clearer. In fact, since all curves start at the value one at $m = 0$ because of our normalization, the experimental data can be similarly normalized without relying on the availability of the fracture toughness value for the onset of crack extension.

The resultant theoretical toughness curves are shown in Fig. 6.4.2 for ε_c^p (the critical plastic strain value) ranging from $11\varepsilon_0$ to $19\varepsilon_0$. It is found that as the

value of the critical plastic strain increases, the toughness curve becomes steeper for higher m values, while at the same time the curve remains fairly flat for lower m values, where m is the ratio of the crack velocity to the shear wave speed.

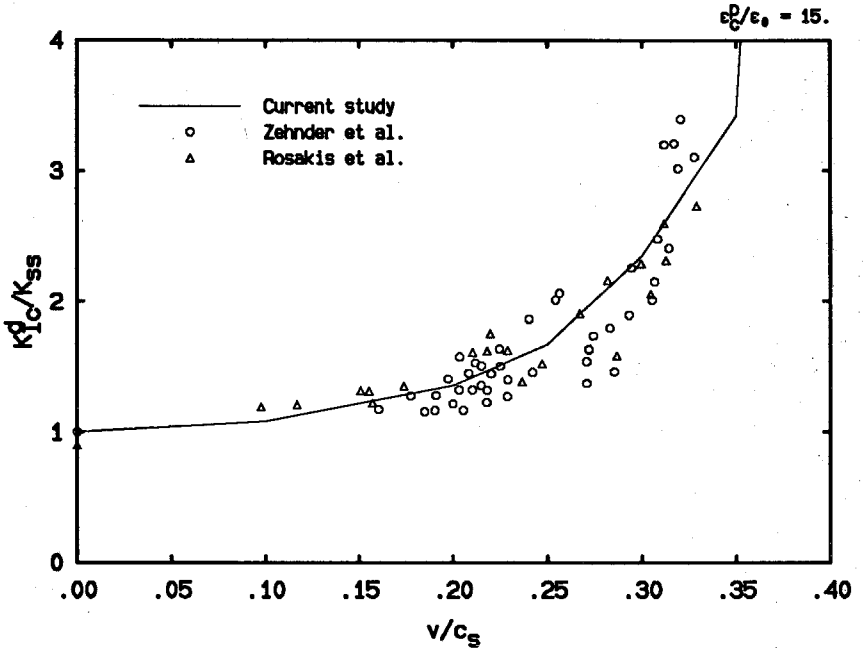

FIGURE 6.4.3 Comparison of the theoretical K_{Ic}^d vs. v relation for $\varepsilon_c^p/\varepsilon_0 = 15$ with the experimental results by Rosakis, Duffy and Freund (1984), and Zehnder and Rosakis (1990a).

Comparisons with experimental data are made in Fig. 6.4.3. Note that the results by Rosakis, Duffy and Freund (1984) and Zehnder and Rosakis (1990a) are obtained from experiments conducted on thin 4340 steel specimen of different geometries and under different loading conditions. The 4340 structural steel is heat-treated however to yield effective stress-strain relations which can be described approximately as elastic-perfectly plastic. The theoretical crack velocity dependence of the dynamic fracture toughness is obtained with the critical effective plastic strain equal to $15\varepsilon_0$. It is seen from Fig. 6.4.3 that the one-parameter theoretical curve fits the whole experimental data amazingly well. This fact seems to strongly suggest that under small-scale yielding conditions the K-criterion can still be used to characterize dynamic crack propagation in materials which fracture in a locally

ductile manner.

If the above calculation is performed between a quasi-static solution and a stationary solution using the same critical plastic strain value, then the ratio between the fracture toughness for fracture initiation and the toughness for steady state quasi-static crack growth can be obtained. For example, if we use our quasi-static solution and the solution by Narasimhan and Rosakis (1988) for the stationary case, the fracture initiation toughness will be approximately 0.62 times the quasi-static value K_{ss}, if $\varepsilon_c^p/\varepsilon_0$ is taken to be 15.

Finally we would like to point out that by applying the above-described procedures theoretical K_{Id}^d vs. v curves of the same character can be obtained for both linear hardening materials and power-law hardening materials. However, it is well known that void growth and coalescence in hardening solids will generally depend on the level of mean stress as well as on the level of effective plastic strain. It is clear from our finite element results that for hardening materials both of the quantities vary significantly with respect to the crack propagation velocity due to stress as well as strain singularities at the crack tip. Hence it appears that a properly modified critical plastic strain criterion, namely a criterion which includes the effect of mean stress or the triaxiality, must be used for dynamic crack propagation in hardening solids in accordance with observed physical phenomena. A modification of such form was provided by McClintock (1968) and was used for Mode I plane strain quasi-static crack growth in a demonstrative manner by Lam (1982), who in his thesis pointed out some difficulties in applying this criterion. It is felt by the current author that more studies are needed as to the appropriateness of this modified criterion before we employ it in an actual computation and interpret the results accordingly.

CHAPTER 7

EFFECTS OF NON-K-DOMINANCE

7.1 INTRODUCTION

This chapter is concerned with the effects of the nonsingular stress terms of the elastic far-field around a crack tip on the active plastic zone, on the near-tip elastic-plastic fields and on the dynamic fracture toughness vs. crack propagation speed relationship.

In the classic small-scale yielding concept (Rice, 1967, 1968a, b), it is assumed that the near-tip elastic-plastic zone is surrounded by an elastic annulus within which the stress state is dominated by the singular K-field, which is often referred to as the K-dominance. Under the K-dominance condition, the near-tip elastic-plastic stress and deformation fields are uniquely characterized by the stress intensity factor K, and their distributions can be obtained by solving an equivalent mathematical boundary layer problem such that as the distance to the crack tip approaches infinity, the K-field is realized (Rice, 1967, 1968a, b).

However, the K-dominance condition is not always achieved in practice, especially under laboratory conditions when tests on small cracked specimens often do not facilitate its existence. In such cases, a boundary layer solution based on the singular term alone certainly is not guaranteed to yield satisfatory results.

In the early seventies, Larsson and Carlsson (1973) had discovered that K-dominance does not always exist for fracture specimens of various types under static loads even within the ASTM (1970) limits specified for small-scale yielding.

They found that solutions for those test specimens from plane strain elastic-plastic finite element analyses differ from each other by 10 to 30 percent in near-tip field quantities such as the plastic zone size, which implies that a boundary layer solution based on K only will provide very inaccurate results in such cases. However, at a suggestion by Rice (see Larsson and Carlsson, 1973; and Rice, 1974), they were able to bring the boundary solution for the crack problem into agreement with the solution for a specific specimen by adding a T-term or the constant stress term—the first nonsingular term—in the Williams's expansion (Williams, 1957) to the boundary layer formulation.

More recently, the issue of K-dominance was studied by Krishnaswamy and Rosakis (1990a), and Krishnaswamy, Rosakis and Ravichandran (1990) concerning the experimental measurement of the dynamic stress intensity factor using the method of caustics, which had been one of the main experimental techniques employed in the investigation of dynamic crack propagation phenomena. They showed that this method at its present stage is not capable of accurately measuring the dynamic stress intensity factor due to the lack of K-dominance near the crack tip during dynamic crack propagation. Consequently, new techniques, such as the *Coherent Gradient Sensor* (CGS) being developed (Tippur, Krishnaswamy and Rosakis, 1990a, b), must be sought in order to determine the dynamic stress intensity factor through measurements of the nonsingular terms as well as the singular term in the crack tip elastic field.

As of today, major interest in the effect of the nonsingular stress terms has been focused on the T-term only since the work of Larsson and Carlsson discussed earlier. This is mainly due to the fact that the T-term is closely related to the stress biaxiality at the front of the crack tip, which has found applications in fatigue crack growth (Leevers and Radon, 1982; Smith and Pascoe, 1983; and Brown and Miller, 1985). Theoretical and numerical approaches have since been developed for the evaluation of the elastic T-term (Leevers and Radon, 1982; Cardew, Goldthorpe,

Howard and Kfouri, 1985; and Kfouri, 1986). A static plane stress finite element study of the biaxial stress effects on the elastic-plastic crack tip displacement fields was completed not long ago by Nicoletto (1988).

In previous chapters, several aspects of steady state dynamic crack propagation in elastic-plastic solids under Mode I plane stress and small-scale yielding conditions have been explored in great detail. To substantiate the earlier findings regarding the near-tip asymptotic field variations and the theoretical dynamic fracture toughness versus crack propagation speed relationship, as well as to assess the influence of the nonsingular stress terms in these areas, a modified boundary layer formulation with a multiterm elastic far-field is performed with the finite element method. The result of this investigation is documented in the following.

7.2 MULTITERM BOUNDARY LAYER FORMULATION

For steady state dynamic crack propagation in linearly elastic solids under Mode I plane deformation conditions, the stress field near the crack tip can be expressed in terms similar to a Williams's series expansion (Williams, 1957) composed of eigen-functions as (see Radok, 1956; and Nishioka and Atluri, 1983)

$$\sigma_{ij} = \frac{K_I^d}{\sqrt{2\pi r}} f_{ij}(\theta, v) + T\delta_{1i}\delta_{1j} + \sum_{n=3}^{\infty} C_n r^{(n-2)/2} g_{ijn}(\theta, v), \tag{7.2.1}$$

where σ_{ij} are stress components, r and θ are the polar coordinates at the crack tip (see Fig. 1.1.1), $f_{ij}(\theta, v)$ and $g_{ijn}(\theta, v)$ are known universal functions of θ and the crack propagation speed v, T is a constant dependent on v, and δ_{ij} is the Kroneker δ symbol. In the following, we shall refer the first term in Eq.(7.2.1) as the singular term or the K-term, the second term in Eq.(7.2.1) as the first nonsingular term or the T-term, the first term under the summation symbol as the second nonsingular term, and so on. Hence a finite element study with multiterm boundary layer formulation will be defined as one which uses one or more nonsignular terms as well as the K-term of the crack tip elastic field as its boundary condition. It is

still required here that the size of the crack tip active plastic zone be small when compared to the size of the domain under consideration. A problem so formulated will be referred here as one which is under conditions of modified small-scale yielding without K-dominance.

To make a parametric study of the effects of the nonsingular stress terms on dynamic crack propagation phenomena, parameters representing the relative dominance of the nonsingular terms with respect to the K-term must be defined at a certain distance from the crack tip. In the present study, the effects of the first two nonsingular terms will be investigated. Using the notations and normalizations defined in Chapter 2, the first three leading terms of the stress and displacement field can be written as follows

$$\sigma_{11} = B\Bigg\{ \Big[(1+2\alpha_l^2-\alpha_s^2)\frac{cos(\theta_l/2)}{\sqrt{r_l}} - \frac{4\alpha_l\alpha_s}{1+\alpha_s^2}\frac{cos(\theta_s/2)}{\sqrt{r_s}}\Big] + \frac{\gamma_1}{\sqrt{L}}\Big[(1+2\alpha_l^2-\alpha_s^2) - \frac{4\alpha_l\alpha_s}{1+\alpha_s^2}\Big] + \gamma_2\Big[(1+2\alpha_l^2-\alpha_s^2)\frac{cos(\theta_l/2)}{(L/\sqrt{r_l})} - \frac{4\alpha_l\alpha_s}{1+\alpha_s^2}\frac{cos(\theta_s/2)}{(L/\sqrt{r_s})}\Big]\Bigg\}, \tag{7.2.2a}$$

$$\sigma_{22} = B\Bigg\{ \Big[-(1+\alpha_s^2)\frac{cos(\theta_l/2)}{\sqrt{r_l}} + \frac{4\alpha_l\alpha_s}{1+\alpha_s^2}\frac{cos(\theta_s/2)}{\sqrt{r_s}}\Big] + \gamma_2\Big[-(1+\alpha_s^2)\frac{cos(\theta_l/2)}{(L/\sqrt{r_l})} + \frac{4\alpha_l\alpha_s}{1+\alpha_s^2}\frac{cos(\theta_s/2)}{(L/\sqrt{r_s})}\Big]\Bigg\}, \tag{7.2.2b}$$

$$\sigma_{12} = B\Bigg\{ 2\alpha_l\Big[\frac{sin(\theta_l/2)}{\sqrt{r_l}} - \frac{sin(\theta_s/2)}{\sqrt{r_s}}\Big] - 2\alpha_l\gamma_2\Big[\frac{sin(\theta_l/2)}{(L/\sqrt{r_l})} - \frac{sin(\theta_s/2)}{(L/\sqrt{r_s})}\Big]\Bigg\}, \tag{7.2.2c}$$

$$u_1 = 4(1+\nu)B\Bigg\{ \Big[\sqrt{r_l}cos(\theta_l/2) - \frac{2\alpha_l\alpha_s}{1+\alpha_s^2}\sqrt{r_s}cos(\theta_s/2)\Big]$$

$$+\gamma_1 \frac{\left[(1+2\alpha_l^2-\alpha_s^2)-\frac{4\alpha_l\alpha_s}{1+\alpha_s^2}\right]}{4(\alpha_l^2-\alpha_s^2)}\left[(\frac{r_l}{\sqrt{L}})cos\theta_l-\frac{(1+\alpha_s^2)}{2}(\frac{r_s}{\sqrt{L}})cos\theta_s\right]$$

$$+\frac{\gamma_2}{3}\left[(\frac{r_l^{3/2}}{L})cos(3\theta_l/2)-\frac{2\alpha_l\alpha_s}{1+\alpha_s^2}(\frac{r_s^{3/2}}{L})cos(3\theta_s/2)\right]\Bigg\}, \qquad (7.2.2d)$$

$$u_2 = 4(1+\nu)B\alpha_l\Bigg\{\left[-\sqrt{r_l}sin(\theta_l/2)+\frac{2}{1+\alpha_s^2}\sqrt{r_s}sin(\theta_s/2)\right]$$

$$+\gamma_1 \frac{\left[(1+2\alpha_l^2-\alpha_s^2)-\frac{4\alpha_l\alpha_s}{1+\alpha_s^2}\right]}{4(\alpha_l^2-\alpha_s^2)}\left[-(\frac{r_l}{\sqrt{L}})sin\theta_l+\frac{(1+\alpha_s^2)}{2\alpha_l\alpha_s}(\frac{r_s}{\sqrt{L}})sin\theta_s\right]$$

$$+\frac{\gamma_2}{3}\left[-(\frac{r_l^{3/2}}{L})sin(3\theta_l/2)+\frac{2}{1+\alpha_s^2}(\frac{r_s^{3/2}}{L})sin(3\theta_s/2)\right]\Bigg\}, \qquad (7.2.2e)$$

where the relative dominance parameters γ_1 and γ_2 are defined as the ratio of the value of the first and the second nonsingular terms, respectively, of the stress component σ_{11} to that of the K-term of σ_{11} at location $\theta = 0^0$ and $r = L(K/\sigma_0)^2$, with L being a dimensionless constant. For the definitions of all other symbols, see section 2.2 of Chapter 2.

Similarly, displacement spatial derivatives with respect to x_1 can be obtained as follows:

$$\frac{\partial u_1}{\partial x_1} = 2(1+\nu)B\Bigg\{\left[\frac{cos(\theta_l/2)}{\sqrt{r_l}}-\frac{2\alpha_l\alpha_s}{1+\alpha_s^2}\frac{cos(\theta_s/2)}{\sqrt{r_s}}\right]$$

$$+\frac{\gamma_1}{\sqrt{L}}\frac{\left[(1+2\alpha_l^2-\alpha_s^2)-\frac{4\alpha_l\alpha_s}{1+\alpha_s^2}\right](1-\alpha_s^2)}{4(\alpha_l^2-\alpha_s^2)}$$

$$+\gamma_2\left[\frac{cos(\theta_l/2)}{(L/\sqrt{r_l})}-\frac{2\alpha_l\alpha_s}{1+\alpha_s^2}\frac{cos(\theta_s/2)}{(L/\sqrt{r_s})}\right]\Bigg\}, \qquad (7.2.3a)$$

$$\frac{\partial u_2}{\partial x_1} = 2(1+\nu)B\Bigg\{\left[\alpha_l\frac{sin(\theta_l/2)}{\sqrt{r_l}}-\frac{2\alpha_l}{1+\alpha_s^2}\frac{sin(\theta_s/2)}{\sqrt{r_s}}\right]$$

$$-\gamma_2\left[\alpha_l\frac{sin(\theta_l/2)}{(L/\sqrt{r_l})}-\frac{2\alpha_l}{1+\alpha_s^2}\frac{sin(\theta_s/2)}{(L/\sqrt{r_s})}\right]\Bigg\}. \qquad (7.2.3b)$$

In the current computation, the dimensionless constant L is chosen as the normalized finite element mesh size which is 4.5 as seen from Fig. 2.3.1. Hence, the parameters γ_1 and γ_2 are actually defined for σ_{11} at the lower right corner of the rectangular domain. To ensure non-K-dominance, the maximum values of γ_1 and γ_2 must be on the order of one. Moreover, for the particular mesh size employed in the boundary layer calculation, it should be checked that the K-term will not become dominant again within any elastic annulus around the crack tip with an inner radius about ten times the size of the active plastic zone.

In the study of Larsson and Carlsson (1973), the ratio of the T-term to $K/\sqrt{a}$ is estimated for several common test specimens under stationary conditions for $a = (0.15)^{-2}(K/\sigma_0)^2$. From these estimations, corresponding γ_1 values can be obtained at a distance to the crack tip of $r = 4.5(K/\sigma_0)^2$. The result is shown in Table 7.2.1.

Table 7.2.1 Values of γ_1 at $r = 4.5(K/\sigma_0)^2$ for various specimens

Case	γ_1
Center-cracked specimen	-0.470
Double edge-cracked specimen	-0.115
Bend specimen	0.0263
Compact tension specimen	0.232

An estimation for the value of the second nonsingular elastic term was recently obtained by Tippur, Krishnaswamy and Rosakis (private communication, 1990) using a newly developed optical technique, the method of coherent gradient sensing (Tippur, Krishnaswamy and Rosakis, 1990a, b). From their static test data for three-point bend specimens made of PMMA, the γ_2 parameter is estimated to be around 0.1 at the distance we defined earlier, namely at $r = 4.5(K/\sigma_0)^2$.

Considering the above factors, we decide to make a parametric study with both γ_1 and γ_2 varying within the range of $[-1.0, 1.0]$. The effects of the T-term will be

studied first for the eight sets of γ_1 values: -1.0, -0.8, -0.6, -0.4, 0.4, 0.6, 0.8 and 1.0. Then, the combined effects of the two leading nonsigular terms will be investigated for the four extreme sets of (γ_1, γ_2) values: (-1.0, -1.0), (-1.0, 1.0), (1.0, -1.0) and (1.0, 1.0).

A Poisson ratio $\nu = 0.3$ is used in all calculation. Due to the large number of computations, the coarser finite element mesh, which has a ratio of the active plastic zone size to that of the smallest near-tip element on the order of 0.8×10^4, is employed here. Most discussions will be confined to the case with a typical crack propagation speed $v = 0.3c_s$ for a typical linear hardening material with hardening parameter $\alpha = 0.4$ as well as for nonhardening materials when $\alpha = 0$. All angular field variations are along a circular path of radius $r/(K/\sigma_0)^2 = 0.6411 \times 10^{-3}$ which is five elements away from the crack tip. Note that the same circular path has been used under K-dominance conditions. Radial field variations are presented along the prospective crack line, with one data point taken from each element starting from the fifth element, if the element at the crack tip is considered as the first one.

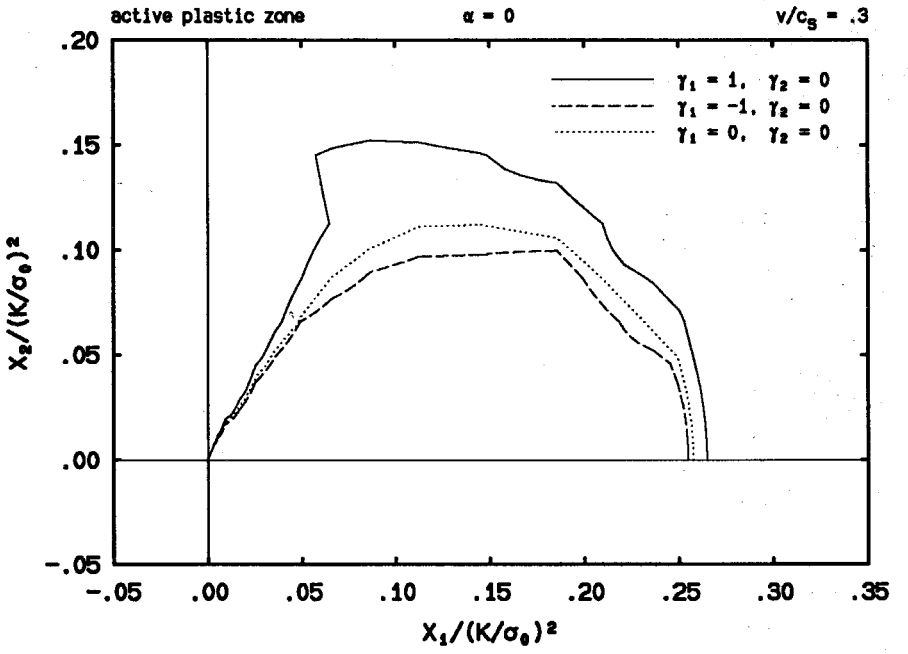

FIGURE 7.3.1a The effect of γ_1 on the shape of the crack tip active plastic zone for $\alpha = 0$ and $v/c_s = 0.3$, plotted in normalized coordinates.

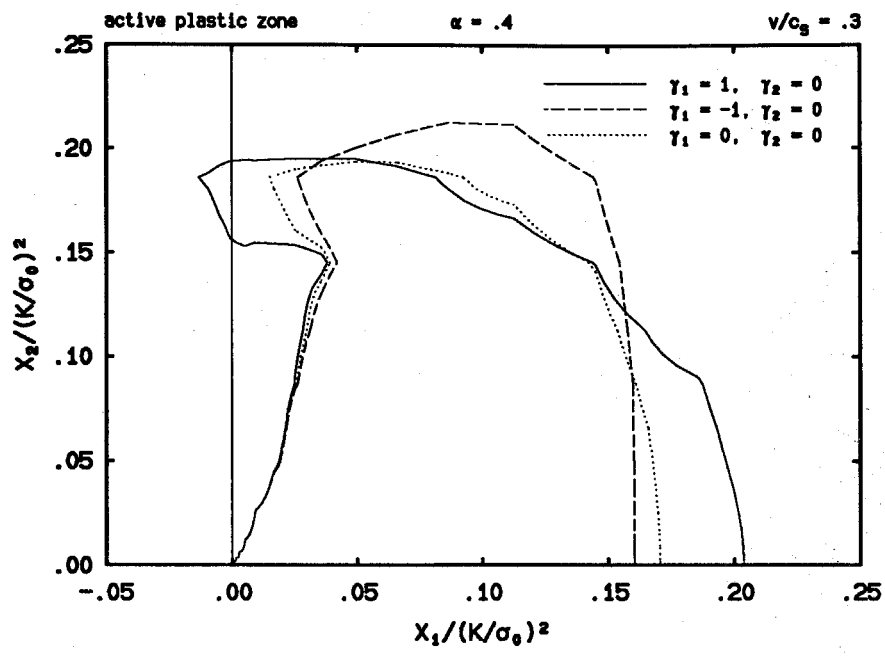

FIGURE 7.3.1b The effect of γ_1 on the shape of the crack tip active plastic zone for $\alpha = 0.4$ and $v/c_s = 0.3$, plotted in normalized coordinates.

7.3 EFFECT ON THE ACTIVE PLASTIC ZONE

The effect of the T-term or γ_1 alone on the crack tip active plastic zone is shown in Fig. 7.3.1. For convenience of discussion, let R_p and H_p denote, respectively, the horizontal and vertical extent of the active plastic zone size. In the case of a nonhardening solid when the linear hardening parameter $\alpha = 0$ (see Fig. 7.3.1a), it is seen that, compared with the K-dominance case $\gamma_1 = 0$, the overall size of the active plastic zone for $\gamma_1 = 1$ is bigger, while that for $\gamma_1 = -1$ is smaller. In the hardening case $\alpha = 0.4$ (see Fig. 7.3.1b), however, the variations are more complicated. For $\gamma_1 = 1$, R_p is much larger than that for $\gamma_1 = 0$ whereas H_p is found to be approximately the same as that for $\gamma_1 = 0$. For $\gamma_1 = -1$, R_p is smaller than that for $\gamma_1 = 0$ and H_p is much larger than that for $\gamma_1 = 0$. A more detailed, more continuous description of the variations of R_p and H_p with respect to γ_1 for both $\alpha = 0$ and 0.4 is presented in Fig. 7.3.1c.

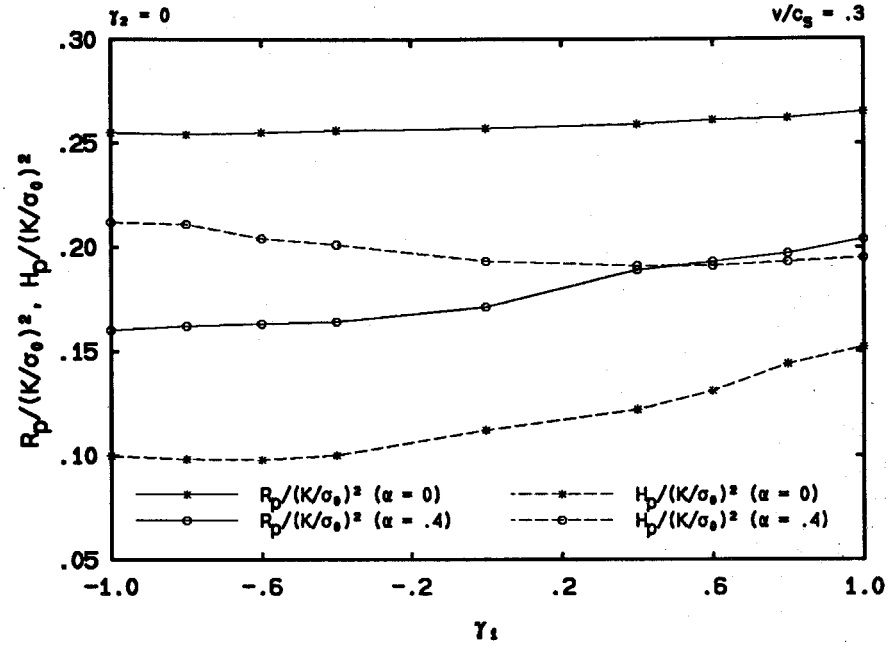

FIGURE 7.3.1c Variations of the normalized horizontal size R_p and vertical size H_p of the crack tip active plastic zone with respect to γ_1 for $\alpha = 0$ and 0.4 and for $v/c_s = 0.3$.

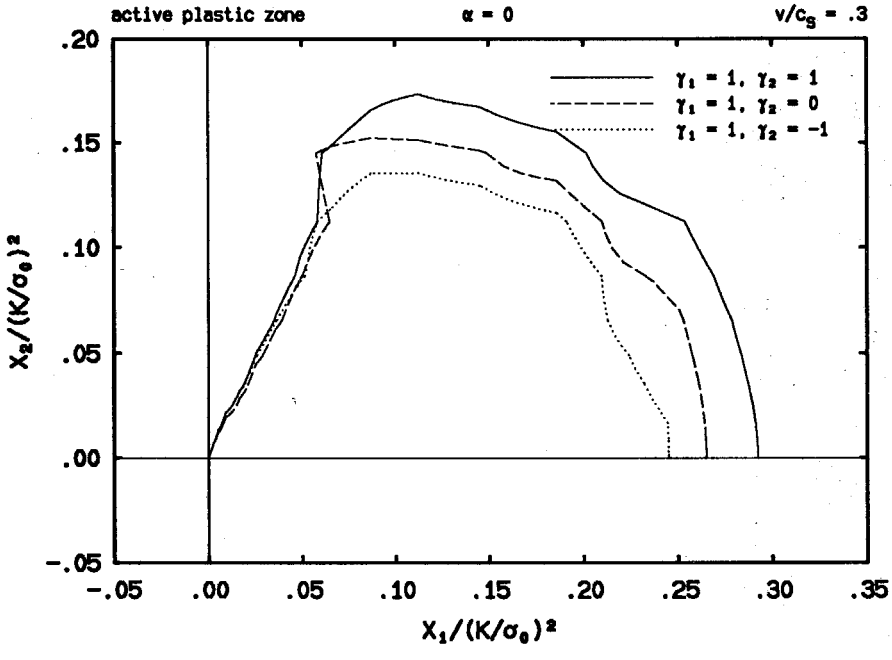

FIGURE 7.3.2a The effect of γ_2 at $\gamma_1 = 1$ on the shape of the crack tip active plastic zone for $\alpha = 0$ and $v/c_s = 0.3$, plotted in normalized coordinates.

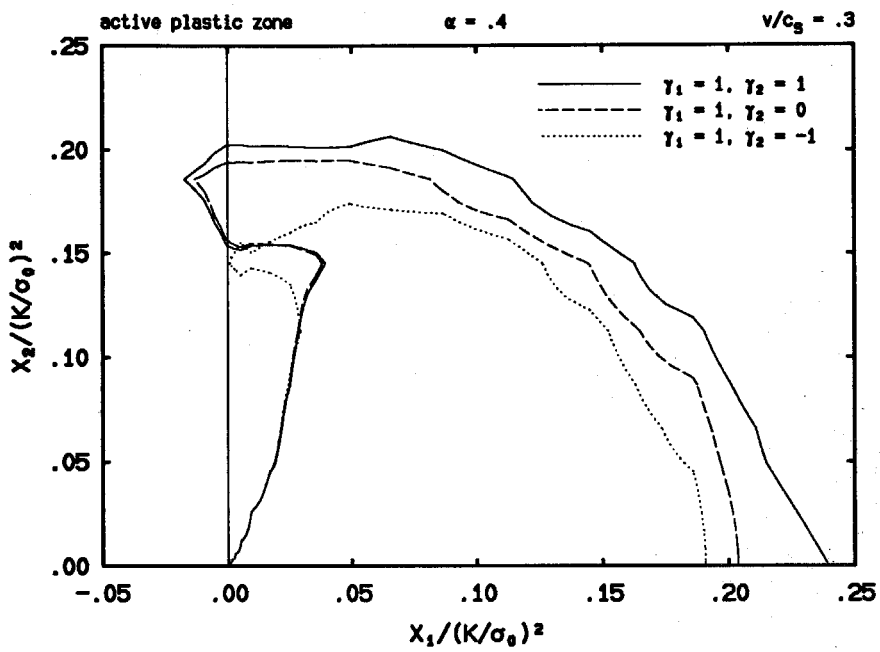

FIGURE 7.3.2b The effect of γ_2 at $\gamma_1 = 1$ on the shape of the crack tip active plastic zone for $\alpha = 0.4$ and $v/c_s = 0.3$, plotted in normalized coordinates.

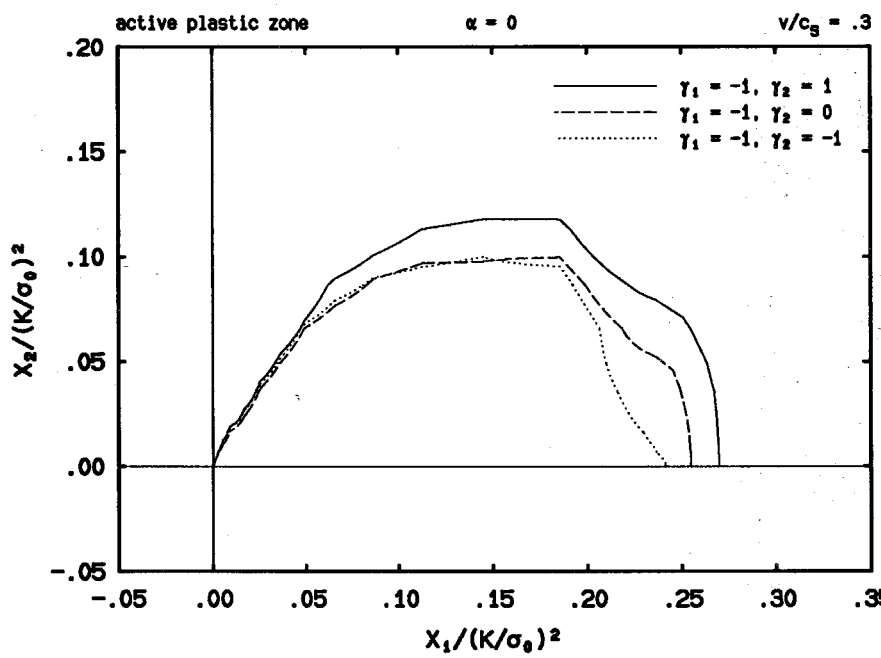

FIGURE 7.3.3a The effect of γ_2 at $\gamma_1 = -1$ on the shape of the crack tip active plastic zone for $\alpha = 0$ and $v/c_s = 0.3$, plotted in normalized coordinates.

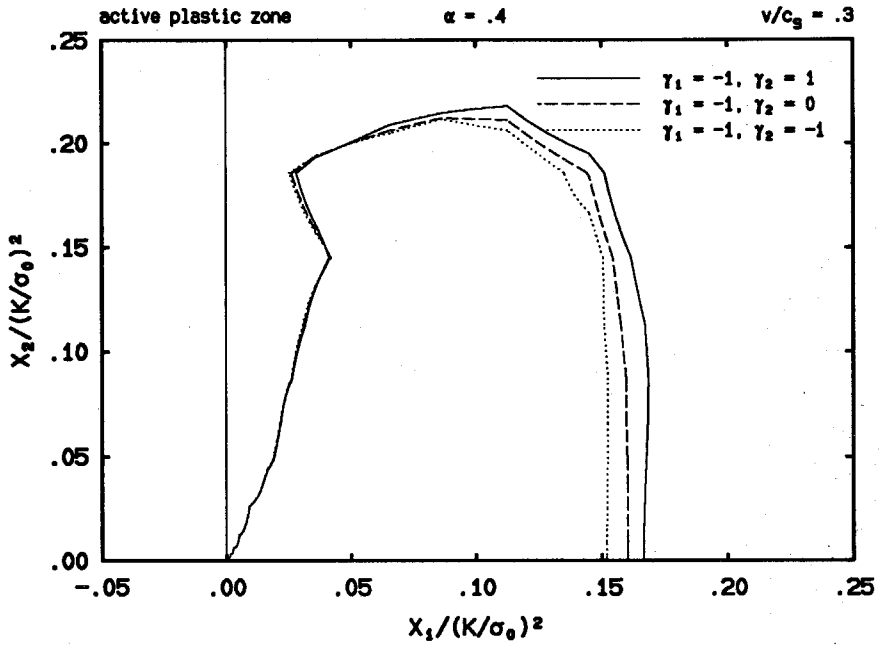

FIGURE 7.3.3b The effect of γ_2 at $\gamma_1 = -1$ on the shape of the crack tip active plastic zone for $\alpha = 0.4$ and $v/c_s = 0.3$, plotted in normalized coordinates.

Shown in Figs. 7.3.2 and 7.3.3 are the combined effects of the first two nonsingular elastic far-field terms or γ_1 and γ_2 on the crack tip active plastic zone for $\gamma_1 = 1$ and $\gamma_1 = -1$, respectively. It is consistently observed that the overall size of the active plastic zone at the two fixed γ_1 values respectively increases as γ_2 increases both for nonhardening materials and for hardening materials.

From the above findings it can be said that the shape as well as the size of the crack tip active plastic zone are quite sensitive to the relative values of the nonsingular elastic terms with respect to that of the singular term. Hence, any estimation based on the K-term alone should be interpreted carefully.

7.4 EFFECT ON THE ANGULAR FIELD VARIATIONS

The effect of γ_1 alone on the angular stress variations is shown in Fig. 7.4.1a and b for $\alpha = 0$ and $\alpha = 0.4$, respectively, at crack propagation $v/c_s = 0.3$. It is observed

that, along the same circular path $r = 0.6411 \times 10^{-3}(K/\sigma_0)^2$ around the crack tip as used under K-dominance conditions, the stress curves are almost identical, which indicates that the T-term on the remote elastic boundary has little influence on the crack tip asymptotic stress field. This point can be further demonstrated from Figs. 7.4.2a and 7.4.2b where the combined effect of γ_1 and γ_2 is illustrated for $\alpha = 0$ and 0.4, respectively. Little difference is found among the stress variations corresponding to different γ_1 and γ_2 values except for the case of $\alpha = 0$ (see Fig. 7.4.2a) where the σ_{11} and σ_{22} curves for $\gamma_1 = 0$ and $\gamma_2 = 0$ are singled out. Yet it must be noted that even in this case the differences are small and that the stress curves for all other γ_1 and γ_2 values almost coincide with one another.

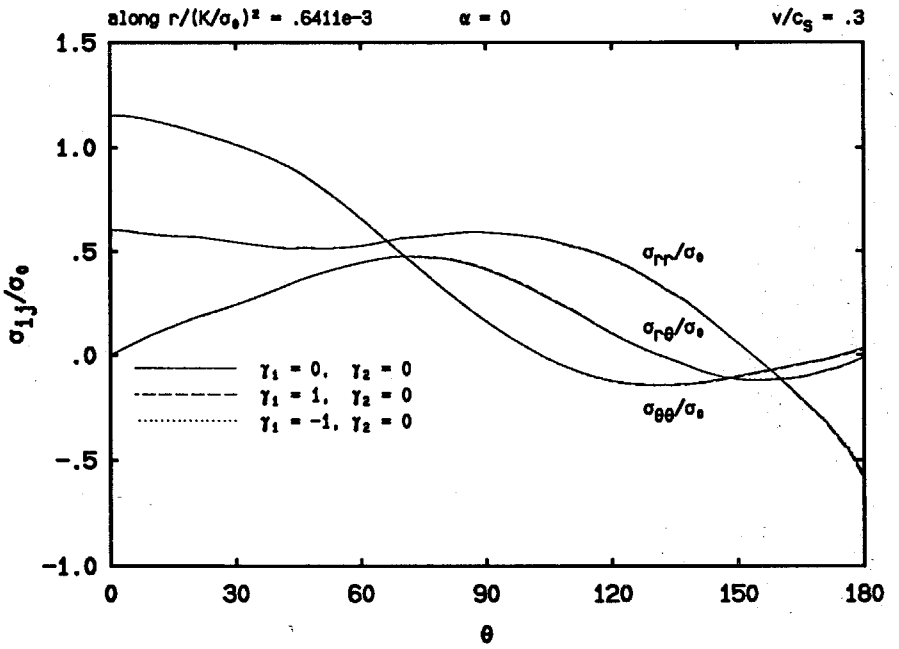

FIGURE 7.4.1a The effect of γ_1 on the angular variations of the polar stress components for $\alpha = 0$ and $v/c_s = 0.3$.

The nonsingular elastic terms are observed to have larger influence on the angular plastic strain variations when compared to those of stresses, as shown in Figs. 7.4.3 and 7.4.4. For example, with the addition of the T-term to the far-field boundary, the relative differences in the magnitude of the effective plastic strain are

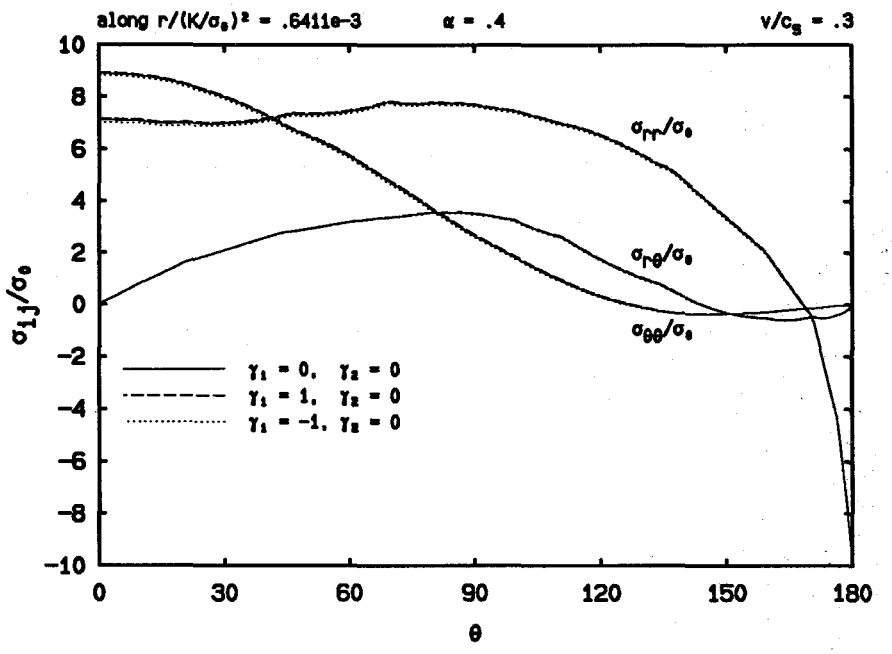

FIGURE 7.4.1b The effect of γ_1 on the angular variations of the polar stress components for $\alpha = 0.4$ and $v/c_s = 0.3$.

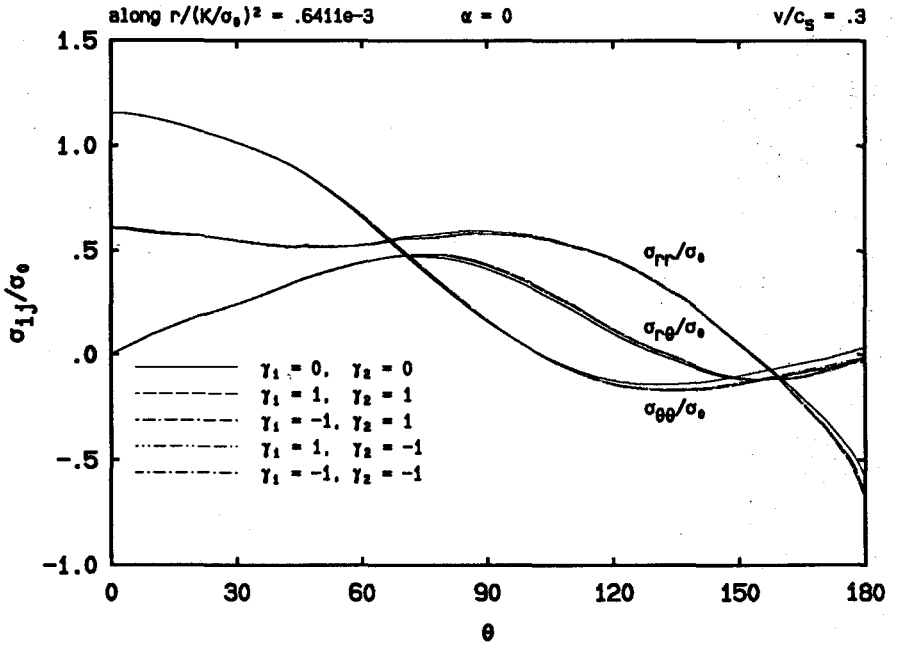

FIGURE 7.4.2a The combined effect of γ_1 and γ_2 on the angular variations of the polar stress components for $\alpha = 0$ and $v/c_s = 0.3$.

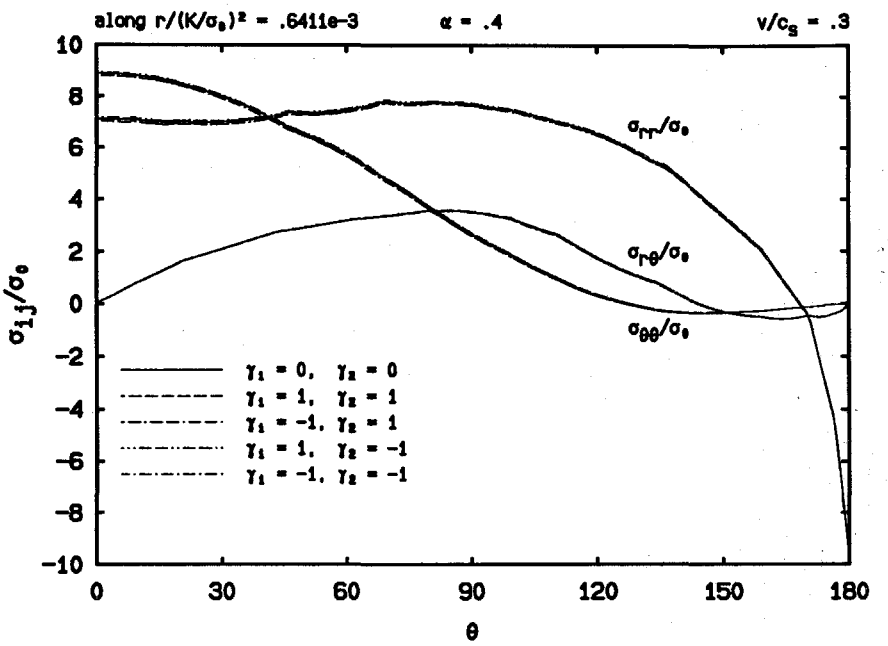

FIGURE 7.4.2b The combined effect of γ_1 and γ_2 on the angular variations of the polar stress components for $\alpha = 0.4$ and $v/c_s = 0.3$.

found to be less than $\pm 3\%$. Moreover, with the addition of both of the nonsingular terms to the far-field elastic boundary, the relative differences are within the range of -0.42% to -7.9%. However, it is discovered that the actual θ-dependence of the plastic strain components are very much the same in all the cases.

It is also worth pointing out that the plastic strain curves corresponding to the same γ_1 values are found to be very close to each other. This tendency can be even more clearly seen from the angular velocity variations to be discussed below. In fact, those curves coincide with each other according to their γ_1 values. This behavior seems to suggest that the effect of γ_1 is dominating compared to that of γ_2.

The effect of the nonsingular elastic terms on the angular variations of the Cartesian velocity component v_2 is consistently very small, as demonstrated in Figs. 7.4.5 and 7.4.6. However, it is interesting to note that the effect of γ_1 and γ_2

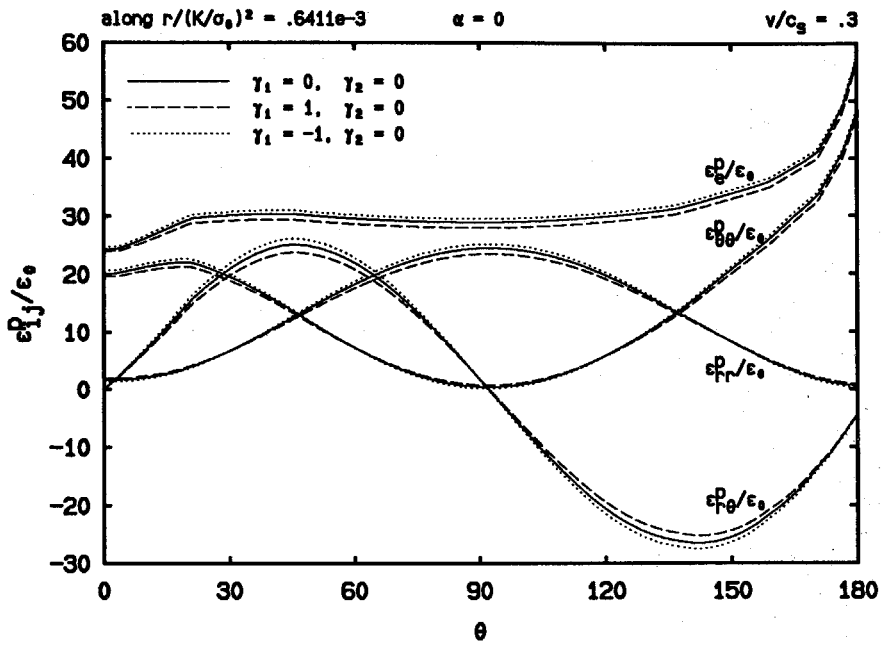

FIGURE 7.4.3a The effect of γ_1 on the angular variations of the effective plastic strain and the polar plastic strain components for $\alpha = 0$ and $v/c_s = 0.3$.

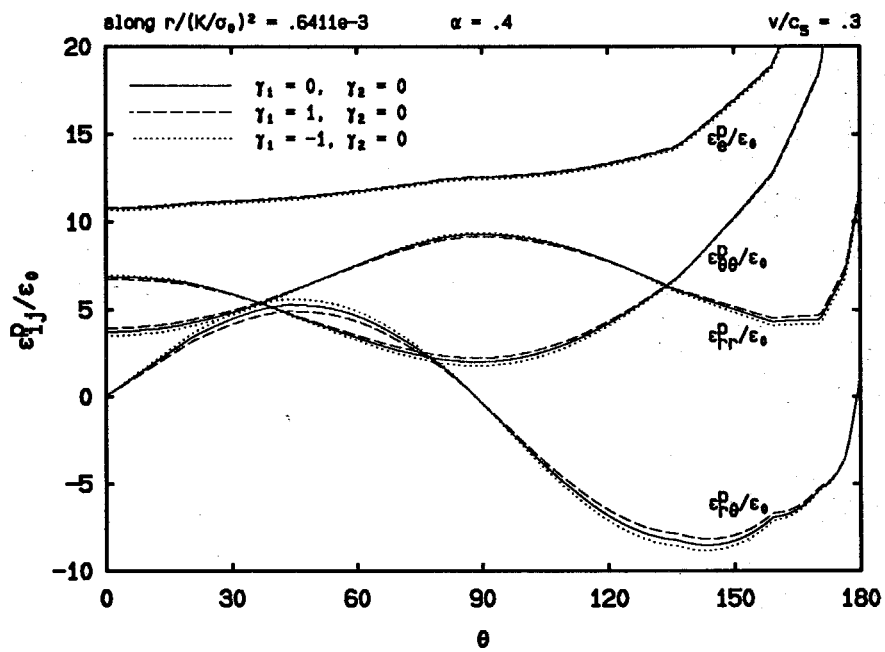

FIGURE 7.4.3b The effect of γ_1 on the angular variations of the effective plastic strain and the polar plastic strain components for $\alpha = 0.4$ and $v/c_s = 0.3$.

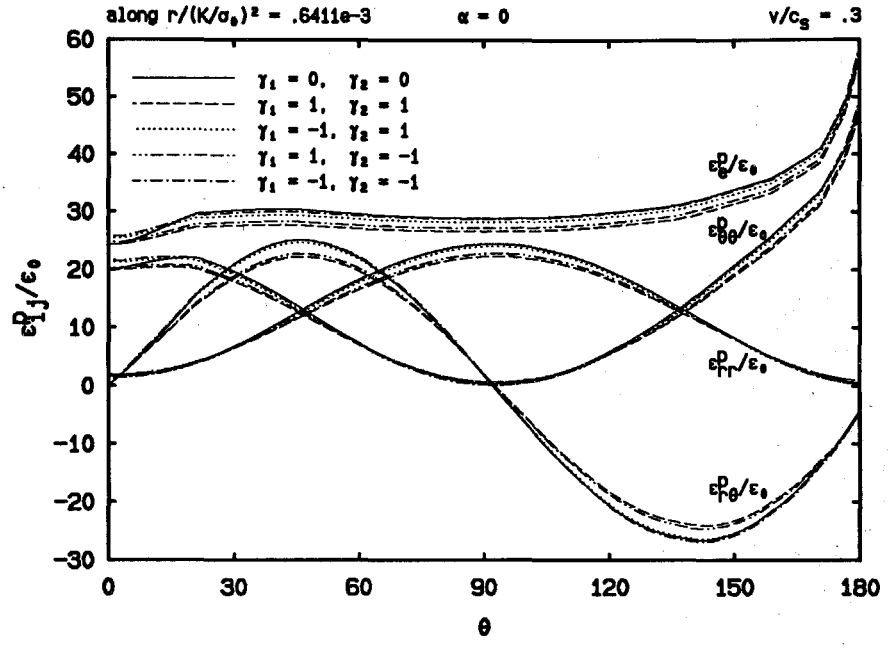

FIGURE 7.4.4a The combined effect of γ_1 and γ_2 on the angular variations of the effective plastic strain and the polar plastic strain components for $\alpha = 0$ and $v/c_s = 0.3$.

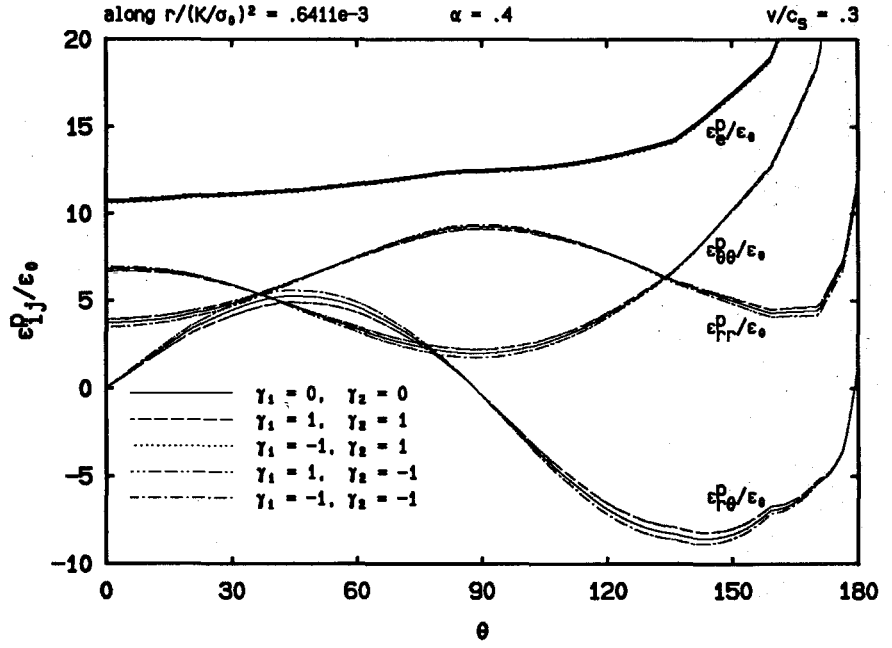

FIGURE 7.4.4b The combined effect of γ_1 and γ_2 on the angular variations of the effective plastic strain and the polar plastic strain components for $\alpha = 0.4$ and $v/c_s = 0.3$.

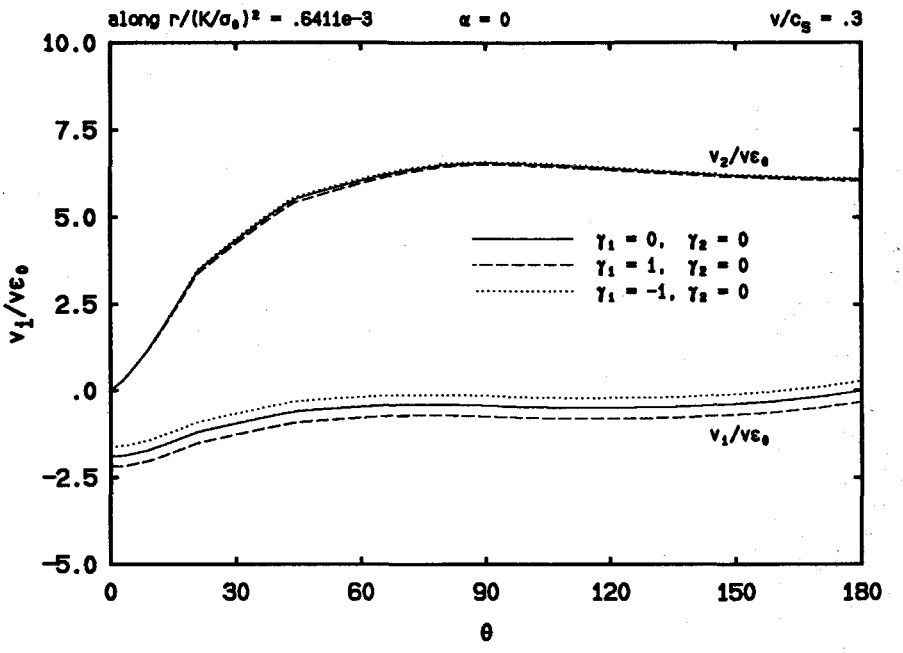

FIGURE 7.4.5a The effect of γ_1 on the angular variations of the Cartesian velocity components for $\alpha = 0$ and $v/c_s = 0.3$.

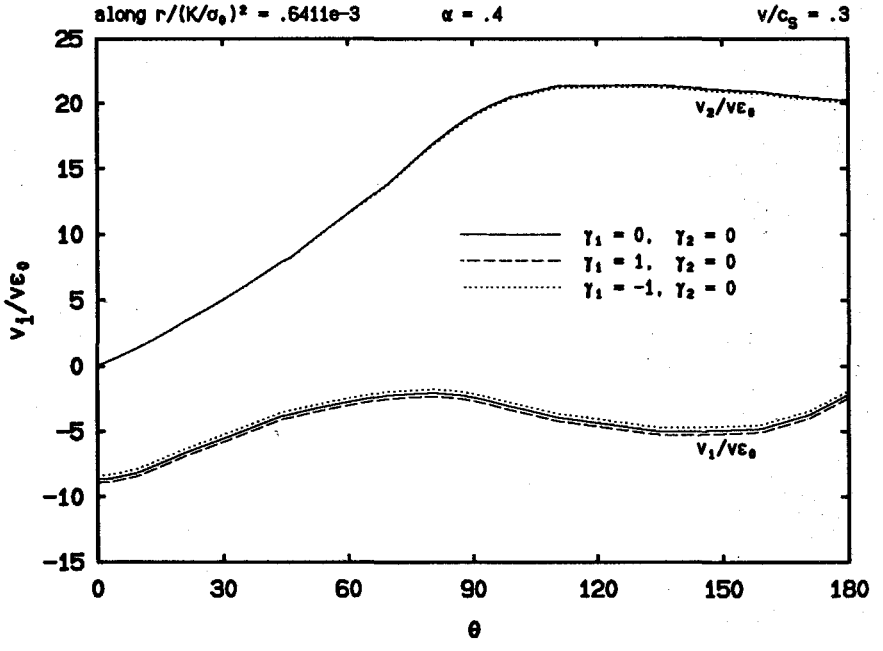

FIGURE 7.4.5b The effect of γ_1 on the angular variations of the Cartesian velocity components for $\alpha = 0.4$ and $v/c_s = 0.3$.

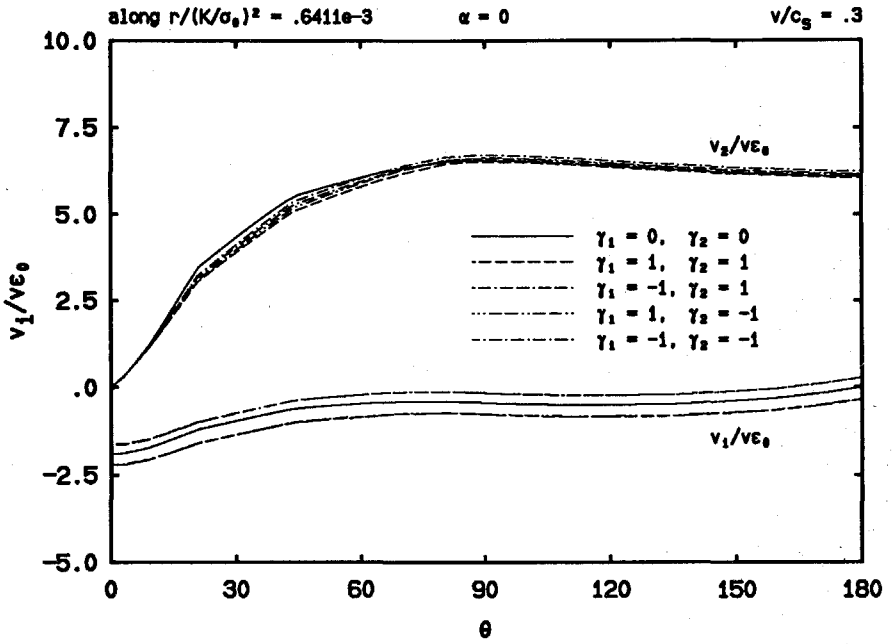

FIGURE 7.4.6a The combined effect of γ_1 and γ_2 on the angular variations of the Cartesian velocity components for $\alpha = 0$ and $v/c_s = 0.3$.

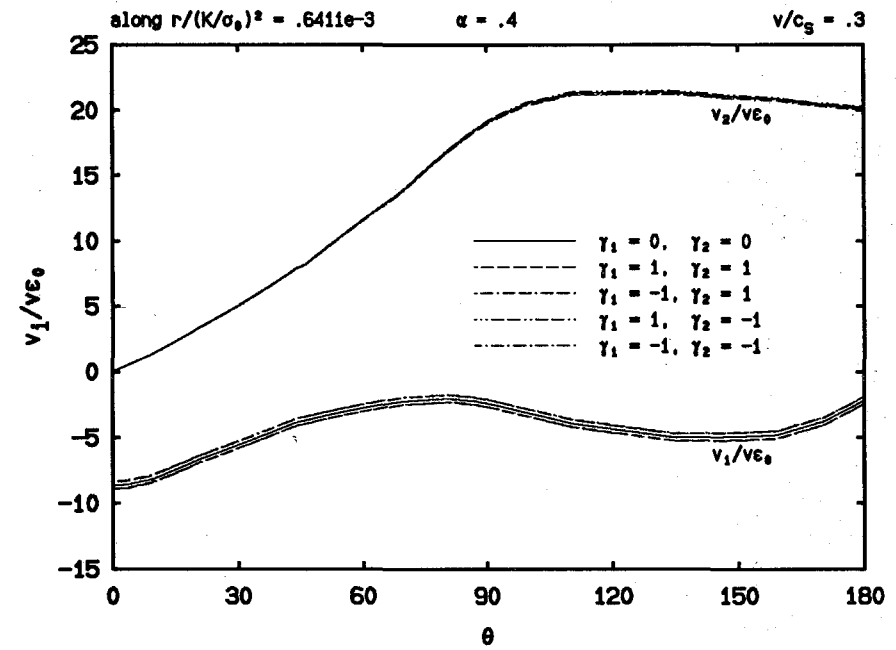

FIGURE 7.4.6b The combined effect of γ_1 and γ_2 on the angular variations of the Cartesian velocity components for $\alpha = 0.4$ and $v/c_s = 0.3$.

on the other velocity component v_1 appears to be, depending on the value of γ_1, just lowering or raising the magnitude of v_1 by an equal constant amount. Recall that during steady state crack propagation, $v_1 = -v\frac{\partial u_1}{\partial x_1} = -v\varepsilon_{11}$, then the above observation can be translated as follows. When $\gamma_1 = 1$ or when a constant tension is added parallel to the x_1 direction, the whole body is stretched accordingly in this direction, which corresponds to a positive increment in ε_{11} or a negative decrease in v_1.

7.5 EFFECT ON THE RADIAL FIELD VARIATIONS

Radial variations of the stress and plastic strain fields will be discussed only along the prospective crack line since they are of most interest there. Shown in Fig. 7.5.1 are the variations of the stress components with respect to the first non-K-dominance parameter γ_1 for the case of $\alpha = 0$. As expected, the magnitude of the 1-1 stress component σ_{11} is increased (or decreased) globally from the K-dominance solution for $\gamma_1 = 1$ (or for $\gamma_1 = -1$) which corresponds to the case that a tension (or compression) is added to the K-field on the far-field elastic boundary. At the same time, the 2-2 stress component σ_{22} is found to vary with an opposite tendency (compared to that of σ_{11}) inside the active plastic zone whose boundary is located approximately at a normalized distance of 0.26 from the crack tip. This opposite behavior of the stress components is apparently due to the requirement of the yield condition with a constant yield stress at $\alpha = 0$. However, for $\alpha = 0.4$ when the yield stress is dependent on the effective plastic strain due to strain hardening, the magnitudes of the two stress components are found to be increased or decreased at the same time (see Fig. 7.5.2), which is because the magnitude of the effective plastic strain is also increased or decreased at the same time as shown later (see Fig. 7.5.6a).

The combined effect of γ_1 and γ_2 on the radial stress variations can be observed from Figs. 7.5.3 and 7.5.4 for $\alpha = 0$ and $\alpha = 0.4$, respectively. It is discovered that

the magnitudes of the two stress components show the same increasing/decreasing tendencies depending on the value of γ_1 only. In fact, the stress curves of both σ_{11} and σ_{22} corresponding to the same γ_1 value, but different γ_2 values, are found to coincide with each other inside the active plastic zone even at locations not far away from the elastic-plastic boundary (see Fig. 7.5.3a). This observation once again suggests that the elastic T-term is the dominating nonsingular term.

Nonetheless, it can be concluded that at locations closer to the crack tip (see Figs. 7.5.1b, 7.5.2, 7.5.3b and 7.5.4), the stress values corresponding to different γ_1 and γ_2 values are approximately the same.

The effect of γ_1 alone on the plastic strain variations along the ray $\theta = 0^0$ is depicted in Fig. 7.5.5. For $\alpha = 0$, the magnitudes of the effective plastic strain ε_e^p and the plastic strain component ε_{22}^p are found to increase at $\gamma_1 = -1$ and to decrease at $\gamma_1 = 1$ when compared with their counterparts' values under K-dominance conditions. Meanwhile, as expected, the plastic strain component ε_{11}^p behaves in just the opposite way. For the case of $\alpha = 0.4$ (see Fig. 7.5.5b), however, the magnitude of ε_e^p is seen to increase as γ_1 increases although ε_{11}^p and ε_{22}^p still show the same behavior as in the case of $\alpha = 0$.

Again, as in the case of stress varaitions, it is discovered that the combined effect of γ_1 and γ_2 on the radial plastic strain variations is mainly influenced by γ_1, which is shown in Fig. 7.5.6.

It is also noted that, in any case, the effect of γ_1 and γ_2 becomes smaller as the distance to the crack tip becomes smaller.

Finally in the section the effect of the nonsingular elastic terms on the crack opening displacement will be described. In Fig. 7.5.7, the normalized vertical displacement along the crack surface is plotted against the normalized distance to the crack tip for the case of $\alpha = 0$. It is first seen that unlike the case of stress and

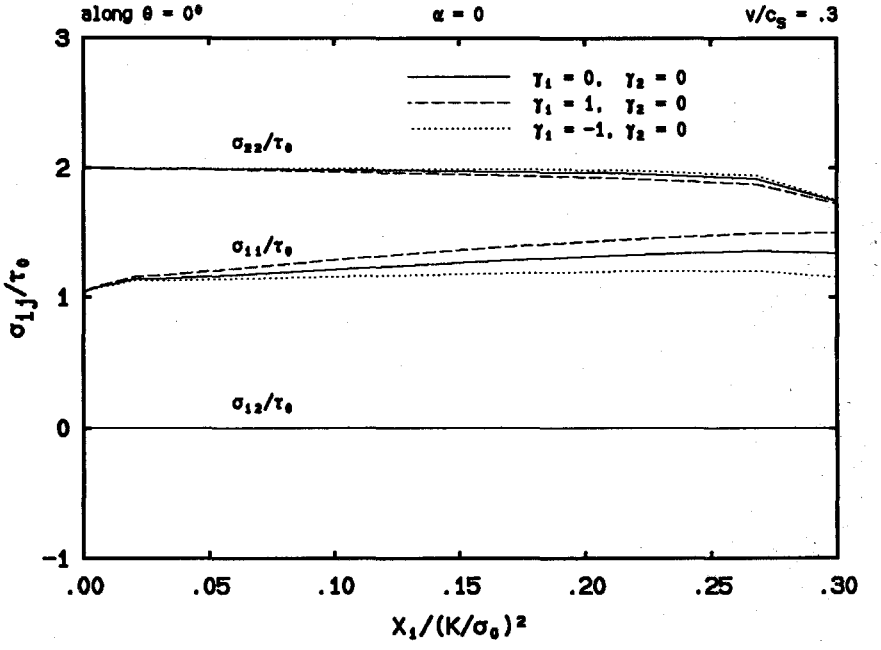

FIGURE 7.5.1a The effect of γ_1 on the radial variations of the stress components for $\alpha = 0$ and $v/c_s = 0.3$, plotted in the normalized coordinates.

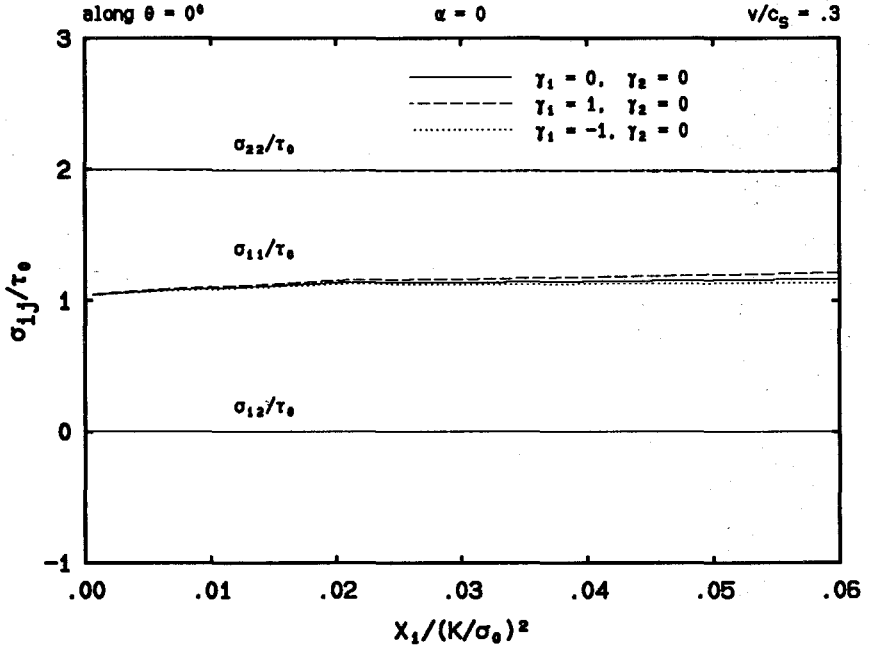

FIGURE 7.5.1b A detailed view of the effect of γ_1 on the radial variations of the stress components for $\alpha = 0$ and $v/c_s = 0.3$, plotted in the normalized coordinates.

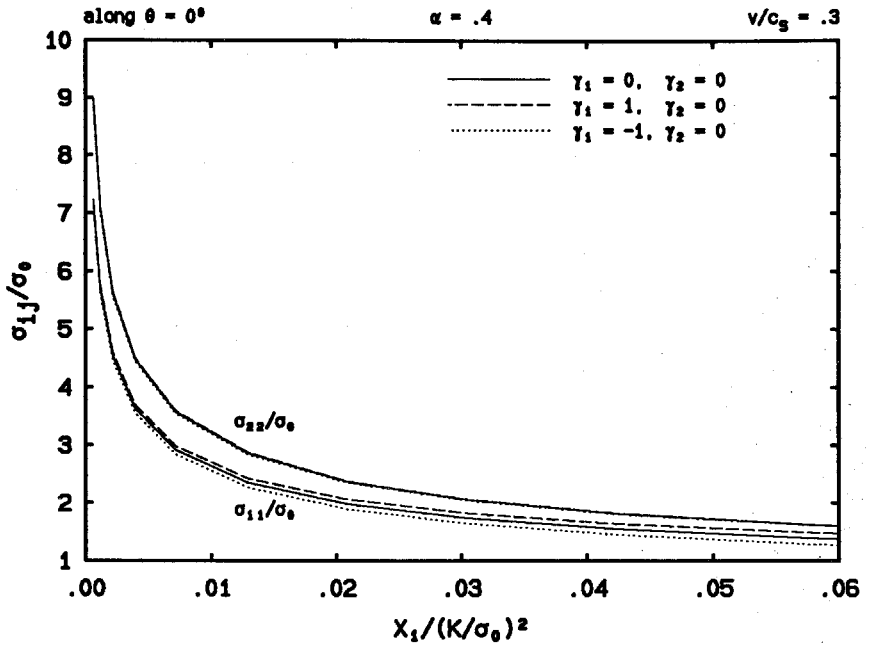

FIGURE 7.5.2 A detailed view of the effect of γ_1 on the radial variations of the stress components for $\alpha = 0.4$ and $v/c_s = 0.3$, plotted in the normalized coordinates.

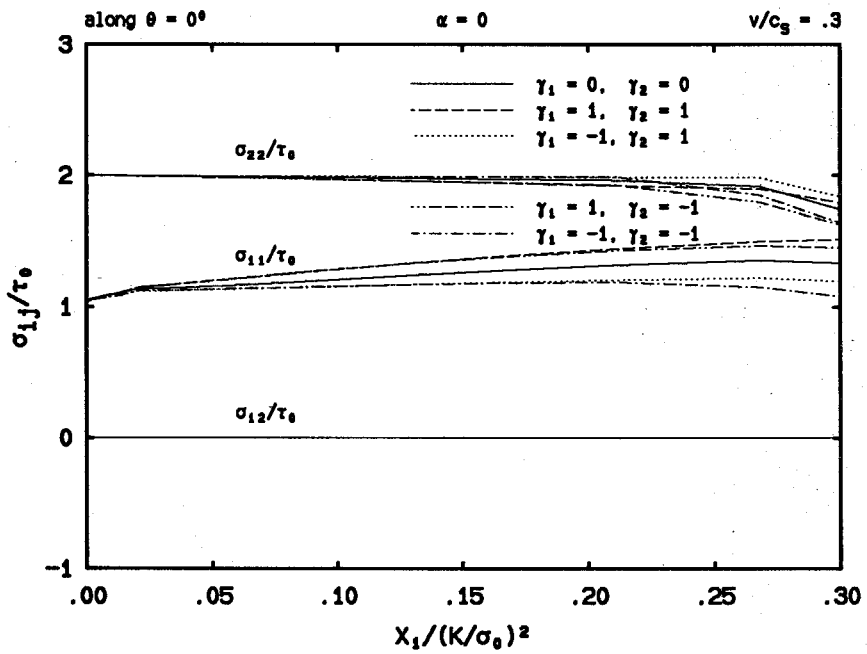

FIGURE 7.5.3a The combined effect of γ_1 and γ_2 on the radial variations of the stress components for $\alpha = 0$ and $v/c_s = 0.3$, plotted in the normalized coordinates.

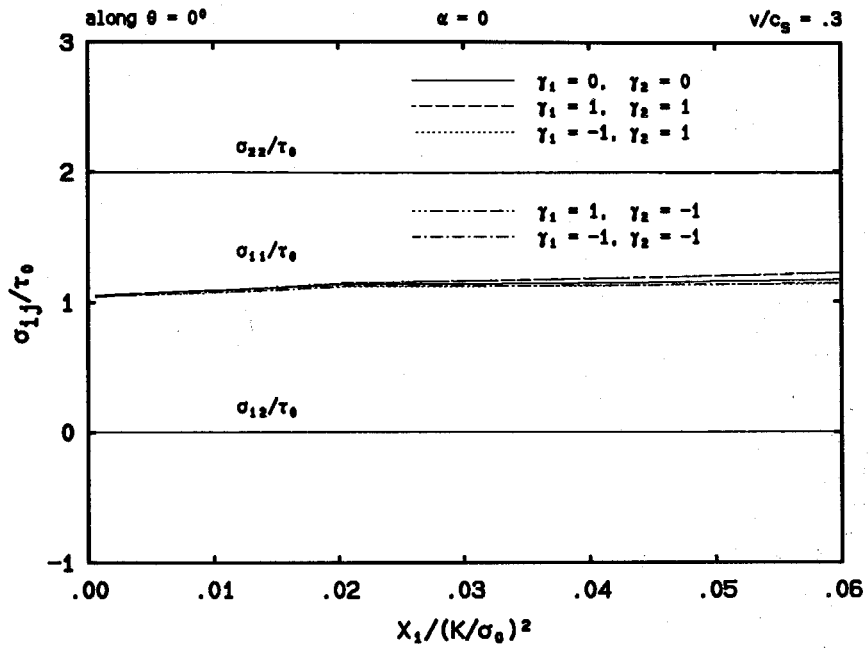

FIGURE 7.5.3b A detailed view of the combined effect of γ_1 and γ_2 on the radial variations of the stress components for $\alpha = 0$ and $v/c_s = 0.3$, plotted in the normalized coordinates.

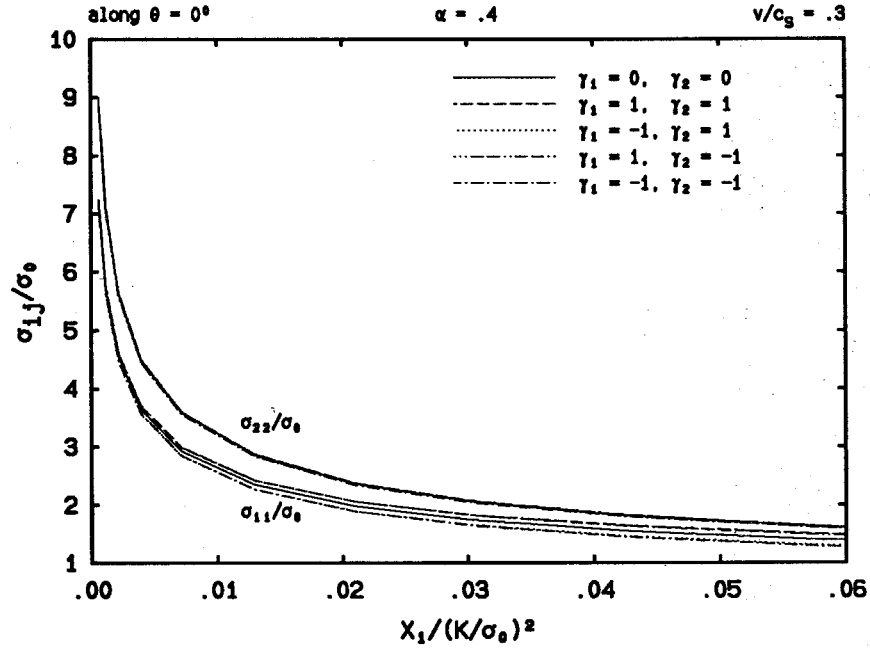

FIGURE 7.5.4 A detailed view of the combined effect of γ_1 and γ_2 on the radial variations of the stress components for $\alpha = 0.4$ and $v/c_s = 0.3$, plotted in the normalized coordinates.

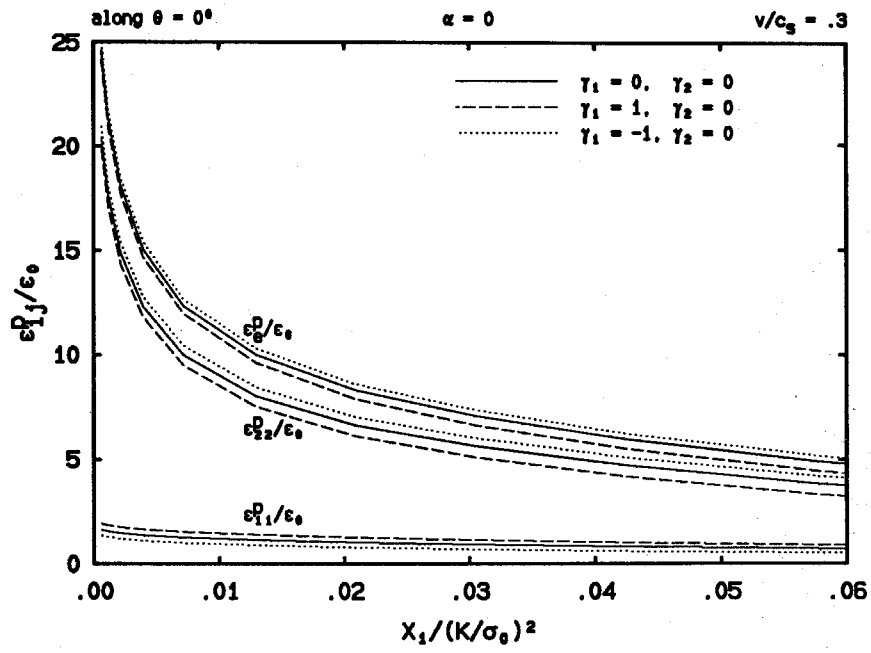

FIGURE 7.5.5a The effect of γ_1 on the radial variations of the effective plastic strain and the plastic strain components for $\alpha = 0$ and $v/c_s = 0.3$, plotted in the normalized coordinates.

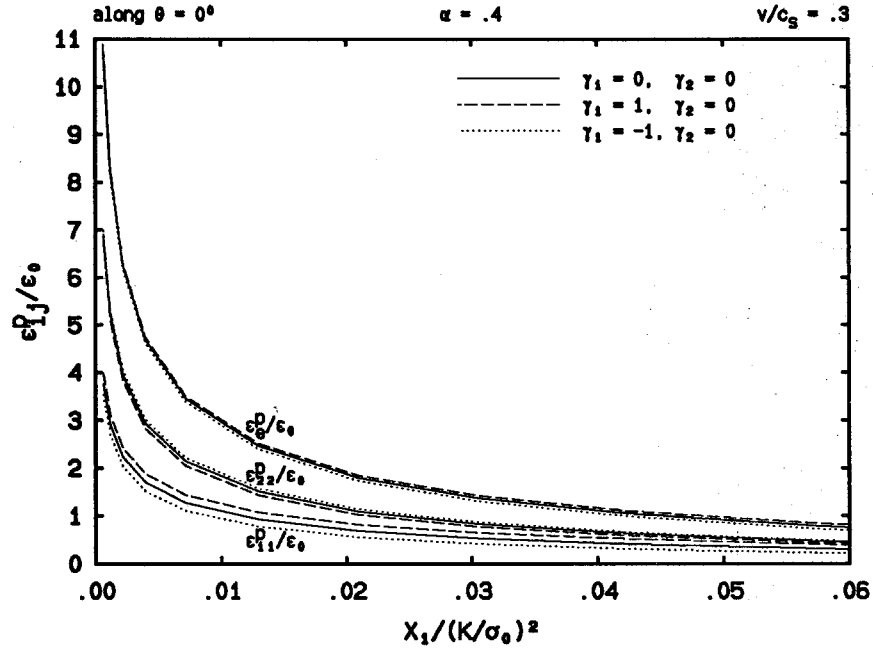

FIGURE 7.5.5b The effect of γ_1 on the radial variations of the effective plastic strain and the plastic strain components for $\alpha = 0.4$ and $v/c_s = 0.3$, plotted in the normalized coordinates.

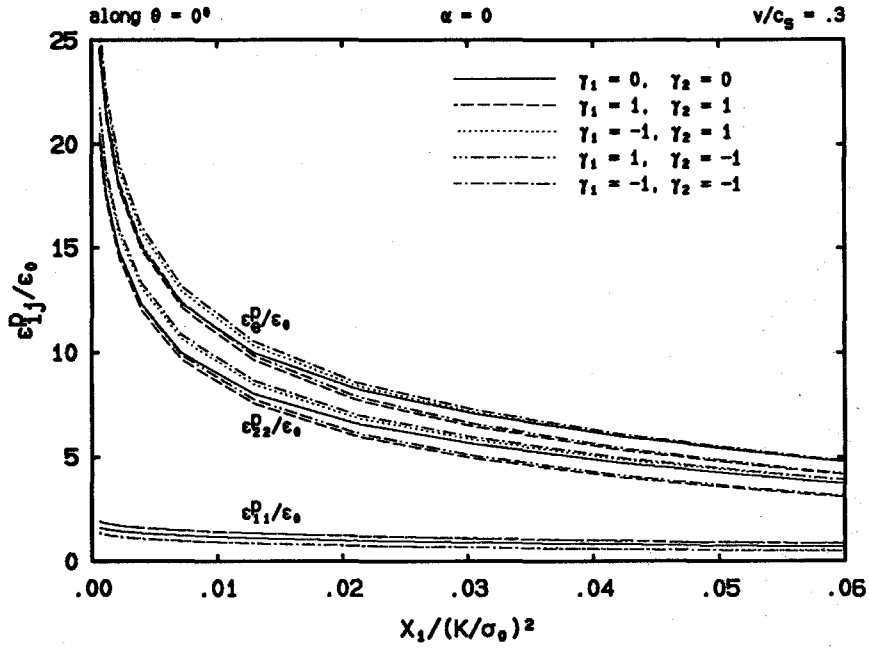

FIGURE 7.5.6a The combined effect of γ_1 and γ_2 on the radial variations of the effective plastic strain and the plastic strain components for $\alpha = 0$ and $v/c_s = 0.3$, plotted in the normalized coordinates.

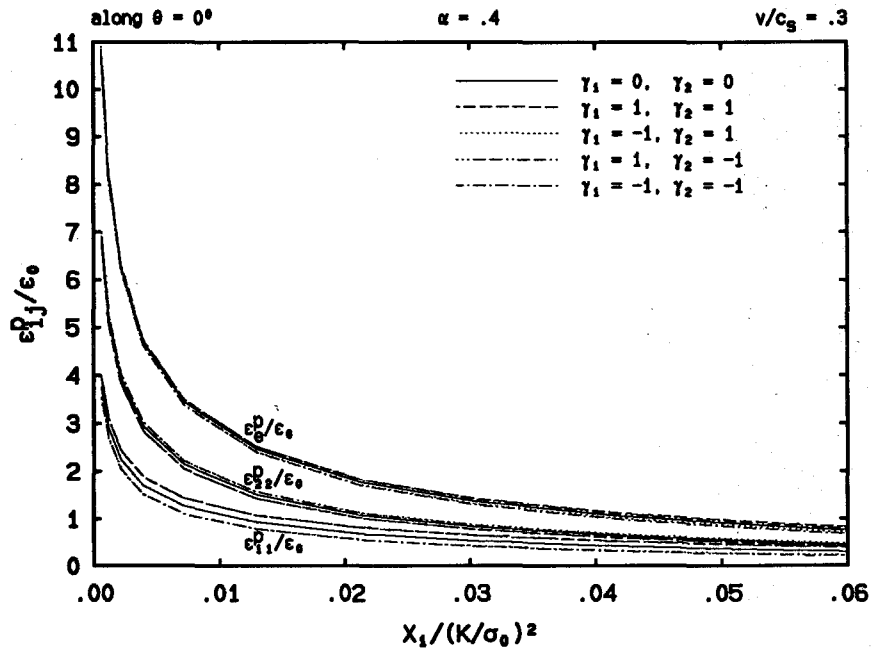

FIGURE 7.5.6b The combined effect of γ_1 and γ_2 on the radial variations of the effective plastic strain and the plastic strain components for $\alpha = 0.4$ and $v/c_s = 0.3$, plotted in the normalized coordinates.

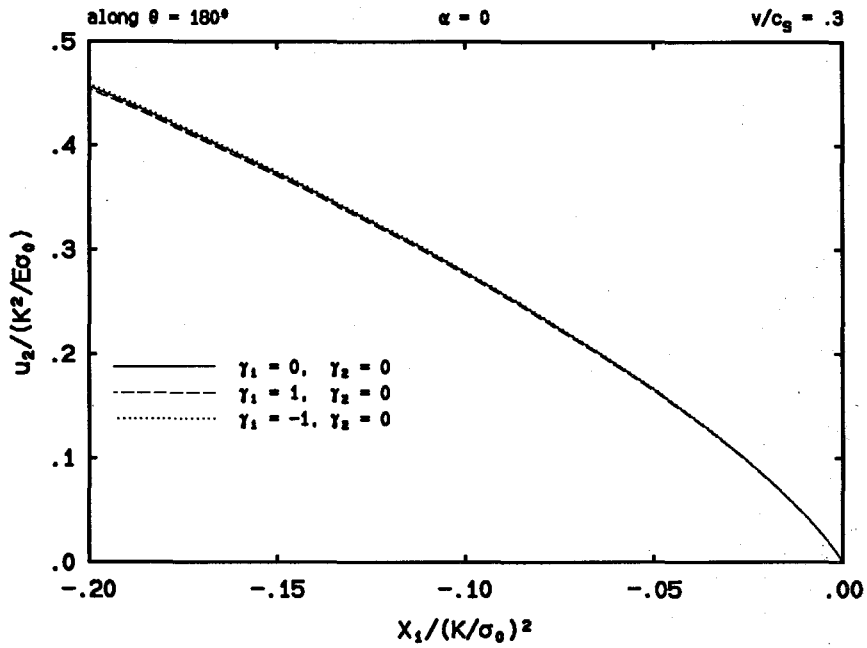

FIGURE 7.5.7a The effect of γ_1 on the radial variations of the vertical displacement component along the crack surface for $\alpha = 0$ and $v/c_s = 0.3$, plotted in the normalized coordinates.

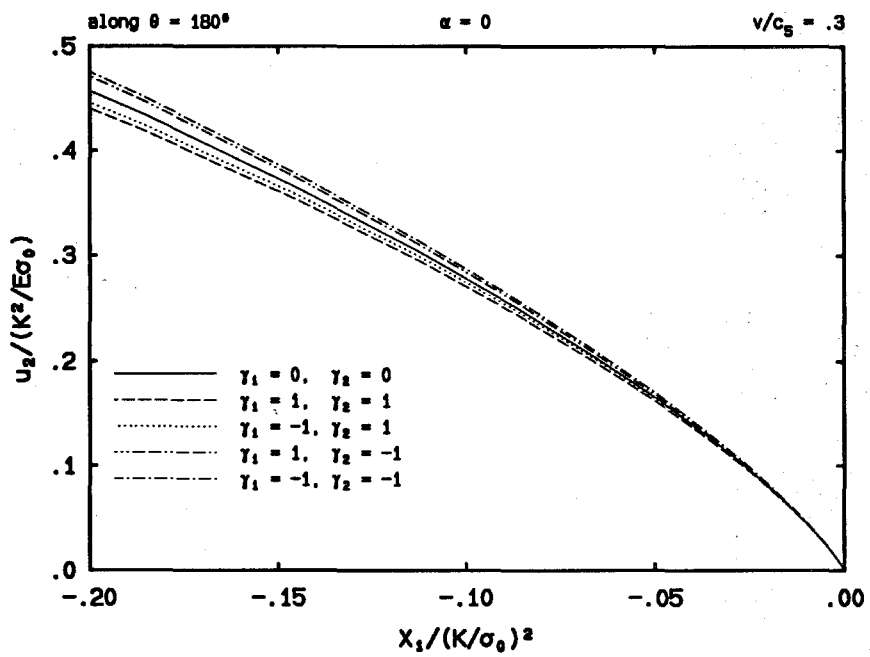

FIGURE 7.5.7b The combined effect of γ_1 and γ_2 on the radial variations of the vertical displacement component along the crack surface for $\alpha = 0$ and $v/c_s = 0.3$, plotted in the normalized coordinates.

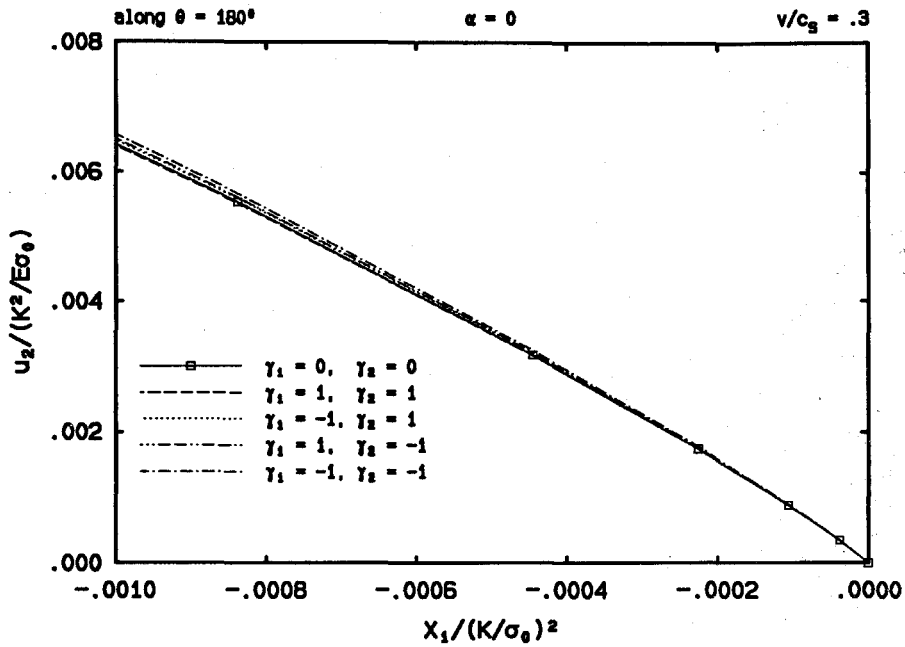

FIGURE 7.5.7c A detailed view of the combined effect of γ_1 and γ_2 on the radial variations of the vertical displacement u_2 along the crack surface for $\alpha = 0$ and $v/c_s = 0.3$, plotted in the normalized coordinates.

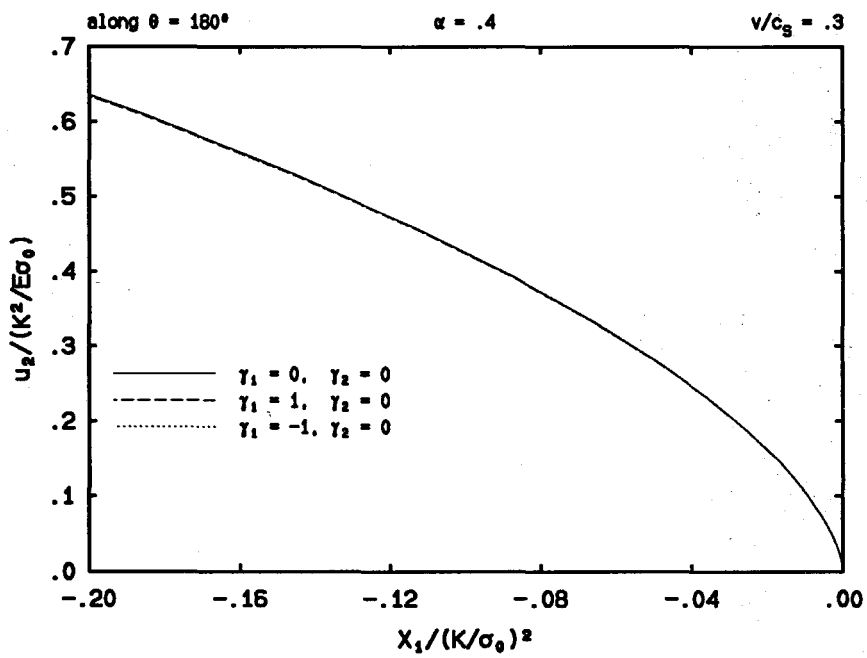

FIGURE 7.5.8a The effect of γ_1 on the radial variations of the vertical displacement component along the crack surface for $\alpha = 0.4$ and $v/c_s = 0.3$, plotted in the normalized coordinates.

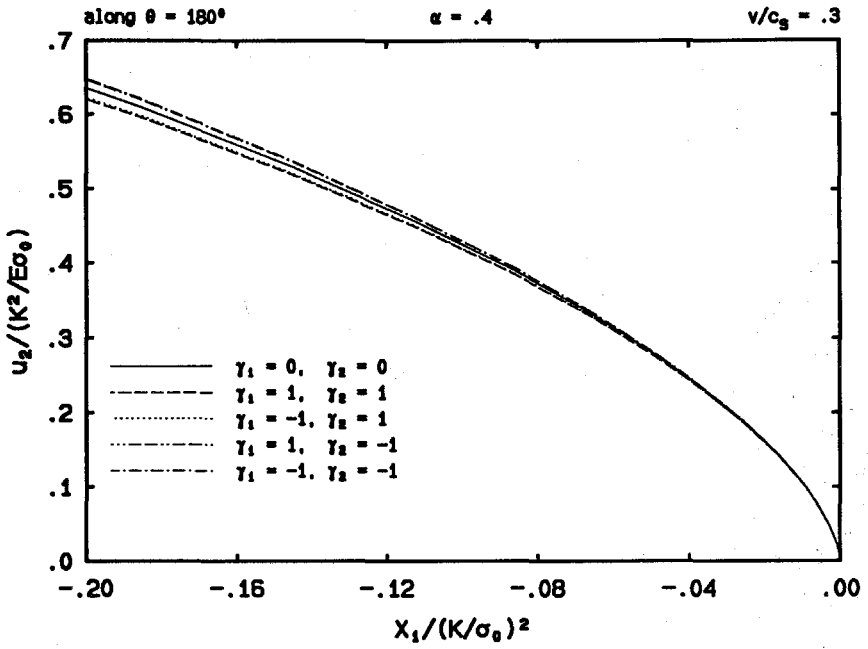

FIGURE 7.5.8b The combined effect of γ_1 and γ_2 on the radial variations of the vertical displacement component along the crack surface for $\alpha = 0.4$ and $v/c_s = 0.3$, plotted in the normalized coordinates.

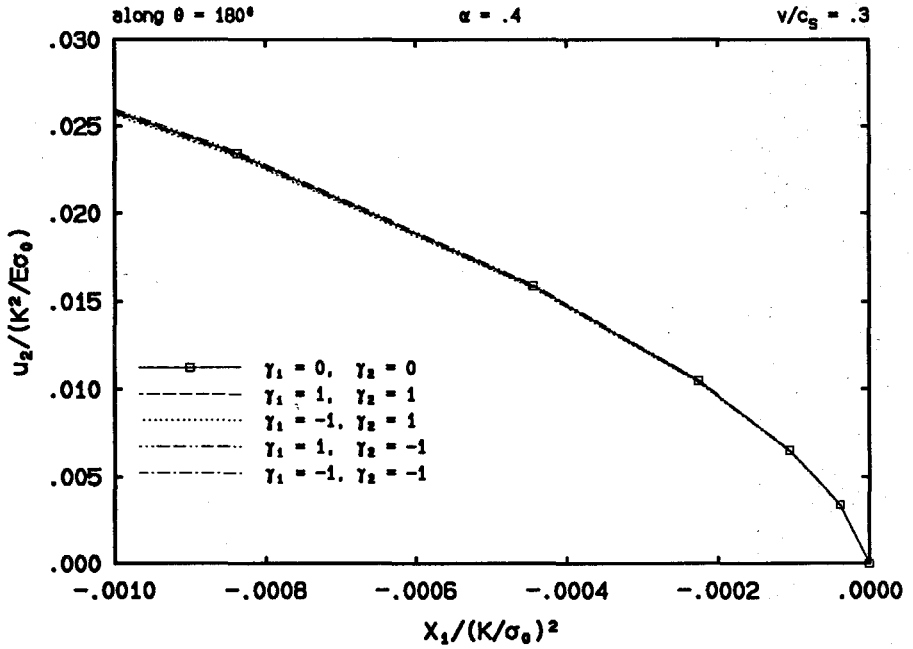

FIGURE 7.5.8c A detailed view of the combined effect of γ_1 and γ_2 on the radial variations of the vertical displacement u_2 along the crack surface for $\alpha = 0.4$ and $v/c_s = 0.3$, plotted in the normalized coordinates.

strain variations, the effect of γ_1 alone is found to be very small even at locations quite far away behind the crack tip (see Fig. 7.5.7a). Furthermore, when the second nonsingular elastic term is also added to the boundary, the magnitude of u_2 immediately changes. It is observed that whether it increases or decreases depends on the value of γ_2 instead of that of γ_1 as in the case of stress and strain variations, which appears to suggest that γ_2 is dominating here. Specifically, at $\gamma_2 = 1$, the magnitude of u_2 is decreased whereas at $\gamma_2 = -1$, it is increased, which seems to have some physical sense. Nevertheless, as the crack tip is approached, as shown in Fig. 7.5.7c, the effect of the nonsingular elastic terms is seen to disappear.

The effect of γ_1 and γ_2 for the case of $\alpha = 0.4$ is very similar to that of $\alpha = 0$ described above, except that the changes of u_2 due to the addition of nonsingular elastic terms to the remote boundary are smaller (see Fig. 7.5.8).

7.6 EFFECT ON THE K_{Ic}^d vs. v RELATIONSHIP

In Chapter 6 we have devised a scheme, after Freund and Douglas (1982), to generate, from the finite element data for the effective plastic strain, theoretical K_{Ic}^d vs. v curves (see Fig. 6.4.2) by assuming a critical plastic strain fracture criterion (McClintock, 1956, 1958; and McClintock and Irwin, 1964). Further, by setting the critical value of the plastic strain ε_c^p to fifteen times that of the initial yield strain ε_0, we demonstrated that the one-parameter theoretical K_{Ic}^d vs. v relationship was able to characterize the main features of the experimental measurements performed by Rosakis, Duffy and Freund (1984), and Zehnder and Rosakis (1990a) on thin 4340 steel plate specimens (see Fig. 6.4.3).

To assess the influence of the nonsingular elastic terms on the theoretically generated K_{Ic}^d vs. v relationship, the scheme devised in Chapter 6 is repeated here. The result of this investigation, using finite element solutions for elastic-plastic materials, is given below.

First of all, the effect of the T-term is examined through a parametric study of γ_1 in the range of [-1, 1]. Plotted in Fig. 7.6.1 are the variations of K_{Ic}^d/K_{ss} with respect to γ_1 at various normalized crack propagation speeds m, where K_{ss} is the steady state fracture toughness for quasi-static crack growth under K-dominance conditions. It is found that the relative deviation from the K-dominance is usually under 4% except that in the cases of $m = 0.1$ and $\gamma_1 = 1$, $m = 0.25$ and $\gamma_1 = 1$ and $m = 0.3$ and $\gamma = -0.8$, it reaches, respectively, 14%, 6% and 9%.

Secondly, when the K_{Ic}^d vs. v relationship is plotted in Fig. 7.6.2 using the same data, it is discovered that the experimentally observed monotonic rising tendency of K_{Ic}^d with respect to v for metal specimens is preserved.

Thirdly, when the second leading nonsingular elastic term is also added to the far-field elastic boundary, the finite element result predicts a further deviation of the normalized toughness values from those obtained under K-dominance conditions, yet with the K_{Ic}^d vs. v relationship still possessing the same characteristics, as illustrated in Fig. 7.6.3. In this case, the maximum relative deviation has been increased up to 22% which occurred for $m = 0.1$, $\gamma_1 = 1$ and $\gamma_2 = 1$.

Nonetheless, if the theoretically predicted K_{Ic}^d vs. v data are plotted together with experimental data, as shown in Fig. 7.6.4, it can be seen that the scattering of the numerical data points due to non-K-dominance is still much less pronounced than those of the experiments. Considering the fact that the present parametric study has already covered quite a large parameter value range compared with real values for some conventional test specimens (see discussions in section 7.2), it seems that the lack of K-dominance alone cannot account for the observed vast range of experimental data scattering. Instead, other factors such as the reliability of the crack propagation velocity measurement (Tippur, private communication, 1990) must be pursued.

In comparing the prediction of the finite element computation with the ex-

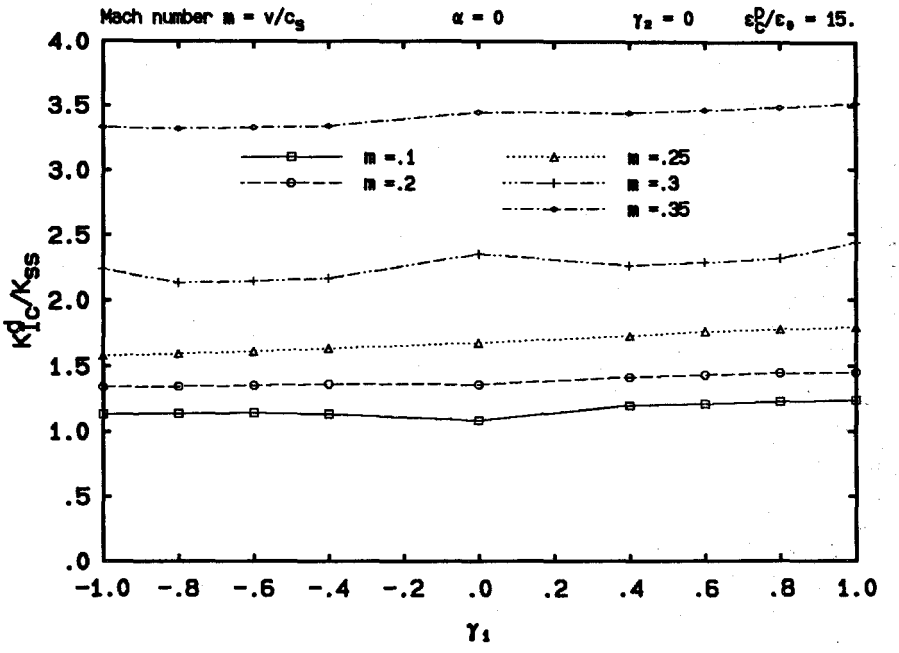

FIGURE 7.6.1 The variations of the normalized dynamic fracture toughness with respect to γ_1 at various crack propagation speeds.

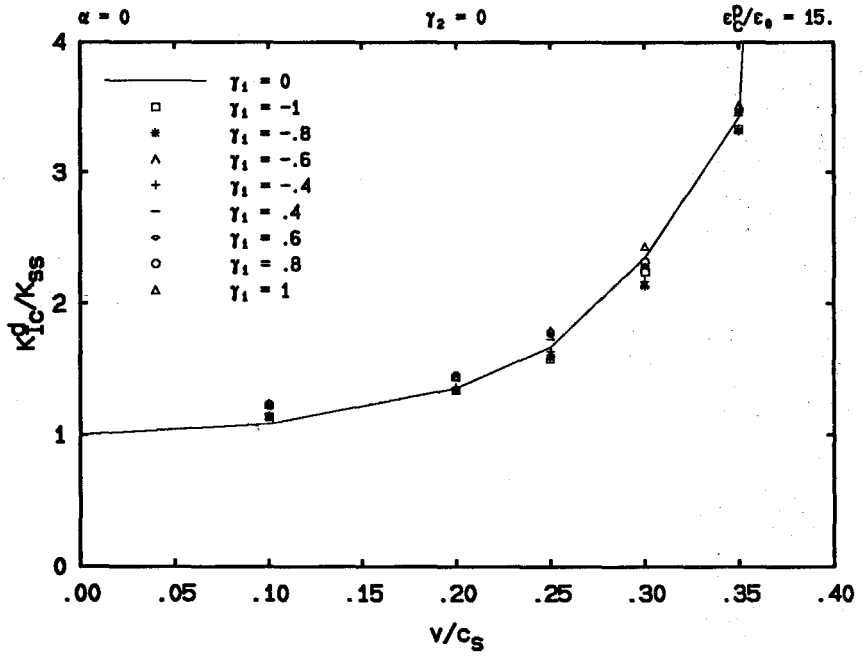

FIGURE 7.6.2 The effect of γ_1 on the K_{Ic}^d vs. v relationship, plotted in normalized coordinates.

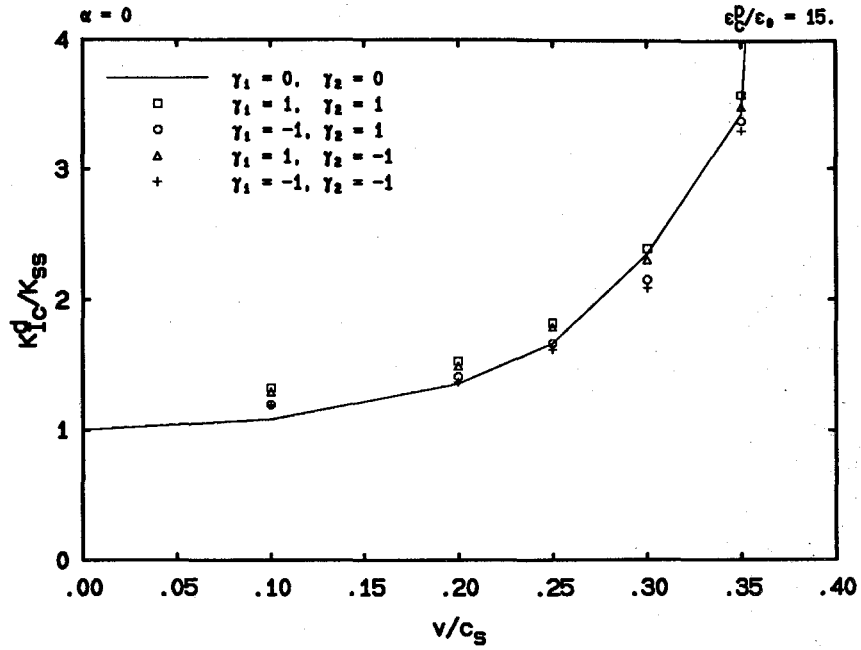

FIGURE 7.6.3 The combined effect of γ_1 and γ_2 on the K_{Ic}^d vs. v relationship, plotted in normalized coordinates.

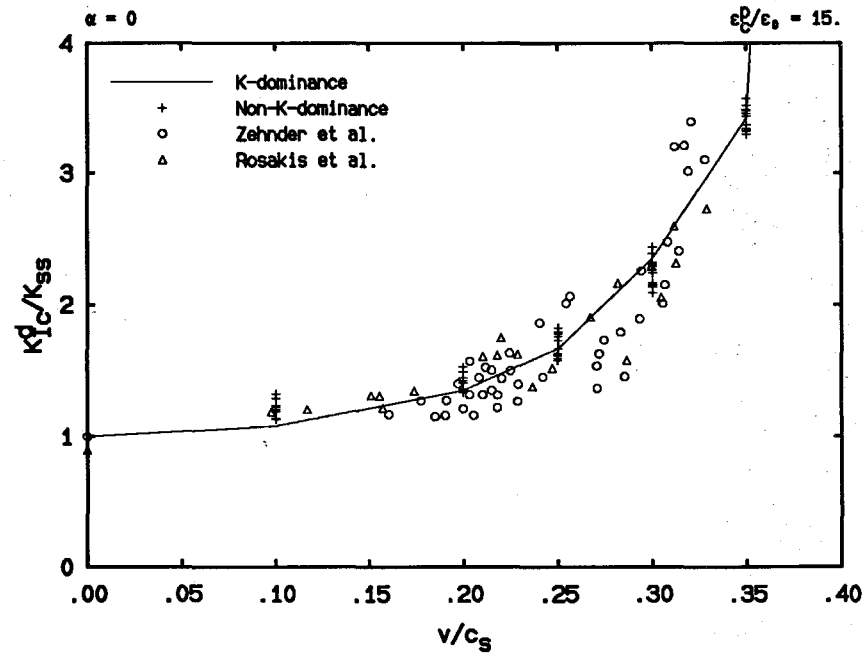

FIGURE 7.6.4 A compilation of the K_{Ic}^d vs. v relationship from the finite element data with and without K-dominance and from experimental measurements of Rosakis, Duffy and Freund (1984) and Zehnder and Rosakis (1990a).

perimental measurements, two important points must be noted. One is that when K-dominance does not exist, the experimental K_{Ic}^{d} data in Fig. 7.6.4 are not the real values of the stress intensity factor. Instead, they include contributions from other nonsingular elastic terms. Yet the data from the numerical calculations represent the real values of K_{Ic}^{d} under the assumed conditions. The other point is that the parameters γ_1 and γ_2 in the finite element computation are defined at a fixed, normalized distance from the crack tip, which in fact corresponds to different physical distances for different K_{Ic}^{d} values. That is to say, an exact non-K-dominance condition is actually characterized by one more parameter, namely the physical location where the relative values of the nonsingular elastic terms are defined. To this end, the present investigation only studied the effect of non-K-dominance for a set of sample points in the parametric space composed of the relative dominance parameters γ_1 and γ_2 as well as the physical distance from the crack tip.

CHAPTER 8

SUMMARY

The present finite element study addresses several issues of interest pertaining to the phenomenon of dynamic crack propagation in elastic-plastic solids. Under conditions of Mode I, plane stress, steady state and small-scale yielding, we investigated the structures of the near-tip stress and deformation fields for three classes of commonly used elastic-plastic material models. A preliminary asymptotic analysis for crack tip stress and velocity fields in elastic-perfectly plastic solids was provided to reveal and explain some special features of the crack tip fields observable only in the case of rapid crack propagation. We studied the theoretical basis of a fracture criterion based on the dynamic stress intensity factor for crack growth in materials which fail in a locally ductile manner. We explored the behavior of crack tip fields under non-K-dominance conditions and its effect on the dynamic fracture toughness vs. crack propagation speed relationship. The main findings of this study are summarized in the following.

8.1 PLASTIC ZONES AND CRACK TIP FIELDS

To start with, observations which are common in all cases investigated will be summarized. First of all, it is found that both the crack propagation speed and the level of strain hardening have a major influence on the size and shape of the active plastic zone at the front of the crack tip. As m or the ratio of the crack speed to that of the elastic shear wave increases, the height and the angular extent of the plastic zone increase accordingly, usually quite substantially, which is true for all materials studied. Comparatively, the size change in the horizontal direction or the

crack growth direction is much smaller; and whether this size increases or decreases depends on the hardening property of the material. For materials with weak or no strain hardening, the horizontal size decreases as m increases. Yet for materials with strong hardening behavior, this size is found to increase to a larger extent as m increases. On the other hand, materials with lower level of strain hardening will always have plastic zones with sizes larger in the horizontal direction and smaller in the vertical direction.

As to the angular variations of the near-tip stress and deformation fields, it is discovered that a compressive stress state always exists behind the crack tip in the direction parallel to that of crack propagation. For all angular ranges, the magnitude of the 2-2 plastic strain component is always much larger than those of the other two in-plane components, which is responsible for the sinusoidal behavior of the polar components. Meanwhile, the vertical component of the velocity field remains positive whereas the other component remains negative with a much smaller magnitude.

Radially, the near tip asymptotic fields possess very different singularities at the crack tip. For elastic-perfectly plastic solids, the finite element solution very near the crack tip strongly suggests that the strain and velocity fields behave as lnr as $r \to 0$, where r is the distance to the crack tip. The stresses are bounded at the crack tip with crack front values close to those predicted asymptotically for quasi-static crack growth, with slight changes for different m values. Strong yet approximately linear variations along the prospective crack line are observed for the radial stress component. For linear hardening elastic-plastic solids, the stress and strain singularities at the crack tip are of the type r^s $(s < 0)$ with s strongly dependent on m, but weakly on the Poisson ration ν. However, for power-law hardening elastic-plastic materials, the singularities at the crack tip are of the type $(lnr)^s$ $(s > 0)$, where s takes different values for stress and strain fields.

Throughout the present study for various elastic-plastic solids, an interesting phenomenon has been consistently observed. Depending on the degree of strain hardening, there seems to exist a transitional crack propagation speed for a given elastic-plastic material. At speeds lower than this value, the crack tip active plastic zones and the near-tip stress and deformation fields show features resembling those for quasi-static crack growth. At speeds higher than this value, however, characteristics distinct from those of quasi-static crack growth are developed.

For all hardening or nonhardening materials, the crack tip active plastic zones are usually found to exist only at the crack front. However, at crack speeds sufficiently large, secondary yield zones will appear along the crack flank. At the same time, kinks will show up in the angular field variations at locations where approximately elastic unloading starts to occur. Further, the value of the horizontal Cartesian component of the velocity field along the crack flank starts to deviate from zero.

It is suggested that if the above behaviors at high crack speeds are the essential features of the dynamic asymptotic crack tip field, then it can be said that the size of the dominance zone of this asymptotic field at the crack tip is extremely small.

8.2 THE FRACTURE CRITERION BASED ON K

A property found for crack growth in all elastic-plastic materials is that at a certain normalized distance at the crack front, the magnitude of the effective plastic strain decreases as m increases. Assuming the validity of a plastic strain based local fracture criterion, which has its bearings from the micromechanical characteristics of void growth and coalesence in ductile fracture, a theoretical dynamic fracture toughness vs. crack propagation speed relationship can be derived from the above effective plastic strain variations. Comparisons with experimental measurements, which are obtained through the use of the fracture criterion directly based on the

far-field dynamic stress intensity, show very good agreement, which strongly indicates the legitimacy, at least approximately, of this K-criterion for dynamic crack propagation in materials such as metals which fail in a locally ductile manner.

8.3 EFFECTS OF NON-K-DOMINANCE

For the non-K-dominance parameters γ_1 and γ_2 (defined in Chapter 7) in the range of [-1, 1], which is large compared to values from some commonly used test specimens, it is observed that the crack tip active plastic zone changes rather substantially both in size and shape from one extreme parameter value to the other. Yet the effect of the nonsingular terms in the elastic far-field on the near tip angular stress varaitions is found to be negligible. Those terms seem to affect the near-tip angular variations of the plastic strain field only in their magnitudes—with small changes—but not in their θ-dependence. The major influence of non-K-dominance on the angular variations of the velocity field is observed for the Cartesian component parallel to the direction of crack growth as if its magnitude is increased or lowered by a small constant amount.

The general tendency of the effects of the nonsingular elastic terms on the stress and plastic strain fields is seen to be mainly characterized by the first term or the T-term. However, the crack opening displacement appears quite insensitive to the existence of the T-term. Nontheless, as the crack tip is approached, all the effects due to the nonsingular elastic terms seem to disappear.

The dynamic fracture toughness vs. crack propagation speed relationship is affected by the nonsingular elastic terms only quantitatively. With the T-term alone, the relative deviation of the normalized dynamic fracture toughness K_{Ic}^{d}/K_{ss} from that under K-dominance conditions will occasionally reach its maximum value which is about 14%. With both nonsingular terms, the maximum relative deviation can take values in the neighborhood of 22%. However, it is noted that even in the

worst case the qualitative behavior of the K_{Ic}^{d} vs. v relationship is preserved.

It must be pointed out that the extent of scattering of the experimental data points in the K_{Ic}^{d} vs. v plot is much larger than that predicted from the present finite element computation with non-K-dominance parameters larger than values for some commonly used test specimens. This observation may suggest that factors other than the lack of K-dominance in experimental measurements must be pursued in order to further our understanding in this and related areas.

8.4 CLOSING COMMENTS

In this study attention is focused on the plane stress approximation of dynamic crack propagation phenomena in elastic-plastic materials. Although we were able to reveal features similar to those observed from experiments, the findings of this investigation must be interpreted cautiously. Due to complicated three-dimensional features involved near a crack edge, ultimate understanding of fracture behavior awaits properly formulated full scale three-dimensional modeling.

References

Achenbach, J.D. and Bazant, Z.P. 1974 " Elastodynamic Near-Tip Stress and Displacement Fields for Rapidly Propagating Cracks in Orthotropic Materials," *Journal of Applied Mechanics* 42, pp. 183-189.

Achenbach, J.D. and Brock, L.M. 1971 "Rapid Extension of a Crack," *Journal of Elasticity* 1, pp. 51-63.

Achenbach, J.D., Burgers, P. and Dunayevsky, V. 1979 "Near-Tip Plastic Deformations in Dynamic Fracture Problems," in *Nonlinear and Dynamic Fracture Mechanics,* ed. N. Perrone and S. N. Atluri, pp. 105-123.

Achenbach, J.D. and Dunayevsky, V. 1981a "Fields near a Rapidly Propagating Crack-Tip in an Elastic Perfectly-Plastic Material," *Journal of the Mechanics and Physics of Solids* 29(4), pp. 283-303.

Achenbach, J.D. and Dunayevsky, V. 1981b "Crack-Tip Plasticity for Rapid Crack Propagation," in *Advances in Fracture Research,* Proceedings of the 5th International Conference on Fracture, ed. D. Francois et al., Pergamon Press, pp. 2205-2213.

Achenbach, J.D. and Dunayevsky, V. 1984 "Crack Growth under Plane Stress Conditions in an Elastic Perfectly-Plastic Material," *Journal of the Mechanics and Physics of Solids* 32(2), pp. 89-100.

Achenbach, J.D. and Kanninen, M.F. 1978 "Crack Tip Plasticity in Dynamic Fracture Mechanics," in *Fracture of Mechanics,* ed. N. Perrone et al., pp. 649-670.

Achenbach, J.D., Kanninen, M.F. and Popelar, C.H. 1981 "Crack-Tip Fields for Fast Fracture of an Elastic-Plastic Material," *Journal of the Mechanics and Physics of Solids* 29(3), pp. 211-225.

Achenbach, J.D. and Li, Z.L. 1984a "Plastic Deformations near a Rapidly Propagating Crack Tip," *Report NU-SML-TR-No.84-1,* Department of Civil Engineering, Northwestern University, Evanston, IL 60201.

Achenbach, J.D. and Li, Z.L. 1984b "Plastic Deformations near a Rapidly Propagating Crack Tip," in *Fundamentals of Deformation and Fracture,* Eshelby Memorial Symposium, ed. B.A. Bilby et al., Cambridge University Press, Cambridge, pp. 217-232.

Achenbach, J.D. and Li, Z.L. 1984c "Plane Stress Crack-Line Fields for Crack Growth in an Elastic Perfectly-Plastic Material," *Engineering Fracture Mechanics* 20(3), pp. 535-544.

Achenbach, J.D., Li, Z.L. and Nishimura, N. 1985 "Dynamic Fields Generated by Rapid Crack Growth," *International Journal of Fracture* 27, pp. 215-227.

Amazigo, J.C. and Hutchinson, J.W. 1977 "Crack-Tip Fields in Steady Crack-Growth with Linear Strain-Hardening," *Journal of the Mechanics and Physics of Solids* 25, pp. 81-97.

Andersson, H. 1973 "A Finite Element Representation of Stable Crack Growth," *Journal of the Mechanics and Physics of Solids* 21, pp. 337-356.

Andersson, H. 1977 "Analysis of a Model for Void Growth and Coalescence Ahead of a Moving Crack Tip," *Journal of the Mechanics and Physics of Solids* 25, pp. 217-233.

Ashby, M.F. 1979 "Micromechanisms of Fracture in Static and Cyclic Failure," in *Fracture Mechanics,* ed. R.A. Smith, Pergamon Press, pp. 1-27.

ASTM STP 527 1974 American Society for Testing and Materials.

Atkinson, C. and Eshelby, J.D. 1968 "The Flow of Energy into the Tip of a

Moving Crack," *International Journal of Fracture* 4, pp. 3-8.

Atluri, S.N. and Nishioka, T. 1985 "Numerical Studies in Dynamic Fracture Mechanics," *Intenational Journal Fracture* 27, pp. 245-261.

Baker, B.R. 1962 "Dynamic Stresses Created by a Moving Crack," *Journal of Applied Mechanics* 29, pp. 449-454.

Begley, J.A. and Landes, J.D. 1972 "The J Integral as a Fracture Criterion," in *Fracture Toughness,* Proceedings of the 1971 National Symposium on Fracture Mechanics, Part II, ASTM STP 514, American Society for Testing and Materials, pp. 1-23.

Bilek, Z. 1980 "Some Comments on Dynamic Crack Propagation in a High Strength Steel," in *Crack Arrest Methodology and Applications, ASTM STP 711,* American Society for Testing and Materials, ed. G.T. Hahn et al., pp. 240-247.

Bishop, R.E.D. 1953 "On Dynamic Problems of Plane Stress and Plane Strain," *Quarterly Journal of Mechanics and Applied Mathematics* 6(2), pp. 250-254.

Bland, D.R. 1956 "The Two Measures of Work Hardening," Proceedings of The 9th International Congress for Applied Mechanics, Brussels, pp. 45-50.

Bowden, F.P., Brunton, J.H., Field, J.E. and Heys, A.D. 1967 "Controlled Fracture of Brittle Solids and Interruption of Electrical Current," *Nature* 216, pp. 38-42.

Brickstad, B. 1983 "A FEM Analysis of Crack Arrest Experiments," *International Journal of Fracture* 21, pp. 177-194.

Brickstad, B. and Nilsson, F. 1980 "Numerical Evaluation by FEM of Crack Propagation Experiments," *International Journal of Fracture* 16, pp. 71-84.

Broberg, K.B. 1960 "The Propagation of a Brittle Crack," *Arkiv für Fysik* 18,

pp. 159-192.

Broberg, K.B. 1967 in *Recent Progress in Applied Mechanics,* ed. K.B. Broberg et al., Almqrist and Wichsell, Stockholm.

Broberg, K.B. 1968 "Critical Review of Some Theories in Fracture Mechanics," *International Journal of Fracture Mechanics* 4, pp. 11-18.

Broberg, K.B. 1971 "Crack-Growth Criteria and Non-Linear Fracture Mechanics," *Journal of the Mechanics and Physics of Solids* 19(6), pp. 407-418.

Broberg, K.B. 1975 "On Stable Crack Growth," *Journal of the Mechanics and Physics of Solids* 23, pp. 215-237.

Broek, D. 1968 "Some Considerations on Slow Crack Growth," *International Journal of Fracture Mechanics* 4, pp. 19-33.

Brown, M.W. and Miller, K.J. 1985 "Mode I Fatigue Crack Growth under Biaxial Stress at Room and Elevated Temperature," in *Multiaxial Fatigue,* ASTM STP 853, American Society for Testing and Materials, pp. 135-152.

Burgers, P. 1980 "Dynamic Linear Elastic Crack Propagation in Anti-Plane Shear by Finite Differences," *International Journal of Fracture* 16(3), pp. 261-274.

Cardew, G.E., Goldthorpe, M.R., Howard, I.C. and Kfouri, A.P. 1985 "On the Elastic T-Term," in *Fundamentals of Deformation and Fracture,* Proceedings of the Eshelby Memorial Symposium, ed. Bilby et al., Cambridge University Press, pp. 465-476.

Chen, E.P. and Sih, G.C. 1977 "Scattering Waves about Stationary and Moving Cracks," in *Mechanics of Fracture* Vol.4, ed. G.C. Sih, pp. 119-212.

Cherepanov, G.P. 1967 "Crack Propagation in Continuous Media," *PMM Applied Mathematics and Mechanics* (English Translation) 31(3), pp. 503-512.

Cherepanov, G.P. 1974 *Mechanics of Brittle Fracture* (English Translation by A.L. Peabody), McGaw and Hill, New York.

Chitaley, A.D. and McClintock, F.A. 1971 "Elastic-Plastic Mechanics of Steady Crack Growth under Anti-Plane Shear," *Journal of the Mechanics and Physics of Solids* 19, pp. 147-163.

Christoffersen, J. and Hutchinson, J.W. 1979 "A Class of Phenomenological Corner Theories of Plasticity," *Journal of the Mechanics and Physics of Solids* 27, pp. 465-487.

Cox, T.B. and Low, J.R., Jr. 1974 "An Investigation of the Plastic Fracture of AISI 4340 and 18 Nickel-200 Grade Maraging Steels," *Metallurgical Transactions* 5, pp. 1457-1470.

Craggs, J.W. 1960 "On the Propagation of a Crack in an Elastic-Brittle Material," *Journal of the Mechanics and Physics of Solids* 8, pp. 66-75.

Curry, D.A. and Knott, J.F. 1980 "Current Aspects of Crack Growth under Monotonic Loading," in *Fracture and Fatigue,* ed. J.C. Radon, Pergamon Press.

Dean, R.H. 1983 "Elastic-Plastic Steady Crack Growth in Plane Stress," in *Elastic-Plastic Fracture: Second Symposium,* ASTM STP 803, ed. C.F. Shih and J.P. Gudas, American Society for Testing and Materials, pp. I-39-I-51.

Dean, R.H. and Hutchinson, J.W. 1980 "Quasi-Static Steady Crack Growth in Small-Scale Yielding," in *Fracture Mechanics: Twelfth Conference,* ASTM STP 700, American Society for Testing and Materials, pp. 383-405.

de Koning, A.U. 1977 "A Contribution to the Analysis of Quasi Static Crack Growth in Sheet Materials," in *Fracture 1977,* Proceedings of the 4th International Conference on Fracture, Vol.3, pp. 25-31.

Deng, X. and Rosakis, A.J. 1990 "Negative Plastic Flow and Its Prevention in Elasto-Plastic Finite Element Computation," *Finite Elements in Analysis and Design* (to appear).

Dong, P. and Pan, J. 1988 "Near-Tip Fields in Elastic Perfectly Plastic Solids," *Preprints of the 25th Annual Technical Meeting,* Society of Engineering Sciences, *University of California, Berkeley.*

Dong, P. and Pan, J. 1989 "Plane-Stress Near-Tip Fields in Elastic Perfectly Plastic Solids under Mixed-Mode Loading Conditions," in *Structural Mechanics in Reactor Technology,* Vol. G, Transactions of the 10th International Conference on Structural Mechanics in Reactor Technology, Los Angeles, pp. 159-164.

Douglas, A.S. 1981 "Dynamic Fracture Toughness of Ductile Materials in Antiplane Shear," *Ph.D. Dissertation,* Brown University, Providence, RI 02912.

Douglas, A.S., Freund, L.B. and Parks, D.M. 1981 "Dynamic Steady Antiplane Shear Crack Growth in an Elastic-Plastic Material," in *Advances in Fracture Research,* Proceedings of the 5th International Conference of Fracture, Vol.5, ed. D. Francois et al., Pergamon Press, pp. 2233-2240.

Drugan, W.J., Rice, J.R. and Sham, T-L. 1982 "Asymptotic Analysis of Growing Plane Strain Tensile Cracks in Elastic-Ideally Plastic Solids," *Journal of the Mechanics and Physics of Solids* 30(6), pp. 447-473.

Dugdale, D.S. 1960 "Yielding of Steel Sheets Containing Slits," *Journal of the Mechanics and Physics of Solids* 8, pp. 100-104.

Dunayevsky, V. and Achenbach, J.D. 1982a "Boundary Layer Phenomenon in the Plastic Zone near a Rapidly Propagating Crack Tip," *International Journal of Solids and Structures* 18(1), pp. 1-12.

Dunayevsky, V. and Achenbach, J.D. 1982b "Radial Nonuniformity of the

Fields near a Moving Crack tip in a Material with Linear Strain Hardening," *Journal of Applied Mechanics* 49, pp. 646-647.

Erdélyi, A. 1956 *Asymptotic Expansions*, Dover Publications, Inc.

Eshelby, J.D. 1969 "The Elastic Field of a Crack Extending Non-Uniformly under General Anti-Plane Loading," *Journal of the Mechanics and Physics of Solids* 17, pp. 177-199.

Freund, L.B. 1972a "Crack Propagation in an Elastic Solid Subjected to General Loading: I. Constant Rate of Extension," *Journal of the Mechanics and Physics of Solids* 20, pp. 129-140.

Freund, L.B. 1972b "Crack Propagation in an Elastic Solid Subjected to General Loading: II. Nonuniform Rate of Extension," *Journal of the Mechanics and Physics of Solids* 20, pp. 141-152.

Freund, L.B. 1972c "Energy Flux into the Tip of an Extending Crack in an Elastic Solid," *Journal of Elasticity* 2, pp. 341-379.

Freund, L.B. 1973 "Crack Propagation in an Elastic Solid Subjected to General Loading: III. Stress Wave Loading," *Journal of the Mechanics and Physics of Solids* 21, pp. 47-61.

Freund, L.B. 1974 "Crack Propagation in an Elastic Solid Subjected to General Loading: IV. Obliquely Incident Stress Pulse," *Journal of the Mechanics and Physics of Solids* 22, pp. 137-146.

Freund, L.B. 1976 "The Analysis of Elastodynamic Crack Tip Stress Fields," in *Mechanics Today* Vol.3, ed. S. Nemat-Nasser, Pergamon, pp. 55-91.

Freund, L.B. 1980 Private Communication to A.J. Rosakis, Presented in *Engineering Fracture Mechanics* 13, pp. 331-347.

Freund, L.B. and Clifton, R.J. 1974 "On the Uniqueness of Plane Elastodynamic Solutions for Running Cracks," *Journal of Elasticity* 4(4), pp. 293.

Freund, L.B. and Douglas, A.S. 1982 "The Influence of Inertia on Elastic-Plastic Antiplane-Shear Crack Growth," *Journal of the Mechanics and Physics of Solids* 30(1/2), pp. 59-74.

Fuller, K.N.G., Fox, P.G. and Field, J.E. 1975 "The Temperature Rise at the Tip of a Fast Moving Crack in Glassy Polymers," in *Proceedings of Royal Society of London, Series A* 341, pp. 537-557.

Gao, Y.C. 1980 "Elastic-Plastic Field at the Tip of a Crack Growing Steadily in Elastic-Perfectly Plastic Medium," *Acta Mechanica Sinica* 1, pp. 48-56.

Gao, Y.C. 1983 "Influence of Compressibility on the Elastic-Plastic Field of a Growing Crack," in *Elastic-Plastic Fracture: Second Symposium,* ASTM STP 803, ed. C.F. Shih and J.P. Gudas, American Society for Testing and Materials, pp. I-176-I-190 .

Gao, Y.C. 1985 "Asymptotic Dynamic Solution to the Mode-I Propagating Crack Tip," *International Journal of Fracture* 29, pp. 171-180.

Gao, Y.C. 1987 "Plane Stress Dynamic Plastic Field near a Propagating Crack Tip," *International Journal of Fracture* 34, pp. 111-129.

Gao, Y.C. and Hwang, K-C. 1981a "Elastic-Plastic Fields in Steady Crack Growth, " in *Three-Dimensional Constitutive Relations and Ductile Fracture,* ed. S. Nemat-Nasser, North-Holland Publishing Company, pp. 417-434.

Gao, Y.C. and Hwang, K-C. 1981b "Elastic-Plastic Fields in Steady Crack Growth in a Strain-Hardening Material," in *Advances in Fracture Research,* Proceedings of the 5the International Conference on Fracture, Vol.2, ed. D. Francois et al., pp. 669-682.

Gao, Y.C. and Nemat-Nasser, S. 1983a "Dynamic Fields near a Crack Tip Growing in an Elastic-Perfectly-Plastic Solid," *Mechanics of Materials* 2, pp. 47-60.

Gao, Y.C. and Nemat-Nasser, S. 1983b "Near-Tip Dynamic Fields for a Crack Advancing in a Power-Law Elastic-Plastic Material: MOdes I,II and III," *Mechanics of Materials* 2, pp. 305-317.

Gao, Y.C. and Nemat-Nasser, S. 1984 "Mode II Dynamic Fields near a Crack Tip Growing in an Elastic-Perfectly-Plastic Solid," *Journal of the Mechanics and Physics of Solids* 32(1), pp. 1-19.

Gao, Y.C., Zhang, X.T. and Hwang, K.C. 1983 "The Asymptotic Near-Tip Solution for Mode-III Crack in Steady Growth in Power Hardening Media," *International Journal of Fracture* 21, pp. 301-317.

Glennie, E.B. 1972 "The Dynamic Growth of a Void in a Plastic Material and an Application to Fracture," *Journal of the Mechanics and Physics of Solids* 20, pp. 415-429.

Griffith, A.A. 1920 "The Phenomena of Rupture and Flow," *Transactions, Royal Society of London, Series A* 221, pp. 163-198.

Griffith, A.A. 1924 "The Theory of Rupture," *Proceedings of the First International Congress of Applied Mechanics,* Delft, Netherlands.

Guo, Q.X. and Li, K.R. 1987 "Plastic Deformation Ahead of a Plane Stress Tensile Crack Growting in an Elastic-Perfectly-Plastic Solid," *Engineering Fracture of Mechanics* 28(2), pp. 139-146.

Hill, R. 1950 *The Mathematical Theory of Plasticity,* Clarendon Press, Oxford.

Hilton, P. and Hutchinson, J.W. 1971 "Plastic Intensity Factors for Cracked Plates," *Engineering Fracture Mechanics* 3, pp. 435-451.

Hinton, E. and Campbell, J.S. 1974 "Local and Global Smoothing of Discontinuous Finite Element Functions Using a Least Squares Method," *International Journal for Numerical Methods in Engineering* 8, pp. 461-480.

Hult, J.A. 1957 "Fatigue Crack Propagation in Torsion," *Journal of the Mechanics and Physics of Solids* 6, pp. 47-52.

Hult, J.A. and McClintock, F.A. 1956 "Elastic-Plastic Stress and Strain Distributions around Sharp Notches under Repeated Shears," in *Proceedings of the 9th International Congress of Applied Mechanics,* Vol.8, pp. 51-58.

Hutchinson, J.W. 1968a "Singular Behaviour at the End of a Tensile Crack in a Hardening Material," *Journal of the Mechanics and Physics of Solids* 16, pp. 13-31.

Hutchinson, J.W. 1968b "Plastic Stress and Strain Fields at a Crack Tip," *Journal of the Mechanics and Physics of Solids* 16, pp. 337-347.

Hutchinson, J.W. 1979 *A Course on Nonlinear Fracture Mechanics,* The Technical University of Denmark.

Hutchinson, J.W. 1983 "Fundamentals of the Phenomenological Theory of Nonlinear Fracture Mechanics," *Journal of Applied Mechanics* 50, pp. 1042-1051.

Hutchinson, J.W. and Paris, P.C. 1979 "Stability Analysis of J-Controlled Crack Growth," in *Elastic-Plastic Fracture,* ASTM STP 668, ed. J.D. Landes et al., pp. 37-64.

Hwang, K.C. and Luo, X.F. 1988 "Perturbation Solution for Near-Tip Fields of Cracks Growing in Elastic Perfectly-Plastic Compressible Materials," in *Recent Advances in Nonlinear Fracture Mechanics,* Proceedings, IUTAM Symposium, Caltech, Pasadena, California.

Irwin, G.R. 1948 "Fracture Dynamics," in *Fracturing of Metals,* American Society for Metals, Cleveland.

Irwin, G.R. 1956 "Crack Propagation in High Strength Steels," in *Proceedings, The Sagamore Research Conference on Strength Limitations of High Strength Metals,* Vol. 2, New York University Research Institute, Syracuse, pp. 289-305.

Irwin, G.R. 1957 "Analysis of Stresses and Strains Near the End of a Crack Traversing a Plate," *Journal of Applied Mechanics* 24, pp. 361-364.

Irwin, G.R. and Koshinen, M.F. 1963 *Transactions, ASME* 85D, pp. 593-594.

Kachonov, L.M. 1974 *Fundamentals of the Theory of Plasticity* (English Translation by M. Konyaeva), Mir Publishers, Moscow.

Kalthoff, J.F. 1983 "On Some Current Problems in Experimental Fracture Mechanics," in *Workshop on Dynamic Fracture,* ed. W.G. Knauss et al., Caltech, Pasadena, CA 91125, pp. 11-35.

Kanazawa, T., Machida, S., Teramoto, T. and Yoshinari, H. 1981 "Study on Fast Fracture and Crack Arrest," *Experimental Mechanics* 21(2), pp. 78-88.

Kanninen, M.F., Popelar, C.H., and Broek, D. 1981 *Nuclear Engineering and Design* 67, pp. 27-55.

Kanninen, M.F., Rybicki, E.F., Stonesifer, R.B., Broek, D., Rosenfield, A.R., Marschall, C.W., and Hahn, G.T. 1979 "Elastic-Plastic Fracture Mechanics for Two-Dimensional Stable Crack Growth and Instability Problems," in *Elastic-Plastic Fracture,* ASTM STP 668, pp. 121-150.

Kfouri, A.P. 1986 "Some Evaluations of the Elastic T-Term Using Eshelby's Method," *International Journal of Fracture* 3, pp. 301.

Kobayashi, T. and Dally, J.W. 1977 "Relation between Crack Velocity and

the Stress Intensity Factors," in *Fast Fracture and Crack Arrest,* ASTM STP 627, American Society for Testing and Materials, ed. G.T. Hahn et al., pp. 257-273.

Kobayashi, T. and Dally, J.W. 1980 "Dynamic Photo-Elastic Determination of $\dot{a}$-K Relation for the 4340 Steel," in *Crack Arrest Methodology and Applications,* ASTM STP 711, American Society for Testing and Materials, ed. G.T. Hahn et al., pp. 189-210.

Kobayashi, A.S. and Mall, S. 1978 "Dynamic Fracure Toughness of Homalite 100," *Experimental Mechanics* 18, pp. 11-18.

Kostrov, B.V. 1966 "Unsteady Propagation of Longitudinal Shear Crack," *Applied Mathematics and Mechanics* (English Translation of PMM) 30, pp. 1241-1248.

Kostrov, B.V. and Nikitin, L.V. 1970 "Some General Problems of Mechanics of Brittle Fracture," *Archiwum Mechaniki Stosowanej* 22, pp. 749-775.

Krishnaswany, S. and Rosakis, A.J. 1990a "On the Extent of Dominance of Asymptotic Elastodynamic Crack-Tip Fields; Part I: An Experimental Study Using Bifocal Caustics," *Journal of Applied Mechanics* (to appear).

Krishnaswany, S. and Rosakis, A.J. 1990b "Quasistatic Crack-Growth under Plane-Stress Conditions in Elastic-Perfectly Plastic Solids: A Note on Regions of Ellipticity and Hyperbolicity," Submitted to *Journal of Applied Mechanics.*

Krishnaswany, S., Rosakis, A.J. and Ravichandran, G. 1990 "On the Extent of Dominance of Asymptotic Elastodynamic Crack-Tip Fields; Part II: Numerical Investigation of Three-Dimensional and Transient Effects," *Journal of Applied Mechanics* (to appear).

Lam, P.S. 1982 "Numerical Analysis of Stable Crack Growth in Elastic-Plastic Materials in Small Scale and General Yielding," *Ph.D. Thesis,* University of Illinois at Urbana-Champaign.

Lam, P.S. and Freund, L.B. 1985 "Analysis of Dynamic Growth of a Tensile Crack in an Elastic-Plastic Material," *Journal of the Mechanics and Physics of Solids* 33(2), pp. 153-167.

Lam, P.S. and McMeeking, R.M. 1984 "Analyses of Steady Quasistatic Crack Growth in Plane Strain Tension in Elastic-Plastic Materials with Non-Isotropic Hardening," *Journal of the Mechanics and Physics of Solids* 32(5), pp. 395-414.

Landes, J.D. and Begley, J.A. 1972 "The Effect of Specimen Geometry on J_{Ic}," in *Fracture Toughness*, Proceedings of the 1971 National Symposium on Fracture Mechanics, Part II, ASTM STP 514, American Society for Testing and Materials, pp. 24-39.

Larsson, S.G. and Carlsson, A.J. 1973 "Influence of Non-Singular Stress Terms and Specimen Geometry on Small-Scale Yielding at Crack Tips in Elatic-Plastic Materials," *Journal of the Mechanics and Physics of Solids,"* 21, pp. 263-277.

Leevers, P.S. and Radon, J.C. 1982 "Inherent Stress Biaxiality in Various Fracture Specimen Geometries," *International Journal of Fracture* 19, pp. 311.

Leighton, J.T., Champion, C.R. and Freund, L.B. 1987 "Asymptotic Analysis of Steady Dynamic Crack Growth in an Elastic-Plastic Material," *Journal of the Mechanics and the Physics of Solids* 35(5), pp. 541-563.

Lin, B-S. 1985 "Elastic Perfectly-Plastic Fields at a Rapidly Propagating Crack Tip," *Applied Mathematics and Mechanics* (English Edition) 6(10), pp. 1017-1025.

Lo, K.K. 1982 "Elastic-Plastic Field at the Tip of a Propagating Shear Crack," *Quarterly of Applied Mathematics* 40, pp. 27-36.

Lo, K.K. and Peirce, D. 1981 "Effect of Yield Surface Vertex on Crack-Tip Fields in Mode III," *Journal of the Mechanics and Physics of Solids* 29(2), pp. 143-152.

Ludwig, P. 1909 *Elements der Technologischen Mechanik,* Berlin.

Luo, X., Zhang, X. and Hwang, K. 1984 "Finite Element Analysis of Mode-I Steady Crack Growth in Plane Stress," in *Proceedings of ICF Internal Symposium on Fracture Mechanics (Beijing),* Science Press, Beijing, China, pp. 138-145.

Majorana, C.E., Odorizzi, S.A. and Vitaliani, R. 1985 "Direct Determinatin of Finite Element Local Smoothing Matrices," *Communications in Applied Numerical Methods* 1, pp. 39-43.

Malkus, D.S. and Hughes, T.J.R. 1978 "Mixed Finite Element Methods—Reduced and Selective Integration Techniques: A Unification of Concepts," *Computer Methods in Applied Mechanics and Engineering* 15, pp. 63-81.

Marcal, P.V. 1965 "A Stiffness Method for Elastic-Plastic Problems," *International Journal of Mechanical Sciences* 7, pp. 229-238.

Marques, J.M.M.C. 1984 "Stress Computation in Elastoplasticity," *Engineering Computation* 1, pp. 42-51.

McClintock, F.A. 1956 "The Growth of Fatigue Cracks under Plastic Torsion," in *Proceedings of International Conference on Fatigue of Metals,* The Institute of Mechanical Engineers, London, pp. 538-542.

McClintock, F.A. 1958 "Ductile Fracture Instability in Shear," *Journal of Applied Mechanics* 25, pp. 582-588.

McClintock, F.A. 1963 "On the Plasticity of the Growth of Fatigue Crack, " in *Fracture of Solids,* ed. Drucker and Gilman, John Wiley and Sons, Inc., pp. 65.

McClintock, F.A. 1965 "Effects of Root Radius, Stress, Crack Growth and Rate on Fracture Instability," *Proceedings of Royal Society (London)* Series A 285, pp. 58-72.

McClintock, F.A. 1968 "A Criterion for Ductile Fracture by the Growth of Holes," *Journal of Applied Mechanics* 35, pp. 363-371.

McClintock, F.A. and Irwin, G.R. 1964 "Plasticity Aspects of Fracture Mechanics," in *Fracture Toughness Testing and Its Applications,* ASTM STP 381, American Society for Testing and Materials, pp. 84-113.

Nagtegaal, J.C., Parks, D.M. and Rice, J.R. 1974 "On Numerically Accurate Finite Element Solutions in the Fully Plastic Range," *Computer Methods in Applied Mechanics and Engineering* 4, pp. 153-177.

Narasimhan, R. and Rosakis, A.J. 1987 "Reexamination of Jumps across Quasistatically Propagating Surfaces under Generalized Plane Stress in Anisotropically Hardening Elastic-Plastic Solids," *Journal of Applied Mechanics* 54, pp. 519-524.

Narasimhan, R., Rosakis, A.J. and Hall, J.F. 1987a "A Finite Element Study of Stable Crack Growth under Plane Stress Conditions: Part I— Elastic-Perfectly Plastic Solids," *Journal of Applied Mechanics* 54, pp. 838-845.

Narasimhan, R., Rosakis, A.J. and Hall, J.F. 1987b "A Finite Element Study of Stable Crack Growth under Plane Stress Conditions: Part II— Influence of Hardening," *Journal of Applied Mechanics* 54, pp. 846-853.

Narasimhan, R. and Rosakis, A.J. 1988 "A Finite Element Analysis of Small-Scale Yielding near a Stationary Crack under Plane Stress," *Journal of the Mechanics and Physics of Solids* 36, pp. 77-117.

Nicoletto, G. 1988 "Biaxial Stress Effects on the Elastic-Plastic Crack-Tip Displacement Fields," Submitted to *International Journal of Plasticity.*

Nilsson, F. 1972 "Dyanmic Stress-Instensity Factors for Finite Strip Problems," *International Journal of Fracture* 8, pp. 403-411.

Nilsson, F. 1974 "A Note on the Stress Singularity at a Nonuniformly Moving Crack Tip," *Journal of Elasticity* 4, pp. 73-75.

Nishioka, T. and Atluri, S.N. 1983 "Path-Independent Integrals, Energy Release Rates, and General Solutions of Near-Tip Fields in Mixed-Mode Dynamic Fracture Mechanics," *Engineering Fracture Mechanics* 18(1), pp. 1-22.

Orowan, E. 1949 "Fracture and Strength of Solids," *Report of Progress in Physics,* Vol.12, Physical Society of London.

Paris, P.C., Tada, H., Zahoor, A. and Ernst, H. 1977 "A Treatment of the Subject of Tearing Instability," *U.S. Nuclear Regularity Commission Report* NUREG-0311 (available through National Technical Information Service, Springfield, VA.

Parks, D.M., Lam, P.S. and McMeeking, R.M. 1981 "Some Effects of Inelastic Constitutive Models on Crack Tip Fields in Steady Quasistatic Growth," in *Advances in Fracture Research,* Proceedings of the 5th International Conference on Fracture, Vol.5, ed. D. Francois et al., pp. 2607-2614.

Phillips, A. 1951 "A General Method of Calculating the Me_{max} Diagram in Plastic Bending of Beams," *Journal of Applied Mechanics* 18(4), pp. 353-358.

Ponte Castañeda, P. 1986 "Asymptotic Fields of a Perfectly-Plastic, Plane Stress Mode II Growing Crack," *Journal of Applied Mechanics* 53, pp. 831-833.

Ponte Castañeda, P. 1987a "Asymptotic Fields in Steady Crack Growth with Linear Strain-Hardening," *Journal of the Mechanics and Physics of Solids* 35(2), pp.227-268.

Ponte Castañeda, P. 1987b "Plastic Stress Intensity Factors in Steady Crack Growth," *Journal of Applied Mechanics* 54, pp. 379-387.

Post, D. 1954 in *Proceedings of the Society for Experimental Stress Analysis* 12, pp. 99-116.

Puttick, K.E. 1959 "Ductile Fracture in Metals," *Philosophical Magazine* 4, pp. 964-969.

Radok, J.R.M. 1956 "On the Solution of Problems of Dynamic Plane Elasticity," *Quarterly Applied Mathematics* 14, pp. 289-298.

Ramberg, W. and Osgood, W.R. 1943 "The Description of Stress-Strain Curves by Three Parameters," *N.A.C.A. Technical Note*, pp. 902.

Ravi-Chandar, K. 1982 "An Experimental Investigation into the Mechanics of Dynamic Fracture," *Ph.D. Dissertation*, Caltech, Pasadena, CA 91125.

Ravi-Chandar, K. and Knauss, W.G. 1984 "An Experimental Investigation into Dynamic Fracture: II. Microstructural Aspects," *International Journal of Fracture* 26, pp. 65-80.

Ravi-Chandar, K. and Knauss, W.G. 1987 "On the Characterisation of the Transient Stress Field near the Tip of a Crack," *Journal of Applied Mechanics* 54, pp. 72-78.

Rice, J.R. 1966 "Contained Plastic Deformation near Cracks and Notches under Longitudinal Shear," *International Journal of Fracture Mechanics* 2, pp. 426-447.

Rice, J.R. 1967 "Mechanics of Crack Tip Deformation and Extension by Fatigue," in *Fatigue Crack Propagation*, ASTM STP 415, American Society for Testing and Materials, pp. 247-311.

Rice, J.R. 1968a "Mathematical Analysis in the Mechanics of Fracture," in *Fracture, An Advanced Treatise*, Vol.II, ed. H. Liebowitz, Academic Press, N.Y. and London, pp. 191-311.

Rice, J.R. 1968b "A Path Independent Integral and the Approximate Analysis of Strain Concentration by Notches and Cracks," *Journal of Applied Mechanics* 35, pp. 379-386.

Rice, J.R. 1975 "Elastic-Plastic Models for Stable Crack Growth," in *Mechanics and Mechanisms of Crack Growth,* Proceedings of April 1973 Conference, British Steel Corp. Physical Metallurgy Centre Report, ed. M. J. May, pp. 14-39.

Rice, J.R. 1973 in Proceedings of The 3rd International Conference on Fracture, Munich.

Rice, J.R. 1974 "Limitations to the Small Scale Yielding Approximation for Crack Tip Plasticity," *Journal of the Mechanics and Physics of Solids* 22, pp. 17-26.

Rice, J.R. 1982 "Elastic-Plastic Crack Growth," in *Mechanics of Solids,* ed. H.G. Hopkins and M.J. Sewell, Pergamon Press, Oxford, pp. 539-562.

Rice, J.R., Drugan, W.J. and Sham, T.L. 1980 "Elastic-Plastic Analysis of Growing Cracks," in *Fracture Mechanics: Twelfth Conference,* ASTM STP 700, American Society for Testing and Materials, pp. 189-221.

Rice, J.R. and Johnson, M.A. 1969 "The Role of Large Crack Tip Geometry Changes in Plane Strain Fracture," in *Inelastic Behavior of Solids,* ed. Kanninen et al., pp. 641-672.

Rice, J.R. and Rosengren, G.F. 1968 "Plane Strain Deformation near a Crack Tip in a Power-Law Hardening Material," *Journal of the Mechanics and Physics of Solids* 16, pp. 1-12.

Rice, J.R. and Sorensen, E.P. 1978 "Continuing Crack-Tip Deformation and Fracture for Plane Strain Crack Growth in Elastic-Plastic Solids," *Journal of the Mechanics and Physics of Solids* 26, pp. 163-186.

Rice, J.R. and Tracey, D.M. 1973 "Computational Fracture Mechanics," in *Numerical and Computer Methods in Structural Mechanics,* ed. S.J. Fenves et al., Academic Press, pp. 585-623.

Rosakis, A.J., Duffy, J. and Freund, L.B. 1984 "The Determination of Dynamic Fracture Toughness of AISI 4340 Steel by the Shadow Spot Method," *Journal of the Mechanics and Physics of Solids* 32, pp. 443-460.

Rosakis, A.J., Ravi-Chandar, K. and Rajapakse, Y. (eds.) 1988 *Analytical, Numerical, and Experimental Aspects of Three Dimensional Fracture Process,* ASME AMD-Vol.91, The American Society of Mechanical Engineers.

Rose, L.R.F. 1976 "Recent Theoretical and Experimental Results on Fast Brittle Fracture," *International Journal of Fracture* 12(6), pp. 799-813.

Schardin, H. 1959 "Velocity Effects in Fracture," in *Fracture,* ed. B.L. Averbach et al., John Wiley and Sons Inc., N.Y., pp. 297-330.

Schreyer, H.L., Kulak, R.F. and Kramer, J.M. 1979 "Accurate Numerical Solutions for Elastic-Plastic Methods," *Journal of Pressure Vessel Technology* 101, pp. 226-234.

Sham, T-L. 1979 *Sc.M. Thesis,* Brown University, Providence, RI 02912.

Sham, T-L. 1983 "A Finite-Element Study of the Asymptotic Near-Tip Fields for Mode I Plane-Strain Cracks Growing Stably in Elastic-Ideally Plastic Solids," in *Elastic-Plastic Fracture: Second Symposium,* Vol.I, ASTM STP 803, ed. C.F. Shih and J.P. Gudas, pp. I-52-I-79.

Shih, C.F. 1973 "Elastic-Plastic Analysis of Combined Mode Crack Problems," *Ph.D. Thesis,* Harvard University, Cambridge, Massachusetts.

Shih, C.F., deLorenzi, H.G., and Andrews, W.R. 1979 "Studies on Crack

Initiation and Stable Crack Growth," in *Elastic-Plastic Fracture,* ASTM STP 668, Americal Society for Testing and Materials, pp. 65-120.

Sih, G.C. 1970 "Dynamic Aspects of Crack Propagation," in *Inelastic Behavior of Solids,* ed. M. F. Kanninen et al., McGraw-Hill Book Company, pp. 607-639.

Sih, G.C. and Chen, E.P. 1977 "Cracks Moving at Constant Velocity and Acceleration," in *Mechanics of Fracture* Vol.4, ed. G.C. Sih, pp. 59-117.

Slepyan, L.I. 1974 "Growing Crack during Plane Deformation of an Elastic-Plastic Body," *Izvestiya Akademii Nauk SSSR, Mekhanika Tverdogo Tela* (English Translation) 9(1), pp. 57-67.

Slepyan, L.I. 1976 "Crack Dynamics in an Elastic-Plastic Body," *Izvestiya Akademii Nauk SSSR, Mekhanika Tverdogo Tela* (English Translation) 11(2), pp. 144-153.

Smith, E.W. and Pascoe, K.J. 1983 "The Behaviour of Fatigue Cracks Subject to Applied Biaxial Stress: A Review of Experimental Evidence," *Fatigue of Engineering Metals and Structures* 6, pp. 201.

Sorensen, E.P. 1978 "A Finite Element Investigation of Stable Crack Growth in Anti-Plane Shear," *International Journal of Fracture* 14(5), pp. 485-500.

Sorensen, E.P. 1979 "A Numerical Investigation of Plane Strain Stable Crack Growth under Small-Scale Yielding Conditions," in *Elastic-Plastic Fracture,* ASTM STP 668, ed. J.D. Landes, J.A. Begley, and G.A. Clarke, Americal Society for Testings and Materials, pp. 151-174.

Takahashi, K. and Arakawa, K. 1987 "Dependence of Crack Acceleration on the Dynamic Stress-Intensity Factor in Polymers," *Experimental Mechanics* 27(2), pp. 195-199.

Tippur, H.V., Krishnaswamy, S. and Rosakis, A.J. 1990a "A Coherent Gradient Sensor for Crack Tip Deformation Measurements: Analysis and Experimental Results," *International Journal of Fracture* (to appear).

Tippur, H.V., Krishnaswamy, S. and Rosakis, A.J. 1990b "Optical Mapping of Crack Tip Deformations Using the Methods of Transmission and Reflection Coherent Gradient Sensing," Submitted to *International Journal of Fracture.*

Tracey, D.M., 1976 "Finite Element Solutions for Crack-Tip Behavior in Small-Scale Yielding," *Journal of Engineering Materials and Technology* 98(2), pp. 146-151.

Weichert, R. and Schoenert, K. 1978 "Heat Generation at the Tip of a Moving Crack," *Journal of the Mechanics and Physics of Solids* 26, pp. 151-161.

Wells, A. A. 1961 "Unstable Crack Propagation in Metals: Cleavage and Fast Fracture," in *Proceedings of the Cranfield Crack Propagation Symposium*, Vol.1, pp. 210-230.

Wells, A.A. 1963 "Application of Fracture Mechanics at and Beyond General Yielding," *British Welding Journal* 11, pp. 563-570.

Wells, A.A. 1965 "Notched Bar Tests, Fracture Mechanics and the Brittle Strengths of Welded Structures," *British Welding Journal* 12(1), pp. 2-13.

Wells, A.A. and Post, D. 1958 in *Proceedings of the Society for Experimental Stress Analysis* 16, pp. 69-92.

Wilkins, M.L. 1964 "Calculation of Elastic-Plastic Flow," in *Methods in Computational Physics,* Vol.3, ed B. Alder et al., Academic Press, pp. 211-263.

Williams, M.L. 1957 "On the Stress Distribution at the Base of a Stationary Crack," *Journal of Applied Mechanics* 24, pp. 109-114.

Yoffe, E.H. 1951 "The Moving Griffith Crack," *Philosophical Magazine* 42, pp. 739-750.

Zehnder, A.T. and Rosakis, A.J. 1990a "Dynamic Fracture Initiation and Propagation in 4340 Steel under Impact Loading," *International Journal of Fracture* (to appear).

Zehnder, A.T. and Rosakis, A.J. 1990b "On the Temperature Distribution at the Vicinity of Dynamically Propagating Cracks in 4340 Steel," *Journal of the Mechanics and Physics of Solids* (to appear).

Zhang, R., Zhang, X. and Hwang, K.C. 1983 "Near-Tip Fields for Plane-Strain Mode-I Steady Crack Growth in Linear Hardening Material with Bauschinger Effect," in *Proceedings of ICF International Symposium on Fracture Mechanics (Beijing)*, Science Press, Beijing, China, pp. 283-290.

Zhang, Z. and Gao, Y.C. 1988 "Plane Stress Dynamic Fields near a Propagating Crack-Tip in a Power-Law Material," *Acta Mechanica Sinica* 4(1), pp. 22-34.